Palaeontologia Electronica
palaeo-electronica.org

A reappraisal of the cranial and mandibular osteology of the spinosaurid *Irritator challengeri* (Dinosauria: Theropoda)

Marco Schade, Oliver W. M. Rauhut, Christian Foth, Olof Moleman, and Serjoscha W. Evers

ABSTRACT

Although originally described almost three decades ago, the holotype of *Irritator challengeri* from the Lower Cretaceous Romualdo Formation of Brazil still represents the most complete spinosaurid skull known to science. Here, we present a detailed description of the skull of *Irritator* based on digital reconstructions from medical and micro computed tomography (µCT) data. Segmentation reveals the near-complete palatal complex and braincase, an unusual morphology of the retroarticular process, a large, ventrally inclined surangular shelf and the tooth replacement pattern. The digitally reconstructed skull anatomy indicates a robust dentition, a field of binocular vision in front of the skull with an inclined snout orientation, a relatively weak but fast bite, as well as laterally spreading and rotating lower jaw rami during jaw opening. We modified an existing phylogenetic matrix of Tetanurae to account for new observations on the morphology of *Irritator* and analysed this using parsimony and Bayesian methods. Results support Spinosauridae as members of Megalosauroidea and recover a monophyletic Carnosauria (Megalosauroidea + Allosauroidea). Parsimony analysis recovers *Monolophosaurus* nested within Megalosauroidea as sister taxon to spinosaurids, but this is not supported by the Bayesian analysis. Bayesian time-calibration and evolutionary rate analysis indicate that spinosaurid evolution happened fast, despite a long ghost lineage of at least 35 million years. High evolutionary rates over a prolonged time can explain the highly derived skull morphology of spinosaurids. This study provides an in-depth look into the evolution of spinosaurid skull anatomy and refines our understanding of these specialized Mesozoic predators.

Marco Schade. University of Greifswald, Institute of Geography and Geology, Palaeontology and Historical Geology, Friedrich-Ludwig-Jahnstraße 17A, 17489, Greifswald, Germany and Zoological Institute and Museum, Cytology and Evolutionary Biology at University of Greifswald, Soldmannstraße 23, 17489 Greifswald, Germany. corresponding author. marco.schade@uni-greifswald.de
Oliver W. M. Rauhut. SNSB - Bayerische Staatssammlung für Paläontologie und Geologie; Department für

Final citation: Schade, Marco, Rauhut, Oliver W. M., Foth, Christian, Moleman, Olof, and Evers, Serjoscha W. 2023. A reappraisal of the cranial and mandibular osteology of the spinosaurid *Irritator challengeri* (Dinosauria: Theropoda). Palaeontologia Electronica, 26(2):a17.
https://doi.org/10.26879/1242
palaeo-electronica.org/content/2023/3821-the-osteology-of-irritator

Geo- und Umweltwissenschaften, Ludwig-Maximilians-Universität; GeoBioCenter, Ludwig-Maximilians-Universität; Richard-Wagner-Str. 10, 80333 Munich, Germany. rauhut@snsb.de
Christian Foth. University of Fribourg, Department of Geosciences, Ch. du Musée 6, 1700 Fribourg, Switzerland. christian.foth@gmx.net
Olof Moleman. Alkmaar, Netherlands. o_moleman@hotmail.com
Serjoscha W. Evers. University of Fribourg, Department of Geosciences, Ch. du Musée 6, 1700 Fribourg, Switzerland. serjoscha.evers@googlemail.com

Keywords: Dinosaur; Theropod; Spinosaurid; Cretaceous; Mesozoic; Brazil

Submission: 10 September 2022. Acceptance: 6 April 2023.

INTRODUCTION

Spinosaurids (Spinosauridae) are an aberrant group of large-bodied theropod dinosaurs, which are so far restricted to the Cretaceous, and have experienced a shift in perception from hunters with piscivorous affinities but an otherwise rather 'normal' theropod body plan (e.g., Charig and Milner, 1986) to a diverse clade, potentially encompassing representatives that foraged under water (e.g., Ibrahim et al., 2014, 2020). Indeed, spinosaurids are unusual theropods that include some of the largest terrestrial predators in Earth's history, such as *Spinosaurus aegyptiacus* (Stromer, 1915; Hone and Holtz, 2017). Whereas other giant theropods are interpreted as hypercarnivorous apex predators (e.g., Molnar and Farlow, 1992), spinosaurids show an aberrant skull morphology that indicates a different feeding ecology. Spinosaurids probably fed on prey items considerably smaller than their own body size, maybe predominantly, but not exclusively, fish (e.g., Taquet, 1984; Charig and Milner, 1986, 1997; Sereno et al., 1998; Rauhut, 2001; Sues et al., 2002; Buffetaut et al., 2004; Dal Sasso et al., 2005; Rayfield et al., 2007; Amiot et al., 2010; Rayfield, 2011; Ibrahim et al., 2014; Schade et al., 2020a; Hone and Holtz, 2021). However, although the name-giving genus *Spinosaurus* was described more than 100 years ago (Stromer, 1915), the skull and the postcranial osteology of spinosaurids is still rather poorly known due to the fragmentary nature of most of the recovered material (e.g., Kellner and Campos, 1996; Taquet and Russel, 1998; Milner, 2003; Dal Sasso et al., 2005; Kellner et al., 2011; De França et al., 2021). Furthermore, some important taxa have so far only received preliminary descriptions (Sereno et al., 1998; Allain et al., 2012; Barker et al., 2021).

Most spinosaurid specimens described so far have no or only very limited skull remains. The original material of *Spinosaurus* only included the anterior ends of the mandibles and a fragment of the maxilla (Stromer, 1915), and only few and fragmentary skull remains were referred to the clade up to the mid-1990s (Taquet, 1984; Buffetaut, 1989, 1992). The most complete specimen was the type of *Baryonyx walkeri*, which includes a complete premaxilla, partial maxilla, nasal, lacrimal, braincase, and several mandibular elements (Charig and Milner, 1986, 1997; see also Sereno et al., 1998). Premaxillae and braincase material are also known for the recently described *Riparovenator milnerae* and *Ceratosuchops inferodios* (Barker et al., 2021), and a snout and further isolated cranial elements, including a braincase, have been referred to *Suchomimus tenerensis* (Sereno et al., 1998; Hendrickx et al., 2016; Sereno et al., 2022), but the latter three taxa lack detailed osteological descriptions. Other specimens mainly include partial snouts (Kellner Campos, 1996; Taquet and Russell, 1998; Dal Sasso et al., 2005; Kellner et al., 2011; Lacerda et al., 2021; Isasmendi et al., 2022), or isolated cranial remains (e.g., Hendrickx et al., 2016; Ibrahim et al., 2014; Arden et al., 2019). The only spinosaurid known from an almost complete skull is the late Early Cretaceous Brazilian taxon *Irritator challengeri* (Figure 1).

The spinosaurid *Irritator* from the Araripe Basin of north-eastern Brazil was initially briefly described and assigned to Maniraptora by Martill et al. (1996). The authors examined the specimen with aid of computed tomography (CT), revealing that the upper jaw was artificially elongated, but, due to the technical limitations of CT devices at that time, little anatomical detail could be gathered from the scans. In the same year, Kellner (1996) suggested that *Irritator* represents a spinosaurid, which was later supported in a more detailed description of the specimen by Sues et al. (2002), after the skull had been more completely prepared. The spinosaurids *Irritator* and *Angaturama limai,* both from the Romualdo Member of the Santana Formation (as formerly considered, see below) of

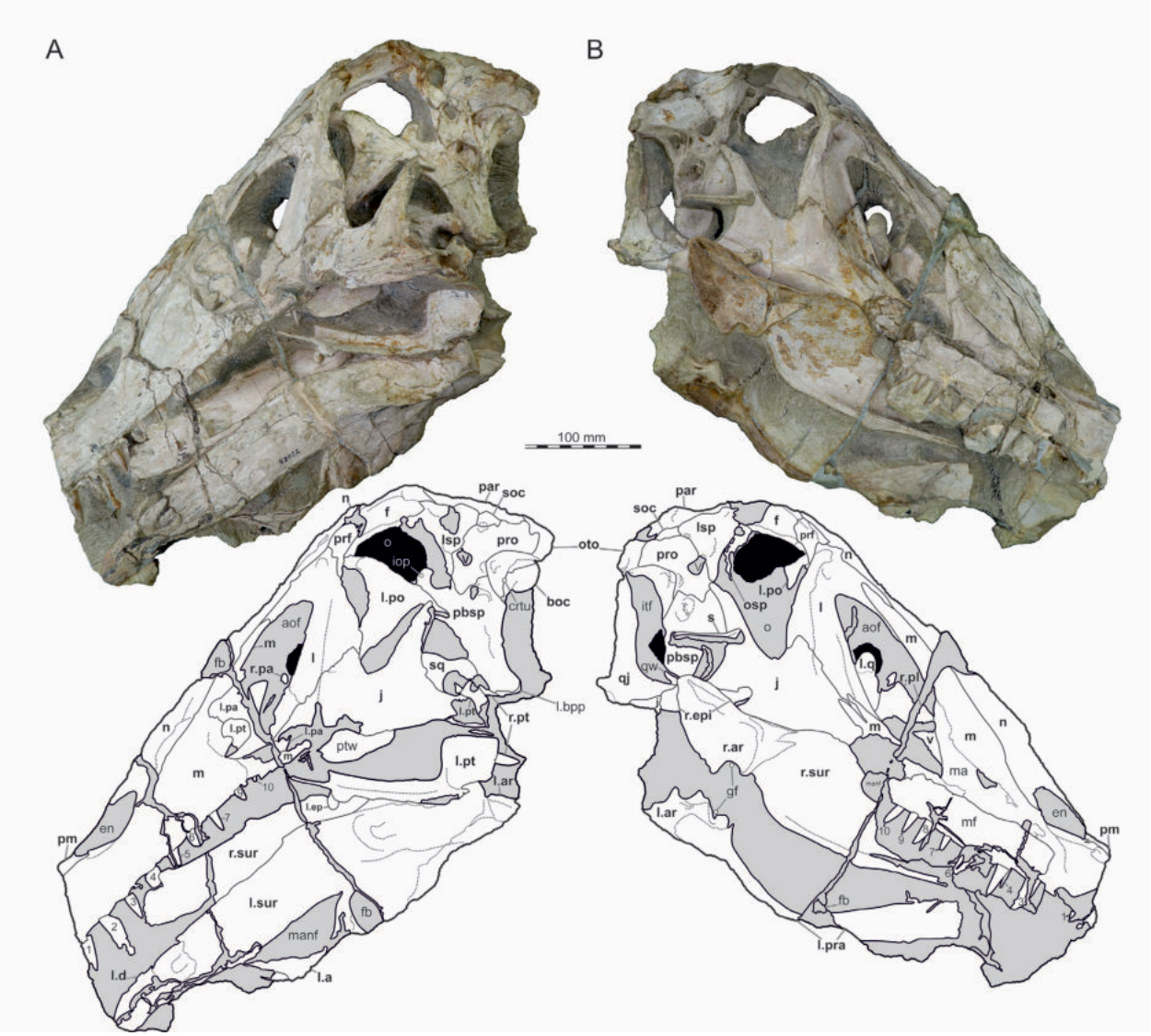

FIGURE 1. Photographs (top) and interpretative line drawings (bottom) of *Irritator challengeri* (SMNS 58022). A, left lateral view; B, right lateral view. Note that bones are labelled in bold, and other anatomical structures in regular font. Also note that tooth positions are numerically labelled but refer to preserved tooth position from anterior to posterior, not to anatomical tooth positions, which are unknown. Abbreviations: an, angular; aof, antorbital fenestra; ar, articular; boc, basioccipital; d, dentary; manf, mandibular fenestra; en, external naris; f, frontal; fb, foreign body; gf, glenoid fossa; iop, interorbital process of parabasisphenoid; itf, infratemporal fenestra; j, jugal; l, lacrimal; l.ar; left articular; l.d, left dentary; l.ep, left ectopterygoid; l.bpp, left basipterygoid process of the parabasisphenoid; l.sur, left surangular; l.sq, left squamosal; l.pa, left palatine; l.pra, left prearticular; l.pt, left pterygoid; l.q, left quadrate; m, maxilla; n, nasal; ma, maxillary antrum; mf, maxillary fragment; r.ar, right articular; r.epi, epipterygoid; r.pa, right palatine; r.sur, right surangular; lsp, laterosphenoid; m, maxilla; n, nasal; o, orbit; osp, orbitosphenoid; oto, otoccipital; pa, palatine; par, parietal; pbsp, parabasisphenoid; pm, premaxilla; po, postorbital; pro, prootic; prf, prefrontal; pt, pterygoid; ptw, pterygoid wing of left quadrate; qw, quadrate wing of right pterygoid; qj, quadratojugal; s, stapes; soc, supraoccipital; sq, squamosal; v, vomer; V, trigeminal nerve foramen (CN V); 1-10 mark preserved tooth positions of the maxillae (because of their size, position 11 and 12 on the maxillary fragment are not visible in this depiction).

Brazil, were described within a period of one month (Martill et al., 1996; Kellner and Campos, 1996). It was hypothesized that both taxa may represent fragments of the same skull (Sereno et al., 1998), since they come from the same area and strata and represent largely complementary portions of the skull. However, Sales and Schultz (2017) pointed out that *Irritator* and *Angaturama* most probably do not represent the same individual, as both seem to preserve the third maxillary tooth

(though see below). They also reported slight differences in proportional size and preservation as evidence against the referral (Sales and Schulz, 2017). In 2020, Schade et al. published the first study of a spinosaurid endocranium, based on the digital braincase endocast of *Irritator* derived from novel CT data. While this study provided information about head posture and neuroanatomy, Schade et al. (2020a) did not present new osteological information from their CT data.

Here, we present a new study of the skull of *Irritator* with the aid of digital segmentation, using the CT data published by Schade et al. (2020a). In addition to studying the skull elements from all sides, we were also able to rearrange the skull bones and mirror elements that are only present from one side (postorbital, quadratojugal, quadrate, squamosal, prearticular and angular). The result (Figures 2-4) is a digital model of the most complete spinosaurid skull known to science, which shows articulations of all the preserved skull bones and allows for further investigations, e.g., of the biomechanics of spinosaurid skulls.

MATERIAL AND METHODS

Segmentation and Digital Reconstruction

The principal specimen analysed here is the holotype skull of the spinosaurid theropod *Irritator challengeri*, SMNS 58022, from the Aptian Romualdo Formation of northeastern Brazil. Comparisons with other spinosaurid skull material is based on first hand observations of *Baryonyx* (NHMUK R9951; MS, OWMR, SWE), *Suchomimus* (MNN GDF 501, referred premaxillae and maxillae cast, MNN GDF 214, referred braincase cast; MS; and original material of these specimens by OWMR, SWE), casts of FSAC KK 11888 ('neotype' of *Spinosaurus aegyptiacus*; SWE, OWMR), a snout referred to *Spinosaurus* (MNHN SAM 124; OWMR), and fragmentary remains tentatively referred to *Camarillasaurus cirugedae* (OWMR, pers. obs. on unpublished material). Additionally, we had a surface scan of the braincase cast referred to *Suchomimus* (MNN GDF 214), produced by MS, available for comparisons. Comparisons with other non-avian theropods are based on first hand observations of many different speci-

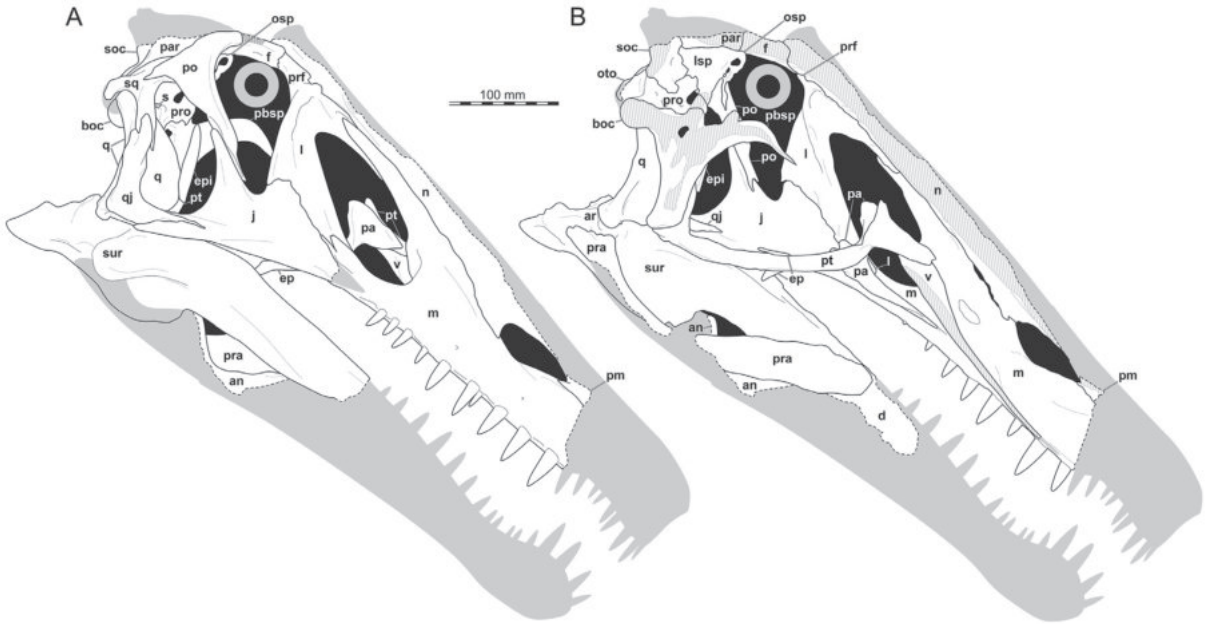

FIGURE 2. Interpretative line drawings of the re-arranged and articulated skull of *Irritator challengeri* (SMNS 58022). A, right lateral view; B, sagittal cut with removed right skull half, revealing medial aspects of the left skull half. Speculatively, grey silhouettes add unknown parts to the skull known from other spinosaurids. Abbreviations: an, angular; ar, articular; boc, basioccipital; d, dentary; ep, ectopterygoid; epi, epipterygoid; f, frontal; j, jugal; l, lacrimal; ls; laterosphenoid; m, maxilla; n, nasal; osp, orbitosphenoid; oto, otoccipital; pa, palatine; par, parietal; pbsp, parabasisphenoid; pm, premaxilla; po, postorbital; pro, prootic; pra, prearticular; prf, prefrontal; pt, pterygoid; q, quadrate; qj, quadratojugal; s, stapes; sur, surangular; soc, supraoccipital; sq, squamosal; v, vomer.

mens (MS, OWMR, CF, SWE) and the cited literature.

Originally, we scanned SMNS 58022 entirely with a medical Siemens Somatom Force (dual source) CT (voltage: 120 kV, X-ray tube current: 1365 µA, exposure time: 154 ms, voxel size: 0.703123 mm × 0.703124 mm × 3 mm) in the Deutsches Herzzentrum in Munich. Additionally, we conducted a second, µCT scan focused only on the braincase, using a Zeiss Metrotom 1500 (voltage: 180 kV, X-ray tube current: 1800 µA, exposure time: 250 ms, voxel size: 0.09713 mm) in the Carl Zeiss Industrielle Messtechnik GmbH in Essingen. The data derived from both scans were published on the online repository MorphoSource for a previous study that examined neuroanatomical features of SMNS 58022 (Schade et al., 2020b; see also Schade et al., 2022; see Data Availability section below). While most of SMNS 58022 was reconstructed using medical CT data, the reconstruction of the braincase (excluding the frontals and parietals) is based on the µCT scan. All elements were segmented manually independently by MS and OM, using Amira (5.6) and 3D slicer (4.10.2), respectively. MS worked with the medical and the µCT data, while OM worked with the medical CT set only. The resulting models were compared to validate the anatomical reconstructions. SWE used the 3D models resulting from the segmentation work of MS to produce figures of isolated elements with Blender (2.79b). OM used his models and the software Blender (2.91) to rearrange the skull bones into their original position. For this, OM mirrored the elements that are only present on one side (postorbital, quadratojugal, quadrate, squamosal, prearticular and angular) and arranged the bones according to their articular facets in cases of disarticulated elements. Additionally, minor retro-deformation was carried out for digital articulation of the skull bones (see Supplementary Data 1 for a description of the reconstruction steps taken).

Phylogenetic Dataset

To explore phylogenetic aspects of the skull anatomy of spinosaurids, we modified the matrix of Rauhut and Pol (2019) for basal tetanurans (Tetanurae). Several spinosaurid taxa were added, including the recently described taxa *Vallibonavenatrix cani* (Malafaia et al., 2020), *Ceratosuchops* and *Riparovenator* (Barker et al., 2021), and the poorly known *Oxalaia quilombensis* (Kellner et al., 2011). Furthermore, we restricted the codings for *Spinosaurus aegyptiacus* to the original material described by Stromer (1915, 1936; Smith et al., 2006), and coded the referred specimens MSNM V 4047 (Dal Sasso et al., 2005), MNHN SAM 124 (Taquet and Russell, 1998) and FSAC KK 11888 (Ibrahim et al., 2014, 2020a, b) as separate operational taxonomic units (OTUs), as two of these (MSNM V 4047, MNHN SAM 124) lack overlap with the original type material, and the referral of FSAC KK 11888 to the same species as *Spinosaurus aegyptiacus* has not been firmly established (see Evers et al., 2015; Kellermann, 2021; Lacerda et al., 2021 contra Ibrahim et al., 2020a; Smyth et al., 2020). The character list was critically evaluated, with a focus on skull characters. Eight of the original characters were deleted, several modified, and a total of 45 characters were added, either from other sources, or as new characters based on our comparisons of non-avian theropod taxa (see Results). The character list is provided as Supplementary Data 2.

The final data matrix thus had 76 OTUs, scored for 395 morphological characters (Supplementary Data 3). Of the characters, 195 are craniodental characters, the rest concern the postcranium.

Parsimony Analyses

Two OTUs, *Oxalaia* and MNHN SAM 124, were subsequently deleted for parsimony analysis, following safe taxonomic reduction criteria (Wilkinson, 1995), as they had very high amounts of missing data (99.7% and 95%, respectively), and all codings completely overlapped with those of MSNM V 4047. As in most palaeontological data sets, missing data is rampant in the resulting data set of 74 taxa and 395 characters; the average proportion of coded characters per taxon is only 40%, with a range from 99% in *Allosaurus fragilis* to only 4% in *Angaturama*.

For a second analysis, we restricted the data matrix to craniodental characters only and deleted all OTUs for which no skull material is known (Supplementary Data 4). In addition, several taxa with limited skull or dental material known could be deleted, following safe taxonomic reduction criteria, including *Coelurus fragilis, Condorraptor currumili, Fukuiraptor kitadaniensis, Magnosaurus nethercombensis, Megaraptor namunhuaiquii* (codings exclude the juvenile material described by Porfiri et al., 2014, as its referral to *Megaraptor* is not entirely certain; Porfiri, pers. comm., 2021), *Saurophaganax maximus,* and "*Szechuanosaurus*" *zigongensis* (in addition to *Oxalaia* and MNHN SAM 124 as mentioned above). The resulting data

matrix for skull characters thus had 54 taxa scored for the 195 cranial, mandibular and dental characters. Missing data is slightly less in this data set, with an average of 49% coded characters per OTU, ranging from 99.5% in *Allosaurus* to 8% in *Angaturama, Australovenator wintonensis* and FSAC KK 11888.

The matrices were analysed under maximum parsimony in the phylogenetic software TNT 1.5 (Goloboff and Catalano, 2016) under the traditional search option, using equally weighted parsimony, with 1000 replicates of Wagner trees, followed by TBR branch swapping. From the resulting equally parsimonious trees (Supplementary Data 5, 6), a strict consensus tree and reduced consensus trees were calculated, using the IterPCR method for the latter (Pol and Escapa, 2009), with the TNT command "pcrprune/>0;nelsen//{0};". Character support of internal nodes was evaluated using the trace character option in Mesquite (Maddison and Maddison, 2021). In order to evaluate the robustness of the results, we also carried out analyses using implied weights (with k=10; Goloboff et al., 2018) in TNT (Supplementary Data 7) for the full character-taxon matrix and evaluated the number of steps needed for alternative placements in Mesquite.

Character Optimization

In order to understand the morphological character transitions implied by our phylogeny as well as the morphological support for internal nodes of the tree, we performed character state optimization in PAUP* 4.0a for Macintosh (Swofford, 2002), as PAUP* allows specification of the optimization criterion, whereas TNT only returns unambiguous synapomorphies. Although we were primarily interested in skull characters, we used the reduced consensus tree from the parsimony analysis using the full matrix for character optimization (Supplementary Data 8). The reason is that we put more credibility in the analysis using the full matrix, and as postcranial synapomorphies could at least also be known this way. As character optimizations should be performed on a fully bifurcated tree, we resolved the polytomies of the reduced consensus tree (Supplementary Data 9). Hereby, we resolved the polytomy within Spinosaurinae by grouping specimens according to geographic provenance, resulting in the following in-group topology for Spinosaurinae: *(Angaturama, Irritator, Spinosaurus,* MSNN V4047). This topology implies close relationships between geographically proximate OTUs, which can be easier justified than resolving this polytomy at random, especially as the geographic OTU pairs in question have sometimes been synonymized with one another. The other polytomies are not further relevant to the objectives of this study (i.e., optimization of synapomorphies) as they are relatively deeply nested within non-megalosauroid groups and alternative resolutions would not affect the results presented herein. The resolution of all polytomies is documented in the respective tree file (Supplementary Data 9). The matrix and tree were combined into a nexus file that is appended as Supplementary Data 10 and served as the file read to PAUP*. We performed the optimization using both accelerated transformations (ACCTRAN) and delayed transformations (DELTRAN) using the “DescribeTrees/ApoList=yes” command in PAUP*. ACCTRAN and DELTRAN are endmembers of a range of possible node positions in which a character state change can occur along a portion of the tree for which the transition cannot be known with certainty, which is either due to missing data or due to conflicting character states for a given character among sister taxa (Agnarsson and Miller, 2008). Unambiguous character state transitions are those in which ACCTRAN and DELTRAN agree. We provide a full list of optimizations (organized by node, but also by character) in which unambiguous, ACCTRAN, and DELTRAN optimizations as found by PAUP* are listed, as Supplementary Data 11. Contrasting ACCTRAN and DELTRAN is important especially for groups such as spinosaurids, in which we have much missing data, and few taxa with extraordinary character coverage, such as *Irritator*: Currently, many cranial and mandibular character states that can only be observed in *Irritator* can either be autapomorphies of the species (under DELTRAN optimization), or spinosaurid synapomorphies (ACCTRAN). Only considering unambiguous synapomorphies (e.g., Rauhut and Pol, 2019; but see Rauhut, 2003; Carrano and Sampson, 2008; Rauhut and Carrano, 2016) is much less informative, as it disregards all of the concerned characters in the spinosaurid example, and thus underestimates the number of traits that are apomorphic among the group, even if the exact nodal appearance of the character state conditions in question cannot be known given the data. PAUP* assigns numerical node labels to internal nodes of the provided phylogeny in its output for the synapomorphy list. For the purpose of communication and easier documentation of synapomorphies, we converted this into a taxonomic code for internal nodes (see Supplementary Data 11). For the discussion

of character support of certain nodes in the main text, we further evaluated the character transformations using the "trace character history" option in Mesquite (Maddison and Maddison, 2021), as this often allows more detailed evaluation of transitions, for example in cases where a character might be inapplicable at a certain node (for which PAUP treats the character state simply as unknown) or a character has been further transformed. We used widely used clade names (e.g., "Megalosauroidea") whenever possible, and these are consistent with the usage of these names in our results (below). For unnamed internal nodes, we used "Taxon A+Taxon B" to indicate a sister-group relationship between two specific taxa. Our code "Taxon A++Taxon C" denotes the group that includes both taxon A, taxon C, their last common ancestor, and all descendants of the latter. Although our optimizations include all characters (Supplementary Data 11), we focus our synapomorphy discussions on skull characters, as this is the partition of the matrix for which *Irritator* and our study provides new evidence.

Bayesian Phylogeny

To explore the temporal framework of spinosaurid evolution, and to estimate rates of character evolution, we performed a Bayesian tip-dating analysis on the full dataset in MrBayes 3.2.7a (Ronquist et al., 2009) in addition to the parsimony analysis. The combined matrix and command list used for this analysis is provided as Supplementary Data 12. For the analysis, we used the same character ordering information and outgroup as in the parsimony analyses. The substitution model was set to the Mkv-model (Lewis, 2001), which models the frequencies of character states as being equal and in which rate variation across characters is drawn from a gamma distribution. The Mkv-model includes an ascertainment bias correction for morphological data so that evolutionary rates are not overestimated. We used an independent gamma rate (IGR, Lepage et al., 2007) relaxed clock, i.e., a clock model in which each branch can have an independent rate. We accounted for uncertainties in the clock rate by specifying a wide clock rate prior with a normal distribution of a mean of 0.001 and variance of 0.1 (Ezcurra et al., 2020). We used first and last appearance dates for all taxa to model uniform age priors and set fossils to be tips. We used a fossilized birth-death (FBD) process for the tree model (Stadler, 2010; Heath et al., 2014) with default values for the individual FBD parameters. We specified a uniform root age prior with a minimum value of 225 Ma and a maximum value of 247.2 Ma, whereby we specified the minimum as the youngest possible age of the outgroup taxon *Eoraptor lunensis* and the maximum as the base (i.e., oldest boundary) of the Anisian. We chose this maximum value as it roughly coincides with divergence time estimates for the origin of Dinosauromorpha from independent studies (Ezcurra et al., 2020). The last appearance of *Eoraptor* and origination time of Dinosauromorpha form a reasonable bracket for the prior on the root age of our tree.

We used four chains and two independent runs of metropolis-coupled Markov chain Monto Carlo algorithms to estimate the posterior distribution and discarded the first 25% of samples for parameter and tree summaries. We changed the chain temperature from the default of 0.1 to 0.5 to facilitate mixing and specified that three swaps of states be attempted between chains at each sample, which were taken at every 500th generation. We implemented a stop rule at 0.01 for the deviation of split frequencies, which was taken to indicate topological convergence (Ronquist et al., 2009), and which was reached after 160,460,000 generations in our analysis. The trace plot produced by the MrBayes sump command indicated stationary convergence as well. Estimated sample sizes (ESS) for all parameters of the analysis comfortably exceeded 200 in each run separately (309 minimum value for the clock rate in one run), indicating parameter convergence of our analysis (Rambaut et al., 2018). The Potential Scale Reduction Factors reached values of 1 for our parameters, furthermore, indicating that between and within run variances of posterior samples were achieved (Gelman and Rubin, 1992; Ronquist et al., 2009). The analysis also showed good mixing at 45–53% successful state exchanges between adjacent chains. MrBayes output files and the log-file containing the sump-outputs that are printed to screen are available at: https://doi.org/10.5281/zenodo.7785634.

To show the temporal framework of spinosaurid evolution, we read the consenus tree with branch lengths from the posterior sample that was output by MrBayes into R v. 4.2.2 (R Core Team 2022) using commands from the phylotate package (Beer and Beer, 2019). We plotted this tree to geological time using commands from the strap package (Bell and Lloyd, 2014), and labelled nodes with their posterior probabilities (PP), whereby nodes with low support (PP < 0.5) were coloured in red. To explore transition rates of char-

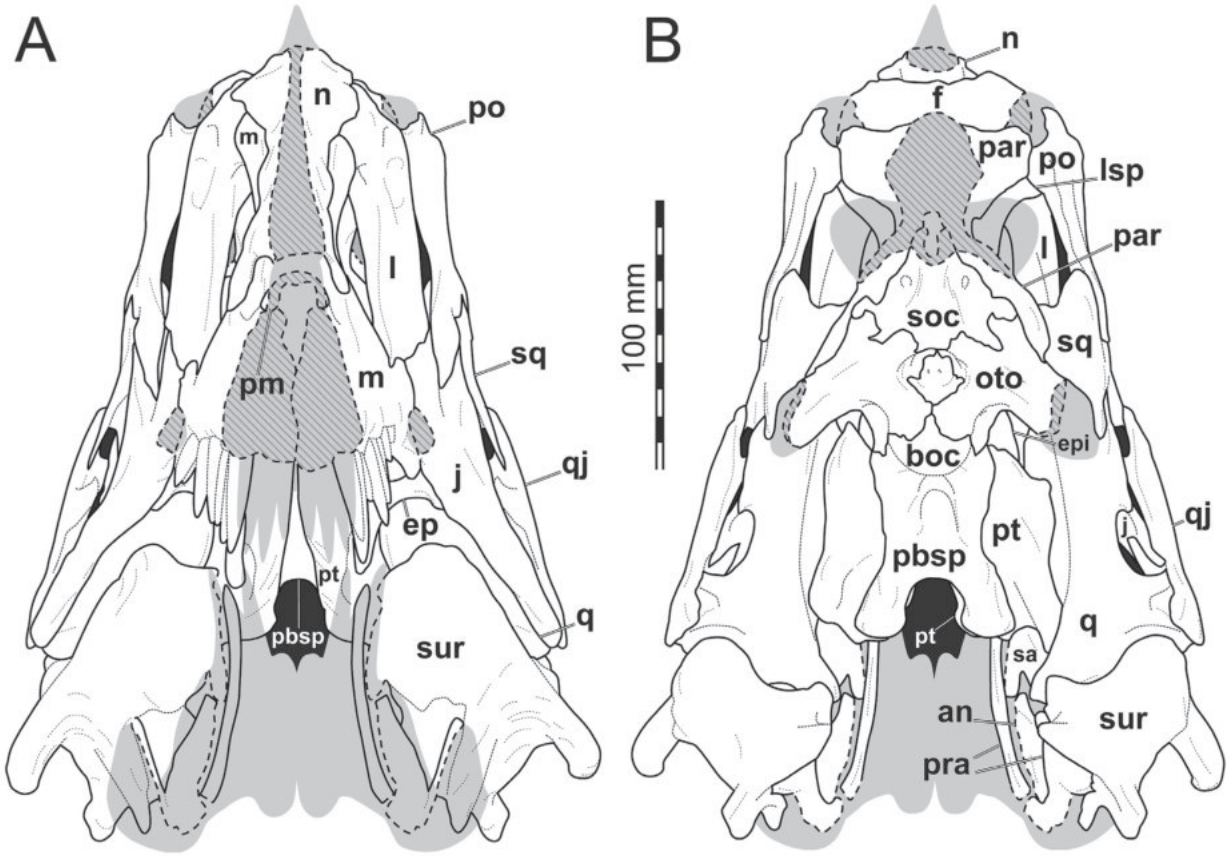

FIGURE 3. Interpretative line drawings of the re-arranged and articulated skull of *Irritator challengeri* (SMNS 58022). A, anterior view; B, posterior view. Speculatively, grey silhouettes add unknown parts to the skull known from other spinosaurids. Abbreviations: an, angular; boc, basioccipital; ep, ectopterygoid; epi, epipterygoid; f, frontal; j, jugal; l, lacrimal; lsp, laterosphenoid; m, maxilla; n, nasal; oto, otoccipital; par, parietal; pbsp, parabasisphenoid; pm, premaxilla; po, postorbital; pra, prearticular; pt, pterygoid; q, quadrate; qj, quadratojugal; sur, surangular; soc, supraoccipital; sq, squamosal.

acter evolution, we additionally read the summary statistics for branch and node parameters from the posterior sample from the MrBayes output. We collapsed nodes from the consensus tree with low support (PP < 0.5) and plotted the resulting tree with its edges coloured according to the median branch rate using commands from the paleotree (Bapst, 2012) and ape (Paradis and Schliep, 2019) packages.

SYSTEMATIC PALAEONTOLOGY

THEROPODA Marsh, 1881
TETANURAE Gauthier, 1986
MEGALOSAUROIDEA Fitzinger, 1843; *sensu* Carrano et al. (2012)
SPINOSAURIDAE Stromer, 1915
SPINOSAURINAE (Stromer, 1915); *sensu* Sereno et al. (1998)

IRRITATOR CHALLENGERI Martill, Cruickshank, Frey, Small and Clarke, 1996

Holotype. SMNS 58022, largely complete skull, missing most of the premaxillae, anterior ends of the maxillae, and anteriormost parts of both mandibles.

Locality and horizon. Near Buxexé, close to Santana do Cariri, Ceará State, northeastern Brazil (see Sues et al., 2002: 535). Lower part of the Romualdo Formation (Santana Formation of some authors; see discussion in Arai and Assine, 2020) of the Santana Group, late Aptian (Arai and Assine, 2020).

Emended diagnosis. The original diagnosis of *Irritator challengeri* by Martill et al. (1996: 5) consisted of a list of skull characters, most of which are common in non-avian theropods (e.g., “maxilla straight with more than 11 teeth”, “orbit ovoid”, “stapes very thin, stick-like with expanded and flattened ends”)

or at least not unique to *Irritator* (e.g., “anterior maxillary teeth are straight, elongate, with sub-oval cross section and unserrated anterior and posterior carinae”, “nasal opening oval, sited some way back from tip of snout”, “infratemporal fenestra almost as large as orbit”) and is thus of limited help to distinguish this species from other theropods.

Sues et al. (2002: 537) gave a shorter diagnosis for the species, based mainly on unique or at least very rare characters, but these authors also noted that the lack of skull material for spinosaurids in general made any definite decision about the apomorphic status of characters tentative. Although some additional spinosaurid skull material has been described since (e.g., Dal Sasso et al., 2005; Kellner et al., 2011; Ibrahim et al., 2014, 2020; Hendrickx et al., 2016; Arden et al., 2019; Barker et al., 2021), the situation has not improved decisively, also because the taxonomic identity of several of these specimens is unclear. In the following emended diagnosis, we thus list characters that are tentatively regarded as apomorphic to *Irritator*, with characters that can be evaluated in at least one other spinosaurid specimen being indicated with an asterisk; future discoveries of more spinosaurid skull material will show if the other characters represent autapomorphies of *Irritator* or synapomorphies of spinosaurids or a subclade thereof. In cases where characters represent a local apomorphy within theropods (i.e., they are present in some other, but distantly related taxa), other occurrences are noted in brackets.

Shelf-like subnarial fossa on the anterior ramus of the maxilla below the posterior end of the external nares* (absent in *Baryonyx*, *Suchomimus*, and a snout referred to *Spinosaurus*: MNHN SAM 124; Charig and Milner, 1997; Sereno et al., 1998; Dal Sasso et al., 2005); widely spaced maxillary teeth, with distance between teeth subequal or greater than mesiodistal length of individual teeth in the anterior part of the maxilla and more closely spaced teeth posteriorly* (absent in *Baryonyx*, *Suchomimus* and snouts referred to *Spinosaurus*: SAM 124 and MSNM V4047; Charig and Milner, 1997; Sereno et al., 1998; Taquet and Russell, 1998; Dal Sasso et al., 2005; similar in *Archaeopteryx lithographica*; Rauhut et al., 2018); posterodorsal end of ascending process of the maxilla tapering and undivided; ascending process extends further posterior than jugal ramus of the maxilla; bipartite jugal ramus of maxilla with a mediolaterally thin process overlapping the lateral surface of the lacrimal and a rod-like process medially to the ventral jugal margin* (however, possibly also present in *Suchomimus;* OWMR, SE, pers. obs., MNN GDF 501; Sereno et al., 1998); jugal with slightly concave ventral margin; facet for contact with the laterosphenoid on postorbital very small and placed entirely on the anterior process of the postorbital (also present in *Dubreuillosaurus valesdunensis;* Allain, 2002); marked lateral ridge on the dorsal half of the squamosal process of the quadratojugal; lack of a well-developed preotic pendant (=ala basisphenoidalis) in the braincase* (this structure is present in *Baryonyx, Suchomimus, Ceratosuchops* and *Riparovenator;* Charig and Milner, 1997; MS, pers. obs. on cast, MNN GDF 214; Barker et al., 2021); pterygoid with rudimentary ectopterygoid process; ectopterygoid with strongly reduced ventral recess (also present in *Ceratosaurus magnicornis* and Abelisauridae; Madsen and Welles, 2000; Sampson and Witmer, 2007) and very small medial pterygoid process; surangular with a broad and strongly ventrolaterally directed, posteriorly flange-like lateral shelf* (absent in *Camarillasaurus*; OWMR, pers. obs. on unpublished material).

DESCRIPTION

General Description

While Sues et al. (2002) were only able to describe the outer morphology of the fossil, our CT and µCT data reveal inner cavities, the non-exposed sides of the skull bones and elements that are at least partly obscured by sedimentary matrix or other bones, some due to taphonomic displacement. Important new features could be revealed on the medial (e.g., maxillae) or lateral (e.g., right surangular) aspects of the cranial material. Some elements are only partly exposed on the fossil but are finely preserved (e.g., palatal elements, quadrate and squamosal, teeth). Furthermore, the right epipterygoid is visible in the specimen but was not mentioned before.

To facilitate comparability with other anatomical descriptions of non-avian theropods, we used anatomical direction terms for SMNS 58022 as if the animal held its skull horizontally.

Skull Openings

As in most archosaurs, the most prominent skull openings of *Irritator* are the external naris, antorbital fenestra, orbit, infratemporal fenestra, and the supratemporal fenestra (Figure 2A). Whereas the first three of these openings can be directly observed in the specimen, the shape of the temporal fenestrae can be estimated from a digital

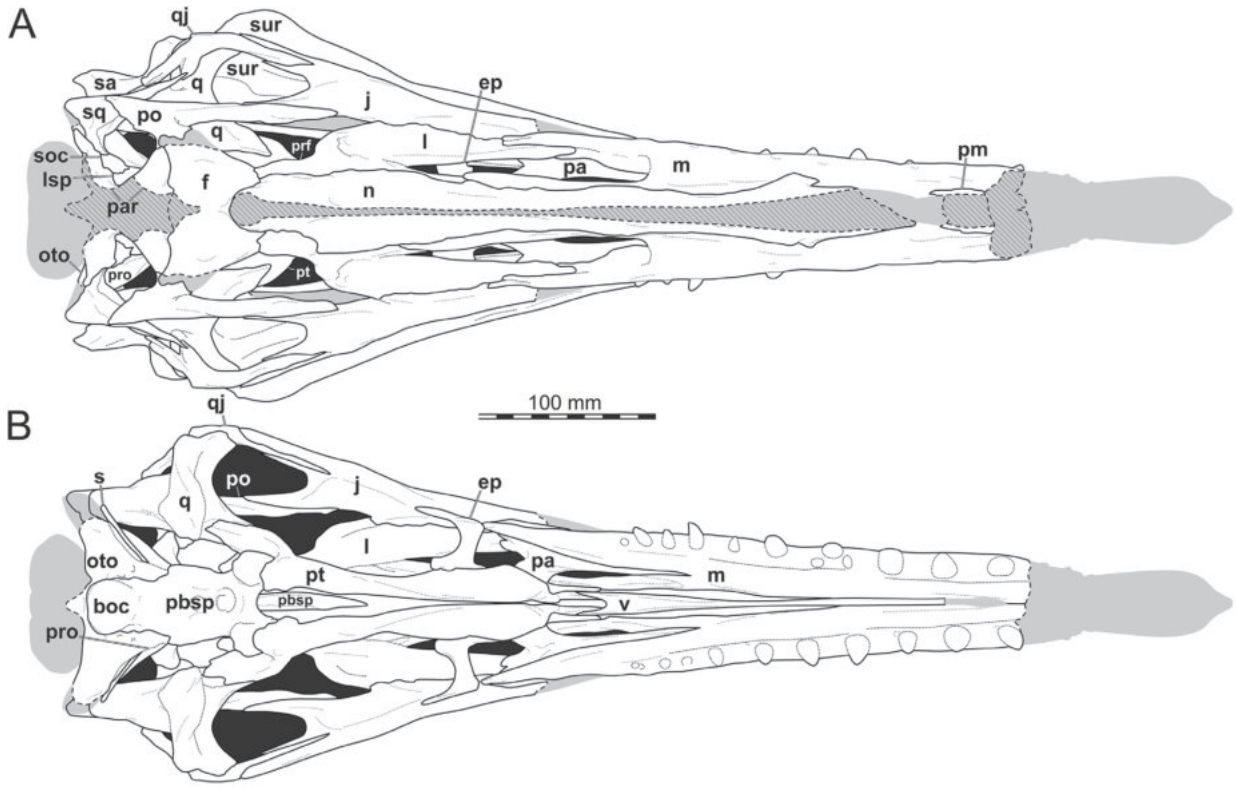

FIGURE 4. Interpretative line drawings of the re-arranged and articulated skull of *Irritator challengeri* (SMNS 58022). A, dorsal view; B, ventral view without the lower jaw. Speculatively, grey silhouettes add unknown parts to the skull known from other spinosaurids. Abbreviations: boc, basioccipital; ep, ectopterygoid; f, frontal; j, jugal; l, lacrimal; lsp, laterosphenoid; m, maxilla; n, nasal; oto, otoccipital; par, parietal; pbsp, parabasisphenoid; pm, premaxilla; po, postorbital; pro, prootic; prf, prefrontal; pt, pterygoid; q, quadrate; qj, quadratojugal; sur, surangular; soc, supraoccipital; sq, squamosal.

re-articulation of the bones that form large parts of their margins. The external naris is roughly oval, anteroposteriorly elongate, and anteroventrally inclined. It is bordered by the premaxilla anteriorly, the nasal posterodorsally and posteriorly, and the maxilla ventrally. The maxillary surface in this region shows no recess for a process of either the nasal or premaxilla, suggesting that the maxillary contribution to the external naris is no artefact of breakage. The anterodorsal margin, which was probably formed by the premaxilla, is not preserved. As in other spinosaurids, such as *Baryonyx* (Charig and Milner, 1986, 1997) and *Suchomimus* (Sereno et al., 1998), the external naris was obviously placed entirely posterior to the premaxillary body, although not to the degree seen in the snouts referred to *Spinosaurus* (Milner, 2001; Dal Sasso et al., 2005). In contrast to MSNM V 4047 and NHMUK PV R 16420 (see Arden et al., 2019; Smyth et al., 2020), the external naris is bordered anteriorly and anterodorsally by the premaxilla in *Irritator*, and not completely enclosed by the maxilla and nasal. Furthermore, it seems to be relatively larger than in those two specimens.

The antorbital fenestra is elongate, suboval in outline and steeply anteroventrally inclined. It is anteroventrally and anterodorsally bordered by the maxilla, and posteroventrally and posterodorsally by the lacrimal. In contrast to most non-avian theropods, the jugal does not participate in the antorbital fenestra. The orbit is reversed drop-shaped, being dorsally wider than ventrally, with the ventral part of the opening flexing slightly anteriorly. Anteriorly, the orbit is bordered by the lacrimal, while the prefrontal forms the anterodorsal margin. Dorsally, the orbit is bordered by the frontal, and posteriorly by the postorbital and the postorbital process of the jugal. The ventral margin is formed by the jugal. The infratemporal fenestra is nearly drop-shaped, being dorsoventrally taller than anteroposteriorly wide, and similar in size to the orbit. It is framed by the jugal anteriorly, the postorbital dorsally, the squamosal posterodorsally, and the quadratojugal posteriorly and posteroven-

trally. The supratemporal fenestra is irregularly oval-shaped and longer anteroposteriorly than wide mediolaterally (Figures 3B, 4A). It is much smaller than the antorbital fenestra, orbit, and the infratemporal fenestra. The parietal forms its anterior, medial, and posterior margin. The postorbital forms the anterior and lateral margin, and the squamosal is situated on the posterior corner of the supratemporal fenestra.

In ventral view, our cranial reconstruction reveals the previously unknown morphology of the palate in *Irritator* (Figures 2B, 4B). The internal narial opening (choana) is displaced posteriorly and situated at the level of the anterior end of the antorbital fenestra; there is thus a partial secondary palate formed by the ventral parts of the maxillae and the vomer. The choana is a strongly anteroposteriorly elongated, anteriorly pointed, drop-shaped opening that is laterally and posteriorly bordered by the palatine, anterolaterally by the maxilla, and medially by the pterygoid and the vomer. The very small, subtriangular palatine fenestra (sometimes called the suborbital fenestra) is anteromedially framed by the palatine, medially by the pterygoid, and posteriorly by the ectopterygoid. It is placed posterolateral to the internal choanae, at about the mid-length of the antorbital fenestra. The lateral and a small part of the anterior border are made up by the maxilla. The notably elongated subtemporal fenestra is surrounded by the ectopterygoid anteriorly, the pterygoid medially, the quadrate posteriorly, the quadratojugal posterolaterally, and the jugal anterolaterally. It is by far the largest opening of the palate and is placed below the posterior end of the antorbital fenestra, the orbit, and the anterior part of the infratemporal fenestra. Due to the anteroventral inclination of the quadrates, its posterior margin is placed entirely anterior to the supratemporal fenestra. Furthermore, the interpterygoid vacuity can be discerned. It is strongly elongated, triangular and becomes narrower anteriorly. Laterally, the pterygoid makes up the border of the vacuity while the posterior margin is formed by the basisphenoid. Anteriorly, the interpterygoid vacuity extends to approximately the half-length of the ectopterygoid, at about the level of the posterior third of the antorbital fenestra.

Premaxilla

Solely the posterior portions of the narial processes of the paired premaxillae are preserved, as a small, exceptionally thin cap on the anteriormost preserved portion of the maxillae on either side of the skull, whereas the premaxillary body and posterodorsal nasal process are missing (Figures 2A, 3A). Because of the incomplete state of preservation, the detailed contacts with surrounding bones are not entirely clear. Usually, however, the premaxilla contacts the maxilla posteroventrally and the nasal posterodorsally and, possibly, the vomer ventromedially.

As the nares are placed entirely posterior to the premaxillary body, there is an undivided, dorsally placed posterior narial process of the premaxilla, as in *Baryonyx* and *Suchomimus* (Charig and Milner, 1986, 1997; Sereno et al., 1998), unlike the situation in most non-avian theropods, in which distinct nasal and subnarial processes extend posteriorly directly from the premaxillary body. The preserved posterior end of the narial process of the premaxilla overlaps the anterior ramus of the maxilla dorsally. Posteriorly, the process has a rounded notch that forms the anteriormost margin of the external naris, and thus represents the branching of the nasal and subnarial processes of the premaxilla. Since the nasal reaches far anteroventrally, it is possible that the premaxilla formed only a small portion of the anterodorsal margin of the external naris in lateral view in *Irritator*. This is also the case in *Baryonyx* and *Suchomimus* in which the long posterodorsal nasal process of the premaxilla is flanked laterally by the anterodorsal premaxillary process of the nasal over most of its length (Charig and Milner, 1997; Sereno et al., 1998).

The preserved part of the premaxilla of *Irritator* clearly contributes to the margin of the external naris, as usual in theropods and also the case in *Baryonyx* and *Suchomimus* (Charig and Milner, 1997; Sereno et al., 1998), but not in a snout referred to *Spinosaurus* (MSNM V4047; Dal Sasso et al., 2005), in which the premaxilla is excluded from the naris. However, the preserved, posteriorly tapering subnarial process of the premaxilla is extremely short in *Irritator*, contrasting the more elongate process in *Baryonyx* and *Suchomimus* (Charig and Milner, 1997; Sereno et al., 1998).

Maxilla

Both maxillae are incomplete anteriorly, but many aspects of their morphology can be discerned (Figures 5, 6). The right maxilla is heavily damaged on its lateral surface along the maxillary body. Here, an elongate, rectangular and toothed fragment is broken away from the rest of the bone (Figures 1B, 6). The maxilla contacts the narial process of the premaxilla anterodorsally, the nasal dorsally, the palatine and vomer medially and the

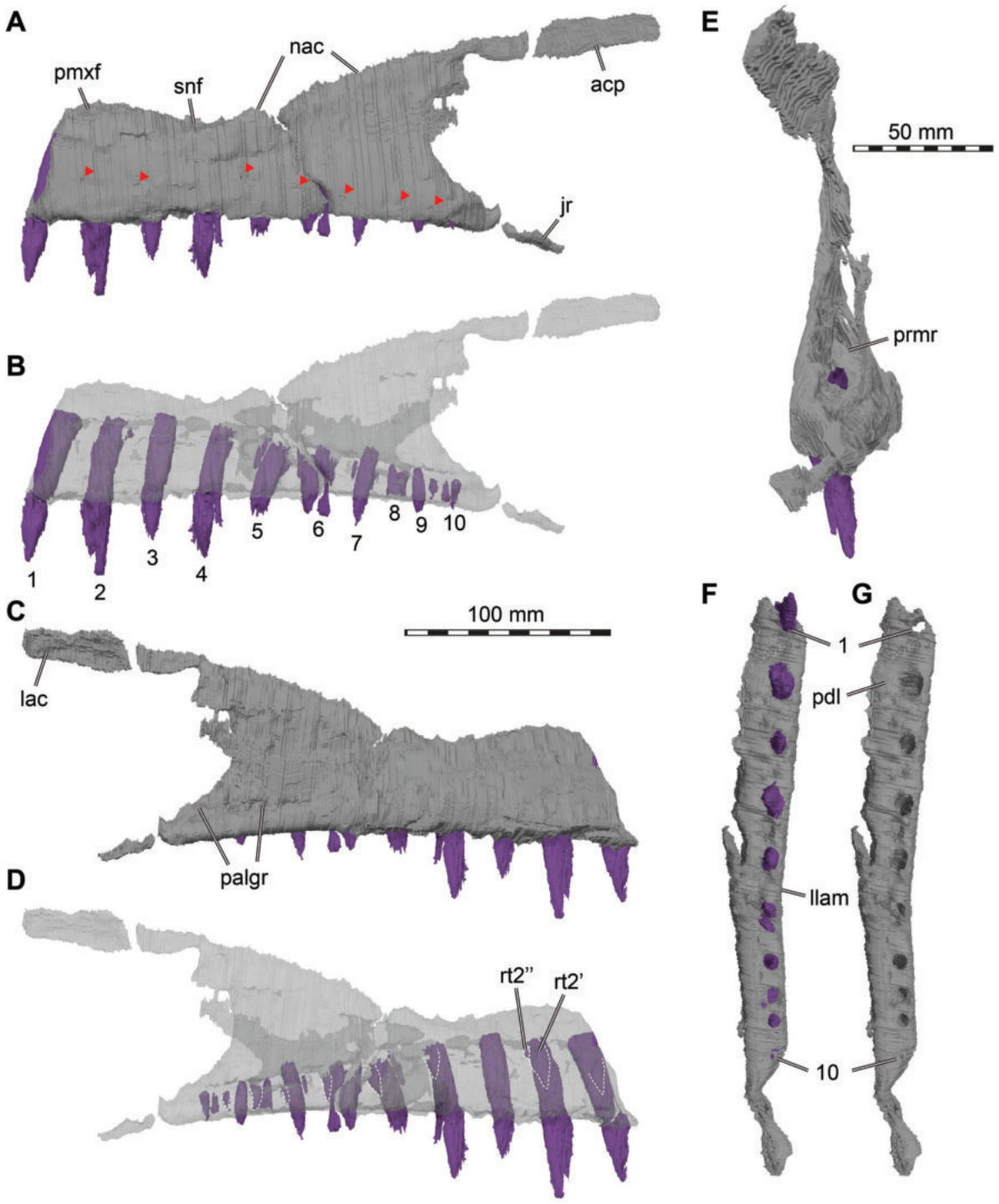

FIGURE 5. 3D renderings of the left maxilla of *Irritator challengeri* (SMNS 58022). A, lateral view; B, lateral view with maxillary bone rendered transparent; C, medial view; D, medial view with maxilla bone rendered transparent; E, posterior view; F, ventral view (anterior to top); G, ventral view without teeth, showing alveoli. Note different scale for E. Also note that tooth positions are numerically labelled but refer to preserved tooth position from anterior to posterior, not to anatomical tooth positions, which are unknown. Replacement teeth are highlighted with dashed lines in D, and different generations are indicated with prime (') or double prime ('') . Red arrow heads point to neurovascular foramina. Abbreviations: acp, ascending process; jr, jugal ramus; lac, lacrimal contact; llam, lateral lamina; nac, nasal contact; palgr, palatine groove; pdl, paradental lamina; pmxf, premaxillary facet; prmr, promaxillary recess; rt, replacement tooth; snf, subnarial fossa.

lacrimal and jugal posteriorly (Figures 2-4); the anterior articulation with the premaxillary body is missing.

The contact area with the lacrimal and jugal is damaged on both sides, but a piece of maxilla remains articulated with these bones on the right side. The ascending process of the right maxilla is broken along a large vertical fracture that separates the snout from the rest of the cranium, but the posterodorsally tapering end of both processes remains in articulation with the respective nasal and lacrimal. The left maxillary body has a better surface preservation than the right pendant, but the ascending process is less well preserved. Furthermore, the posterior process of the left maxilla that articulates with the lacrimal and jugal is missing.

The maxilla is comparatively slender and low. The well-developed ascending process has an anteroposteriorly long base and is inclined more steeply (around 25°) than in *Suchomimus*, in which the process is almost horizontally orientated over its entire length (Sereno et al., 1998). The inclination of the ascending process is much steeper in other megalosauroids, such as *Afrovenator abakensis* (Sereno et al., 1994), *Dubreuillosaurus* (Allain, 2002), *Duriavenator hesperis* (Benson, 2008), and *Torvosaurus tanneri* (Hendrickx and Mateus, 2014). The entire anterodorsal margin of the process is gently convex and lacks a marked change in orientation, as it is present in coelophysids (e.g., Raath, 1977), *Monolophosaurus jiangi* (Zhao and Currie, 1994; Brusatte et al., 2010), the allosauroid *Asfaltovenator vialidadi* (Rauhut and Pol, 2019), and many megalosaurids (e.g., Sereno et al., 1994; Allain, 2002; Benson, 2008; Hendrickx and Mateus, 2014; Rauhut et al., 2016). The ascending process of *Irritator* becomes very slender and tapers posteriorly and articulates with the nasal dorsomedially and with the lacrimal posteromedially, which the ascending process overlies laterally. In contrast to most non-avian theropods, the posterior end of the ascending process does not bifurcate to receive the anterior end of the lacrimal but tapers to a point, which laterally overlies an extensive articular facet on the lateral side of the anterior end of the lacrimal. Another very unusual feature of the maxilla of *Irritator* is that the ascending process extends further posteriorly than the jugal ramus of this bone, reflecting the strong anteroventral inclination of the ventral ramus of the lacrimal.

The elongated body of the maxilla of *Irritator* is morphologically like those of other known spinosaurids. As in these, this elongate shape is mainly caused by the greatly elongated anterior ramus. The anterior ramus contacts the premaxilla anterior to the level of the external nares, as in other spinosaurids (Charig and Milner, 1986; Sereno et al., 1998; Dal Sasso et al., 2005). The maxilla forms most of the ventral and the posteroventral margin of this opening, as in a snout referred to *Spinosaurus* (Dal Sasso et al., 2005), but in contrast to *Suchomimus*, where most of the anteroventral border of the nares is formed by the subnarial process of the premaxilla, and the maxilla has only a small participation in the narial opening (Sereno et al., 1998). A narrow longitudinal groove with sharp lateral and medial margins is present on the dorsal surface of the maxilla anterior to the naris and below its anterior margin, marking the facet for the contact with the narial process of the premaxilla. Posterior to this groove, the dorsal surface of the maxilla forms a subnarial fossa in the form of a posteriorly widening shelf below the posterior part of the nares. In its anterior portion, the shelf is strongly laterodorsally directed, with the medial rim of the articular groove for the premaxilla forming a sharp medial rim of the shelf. This medial crest becomes lower posteriorly, and the shelf twists into a more dorsally facing position in its posterior part. Its lateral margin is formed by a low ridge that becomes more conspicuous posteriorly and leads into the anterodorsal margin of the ascending process of the maxilla. An intermaxillary contact is present ventrally in the anterior part of the anterior maxillary ramus, and the thin vomer is also contacted in this region. Together, these bones form a short secondary palate below the anteriorly narrow and posteriorly widening nasal vestibule. In anterior view, breakage reveals that the anterior maxillary rami are triangular in cross section and broadly contact each other dorsoventrally, except for their upper third where the anteroposteriorly long sinus of the nasal vestibule is situated (Figure 3A). The anteromedial surface of each maxilla is slightly roughened for the articulation with the respective counterpart. Dorsal to the fourth preserved alveolus and posterior to the end of the premaxillary subnarial process, the left maxilla is dorsoventrally narrowest, as the margin of the bone forms a concave notch along the margin of the external naris (Figure 5A-D).

In addition to the lacrimal contact of the ascending process, a second contact with the lacrimal is present ventral to the antorbital fenestra, where the maxilla bifurcates into a posterodorsal process that contacts and overlaps the anteroventral end of the lacrimal laterally, and a posteroven-

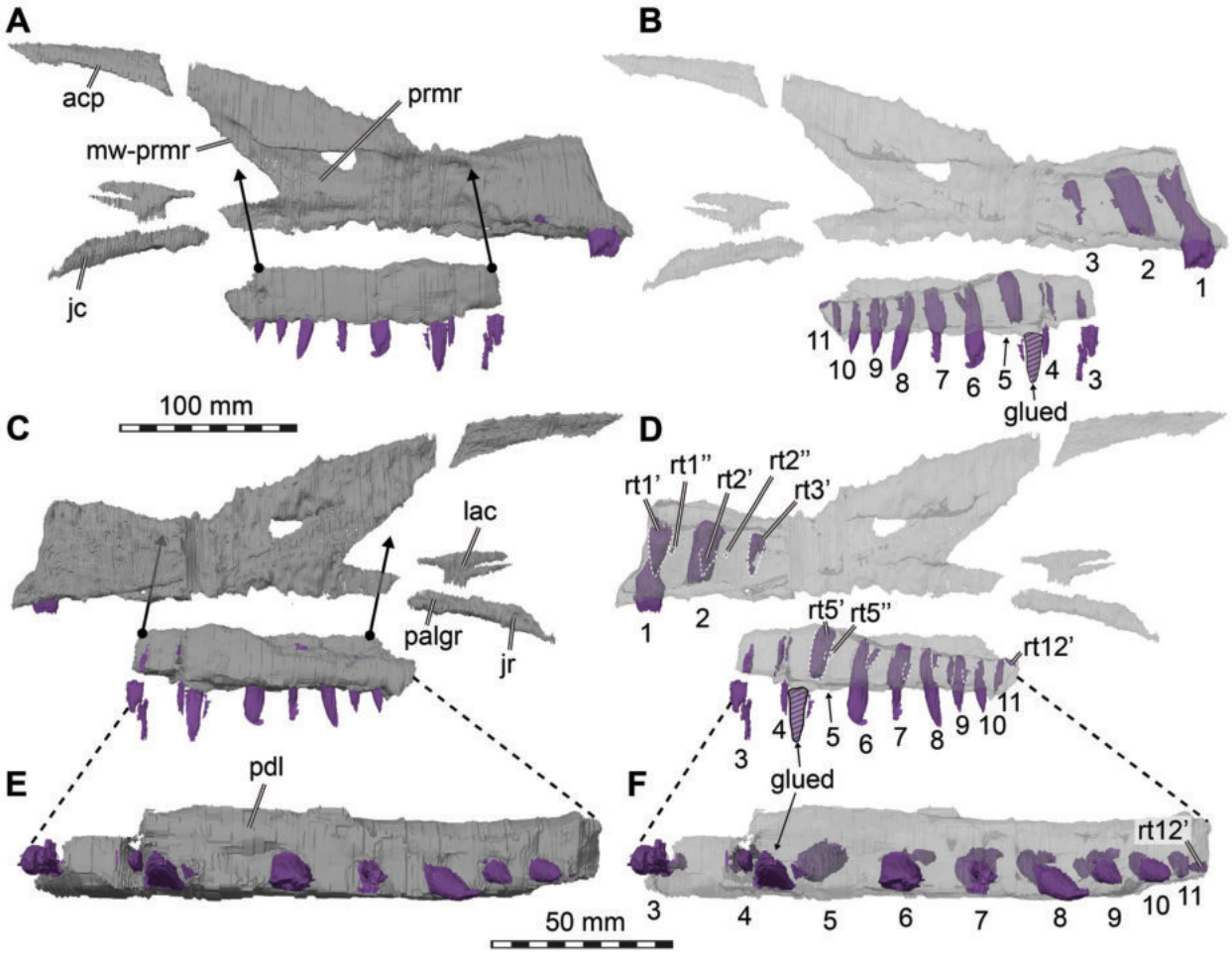

FIGURE 6. 3D renderings of the right maxilla of *Irritator challengeri* (SMNS 58022). A, lateral view; B, lateral view with maxillary bone rendered transparent; C, medial view; D, medial view with maxillary bone rendered transparent; E, ventral view of tooth row fragment; F, ventral view with maxillary bone rendered transparent. Note different scale for E–F. Also note that tooth positions are numerically labelled but refer to preserved tooth position from anterior to posterior, not to anatomical tooth positions, which are unknown. Replacement teeth are highlighted with dashed lines in D, and different generations are indicated with prime (') or double prime ('') . Arrows in A and C indicate approximate original position of tooth-bearing fragment. Abbreviations: acp, ascending process; jr, jugal ramus; lac, lacrimal contact; mw-prmr, medial wall of promaxillary recess; palgr, palatine groove; pdl, paradental lamina; prmr, promaxillary recess; rt, replacement tooth.

tral process that additionally contacts the jugal, palatine, and possibly the ectopterygoid (Figures 2A, 6A).

The lateral surface of the maxilla bears a single row of broadly spaced neurovascular foramina, each of which is positioned approximately between individual tooth positions (Figure 5A). There are at least seven neurovascular foramina on the lateral surface of the left maxilla, leading to the anteroposteriorly long neurovascular canal, which housed the trigeminal nerve and blood vessels. Due to the limits of resolution in the CT data and preservation, the neurovascular canals could not be followed over their entire length in both maxillae. Such canals are also known from other spinosaurids (Rayfield et al., 2007), megalosauroids (Benson, 2008; Rauhut et al., 2020) and other non-avian theropods (Barker et al., 2017). Seemingly unlike *Baryonyx* and *Suchomimus* (Charig and Milner, 1997; Sereno et al., 1998), *Irritator* does not bear one foramen per alveolus. On the left maxilla, the foramina in *Irritator* are approximately situated above the second, third, fifth and sixth preserved alveoli as well as between the sixth and seventh, above the eight, and between the ninth and tenth. Additionally, the foramina tend to be positioned dorsoventrally higher the more anteriorly they are.

The antorbital fossa seems to have been small and mainly restricted to the anterior rim of the antorbital fenestra, although the medial wall of the fossa is incompletely preserved on both sides. In contrast to most non-avian theropods, but like in *Suchomimus* (OWMR, SE, pers. obs., MNN GDF 501; Sereno et al., 1998), the fossa has a sharp and overhanging anterior and anteroventral rim and does not extend onto the jugal ramus of the maxilla. Dorsally, the fossa more gradually fades into the lateral surface of the process of the ascending process bordering the antorbital fenestra dorsally, but over most of the length of this process, its lateral surface is not notably depressed. Despite the damaged medial wall of the fossa, it seems almost certain that no distinct maxillary fenestra was present, as there would be very little space for such an opening. Ventrally, a natural rim of the medial lamina of the antorbital fossa is preserved and disappears below an overhanging lateral lamina in lateral view, being strongly indented anteriorly in the ventral part in medial view. In general, the medial wall gives a similar impression as in *Suchomimus* (Sereno et al., 1998), being more extensive dorsally than ventrally, although more extremely so than in the latter taxon, in which parts of the medial lamina are also visible on the ventral end of the antorbital fossa in lateral view. A feature revealed by the break of the right maxilla (see Sues et al., 2002, fig. 1B) and our CT data is the presence of a large antrum, invading the base of the ascending process and the anterior ramus of the maxilla from the anterior margin of the antorbital fenestra, and extending approximately from the fourth to the tenth preserved tooth position within the left maxilla (Figure 5B, D, E). The antrum is connected to the external antorbital fenestra (sensu Witmer, 1997) by a dorsoventrally large, posteriorly opening, funnel-like foramen, like the condition in *Suchomimus* (MNN GDF 501; Sereno et al., 1998) and *Wiehenvenator albati* (Rauhut et al., 2016), although both the antrum and the foramen are relatively smaller in the latter taxon, in accordance with the much less extensive base of the ascending process. A thin, dorsoventrally slightly medially convex wall borders the antrum medially and connects the dorsal margin of the alveolar maxillary body with the medial side of the anterodorsal margin of the ascending process (Figure 5E). Like in *Allosaurus* (Madsen, 1976; Witmer, 1997), this medial wall is anterodorsally perforated by a large, oval opening that connects the antrum with the space just posterior to the internal naris (see also Sues et al., 2002). This opening is preserved on both sides, although the margins seem to be largely broken, and on the left side, the medial wall posterior to it is largely broken away. Sues et al. (2002) identified the large recess in the base of the ascending process as the maxillary antrum, but its position anterior to the antorbital space and its connection to the latter by a posteriorly opening foramen are more consistent with an interpretation as the promaxillary recess, with the foramen representing the promaxillary foramen. The left promaxillary recess reaches anteroventrally deep where it seems to meet the neurovascular canals ventral to the posterior margin of the external naris. This is like the condition in *Suchomimus* and the spinosaurid maxillary fragment ICMWS 2014.95 (OWMR, SE, pers. obs., MNN GDF 501; Munt et al., 2017).

The maxillary body and the elongate anterior ramus of *Irritator* form the tooth-bearing part of the bone. Ten tooth positions are preserved on the left side and 12 on the right side (though, see details in the dentition section). Sales and Schultz (2017) interpreted the alveoli they recognized to represent tooth positions 3 to 12 and suggested that the fourth maxillary tooth seems to generally be the largest in spinosaurids, and thus the second preserved alveolus of the left side in *Irritator* should represent this tooth position. However, the situation is not quite as clear as that: In *Baryonyx*, maxillary tooth positions 2 to 4 are of subequal size, with the third alveolus seemingly being slightly larger than the fourth (NHMUK R 9951; Charig and Milner, 1997), and in *Suchomimus*, maxillary tooth positions three to six are largest and approximately subequal in size (OWMR, pers. obs., MNN GDF 501; Sereno et al., 1998). Although the posterior part of each maxilla is damaged in *Irritator*, the alveolar size of the posteriormost preserved tooth position on the right side, along with the geometrical arrangement of the skull bones in this area, may suggest that no further teeth were present posterior to this tooth. Anteriorly, it is likely that additional maxillary teeth were once present.

A very unusual condition for theropods found in *Irritator* is that the maxillary teeth are very widely spaced, with the space between individual teeth being more than the mesiodistal length of the alveoli (Figures 1-2, 4B, 5-6). It is noteworthy that wide tooth spacing to this degree is otherwise predominantly observed in longirostrine aquatic taxa, including polycotylid plesiosaurs (e.g., Fischer et al., 2018) and derived tomistomine crocodylians (e.g., Brochu, 2001). However, this wide tooth spacing is not present in other spinosaurid snouts

(Charig and Milner, 1997; Sereno et al., 1998; Taquet and Russell, 1998; Dal Sasso et al., 2005) and also present in non-aquatic taxa, for instance *Archaeopteryx* (Rauhut et al., 2018), many pterosaurs (e.g., Wellnhofer, 1975; Andres et al., 2010; Pêgas et al., 2021), and some squamates (e.g., Conrad, 2008, 2012). Individual alveoli are almost round (Figure 5G) and slightly longer mesiodistally than wide labiolingually, as in other spinosaurids, but unlike the rectangular alveoli of abelisaurids (e.g., Smith, 2007) or the much more elongate alveoli of most non-avian theropods. The depth of the alveoli extends to almost the dorsal margin of the maxillary body in the anterior ramus, but diminishes below the promaxillary recess (Figures 5B, D, 6B, D).

The ventral surface of the maxilla forms a buccal lamina, a notable longitudinal labial groove, and a prominent, swollen medial ridge (Figures 4B, 5F, G, 6E). As in other spinosaurids (e.g., *Baryonyx*; NHMUK 9551; *Suchomimus*; GDF 501), this medial ridge represents a ventrally expanded paradental lamina (the lamina covering the nutrient groove at the dorsal end of the interdental plates; see Hendrickx and Mateus, 2014) that covers the interdental plates medially. The latter seem to be completely fused and are separated from the paradental lamina by a deep but narrow incision. The medial ridges formed by the swollen paradental laminae constitute the secondary palate below the nasal passage. Both medial ridges are close and in parallel to each other anteriorly but diverge at the fourth preserved maxillary alveolus. The medial ridge reaches at least to the last preserved tooth positions. A similar ridge is also known from *Baryonyx, Suchomimus* and *Spinosaurus* (Charig and Milner, 1997; Sereno et al., 1998, Dal Sasso et al., 2005).

The medial surface of the maxilla bears a deep and anteroposteriorly long depression that receives the maxillary process of the palatine. This depression is positioned dorsal to the posterior portion of the median ridge and extends anteriorly to the level of the middle portion of the promaxillary recess, at the space between the sixth and seventh preserved alveolus. Below the promaxillary recess, the alveolar part of the medial side of the maxilla bulges slightly medially, whereas the medial side of the anterior ramus is flat for the contact with the opposite side. A prominent lingual bar or lingual bulge, as it is present in many basal tetanuran theropods (Carrano et al., 2012), is absent.

In *Irritator*, the configuration of the maxilla, lacrimal and jugal excludes the jugal from the antorbital fenestra (Figures 1, 2A), like the condition in *Ceratosaurus* where, however, this point is situated more posteriorly (Gilmore, 1920; Madsen and Welles, 2000). The posteroventral contacts of the maxilla and the morphology of the respective maxillary process of the jugal are hard to determine with certainty due to breakage on either side of the specimen. However, on the right side, there are two main pieces of the maxilla preserved: a mediolaterally thin, posteriorly tapering and posterodorsally directed piece that overlaps the lateral surface of the anteroventral end of the lacrimal and contacts the dorsal margin of the jugal (Figures 1B, 2A, 6). This process is posteriorly bifurcated into two thin rami, which are visible in the fossil (see Sues et al., 2002: fig. 1B). The second main piece of the posterior maxillary process is a posteriorly tapering process that aligns with the ventral skull margin and articulates with the ventromedial surface of the jugal and possibly the ventral surface of the lacrimal (Figures 4B, 6). This process extends to the position of the ectopterygoid, possibly contacting its anterior end. These two main pieces suggest that the posterior maxillary process was bifurcated into a dorsal ramus that framed the lacrimal-jugular area laterally, and a ventral ramus that framed this region medially. Therefore, the posteroventral process of the maxilla brackets the jugal and lacrimal in a 'paperclip-like' fashion that is unknown in other theropods, with the possible exception of *Suchomimus*, which also seems to have a bifurcated posterior end of the maxilla (OWMR, SE, pers. obs., MNN GDF 501; Sereno et al., 1998).

Nasal

The nasals are nearly completely preserved (Figures 1-2, 4A, 7) with only slight breakage that has occurred on the anterior end of the bones, but much of their surface is somewhat abraded. The paired nasals are fused with each other on their posteriormost third, but a suture is traceable anteriorly (Figure 8). However, we segmented the nasals from the CT data as a single element, and the right and left nasals are described together in the following account. The nasal contacts the premaxilla anteriorly, the maxilla and lacrimal ventrally and the prefrontal and frontal posteroventrally, forming the skull roof between the external nares and the orbit (Figures 2-4). The CT data suggest that there is an artificial insertion of a foreign body in the nasals, close to their mid-length, within a major fracture (Figures 1, 7); thus, this part has not been considered in the description.

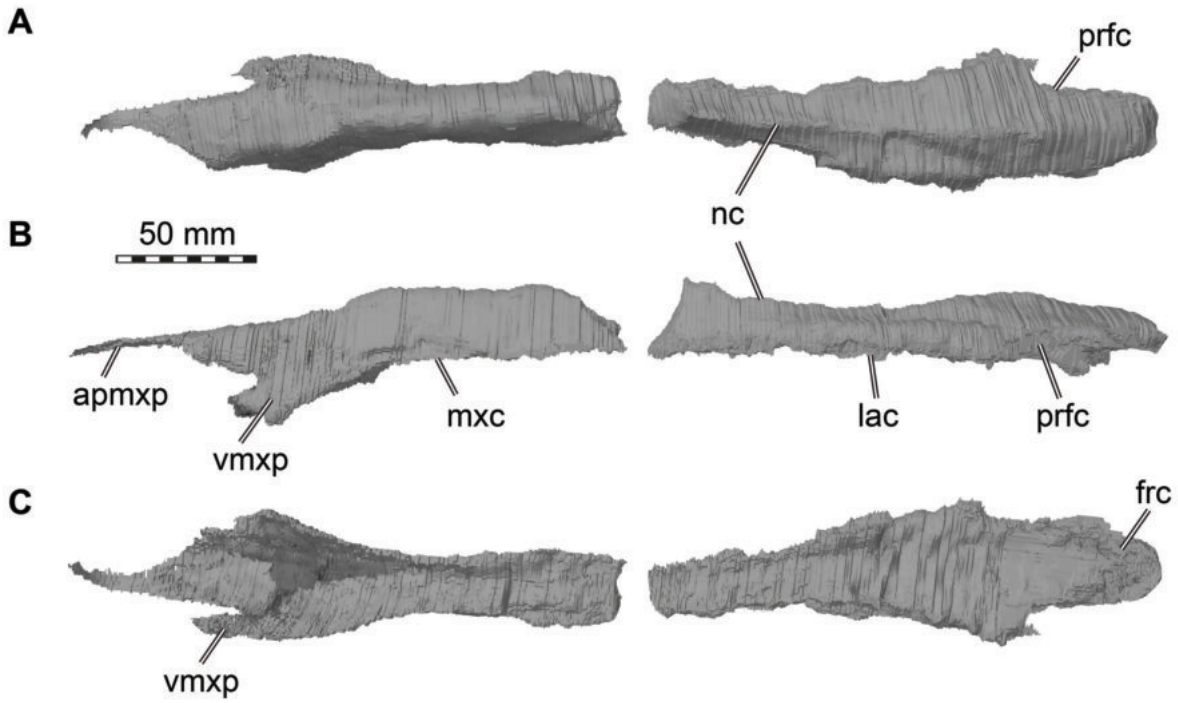

FIGURE 7. 3D renderings of the fused nasals of *Irritator challengeri* (SMNS 58022). A, dorsal view; B, left lateral view; C, ventral view. Abbreviations: apmxp, anterior premaxillary process; frc, frontal contact; lac, lacrimal contact; mxc, maxillary contact; nc, nasal crest; prfc, prefrontal contact; vmxp, ventral maxillary process.

Whereas the posterior part of the nasal forms the dorsal skull roof, the bone curves ventrally in its anterior part to form parts of the lateral wall of the snout in front of the ascending process of the maxilla. As preserved, right and left external nares are anteriorly confluent with one another, but we assume that this is due to breakage, and the premaxillae and nasals would have formed a midline contact that separates each narial opening from one another. Anteriorly, the dorsal and posterior margin of the external naris is formed by an oval notch produced by a dorsal premaxillary and a ventral maxillary process of the nasal. The premaxillary process is only preserved on the right side, but its anterior end is missing. The process tapers anteriorly when seen in lateral view. The maxillary process of the nasal projects anteroventrally and overlies the maxilla laterally, forming an arch over the interior of the snout. The ventral margin of the nasal which meets the maxilla ascends from the maxillary process posteriorly along the anterodorsal margin of the ascending process of the maxilla. Here, the nasal slightly overlaps the maxilla dorsolaterally in its anterior portion, whereas the posterior end of the ascending process of the maxilla abuts the ventrolateral rim of the nasal laterally. Posteriorly, the nasals become dorsoventrally thicker, and their ventral surface becomes less arched and nearly flat. On the dorsal surface, the remnant of a nasal crest is preserved and extends from shortly posterior to the external naris to nearly the posterior end of the bone. The nasal crest seems to have been dorsoventrally tall around the mid-length of the nasals but becomes lower and transversely thinner posteriorly, and it disappears around 5 cm before the rounded posterior margin of the nasal. Thus, the crest is not as pronounced in *Irritator* as it is in *Baryonyx* and *Suchomimus*, where it extends to the posterior end of the nasal, forming a nasal cornet (Charig and Milner, 1997; MS, pers. obs. on cast, MNN GDF 214 referred to *Suchomimus*). A transverse posterior expansion of the crest at the level of the nasal-prefrontal contact, as is present in *Baryonyx* and *Suchomimus* (Charig and Milner, 1997; MS, pers. obs. on cast, MNN GDF 214) is absent in *Irritator*, but the dorsal surface lateral and posterior to the crest is gently convex. However, it should be noted that the exact shape of the crest was likely affected by the abrasion of the dorsal surface of the nasals, especially in its anterior part, and it cannot be excluded that the crest continued anterior to the mid-length of the nasal. In contrast to a partial nasal referred to *Spinosaurus* (Dal Sasso et al., 2005), the crest is solid

and not pneumatized in *Irritator*. Sales and Schultz (2017) mention that an autapomorphy of *Irritator* is a knob-like projection at the end of the sagittal crest of the nasals. We interpreted this morphology (newly coded as character 46) to be present in several spinosaurids *(Baryonyx, Suchomimus, Riparovenator)* but not in *Irritator*, although it must be mentioned that this area is poorly preserved in the latter.

In contrast to various basal tetanurans (Rauhut, 2003), the nasal of *Irritator* does not contribute to the antorbital fossa. Instead, the joined nasals dorsally overlie the ascending process of the maxilla, the lacrimal and the prefrontal. The nasals are mediolaterally broadest just posterior to the position of the small lacrimal boss. In this region, the nasal forms a posterior notch for the prefrontal, and the lateral margin of the nasal inserts between the lacrimal boss and the prefrontal (Figures 7A, C, 8), resulting in an arrowhead-like shape of the posterior nasal, as in *Baryonyx* (Charig and Milner, 1997). This is better preserved on the right side. Posteromedial to the notch, Sues et al. (2002) inferred that a potential postnasal fenestra (named after the posterolateral notch in the nasal of *Baryonyx*; Charig and Milner, 1997) in *Irritator* has rather been produced by the “dorsal displacement” of the nasal from the prefrontal, lacrimal and frontal contact. Seemingly, this "fenestra" is rather a superficial depression between the prefrontal, frontal and nasal that is filled with sediment. The CT data suggest a tightly fitting articulation of these bones here, with the nasal being considerably thickened in this region.

Based on our CT data, the nasals show an offset ventral platform (Figure 7C) that is wedged between the nasal processes of the frontals. The nasal processes of the frontal receive the nasals mainly anteromedially, and the posterior surface of the platform abuts the anteromedial surface of the frontals. In lateral view, the posteriormost portion of the nasal overlies the frontals dorsally and the frontals dip beneath the nasal anteriorly. A ventral median ridge, as present in *Baryonyx* (Charig and Milner, 1997), is absent in *Irritator*.

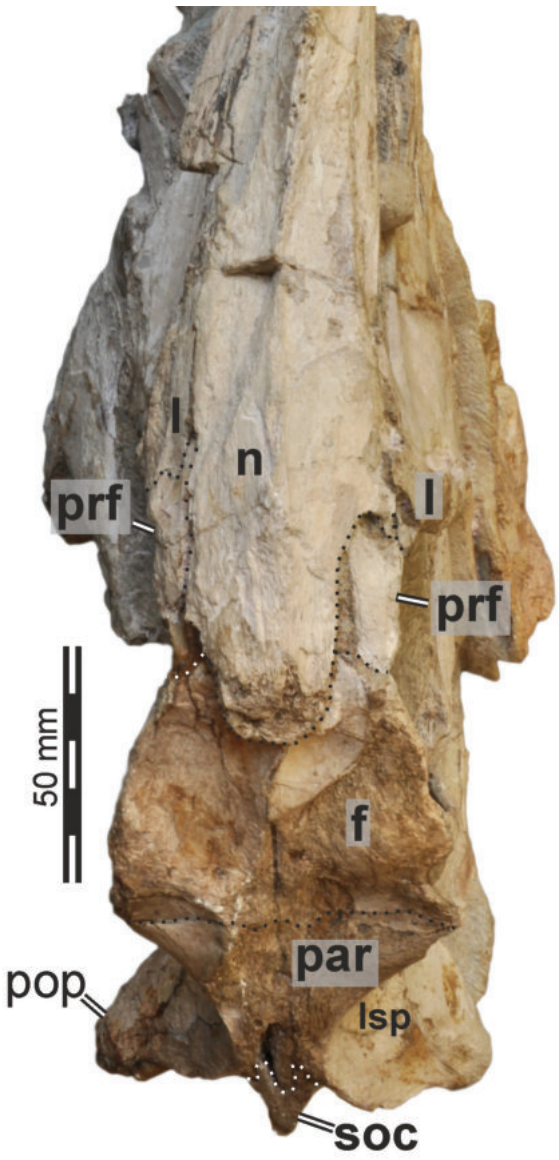

FIGURE 8. Photograph of posterior skull roof of *Irritator challengeri* (SMNS 58022) in dorsal view. Note that bones are labelled in bold, and other anatomical structures in regular font. Dashed lines mark sutures. Abbreviations: f, frontal; l, lacrimal; lsp, laterosphenoid; n, nasal; par, parietal; pop, paroccipital process; prf, prefrontal; soc, supraoccipital.

Lacrimal + Prefrontal

Both lacrimals and prefrontals are preserved (Figures 1, 9). Although the sutures between the lacrimal and the prefrontal are at least partially clearly visible on the fossil (Figure 10), these bones cannot be distinguished in the CT data, which might suggest a certain degree of fusion internally, as generally all other sutures are distinguishable in the specimen, including those of tightly appressed braincase bones. Therefore, we segmented the lacrimal and prefrontal as a single model for each side. Both elements are described together, but lacrimal and prefrontal features are described separately as much as possible.

The lacrimal contacts the maxilla anteriorly, the nasal dorsally, the prefrontal posteromedially

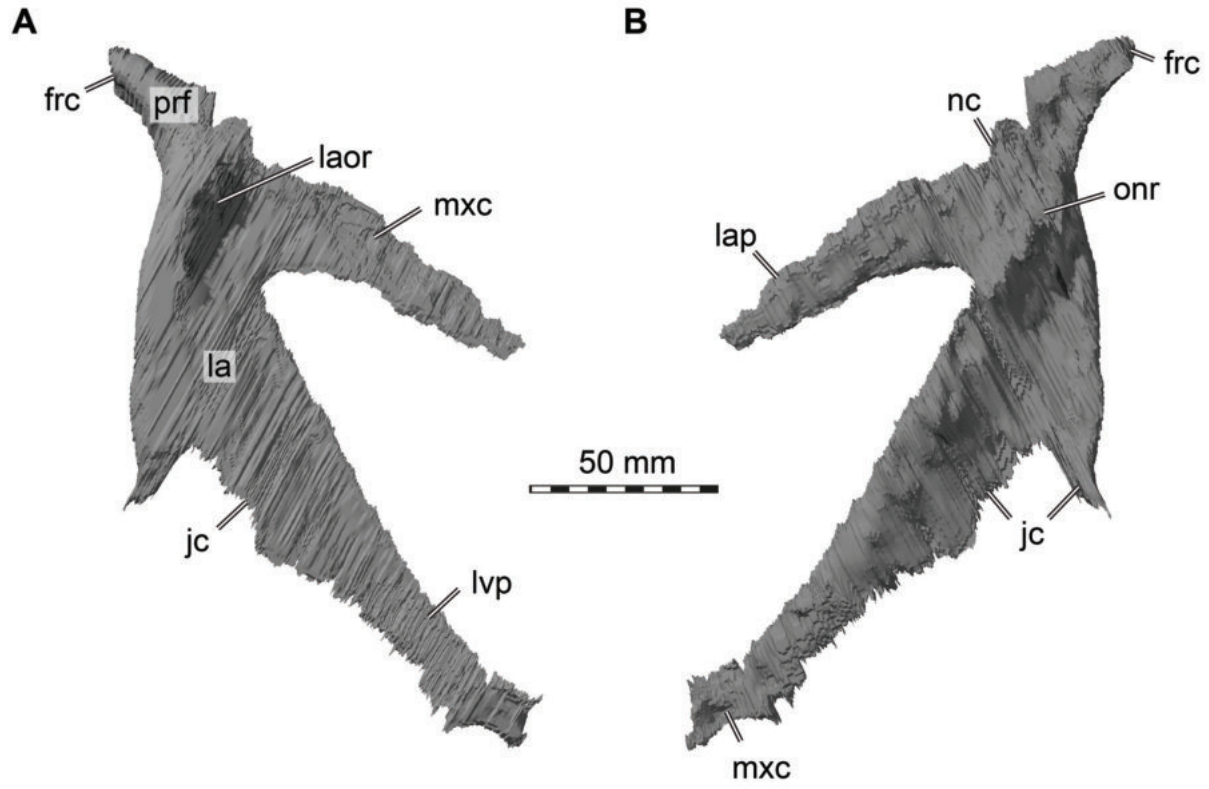

FIGURE 9. 3D renderings of the right lacrimal and prefrontal of *Irritator challengeri* (SMNS 58022). Note that sutures between these two bones could not be identified in the CT data, but externally visible sutures on the specimen show that these bones are only partially fused (see Figure 10). A, lateral view; B, medial view. Abbreviations: frc, frontal contact; jc, jugal contact; la, lacrimal; laor, lacrimal antorbital recess; lap, lacrimal anterior process; lvp, lacrimal ventral process; mxc, maxillary contact, nc, nasal contact; onr, orbitonasal ridge; prf, prefrontal.

and the jugal ventrally (Figures 2-4). The right lacrimal is in a better condition than the left one, still showing a distinct lacrimal recess (Figures 1, 9-11). As is typical in non-avian theropods (Gauthier, 1986; Rauhut, 2003), the lacrimal has an inverted L-shape, but with an acute angle of c. 30–35° (as measured between the dorsal and posteroventral margins of the antorbital fenestra), rather than almost right-angled between the anterior and ventral processes, as in *Baryonyx* and *Suchomimus* (Charig and Milner, 1997; MS, pers. obs. on cast, MNN GDF 214). The anterior process is approximately 68% of the length of the ventral process (both measured from the posterodorsal edge of the lacrimal to the tip of the respective process), and due to the strong anteroventral inclination of the latter, its tip is located anterior to the anterior end of the anterior process, a condition that seems to be unique relative to non-spinosaurid theropods. The posterodorsal part of the medial lacrimal surface articulates with the prefrontal. Anterodorsally, the lacrimal has an anterior process that forms the posterior part of the dorsal margin of the antorbital fenestra, and which is partially overlapped by the maxilla laterally and the nasal dorsally. This process is mediolaterally thin and dorsoventrally tall at its base while tapering anteriorly. Its dorsal margin is slightly convex proximally and becomes straight distally, whereas the ventral margin is gently concave, forming the margin of the antorbital fenestra.

Posterior to the anterior process of the lacrimal, at the base of the ventral process, the posterior margin of the lacrimal which frames the anterior orbital margin is mediolaterally thickened. This thickened part of the lacrimal bears a dorsoventrally tall recess, which faces anteriorly and forms the posterior end of the antorbital fossa. The recess contains four dorsoventrally aligned main depressions that are separated from each other by mediolaterally oriented ridges. The second depression from dorsally is the smallest but seems to represent a pneumatic foramen to a very small cavity network, stretching ventrally. CT data show that where the ridge that houses the lacrimal recess

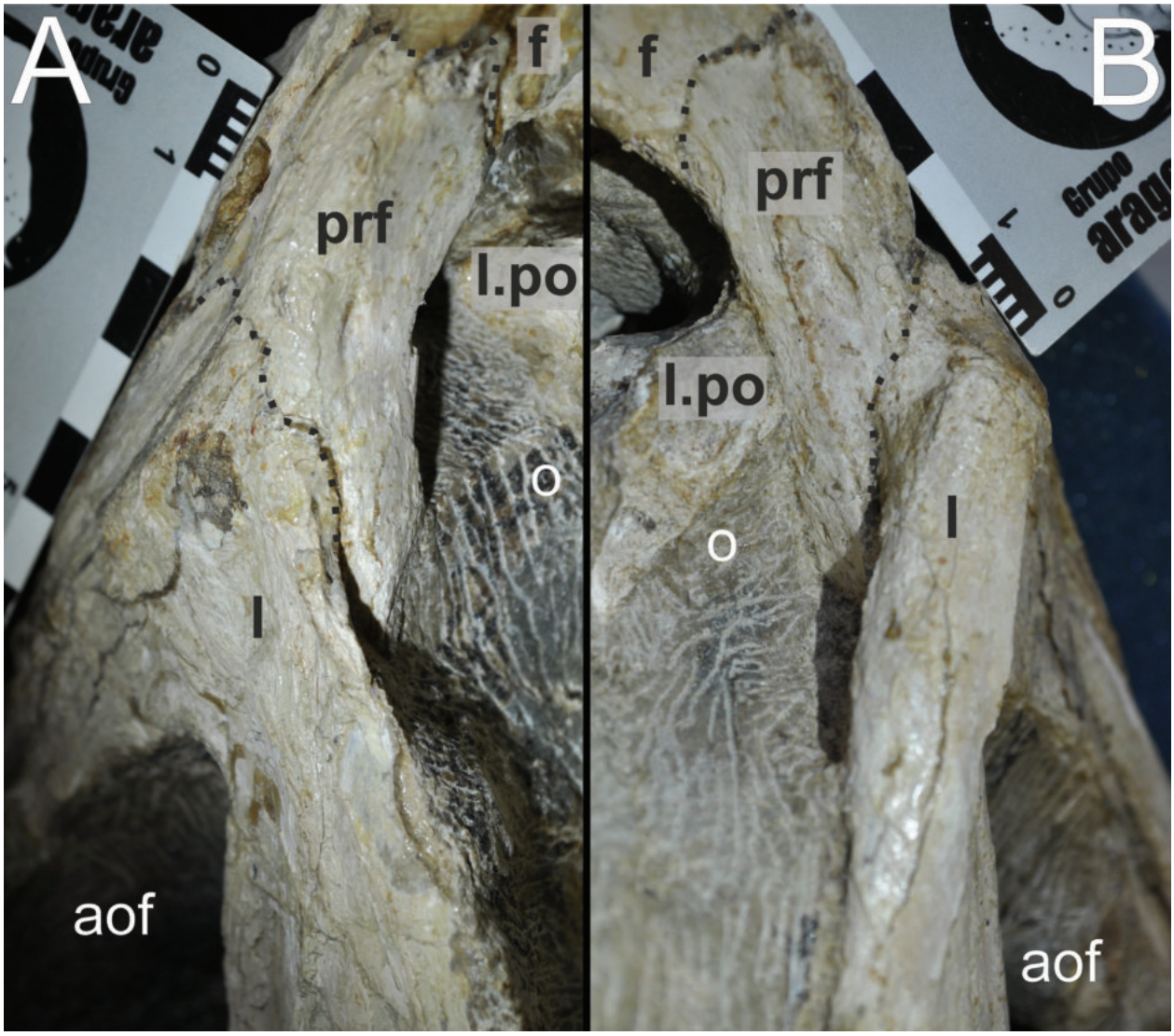

FIGURE 10. Close-up photographs of the lacrimal/prefrontal region of *Irritator challengeri* (SMNS 58022). A, left posterolateral view; B, right posteroventral view. Note that bones are labelled in bold, and other anatomical structures in regular font. Dashed lines mark sutures. Abbreviations: aof, antorbital fenestra; f, frontal; l, lacrimal; l.po, left postorbital; o, orbit; prf, prefrontal.

flattens laterally, some other small cavities are situated without any obvious connection to a pneumatic foramen. The lacrimal recess of *Baryonyx* is anteroposteriorly and dorsoventrally larger than in *Irritator* (Charig and Milner, 1997). Furthermore, the lamina that covers the recess laterally extends ventrally onto the ventral process of the lacrimal and marks the posterior border of the antorbital fossa in both taxa. The recess was originally covered by a very thin, bulbous bony lamina, which was apparently lost during preparation (Figure 11).

The ventral process of the lacrimal forms the articulation with the maxilla, jugal, and likely the palatine. The process is strongly anteroposteriorly expanded ventrally, making it roughly triangular. The expansion is mainly anteroventral, so that the lacrimal orbital margin is only about 72% of the length of the respective margin of the antorbital fenestra. As in other spinosaurids (Charig and Milner, 1997; Sereno et al., 1998), the anteroventral inclination of the anterior margin of the process results in an oval antorbital fenestra of which the lacrimal forms a substantial part of the posteroventral margin. Whereas the rim of the antorbital fenestra is very gently concave, the orbital margin of the ventral process is slightly convex; a suborbital spur or process is absent. The orbital margin of the ventral process is mediolaterally notably

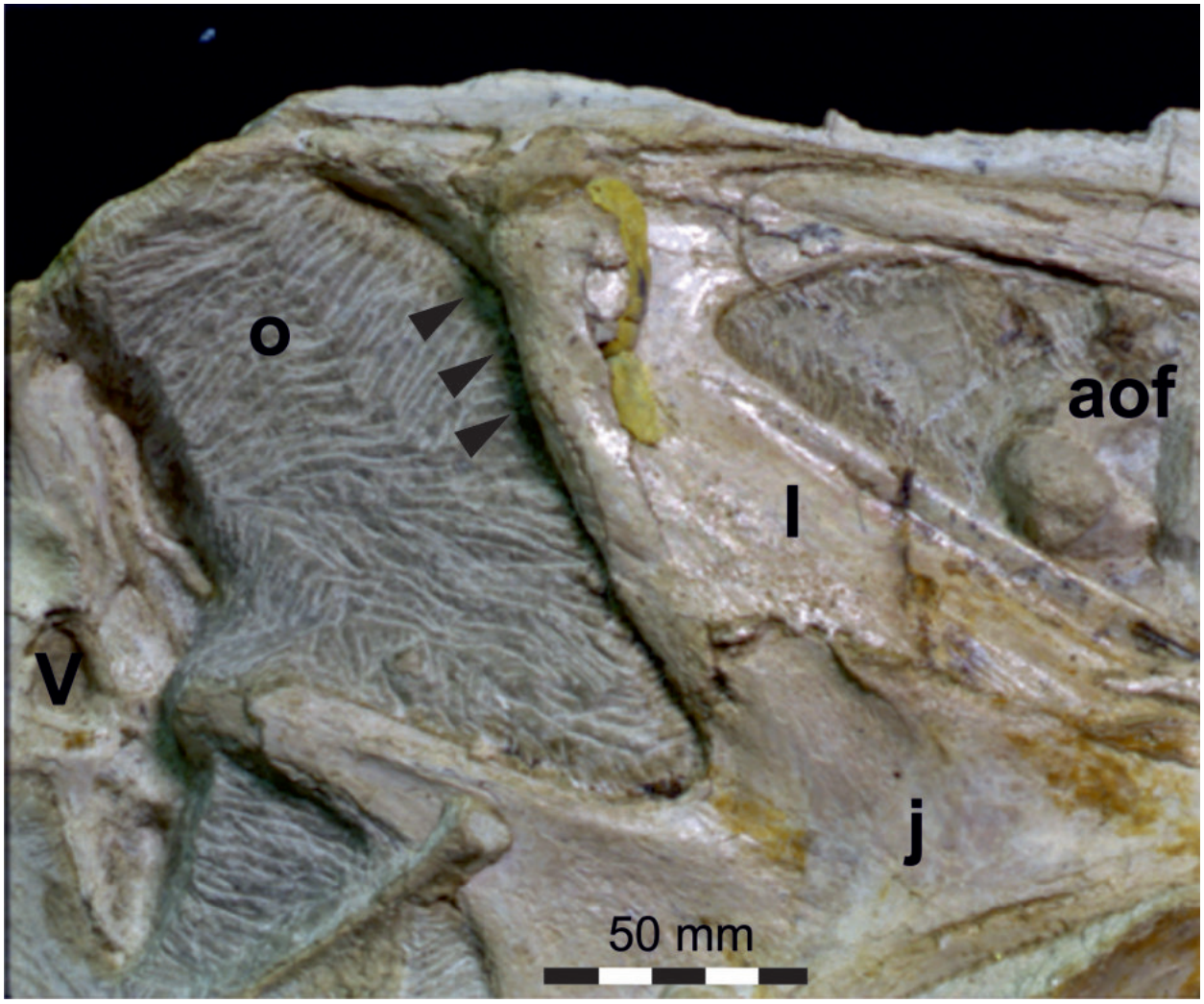

FIGURE 11. Close-up photograph of the lacrimal region of *Irritator challengeri* (SMNS 58022) in an earlier stage of preparation. Right lateral view. Arrows indicate the formerly more complete lamina on the dorsolateral aspect of the lacrimal. Abbreviations: aof, antorbital fenestra; j, jugal; l, lacrimal; o, orbit; V, trigeminal nerve foramen (CN V).

convex and thickened dorsally in the area of the lacrimal recess but becomes gradually thinner towards the jugal contact. The rim of the antorbital fenestra is also slightly thickened, but much less so than the orbital margin. The position of the lacrimal foramen and course of the lacrimal canal could not be established. Even more than in other basal tetanurans (Evers et al., 2020), the distal end of the ventral process articulates widely with the jugal ventrally and the maxilla anterolaterally. Unlike in most basal tetanurans, however, the lacrimal and maxilla exclude the jugal from participating in the margin of the antorbital fenestra (Evers et al., 2020). The ventral margin of the lacrimal articulates with the jugal along a relatively simple contact, with the suture being notably anteroventrally inclined. A broad overlap of the jugal over the ventral lamina of the lacrimal, as is plesiomorphically present in Saurischia (Sereno and Novas, 1993) does not seem to be present, although it cannot be completely excluded that this might be due to a lack of resolution of the CT data, as this lamina is extremely thin in many non-avian theropods. Shortly before both bones form the anteroventral margin of the orbit, a notch is developed within the ventral margin of the lacrimal. A similar notch can also be discerned in *Allosaurus*, albeit without an anteroventrally inclined suture between the jugal and the lacrimal (Evers et al., 2020). The contact with the maxilla seems to be restricted to the anteroventral portion of the ventral process of the lacrimal, which is overlapped by the dorsal posterior process of the maxilla laterally (Figure 2A). This contrasts with most non-avian theropods, in

which the base of the lacrimal broadly contacts the dorsomedial surface of the maxilla medial to the jugal (Evers et al., 2020).

As with the antorbital fossa on the maxilla, a clearly defined antorbital fossa is only present in front of the lacrimal recess. The sharply defined rim of the fossa extending ventrally from the lacrimal recess ends at about the half-height of the posterior margin of the ventral process. Below this point, the lateral surface gradually deepens anteriorly, but a clearly rimmed antorbital fossa is absent. However, in contrast to most non-avian theropods, including *Baryonyx* (Charig and Milner, 1997), but except for, e.g., *Torvosaurus* (Britt, 1991), the dorsal and ventral parts of the lacrimal antorbital fossa on the ventral process are confluent and not interrupted by an anterior expansion of the lateral lamina of the lacrimal. On the anterior process, there is also no defined rim of the antorbital fossa, but the lateral surface of the process is level with the lateral surface of the lacrimal anterior to the lacrimal recess, indicating that most of the process might have been occupied laterally by the antorbital fossa. The dorsal part of the anterior half of the process is very slightly depressed where it is overlain laterally by the posterior end of the ascending process of the maxilla.

Medially, the lacrimal shows two well-developed ridges (Figure 9) that extend along the dorsal margin of the anterior process and the anterior margin of the ventral process and are aligned posterodorsally with the anterior and ventral processes of the prefrontal, respectively. The prominent orbitonasal ridge of the lacrimal and prefrontal thus extends from the posteromedial portion of the prefrontal to the anteroventral corner of the ventral process of the lacrimal. Here, the palatine possibly meets the lacrimal medially with a small lateral process. In *Baryonyx*, a very similar orbitonasal ridge is present (Charig and Milner, 1997). However, the ridge in *Baryonyx* is divided into a sharp anterior and a sharp, parallel posterior crest by a longitudinal trough. Such a trough, although less deep and less clearly defined, might be present in the left lacrimal of *Irritator*, but this element is rather poorly preserved. In the better preserved right lacrimal of *Irritator*, the orbitonasal ridge is broad and anteroposteriorly rounded below the prefrontal. In its ventral third, the posteroventral border of the ridge forms a sharp and very slightly overhanging crest. The medial surface of the ventral process posterior to the orbitonasal ridge is triangular in outline and gently concave between the ridge and the thickened orbital margin.

The ridge along the dorsal rim of the anterior process is slightly thinner than the orbitonasal ridge and disappears anteriorly at approximately the mid-length of the anterior process (as measured from the rim of the antorbital fenestra). In the proximal portion of the anterior process, this ridge is triangular in cross-section, with a flattened, dorsomedially facing surface and a mediolaterally shorter, also somewhat flattened, ventrally facing shelf. The surface between the two ridges, medial to the external lacrimal recess, is slightly concave and forms a deep recess anterior to the prefrontal.

The prefrontal is medially positioned with respect to the lacrimal, and its anterior and anteroventral processes contact the medial surface of the latter, whereas the short but stout posterior process extends posterior to the level of the lacrimal (Figures 9-10). As in most basal tetanuran theropods, the prefrontal is a roughly hook-shaped element, with distinct anterior and anteroventral processes, which meet each other at an angle of 30–35°. Since the prefrontal seems to be at least partially fused with the lacrimal, the exact extent of the anterior and anteroventral processes cannot be discerned with certainty, but the morphology of the prefrontal-lacrimal complex and the sutures visible on the actual specimen give some indication of their morphology. The anteroventral process of the prefrontal contributes to the orbitonasal ridge and seems to extend to approximately one-third of the height of the orbit. Posterodorsally, the ridge is continuous with the crista cranii of the frontals, which separate the sulcus olfactorius medially from the lateral orbital facet. The anterior prefrontal process is shorter than the anteroventral process and defines the dorsal margin of a posterodorsal recess of the internal antorbital space in the region where lacrimal, prefrontal and nasals contact each other. The posterior process of the prefrontal is visible in the lateral view of the skull and bridges the space between frontals and lacrimal. The prefrontal forming a considerable part of the anterodorsal margin of the orbit, such that it is visible in lateral view, contrasts with many other basal tetanurans (e.g., *Sinraptor dongi* and *Allosaurus*; Madsen, 1976; Currie and Zhao, 1994; Chure and Loewen, 2020).

Frontal

Both frontals are preserved (Figure 12). Although the interfrontal suture is discernible on the fossil (Figure 8), it was not possible to individually reconstruct them, as they appear confluent in the CT data, and thus are described in unison

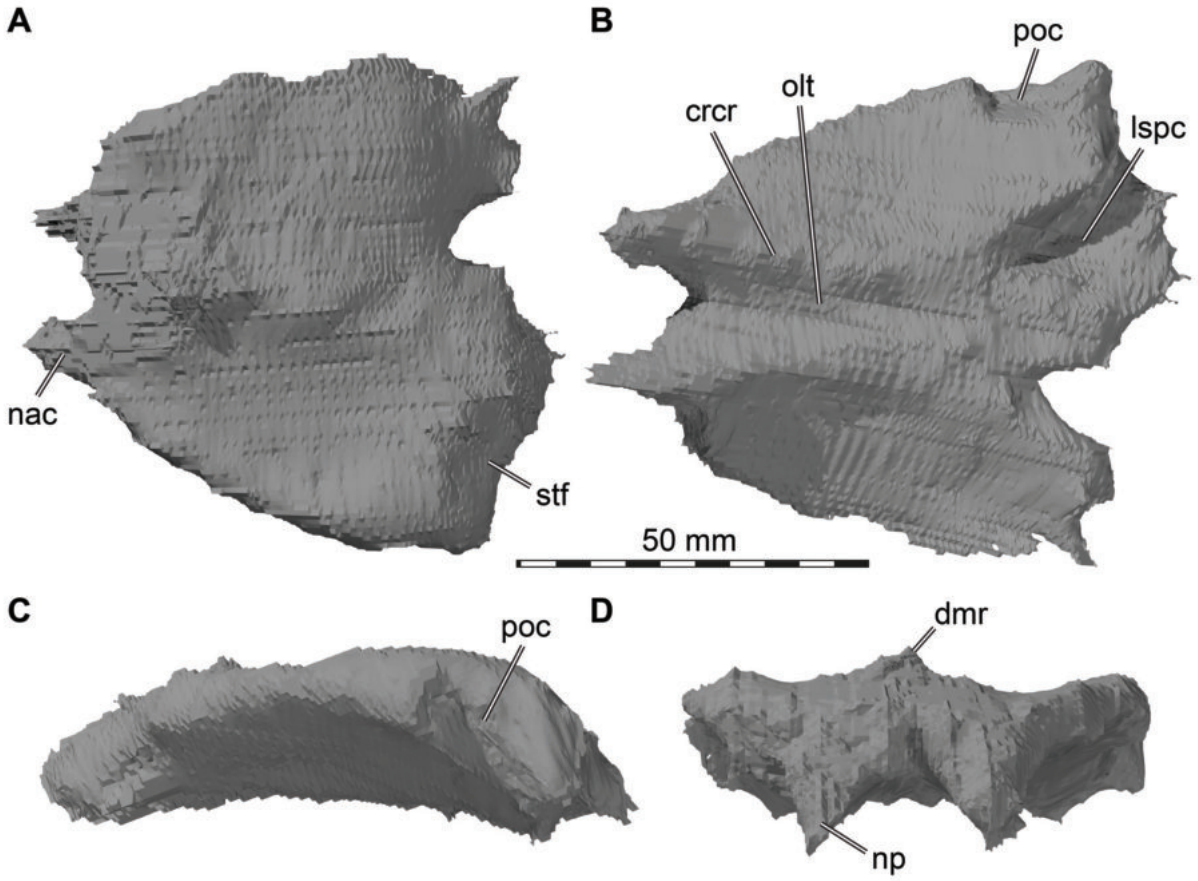

FIGURE 12. 3D renderings of the right and left frontals of *Irritator challengeri* (SMNS 58022). Note that the interfrontal contact could not be identified in the CT data, but externally visible sutures on the specimen show that these bones are only partially fused (see Figure 8). A, dorsal view; B, ventral view; C, left lateral view; D, anterior view. Abbreviations: crcr, crista cranii; dmr, dorsal median ridge; lspc, laterosphenoid contact; nac, nasal contact; np, nasal process; olt, olfactory tract, poc, postorbital contact, stf, supratemporal fossa.

here. The frontal contacts the nasal anteriorly, the prefrontal anterolaterally, the parietal posteriorly, the postorbital posterolaterally, and the orbitosphenoid and laterosphenoid posteroventrally (Figures 2-4). Dorsally, a low median ridge extends along the frontals, subdividing the otherwise nearly flat skull roof; this ridge is only preserved on the anterior half of the frontals, as the dorsal surface of the posterior half is largely abraded. In contrast to many other megalosauroids (e.g., Allain, 2002; Sadleir et al., 2008), the basal tetanuran *Piatnitzkysaurus floresi* (Rauhut, 2004), and Metriacanthosauridae (IVPP 10600; Currie and Zhao, 1994), but similar to the condition in *Acrocanthosaurus atokensis* (Eddy and Clarke, 2011) and other Carcharodontosauridae (e.g., Coria and Currie, 2002), the frontals are rather short and broad, the articulated elements being slightly broader mediolaterally than long anteroposteriorly. The frontals are mediolaterally widest on their posterior end and become narrower towards the nasals anteriorly. However, a marked postorbital process in the posterior part, as is, for example, present in *Allosaurus* (Gilmore, 1920; Chure and Loewen, 2020), is absent, and the orbital margins are very slightly convex in dorsal view. The frontal is vaulted, so that the posterior part flexes downwards regarding the anterior portion, which is aligned with the dorsal surface of the nasal (Figures 1, 2, 12). This contributes to the snout inclination that we have argued for on the grounds of horizontal semicircular canal orientation in a previous study (Schade et al., 2020a).

In contrast to most non-avian theropods, the frontals become gradually thicker anteriorly. In general, the frontal is rather massive, with its maximal thickness (c. 18 mm) being more than 25% of its anteroposterior length. Anteriorly, the frontal articulates with the nasal in a complex suture. As noted above, dorsally, the low and rounded posteriormost

portion of the nasals rests upon a roughened and semicircular medial surface of the frontals. This relatively short dorsal posterior process of the nasal is offset from the thickened main nasal body by a marked step, below which the nasal is slotted in between the lateral nasal processes and abuts the anterior end of the thickened frontals. In most basal tetanuran theropods, the frontals usually bear long, plate-like anterior projections that are extensively overlapped dorsally by the nasals (e.g., *Dubreuillosaurus*: Allain, 2002; *Sinraptor*: Currie and Zhao, 1994), which differs from the condition in *Irritator*. In addition, the anterior end of the frontal contacts the prefrontal anterolaterally. In contrast to the condition in the vast majority of non-avian theropods, the facet for the prefrontal is not developed as a deep socket but has a rather flat to only slightly concave surface and faces more anteriorly than laterally.

In ventral view, the frontal complex of *Irritator* bears two small anterior processes that contact the nasals medially and the respective prefrontals anteriorly and laterally. While the right suture between frontal and prefrontal is rather straight in ventral view, the left frontal seems to bear a ventrolateral notch for the respective prefrontal (Figure 10), which might be a result of breakage). The medial orbitonasal ridge of the lacrimal and the prefrontal continues posteriorly to form paired ventral ridges of the frontal, the cristae cranii, which define the olfactory tract impression (sulcus olfactorius). Compared to other basal tetanuran theropods, the cristae cranii are pronounced, though not to the extent seen in Troodontidae (see Rauhut, 2003, fig. 11C). The olfactory tract is narrow posteriorly (c. 10 mm), but widens gradually anteriorly to a width of c. 15 mm. A large anterior expansion, as is present in *Allosaurus*, is absent. The cristae cranii become slightly higher and more sharply defined anteriorly. The orbital facets are roughly trapezoidal in outline, being wider posteriorly than anteriorly, and are very gently concave anteroposteriorly but more or less straight mediolaterally, being inclined gently dorsolaterally. The frontal forms most of the dorsal border of the orbit, and the lateral margin of the bone forms a rather sharp lateral rim (Figures 1, 2).

The supratemporal fossa on the posterodorsal surface of the frontal is a shallow but mediolaterally wide depression (Figure 12A). It is clearly delimited anteriorly and medially by low ridges and faces mainly posterodorsally, unlike the situation in many basal tetanurans, in which this fossa faces mainly dorsally, but comparable to the morphology seen in many non-avian Coelurosauria (Rauhut, 2003). However, the frontal is excluded from the supratemporal fenestra by the parietal. In lateral view, the frontals show a slight arc on the dorsal margin of the orbit. The frontal articulates with the anterior process of the postorbital via a shallow and anteroposteriorly short depression which is clearly visible on the left side.

At the posterior end, the frontals contact the anterior end of the parietals dorsally and the laterosphenoids ventrally. In ventral view, there is a notch on each side of the posterior end of the olfactory tract impression. Here, the articulation surface for the medial head of the laterosphenoid is discernible (Figure 12B).

There are small cavities within the frontals that seem to be arranged in anteroposteriorly oriented, ‘dashed’ rows. On either side of the dorsal median ridge, one such row is clearly discernable. The cavities are rarely interconnected and are not associated with a pneumatic foramen.

Parietal

Both parietals are preserved but are incomplete (Figure 13). The transverse nuchal crest is completely absent, and the dorsal surfaces of both parietals are broken and eroded in most places, especially posteriorly (Figures 8, 14). This is most obvious in comparison with a braincase that is probably referable to *Suchomimus*, where an anteroposteriorly and mediolaterally very prominent, mainly laterally pointing transverse nuchal crest is present (MS, pers. obs. on SMNS cast of MNN GDF 214). Additionally, the condition in *Suchomimus*, *Ceratosuchops*, and *Riparovenator* suggests a relatively anteroposteriorly longer supratemporal fossa on the anterior lateral wing of the parietal in these taxa (MS, pers. obs. on cast, MNN GDF 214; Barker et al., 2021). The parietal contacts the frontal anteriorly, the postorbital anterolaterally, the laterosphenoid anteroventrally, the supraoccipital posteriorly and ventrally, and the otoccipital and squamosal posteroventrally (Figures 2-4). In general, this bone seems to be less massive than the frontal, although its thickness has certainly been affected by the abrasion of its dorsal surface.

In dorsal view, the parietals form a straight and mediolaterally wide frontoparietal contact (Figures 3B, 4A, 8). Anterolaterally, the lateral tip of the parietal articulates with the postorbital, and, whereas the parietal articulates with the frontal on the skull roof, its anteroventral margin contacts the lateral process of the laterosphenoid. Anterolaterally, the parietal forms a dorsally facing shelf of the

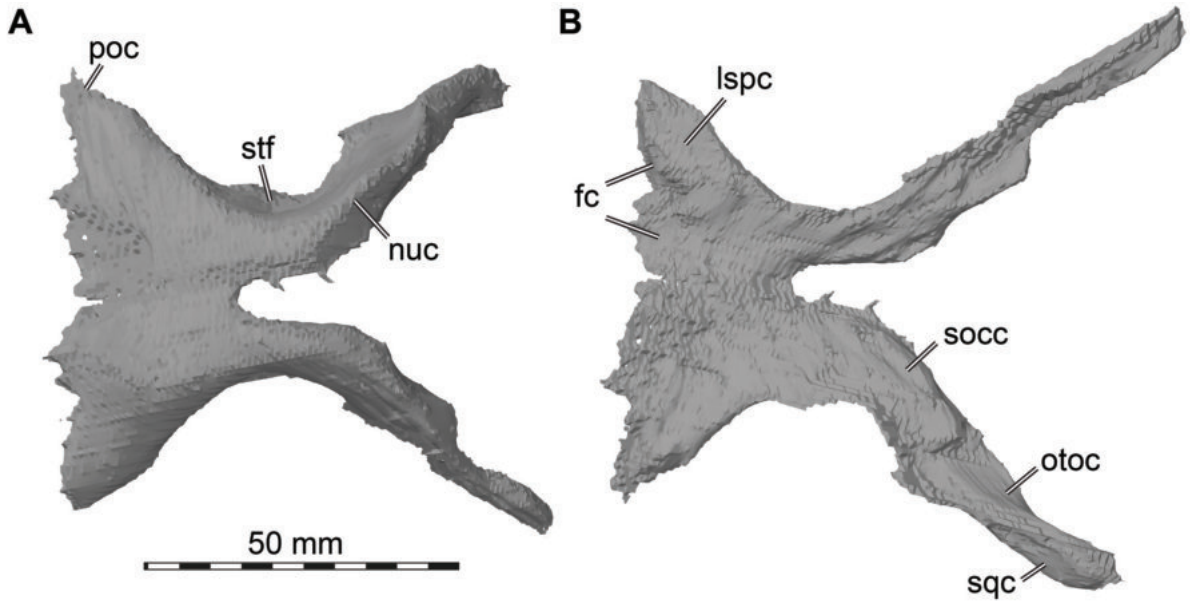

FIGURE 13. 3D renderings of the right and left parietals of *Irritator challengeri* (SMNS 58022). A, dorsal view; B, ventral view. Abbreviations: fc, frontal contact; lspc, laterosphenoid contact; nuc, nuchal crest base; oto, otoccipital contact; poc, postorbital contact, socc, supraoccipital contact; stf, supratemporal fossa; sqc, squamosal contact.

supratemporal fossa that is continuous with the portion of the fossa on the frontal and clearly delimited by a raised rim medially, placed c. 10 mm lateral to the midline of the joined parietals. The midsection of the parietals is constricted to approximately one-third the width of the frontal suture. Whereas the anterior portion is flat and faces dorsally, in the mid-section, the sides curve downwards towards the contact with the lateral braincase wall, formed by the laterosphenoid, and, more posteriorly, the otoccipital. The lateral surface is deeply concave anteroposteriorly in dorsal view, forming the medial border of the supratemporal fossa. A median sagittal ridge, as seen in *Suchomimus* and *Ceratosuchops* (MS, pers. obs. on cast, MNN GDF 214; Barker et al., 2021), might have been present, but if so, was eroded in *Irritator*. Posteriorly, the parietals of *Irritator* diverge laterally into two more vertically oriented, posterolateroventrally directed occipital wings, which articulate on the dorsal skull surface along the contact of the paraoccipital processes and the squamosal. As described by Sues et al. (2002), the distal ends of the wings taper and are slightly twisted (Figures 8, 13-14). Posteromedially, the parietals receive a bifurcating process of the supraoccipital. Here, breakage creates a hole that penetrates through the skull roof and exposes parts of the interior of the braincase.

The parietals contact the laterosphenoids ventrally, with the laterosphenoid buttressing the parietal along nearly its entire length. In the posteriormost section only, the parietals rest upon the supraoccipital and the otoccipital. There are very small, isolated cavities within the parietal. In dorsal view, these are situated posterolaterally to the hole that leads into the braincase.

Postorbital

Only the left postorbital is preserved (Figure 15). As noted by Sues et al. (2002), it has been disarticulated from its surrounding bones and turned around 45° so that the distal half of the descending jugal process is hidden by matrix and the lacrimal, and only the lateral side of the area where the three rami meet is exposed (Figure 1A). Our CT data made it possible to reconstruct the complete morphology of the postorbital. The element is T-shaped, anteroposteriorly short, mediolaterally thin, and dorsoventrally tall, with the ventral process being about twice as long as the approximately equally long anterior and posterior processes. As is usual in basal tetanurans, both the anterior and posterior process are set at an angle of approximately 90° towards the ventral process, whereas the anterior process is directed anterodorsally in many non-avian coelurosaurs (e.g., Makovicky et al., 2004; Norell and Makovicky, 2004; Rauhut et al., 2018). The lateral and

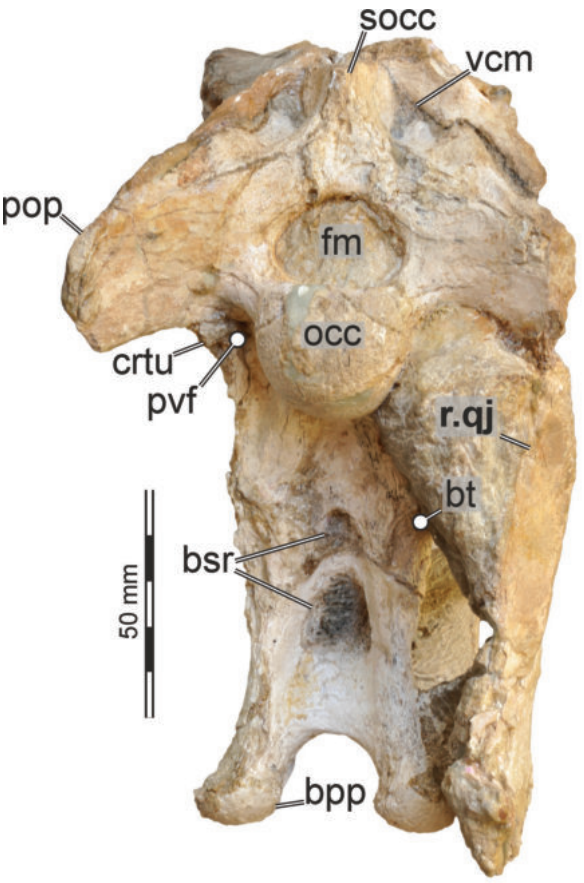

FIGURE 14. Photograph of the braincase of *Irritator challengeri* (SMNS 58022) in posterior view. Note that bones are labelled in bold, and other anatomical structures in regular font. Abbreviations: bpp, basipterygoid process of parabasisphenoid; bsr, basisphenoid recess; bt, basal tuber; crtu, crista tuberalis; fm, foramen magnum; occ, occipital condyle; pop, paroccipital process; pvf, posterior vagal foramen; r.qj, right quadratojugal; socc, supraoccipital crest; vcm, vena capitis media foramen.

medial surfaces of the postorbital are generally smooth. The postorbital contacts the frontal, parietal and laterosphenoid anteromedially, the squamosal posteriorly and the jugal ventrally.

The anterior (frontal) process of the postorbital forms the posterodorsal margin of the orbit. The process articulates with the frontal, parietal and laterosphenoid medially, so that the frontal is more laterally positioned than other bones that are involved in contributing to the dorsal orbital margin (Figures 2-4). In anterior view, the broad anterior surface of the postorbital, which forms the posterior wall of the orbital fossa, is entirely exposed. This indicates that the eyes may have faced at least partially forward, allowing for some stereoscopic vision (see also Stevens, 2006; Arden et al., 2019). The anterior end of the frontal process of the postorbital is blunt and slightly downturned. A notable supraorbital rugosity is absent, in contrast to some large megalosaurids, such as *Torvosaurus* (Britt, 1991) and *Wiehenvenator* (Rauhut et al., 2016), and allosauroids, such as *Allosaurus* (Madsen, 1976), *Sinraptor* (Currie and Zhao, 1994), and *Acrocanthosaurus* (Eddy and Clarke, 2011). However, at the anterolateral end of the raised orbital margin, a small, anteroposteriorly elongate lateral tubercle is present.

On the medial surface of the anterior process, the postorbital forms an anteroposteriorly broad but mediolaterally short shelf, the medial surface of which bears the articulation facets for the medially adjacent bones (Figure 15C). A large anterior socket for the articulation with the frontal is subdivided by two anterodorsally inclined ridges into two, anterodorsally open slots that indicate the facets for the frontal anteriorly and the parietal posteriorly. A small, oval depression posteroventral to these facets receives the lateral laterosphenoid head. This socket for the laterosphenoid is thus relatively smaller than in most non-avian theropods and entirely placed on the anterior process of the postorbital, whereas it is usually found at the junction of the three postorbital processes (e.g., Madsen, 1976; Currie and Zhao, 1994). A thickened area just dorsal to this socket probably represents the contact with the lateralmost tip of the parietal. The morphology of the medial surface of the anterior process is very similarly developed in the megalosauroid *Dubreuillosaurus* (Allain, 2002). In dorsal view, the posterior border of this medial shelf marks the anterior border of the supratemporal fenestra, and its dorsal surface flexes anterodorsally to form the postorbital portion of the supratemporal fossa, which is thus directed posterodorsally, as the frontal supratemporal fossa.

The anterior and posterior processes of the postorbital form a dorsal bar that contributes to the T-shape of the element. The dorsal margin of the postorbital that links these processes is straight and has a sharp edge along the lateral margin of the supratemporal fenestra, where the dorsomedially curving lateral side meets the vertical medial side in a sharp angle.

The short and straight posterior (squamosal) process of the postorbital fits into a deep notch, formed between two anterior processes of the squamosal. The posterior process of the postorbital tapers posteriorly and bears an anteroposteriorly elongated medial ridge that would have been

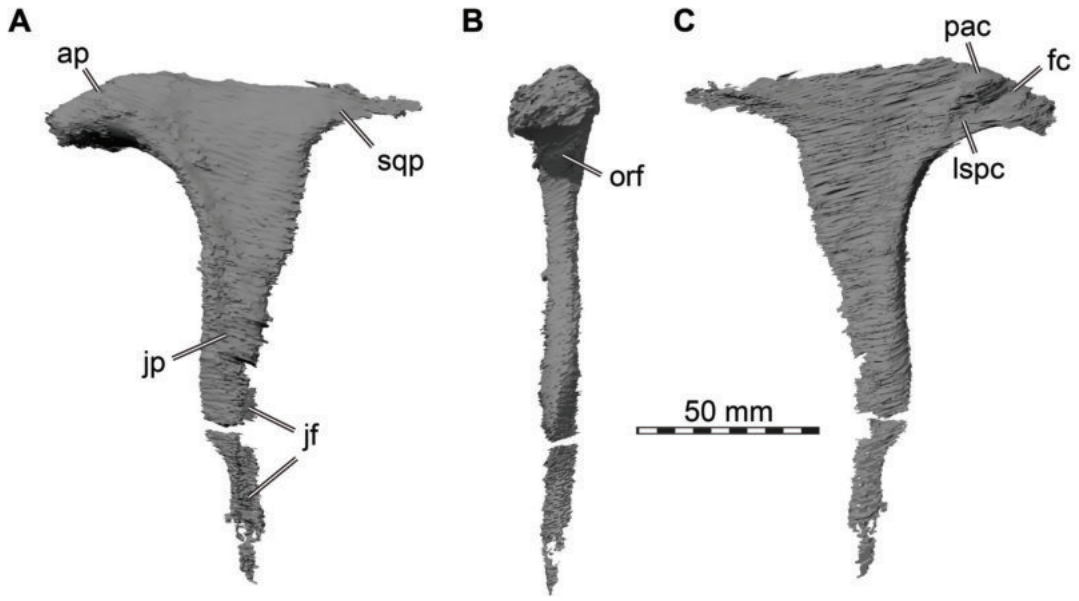

FIGURE 15. 3D renderings of the left postorbital of *Irritator challengeri* (SMNS 58022). A, lateral view; B, anterior view; C, medial view. Abbreviations: ap, anterior process; fc, frontal contact; jf, jugal facet; jp, postorbital jugal process; lspc, laterosphenoid contact; orf, orbital fossa; pac, parietal contact; sqp, squamosal process.

wedged between the anterior processes of the squamosal, giving this process a twisted appearance, reminiscent of the 'helical' articulation between the postorbital and squamosal seen in many carcharodontosaurids (Carrano et al., 2012). The squamosal process of the postorbital and the two anterior processes of the squamosal separate the supratemporal fenestra from the infratemporal fenestra.

The ventrally descending (jugal) process of the postorbital is broken in the center, but the distal third could be identified in the CT data, being in close association with the rest of the bone (Figure 15). The process tapers ventrally. Its anterior margin represents the posteroventral border of the orbit. The entire orbital margin is mediolaterally expanded to form the posterior orbital fossa, but the width of the fossa narrows ventrally (Figure 15B). Therefore, both the lateral and the medial orbital margin stand out from the surface of the postorbital as slightly raised ridges (Figure 3A). At the level of the contact with the jugal, where the orbit becomes ventrally constricted between lacrimal, postorbital and jugal, the expanded anterior surface of the postorbital gives way to an anterior ridge with a sharp edge. The dorsal half of the posterior margin of the ventral postorbital process forms the anterodorsal margin of the infratemporal fenestra and is gently convex in lateral view. Around its mid-length, the posterior margin of the jugal process of the postorbital becomes straight to slightly concave and deeply recessed posteriorly, forming a U-shaped cross-section that receives the posterodorsal process of the jugal, as in megalosaurids (Britt, 1991; Sereno et al., 1994; Allain, 2002; Sadleir et al., 2008; Rauhut et al., 2016). Concerning the two other postorbitals that have recently been assigned to spinosaurids (*Ceratosuchops*, Barker et al., 2021; *Suchomimus*, Sereno et al., 2022), it might be worth mentioning that the postorbital of *Irritator* is a much more delicate bone (especially on its dorsal portion) in comparison to these elements. Whereas the anterior process of the postorbital of *Irritator* is generally mediolaterally slender and lacks a prominent orbital boss or brow, a mediolaterally wide anterior process and a thickened brow are developed in material assigned to *Ceratosuchops* (Barker et al., 2021) and *Suchomimus* (Sereno et al., 2022), and the latter shows clear rugosities, as it is common in carcharodontosaurids (e.g., Motta et al., 2016). Furthermore, the mediolaterally widened, spoon-shaped posterodorsal articular facet for the squamosal is much wider in the elements referred to *Ceratosuchops* (Barker et al., 2021) and *Suchomimus* (Sereno et al., 2022) than in *Irritator*. Such a widened posterior process of the postorbital, resulting in a helical articulation with the squamosal, was considered to represent a carcharodontosaurid synapomorphy by Carrano et al. (2012). Additionally, there is no infraorbital pro-

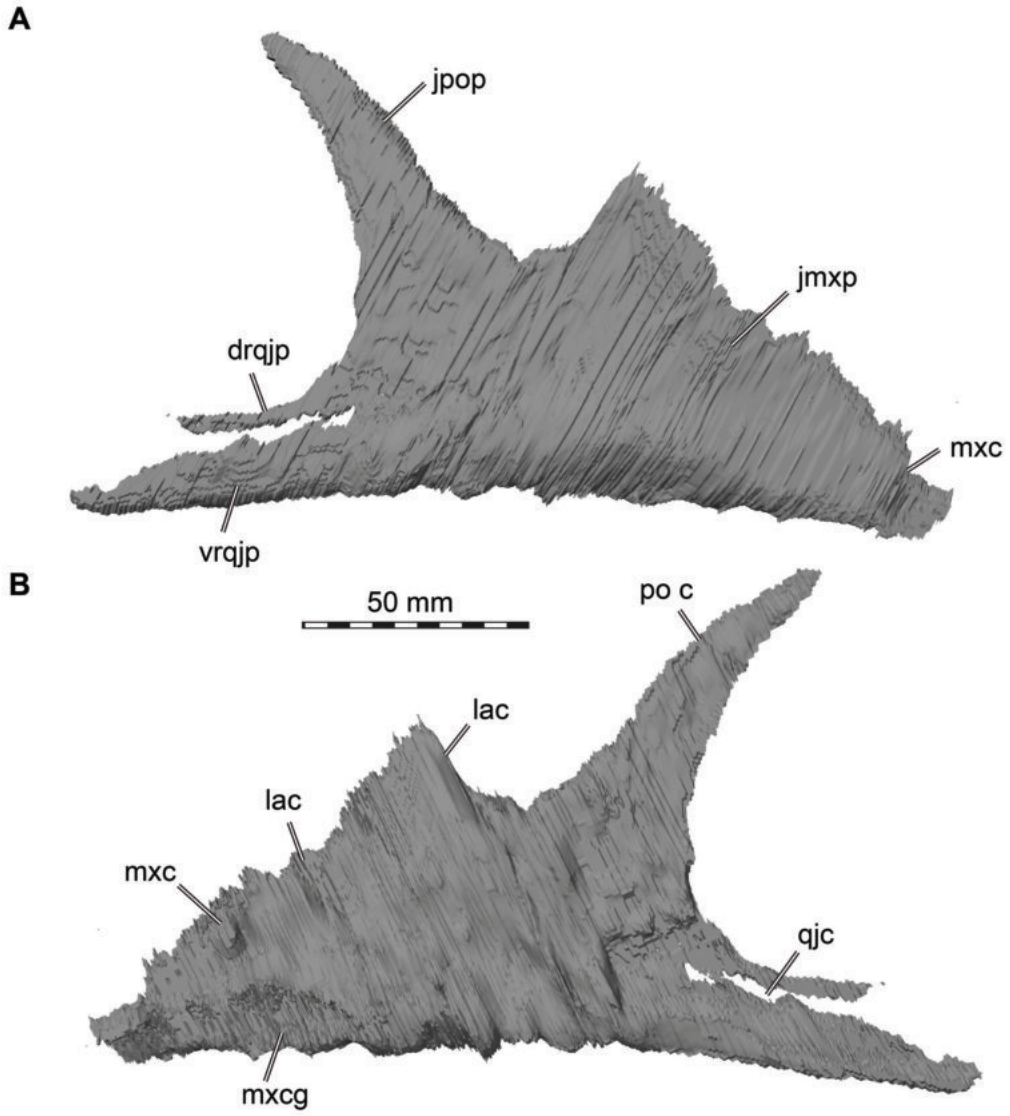

FIGURE 16. 3D renderings of the right jugal of *Irritator challengeri* (SMNS 58022). A, lateral view; B, medial view. Abbreviations: drqjp, dorsal ramus of quadratojugal process; jmxp, maxillary process; jpop, postorbital process; lac, lacrimal contact; mxc, maxillary contact; mxcg, maxillary contact groove; poc, postorbital contact; qjc, quadratojugal contact; vrqjp, ventral ramus of quadratojugal process.

cess in *Irritator* and the material assigned to *Suchomimus* (Sereno et al., 2022); on the other hand, there is a well-developed infraorbital process in the postorbital referred to *Ceratosuchops* (Barker et al., 2021). Such an infraorbital process is also prominent in carcharodontosaurids (Sereno et al., 1996; Sereno and Brusatte, 2008; Motta et al., 2016; Canale et al., 2022). Thus, in comparison with the postorbital of *Irritator*, it seems possible that the postorbitals were erroneously referred to spinosaurids. The element referred to *Ceratosuchops* (which also differs somewhat in preservation from the rest of the material) might represent the early branching carcharodontosaurian *Neovenator salerii*, which is from the same stratigraphic unit (Brusatte et al., 2008), whereas both the postorbital and the frontal referred to *Suchomimus* by Sereno et al. (2022) are reminiscent of the respective elements of the early carcharodontosaurzid *Eocarcharia dinops* from the same formation (Sereno and Brusatte, 2008).

Jugal

Both jugals are preserved (Figure 16), but the right jugal is better preserved than the left (Figure 1). The jugal has three primary processes (maxillary, quadratojugal, and postorbital process), which contact the maxilla anteriorly and medially, the lacrimal anterodorsally, the postorbital posterodorsally, the quadratojugal posteriorly, and the ectopterygoid medially. The jugal body is mediolaterally thin but notably thickened towards its ventral margin, forming a dorsoventrally broad longitudinal ridge on the lateral side just above the ventral margin, as is present in many non-avian theropods, and a medially thickened ventral rim. The ventral margin of the jugal is very slightly concave, in contrast to the usually convex ventral margin of the jugal in most non-avian theropods (Sullivan and Xu, 2017).

The anterior process is triangular in front of the orbit in lateral outline, with the posterior part of the process being dorsoventrally expanded in comparison with the suborbital jugal body, while the anterior end tapers into an acute angle. The anterior process articulates with the maxilla, lacrimal, and probably the ectopterygoid medially (Figures 2-4). As described in the maxilla section, the maxilla has two posterior rami, the ventral of which contacts the ventromedial surface of the anterior process of the jugal, whereas the dorsal maxillary process contacts the dorsolateral margin of the jugal, thus tightly interlocking the cheek region. The jugal has a groove along its ventromedial surface for the posteroventral process of the maxilla. Just posterior to the contact with this maxillary process, the ectopterygoid contacts the medial surface of the jugal. However, the exact nature of this contact is unclear due to disarticulation of the ectopterygoid in the fossil and the lack of a clear ectopterygoid facet on the reconstructed medial jugal surface based on the CT data. The ventral process of the lacrimal contacts the mostly straight, anteroventrally inclined dorsal margin of the anterior process. The highest dorsoventral extent of the anterior process marks the transition point to the orbital margin of the jugal. Here, the dorsal margin of the jugal slopes down, forming a narrowly rounded anteroventral rim of the orbital opening. The suborbital body of the jugal is notably high, being almost 2.5 times the height of the quadratojugal process.

The postorbital process of the jugal is elongate, triangular in lateral outline and posterodorsally inclined, with a slightly convex anterior and a gently concave posterior margin. The process is not as steep as in other large-bodied theropods like, for example, *Majungasaurus crenatissimus* (Sampson and Witmer, 2007), *Acrocanthosaurus* (Eddy and Clarke, 2011), and *Alioramus altai* (Brusatte et al., 2012). The elongated process is slender and tapers into a rounded dorsal tip. A marked, rounded lateral ridge is present along the contact with the postorbital and the posteroventral margin of the orbit, as in some other non-avian theropods (e.g., *Acrocanthosaurus*; Eddy and Clarke, 2011).

Posteriorly, a long and slender quadratojugal process of the jugal is developed. This process bifurcates into two rami, which receive the quadratojugal; this bifurcation extends anteriorly to the level of the posterior border of the postorbital process. The dorsal quadratojugal process of the jugal is dorsoventrally narrower and anteroposteriorly shorter than its ventral counterpart, which is more robust and embraces the ventral margin of the quadratojugal (Figures 2A, 16). A longitudinal groove flanks the incision between the two processes along the ventral process on the medial side, and the distal end of the ventral process flexes medially in its ventral part. Together with the postorbital process, the quadratojugal process of the jugal forms the anteroventral border of the infratemporal fenestra (Figure 2A). Whereas the dorsal quadratojugal process of the jugal reaches only slightly posterior to the mid-length of this opening, the ventral process extends to the level of its posterior border.

In this context, it may be worth mentioning that the element that was identified as the jugal in the holotype of *Baryonyx* does not resemble the jugal of *Irritator*, since the supposed dorsal border that makes up the ventral margin of the orbit is much smaller and there are medial articulation facets on this element that do not have an equivalent in *Irritator*. This bone of *Baryonyx* may rather represent a prearticular (as suggested by Sereno et al., 1998), with the putative quadratojugal contact instead being the contact for the surangular and articular, and the ectopterygoid facet instead being the facet for the angular.

Quadratojugal

Only the right quadratojugal is preserved (Figures 1B, 17). It is L-shaped, with a tall dorsal process articulating with the quadrate medially and the squamosal dorsally, and a slightly shorter anterior process that meets the posterior process of the jugal (Figures 2-4). The two processes of the quadratojugal meet at an angle of approximately 90° and form the concave posteroventral margin of

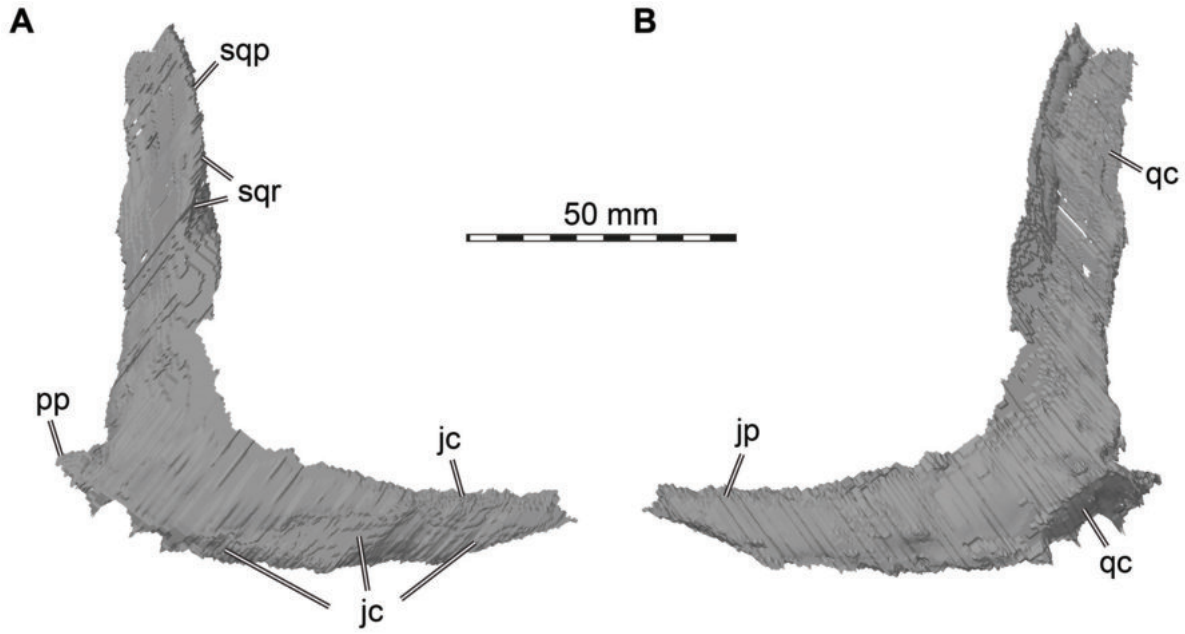

FIGURE 17. 3D renderings of the right quadratojugal of *Irritator challengeri* (SMNS 58022). A, lateral view; B, medial view. Abbreviations: jc, jugal contact; jp, jugal process; pp, posterior process; qc, quadrate contact; sqp, squamosal process; sqr, squamosal ridge.

the infratemporal fenestra. It might be worth mentioning here that the bone figured as the quadrate of *Irritator* by Hendrickx et al. (2016: fig. 9M, N) represents a part of the quadratojugal, and the structure identified as the quadrate foramen by these authors is a break in this bone.

The jugal process of the quadratojugal gradually tapers anteriorly over its entire length. The margin of the quadratojugal that is exposed in the infraorbital fenestra is sharp-edged, whereas the anterior third of the anterior process that is wedged between the jugal is shaped to facilitate this articulation: the dorsal surface is slightly broadened, and a clear facet is developed on the ventrolateral surface of the anterior process. This facet is offset from the laterally exposed part of the process by a notable 'step' and would have been covered laterally by the ventral posterior process of the jugal, fitting into the groove on the medial side along the dorsal rim of the ventral posterior process of the jugal (Figures 2, 4B).

The posteroventral region of the quadratojugal has a roughened medial surface for the articulation with the quadrate. Along this articulation, the posterior margin of the quadratojugal is gently curved posteromedially towards the quadrate, wrapping around the posteroventral margin of the latter (Figures 1B, 2A, 3B, 14), as is the case in many non-avian theropods (Rauhut, 2003). Here, a small, tab-like posterior process possibly marks the posteriormost contact between the two bones (Figures 3B, 17).

The dorsal squamosal process of the quadratojugal is an anteroposteriorly comparatively wide, but mediolaterally thin, plate of bone. At about its mid-height, a ridge appears towards its anterior margin that extends dorsally, forming a marked, anterolaterally directed edge. In the ventral part, where this edge is developed as a lateral ridge, a thin sheath of bone is present, facing somewhat anteromedially. The region posterior to the ridge and the emerging dorsal edge is inclined posteromedially, resulting in a slightly posteromedially twisted appearance of the process. The dorsal part of the squamosal process is damaged, but the contact area for the quadratojugal on the squamosal indicates that it was possibly tongue-shaped originally. The dorsal end of the quadratojugal was wedged between two slender processes of the squamosal, forming a large contact area with the latter bone (Figure 2A), while the medial sheath further contacts the lateral margin of the dorsal quadratojugal flange of the quadrate (Figure 3B).

Squamosal

The squamosal is solely represented by the left element, which is damaged by a mediolaterally oriented subvertical crack on its main body (Figure 18). It is preserved anterior to the basisphenoid (Figure 1A) and hence is situated far more ventro-

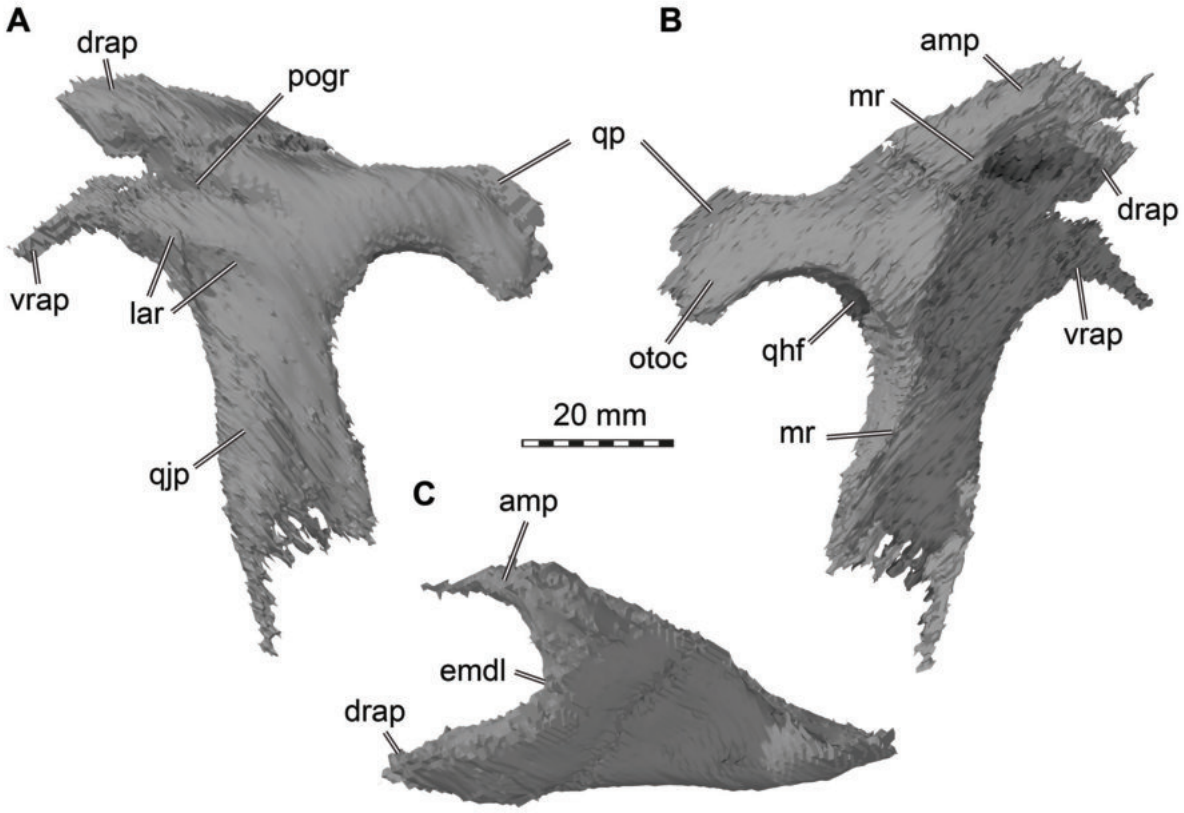

FIGURE 18. 3D renderings of the left squamosal of *Irritator challengeri* (SMNS 58022). A, lateral view; B, medial view; C, dorsal view. Abbreviations: amp, anteromedial process; drap, dorsal ramus of anterior process; emdl, emarginated dorsal lamina; lar, lateral ridge; mr, medial ridge; pogr, postorbital groove; qhf, quadrate head facet; qjp, quadratojugal process; qp, quadrate process; vrap, ventral ramus of anterior process.

medially and anteriorly in the fossil compared to its usual anatomical position. Our CT data reveal an almost completely preserved squamosal. The squamosal contacts the postorbital anteriorly, the parietal, otoccipital, and possibly the supraoccipital posteriorly and medially, and the quadrate and quadratojugal ventrally (Figures 2-4). As it is usual in non-avian theropod squamosals, the bone is composed of four processes, an anterior postorbital process, a posterior process forming the roof of the cavity for the quadrate articulation, a ventral quadratojugal process, and a posteriorly placed medial process for the contact with the parietal.

The element has the greatest extent in its dorsoventral dimension, due to a long, descending quadratojugal process, but has unusually short anterior and medial processes, although it cannot be excluded that the anterior end of the anterior process is missing. The bone forms the posterodorsal margin of the infratemporal fenestra and parts of the lateral and the posterior margin of the supratemporal fenestra.

The dorsal surface of the squamosal body bears a large, shallow depression, resulting in a markedly concave outline of the dorsal margin between the anterior and posterior processes in lateral view. In lateral view, the squamosal has a short, bifurcated anterior postorbital process (whereas the postorbital articulated mainly laterally with the squamosal in *Irritator*, material assigned to *Suchomimus* suggests a mediolaterally wide articulation on the ventral surface of the dorsal branch of the anterior process; Sereno et al., 2022). The dorsal branch of the process is slightly shorter than its ventral counterpart and has a blunt anterior end, although it cannot be excluded that a small portion of the bone might be missing here. This dorsal branch is considerably anterodorsally directed in comparison to the quadratojugal and posterior processes. The ventral branch is slightly flexed anteroventrally, resulting in a continuously curved posterodorsal border of the infratemporal fenestra, in which the anterior part of the dorsal margin of this opening stands at an angle of c. 90° towards

the posterior margin. The ventral branch of the anterior process has a shallow lateral ridge and a pointed tip. The lateral ridge is less pronounced than in many other non-avian theropods, such as *Allosaurus* (Gilmore, 1920; Chure and Loewen, 2020), and extends posteriorly to the level of about half the anteroposterior length of the ventral process. Where both branches of the anterior process meet, they form a distinct longitudinal lateral groove that receives the squamosal process of the postorbital. The groove becomes shallower posteriorly, extending onto the mid-length of the squamosal body. However, it is deeper than high over its entire length, in accordance with the transversely broadened posterior end of the postorbital.

The medial process is placed at about the anteroposterior mid-length of the squamosal. It is triangular in outline in dorsal view and anteromedially directed. The medial process is almost as long as the dorsal branch of the anterior process (in contrast to material assigned to *Suchomimus*, where the medial process is relatively smaller and more strongly medially directed; Sereno et al., 2022). In contrast to several non-avian theropods, including Ceratosauria (Gilmore, 1920; Madsen and Welles, 2000; Sampson and Witmer, 2007; Pol and Rauhut, 2012), Allosauroidea (e.g., Madsen, 1976; Currie and Zhao, 1994; Eddy and Clarke, 2011), and a few others, the dorsal lamina between the anterior and medial process is emarginated by the supratemporal fenestra and thus concave to angled in dorsal view. The small lamina overhangs the cavity of the supratemporal fenesta, the posterolateral wall of which is formed by the main body of the squamosal. Three notable depressions are present in this wall, two are mainly posteriorly excavated. The dorsalmost depression is at the level of the base of the anterior and medial process. Ventroposteriorly, the second depression is situated at the base of the ventral process, and a third depression is more laterally excavated further ventrally, at about the mid-height of the main body of the ventral process.

A large facet for the articulation of the quadrate head is formed by the posterior process and the descending quadratojugal process. The proximal part of the posterior process is perpendicular to the ventral process, but the posterior process is flexed strongly posteroventrally, resulting in a semicircular outline of the notch for the quadrate in lateral view. There is no anteroventrally pointing flange on the posterior part (Figure 18) that would cover the quadrate head laterally, as occurs in metriacanthosaurids (e.g., Currie and Zhao, 1994) and *Acrocanthosaurus* (Eddy and Clarke, 2011), so the quadrate head is fully exposed in lateral view in the articulated skull (Figure 2A). In dorsal view, the posterior process forms a narrow triangle, with a pointed posterior tip laterally and a steeply anteromedially inclined medial edge, where the squamosal would have contacted the paroccipital process. This medial margin is rather sharp, while the lateral margin is rounded. The angle between the lateral and medial edge in dorsal view is slightly less than 45°. In ventral view, the process forms a triangular, anteroposteriorly strongly and mediolaterally weakly concave articulation facet for the quadrate head. The posteromedial side of the process that articulates with the paroccipital process bears a horizontal concavity. Anteriorly, between the base of the anteromedial process and the posterior process is a shallow medial depression. Furthermore, there is a marked medial ridge, extending from the anteromedial process to the posterior end of the posterior process, which forms the medial border of the quadrate head articulation surface.

The long quadratojugal process of the squamosal is straight and ventrally directed. It is anteroposteriorly wide and mediolaterally thin. The posterior margin of the process forms a vertically orientated, mediolaterally expanded, and ventrally thinned articulation facet for the quadrate head and shaft. The ventral end of the process has a concave margin between the thin but distinct anterior and posterior ventral processes. The anterior process is considerably longer than the posterior process; together, these two processes would have clasped the dorsal end of the quadratojugal (between these two processes, a thin lamina seems present in the squamosal assigned to *Suchomimus*; Sereno et al., 2022).

A network of different-sized cavities is present within the squamosal body, mainly behind the crack. Some further small cavities are scattered at the lateral base of the dorsal postorbital process. In a posterior direction, the cavities become bigger, interconnected, and extend ventrally and medially. The posteriormost cavities are situated dorsally to the articulation surface for the quadrate head. No unequivocal connection of this network to a pneumatic foramen could be identified.

Quadrate

Only the left quadrate is preserved (Figures 1, 19). Other than a mediolaterally oriented crack on the upper half of the quadrate foramen, the bone is complete. It is disarticulated from its original position. In the fossil, the quadrate head is visible

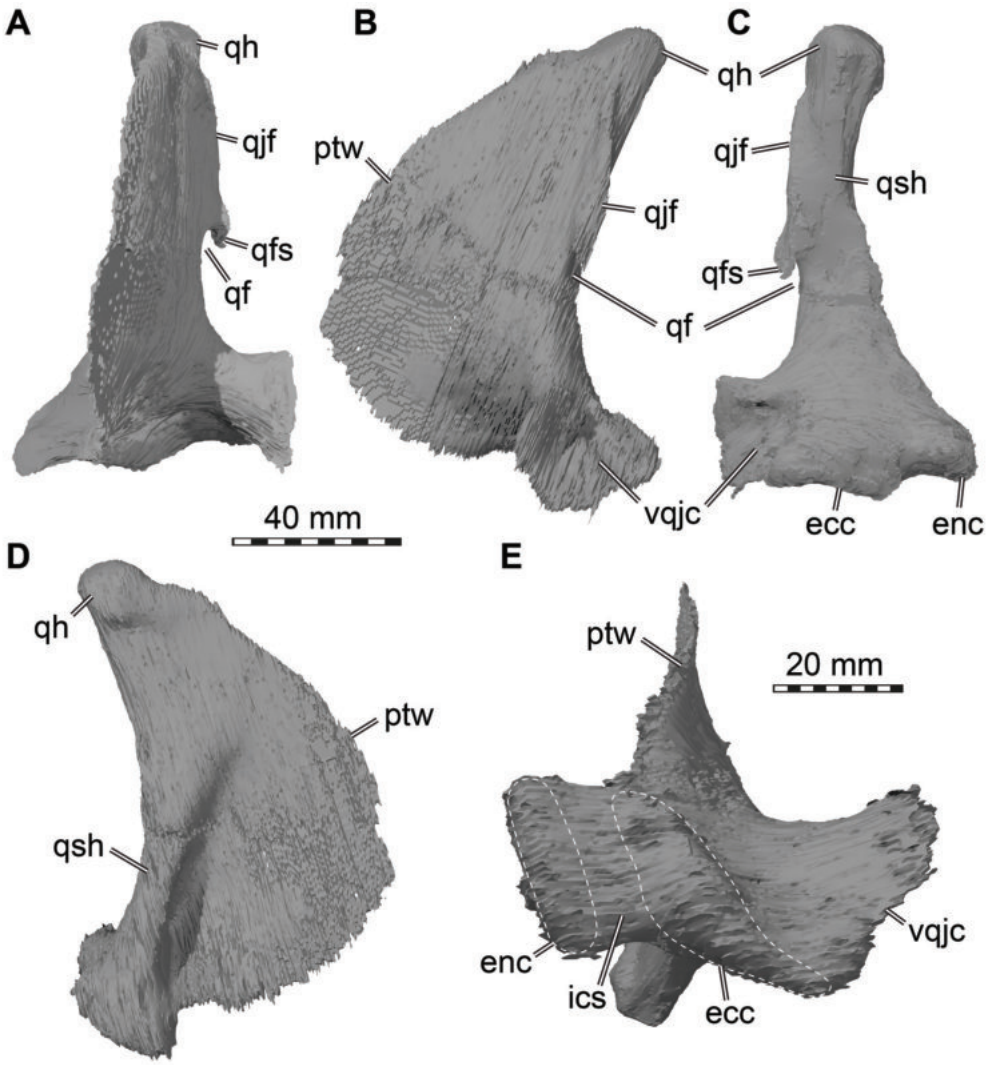

FIGURE 19. 3D renderings of the left quadrate of *Irritator challengeri* (SMNS 58022). A, anterior view; B, lateral view; C, posterior view; D, medial view; E, ventral view (anterior at top). Note that A–D are to same scale, E with separate scale bar. Dashed lines in E are approximate shapes of quadrate articulation condyles. Abbreviations: ecc, ectocondyle; enc, entocondyle; ics, intercondylar sulcus; ptw, pterygoid wing; qh, quadrate head; qjf, quadratojugal flange; qf, quadrate foramen; qfs, quadrate foramen spur; qsh, quadrate shaft; vqjc, ventral quadratojugal contact.

through the right antorbital fenestra, while the left lateral aspect of the pterygoid flange is exposed below the left jugal. However, we were able to fully reconstruct the quadrate with the help of CT data. The quadrate contacts the pterygoid and, possibly, the epipterygoid anteriorly, the quadratojugal laterally, the squamosal and possibly the otoccipital dorsally, and the surangular and articular ventrally (Figures 2-4).

The quadrate is dorsoventrally tall with the quadrate head forming the apex of the bone and the contact with the squamosal. The quadrate shaft connects the quadrate head with the mediolaterally wide base, where the quadrate articulates with the lower jaw. Anteriorly, the quadrate forms an expanded, semi-oval sheet of bone, the pterygoid wing.

The dorsal quadrate head is developed as a semicircular condyle in medial or lateral view, as in non-avian theropods. In proximal outline, the head is subquadrangular in outline, as in *Baryonyx*, but unlike the more triangular shape seen in a quadrate referred to *Suchomimus* (Hendrickx et al., 2016). The quadrate head of *Irritator* is slightly wider mediolaterally than long anteroposteriorly, and its anterior side is slightly wider than the posterior one. Our skull reconstruction shows that the quadrate head was capped by the squamosal, and

posteromedially additionally braced by the anterolateral surface of the paroccipital process of the otoccipital. The posterior margin of the quadrate shaft is distinctly concave between the quadrate head and ventral articulation surface for the jaw; however, both the dorsal and ventral half of the shaft are posteriorly rather straight, with a marked flexure at about mid-height of the bone. The quadrate shaft is slightly bent medially, mainly caused by the marked medial expansion of the ventral end and a medial expansion of the quadrate head, like the juvenile spinosaurid quadrate FSAC KK 18120 (Lakin and Longrich, 2019). In contrast, the quadrates of *Baryonyx* and *Suchomimus* are rather laterally inclined, with a slightly convex medial margin of the shaft (Hendrickx et al., 2016). The quadratojugal flange is represented by an offset ridge, extending on the lateral side of the quadrate shaft. Its dorsal end is placed just below the quadrate head, at about the anteroposterior mid-width of the shaft, but it then extends posteroventrally and follows the posterolateral edge of the quadrate shaft. Ventrally, at about the half height of the quadrate, the ridge gives way to the quadrate foramen, which is proportionally larger than in material assigned to *Spinosaurus* (Hendrickx et al., 2016). The foramen in *Irritator* is shaped like an elongate drop in outline, becoming wider ventrally. The medial margin of the foramen is formed by the lateral side of the quadrate shaft, while the ventral margin is formed by a short but broad lateral process that forms the ventral quadratojugal contact. The foramen is laterally open but would have been enclosed by the quadratojugal in the articulated skull. Only at the dorsal end of the foramen, a small ventral spur of the lateral edge of the quadratojugal forms a small part of its lateral border. The ventral quadratojugal contact is broad, and forms a posterodorsally open, cup-shaped articulation facet for the quadratojugal.

Ventrally, the quadrate is expanded to more than three times the minimal width of the quadrate shaft, with most of this expansion being accounted for by the medial side. It articulates with the lower jaw via two quadrate condyles. The slightly curved, laterally concave, lens-shaped, and somewhat mediolaterally oriented ectocondyle lies lateral to the smaller and anteromedially-to-posterolaterally oriented entocondyle (Figure 19E). The medial half of the articular end with the entocondyle is approximately twice as deep anteroposteriorly as the lateral half. The condyles are separated by a broad, shallow intercondylar sulcus that is slightly anteromedially inclined. The intercondylar sulcus is more distinct than in other spinosaurids, e.g., FSAC KK 18120, *Spinosaurus*, and *Baryonyx* (Lakin and Longrich, 2019; Hendrickx et al., 2016).

Anteriorly, the quadrate forms a laminar process, the pterygoid wing, which extends almost over the entire height of the element from the quadrate head to the intercondylar sulcus at the base of the quadrate. The anterior margin of the pterygoid wing is convex, and the wing is anteroposteriorly deepest around its mid-height. This part of the wing overlies the quadrate ramus of the pterygoid laterally, and possibly is in contact with the epipterygoid at its anterior end (Figure 2A). The entire pterygoid wing is gently convex laterally. On the medial side, there is a large, oval fossa at the base of the pterygoid wing. This fossa houses a small pneumatic foramen in its deepest part, leading to a small medial cavity at the base of the quadrate shaft. In contrast to other non-avian theropods (e.g., *Sinraptor*; Currie and Zhao, 1994), the ventral rim of the pterygoid wing does not seem to be flexed medially to form a medial shelf underneath the pterygoid (Figure 19A).

CT data reveal that there is a dorsoventrally tall network of irregularly formed cavities situated within the quadrate shaft. This network extends from the anterior margin of the quadrate head to the lower half of the quadrate foramen. This network of cavities does not seem to have a connection to an external pneumatic foramen.

Braincase

The braincase of *Irritator* is nearly completely preserved, with most bones in near-perfect articulation with one another (Figures 8, 14, 20-26). The general shape of the dorsoventrally high and anteroposteriorly short braincase has been described by Sues et al. (2002), as has the shape and size of the foramen magnum and many aspects of the directly visible morphology of the braincase elements and the openings for nerves and blood vessels.

The cavity for the vestibular apparatus is housed within the prootic (anterolaterally), otoccipital (posteroventrally), and the supraoccipital (posterodorsally). The cavity for the cochlea is formed by the prootic, otoccipital, and basioccipital. The floccular fossa is contained within the prootic, supraoccipital, and otoccipital (distally).

The following description of the braincase bones is based on the bone surfaces directly visible on the specimen and models that were segmented from the µCT data. Our braincase models are solely based on µCT data (except for the rear-

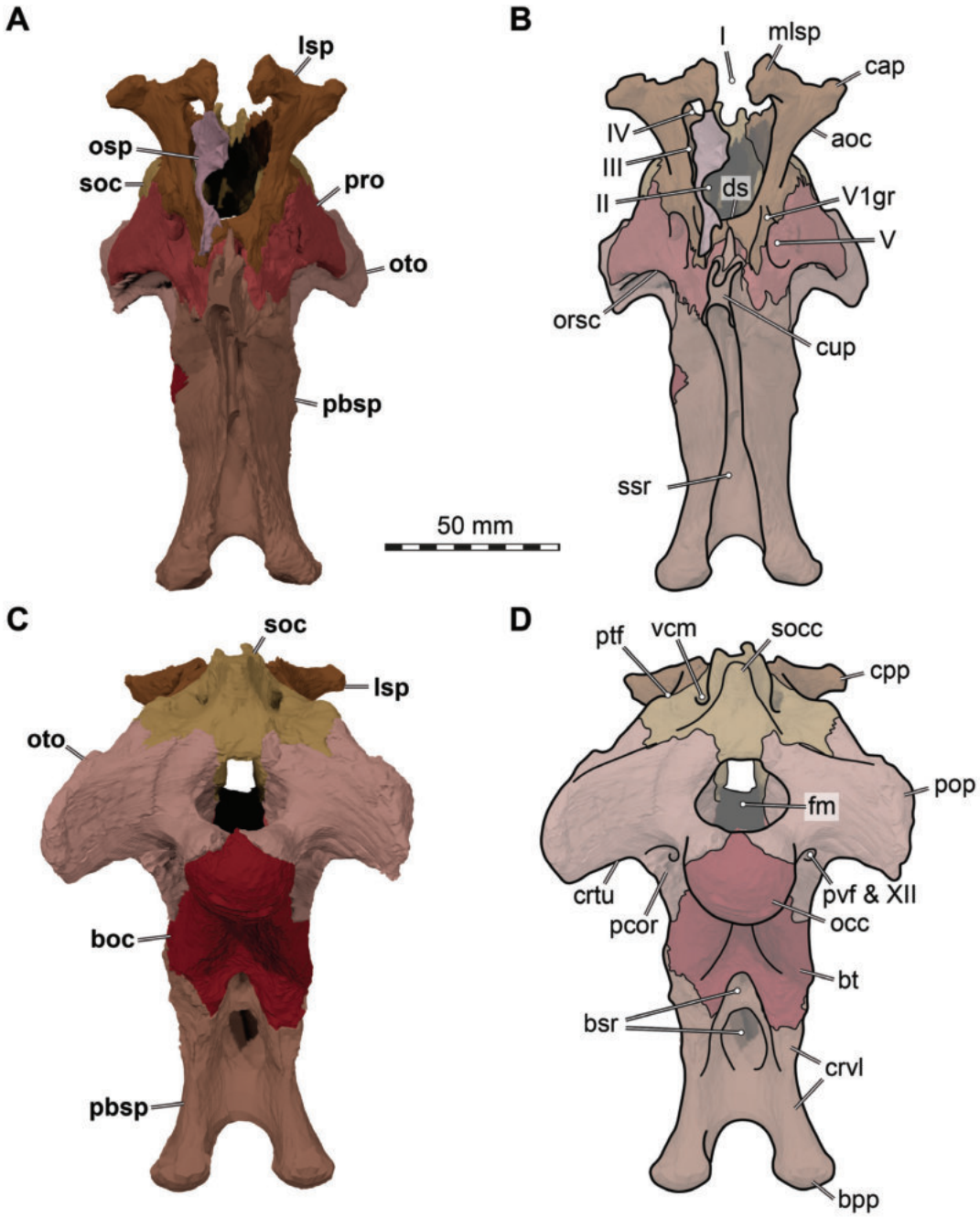

FIGURE 20. 3D renderings of the articulated braincase elements of *Irritator challengeri* (SMNS 58022). A, anterior view; B, anterior view with interpretative line drawings; C, posterior view; D, posterior view with interpretative line drawings. Note that bones are labelled in bold, and other anatomical structures in regular font. Abbreviations: aoc, antotic crest; boc, basioccipital; bpp, basipterygoid process; bsr, basisphenoid recess; bt, basal tuber; cap, capitate process; crtu, crista tuberalis; crvl, crista ventrolateralis; cup, cultriform process; ds, dorsum sellae; fm, foramen magnum; lsp, laterosphenoid; mlsp, medial laterosphenoid process; occ, occipital condyle; osp, orbitosphenoid; oto, otoccipital; orsc, orbitosphenoidal crest; pbsp, parabasisphenoid; pcor, paracondylar recess; pop, paroccipital process; pro, prootic; ptf, posttemporal fenestra; pvf and XII, posterior vagal foramen and hypoglossal nerves (CN XII), see Figure 23 for details of this region; soc, supraoccipital; socc, supraoccipital crest; ssr, subsellar recess; vcm, vena capitis media foramen; I, olfactory nerve (CN I) foramen; II, optic nerve (CN II) foramen; III, oculomotor nerve (CN III) foramen; IV, trochlear nerve (CN IV) foramen; V, trigeminal nerve (CN V) foramen; V_1gr, ophthalmic groove for V_1 branch.

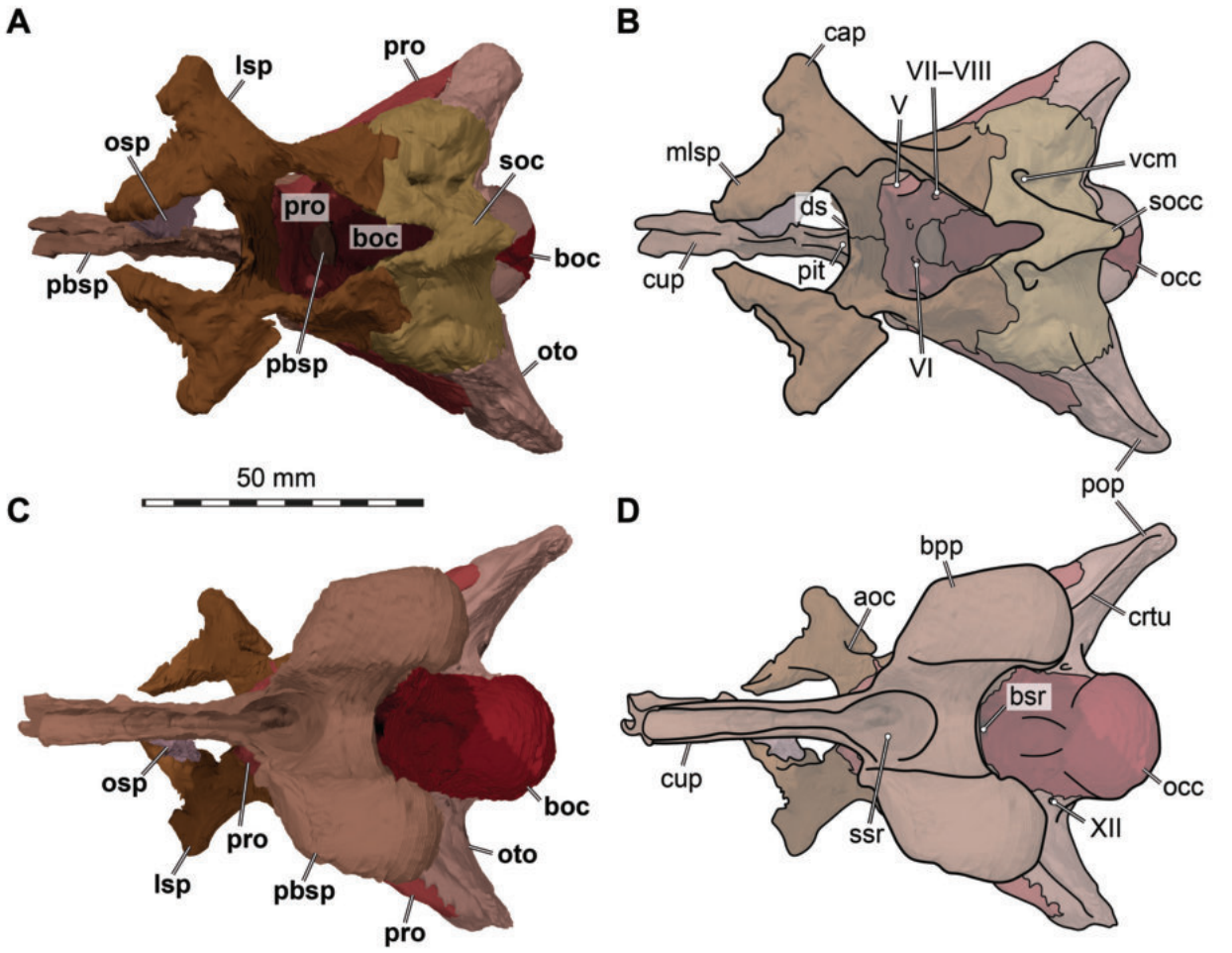

FIGURE 21. 3D renderings of the articulated braincase elements of *Irritator challengeri* (SMNS 58022). A, dorsal view; B, dorsal view with interpretative line drawings; C, ventral view; D, ventral view with interpretative line drawings. Note that bones are labelled in bold, and other anatomical structures in regular font. Abbreviations: aoc, antotic crest; boc, basioccipital; bpp, basipterygoid process; bsr, basisphenoid recess; cap, capitate process; crtu, crista tuberalis; cup, cultriform process; ds, dorsum sellae; lsp, laterosphenoid; mlsp, medial laterosphenoid process; occ, occipital condyle; osp, orbitosphenoid; oto, otoccipital; pbsp, parabasisphenoid; pit, pituitary fossa (sella turcica); pop, paroccipital process; pro, prootic; soc, supraoccipital; socc, supraoccipital crest; ssr, subsellar recess; vcm, vena capitis media foramen; V, trigeminal nerve (CN V) foramen; VI, (posterior) foramen for abducens nerve (CN VI); VII–VIII, medial fossa for entry of facial nerve (CN VII) and optic nerve (CN VIII) into prootic; XII, hypoglossal nerve (CN XII) foramen.

ranged skull reconstructions, which source from the medical CT data only; see Figures 2-4), so do not include the entirety of the cultriform process of the parabasisphenoid, which is located mostly outside of the region that underwent µCT scanning.

Supraoccipital

The supraoccipital is present but lacks its dorsalmost portion (Figures 1, 8, 14). It is an unpaired bone, forming the dorsal part of the occipital complex (Figures 20-24). Our µCT data suggest that an elongate and roughly rectangular portion of the supraoccipital is exposed on the lateral surface of the braincase, dorsal to the prootic and bordered posteriorly by the otoccipital, dorsally by the parietal, and anteriorly by the laterosphenoid. Although the sutures are difficult to discern in the scan, the relationships between these elements can be confirmed on both sides of the braincase directly on the fossil (Figure 1). This exposure is unusual for non-avian theropods (see, e.g., *Majungasaurus*; Sampson and Witmer, 2007; *Allosaurus*; Chure and Loewen, 2020; *Murusraptor barrosaensis*; Paulina-Carabajal and Currie, 2017; see also Paulina-Carabajal, 2015). However, the bone surface of this anterolateral exposure of the supraoccipital

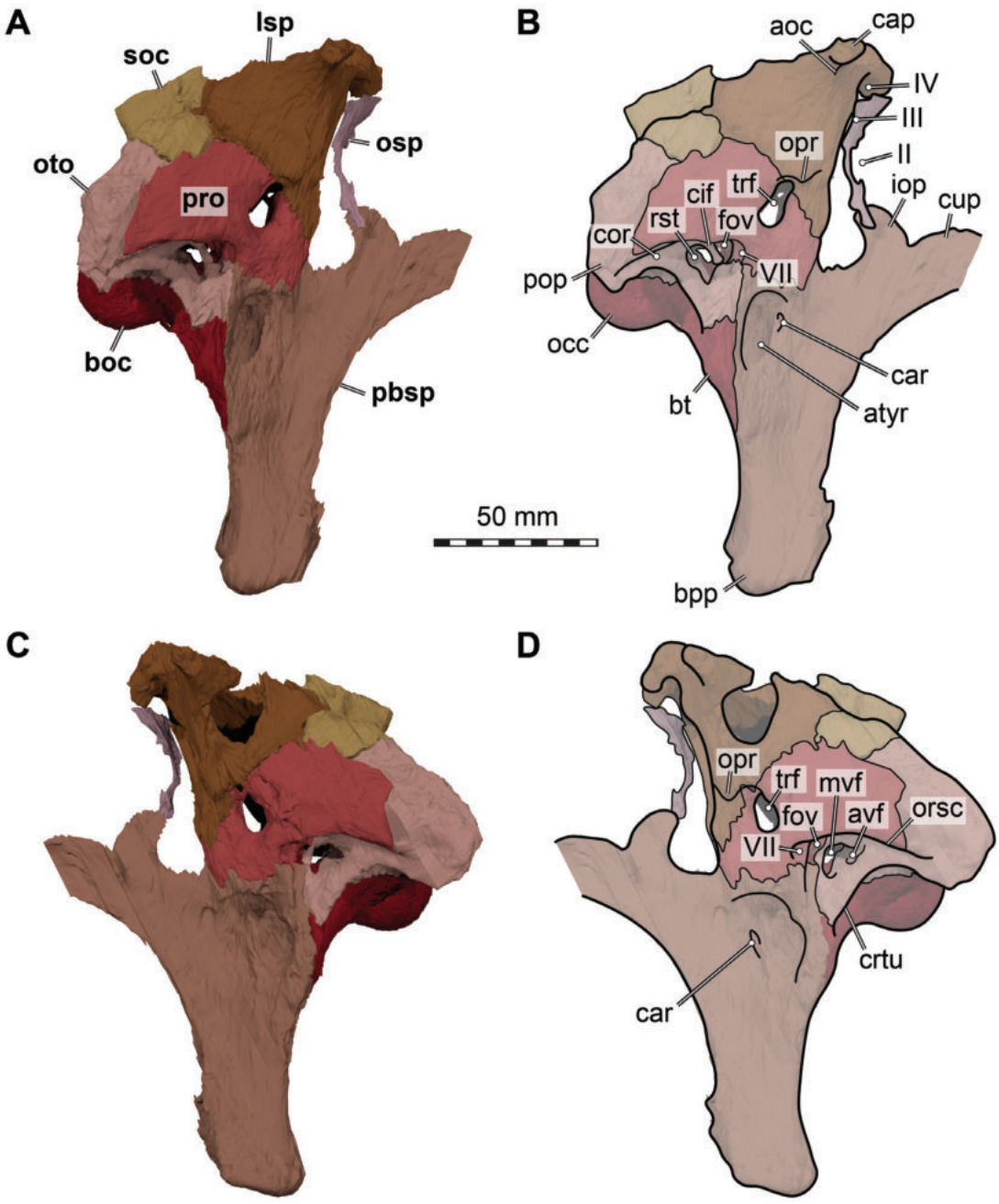

FIGURE 22. 3D renderings of the articulated braincase elements of *Irritator challengeri* (SMNS 58022). A, right lateral view; B, right lateral view with interpretative line drawings; C, left lateral view; D, left lateral view with interpretative line drawings. Note that bones are labelled in bold, and other anatomical structures in regular font. Abbreviations: aoc, antotic crest; atyr, anterior tympanic recess; avf, (anterior) vagal foramen (connecting recessus scalae tympani region with paracondylar recess via a vagal canal); boc, basioccipital; bt, basal tuber; cap, capitate process; car, external foramen for the internal carotid artery (=vidian) canal; cor, columella recess; cif, crista interfenestralis; crtu, crista tuberalis; cup, cultriform process; fov, fenestra ovalis; iop, interorbital process of the parabasisphenoid; lsp, latero-sphenoid; mvf, medial vagal foramen (connecting brain cavity with recessus scalae tympani); occ, occipital condyle; opr, ophthalmic ridge defining groove for ophthalmic branch (CN V_1); oto, otoccipital; orsc, orbitosphenoidal crest; pbsp, parabasisphenoid; pop, paroccipital process; pro, prootic; rst, recessus scalae tympani/tympanic region of middle ear; soc, supraoccipital; II, medially open foramen for optic nerve (CN II); III, oculomotor nerve (CN III) foramen; IV, trochlear nerve (CN IV) foramen; V, trigeminal nerve (CN V) foramen; VII, facial nerve (CN VII) foramen.

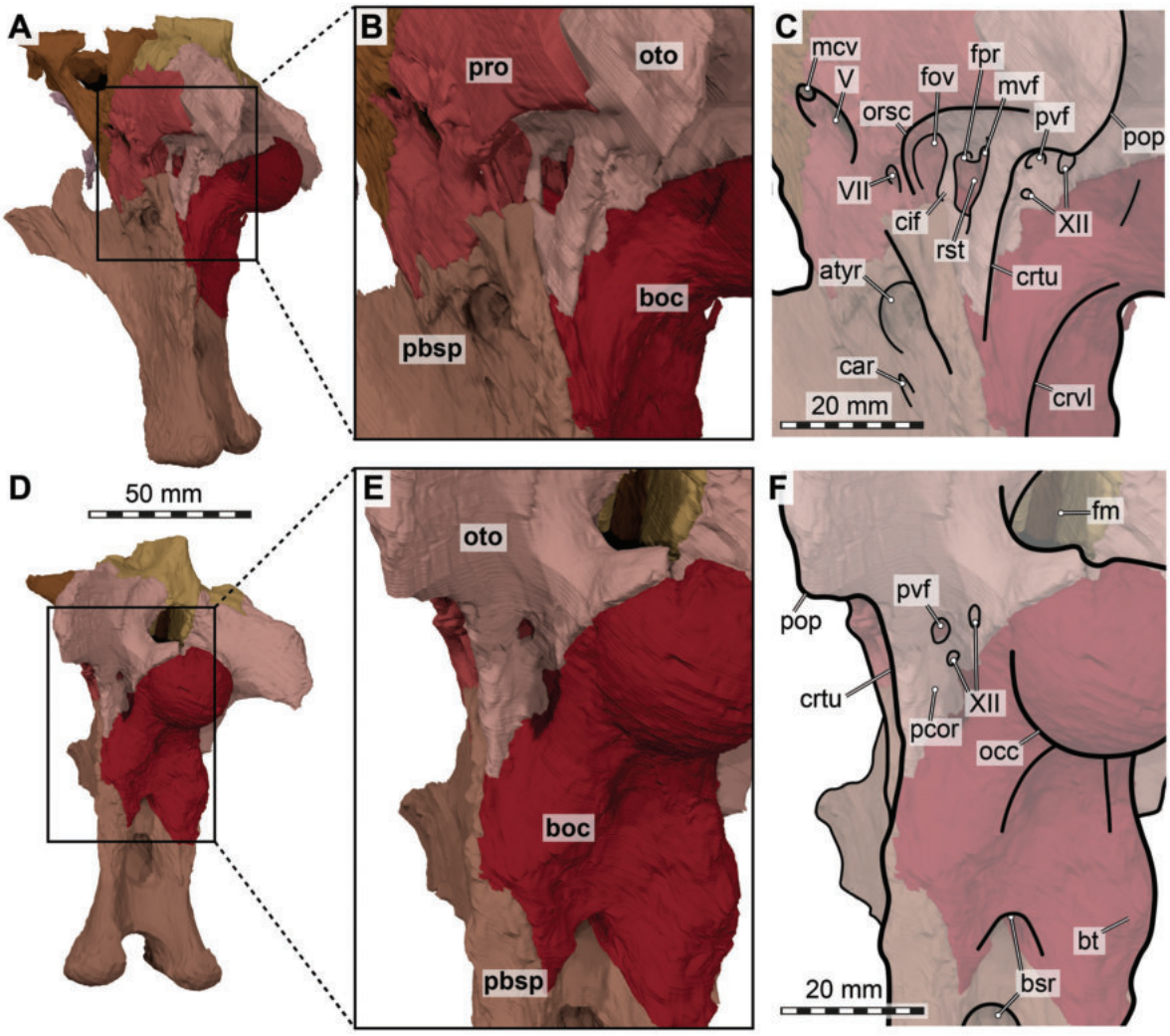

FIGURE 23. 3D renderings of the articulated braincase elements of *Irritator challengeri* (SMNS 58022). A, slightly posteriorly rotated view of left side; B, detailed view of tympanic region; C, as B, with interpretative line drawings; D, strongly posteriorly rotated view of left side; E, detailed view on paracondylar region; F, as E, with interpretative line drawings. Note that bones are labelled in bold, and other anatomical structures in regular font. Abbreviations: atyr, anterior tympanic recess; boc, basioccipital; bsr, basisphenoid recess; bt, basal tuber; car, external foramen for the internal carotid artery (=vidian) canal; cif, crista interfenestralis; crtu, crista tuberalis; crvl, crista ventrolateralis; fm, foramen magnum; fov, fenestra ovalis; fpr, fenestra pseudorotunda (anteroposterior opening between labyrinth cavity and recessus scalae tympani); mcv, mid cerebral vein foramen; mvf, medial vagal foramen (connecting brain cavity with recessus scalae tympani); occ, occipital condyle; oto, otoccipital; orsc, orbitosphenoidal crest; pbsp, parabasisphenoid; pcor, paracondylar recess; pop, paroccipital process; pro, prootic; pvf, posterior vagal foramen; rst, recessus scalae tympani/tympanic region of middle ear; V, trigeminal nerve (CN V) foramen; VII, facial nerve (CN VII) foramen; XII, hypoglossal nerves (CN XII) foramina.

is markedly rugose, and thus it cannot be excluded that this area was originally covered by a lamina of the parietal. The supraoccipital contacts the parietal anteriorly, dorsally, and laterally, the laterosphenoid and prootic anteriorly, and the otoccipital posteroventrally.

In relation to the dorsal surface of the parietal and the posterior surfaces of the otoccipitals and basioccipital, the supraoccipital slopes anterodorsally at an angle of approximately 45°. It bears a centrally situated supraoccipital crest (nuchal crest of Sues et al., 2002 and Sampson and Witmer, 2007) on its posterodorsal surface. While most of the crest is broken off, a remnant of the base is still preserved. The crest becomes more prominent dorsally, but due to the inclination of the supraoc-

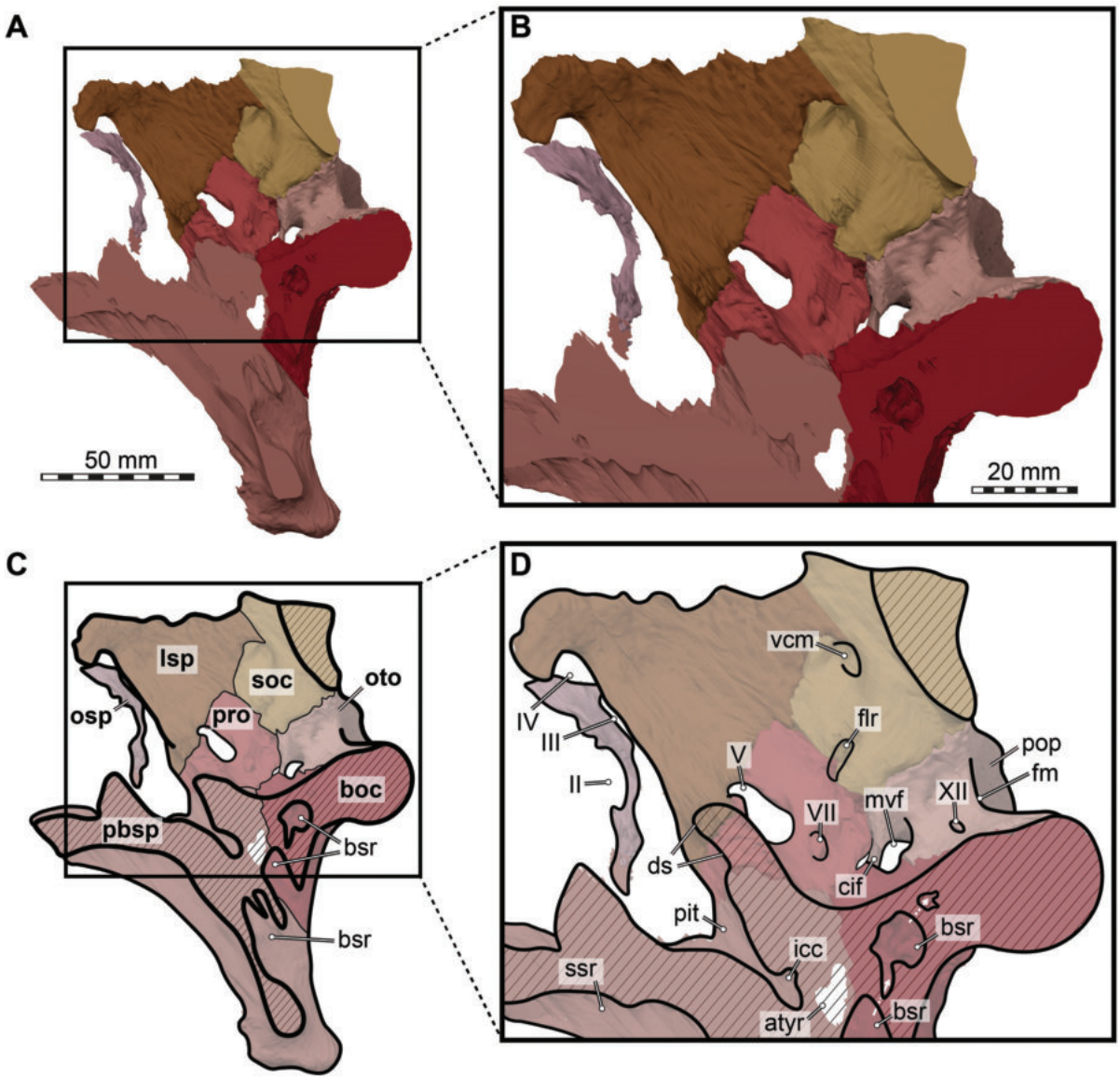

FIGURE 24. 3D renderings of the sagitally sectioned articulated braincase elements of the right side of *Irritator challengeri* (SMNS 58022) in medial view. A, complete rendering of right side; B, detailed view endocranial cavity; C, as A, with interpretative line drawings; D, as B, with interpretative line drawings. Note that bones are labelled in bold, and other anatomical structures in regular font. White arrows indicate internal connections of basisphenoid recess not covered in section. Abbreviations: atyr, anterior tympanic recess; boc, basioccipital; bsr, basisphenoid recess; cif, crista interfenestralis; ds, dorsum sellae; flr, floccular recess opening; fm, foramen magnum; icc, internal carotid artery (=vidian) canal; lsp, laterosphenoid; mvf, medial vagal foramen (connecting brain cavity with recessus scalae tympani); osp, orbitosphenoid; oto, otoccipital; pbsp, parabasisphenoid; pit, pituitary fossa; pop, paroccipital process; pro, prootic; soc, supraoccipital; ssr, subsellar recess; vcm, vena capitis media foramen; II, medially open foramen for optic nerve (CN II); III, oculomotor nerve (CN III) foramen; IV, trochlear nerve (CN IV) foramen; V, trigeminal nerve (CN V) foramen; VII, facial nerve (CN VII) foramen; XII, hypoglossal nerves (CN XII) foramina.

cipital, its posterior margin remains vertical above the foramen magnum in lateral view. In *Baryonyx, Suchomimus*, and *Ceratosuchops*, the crest is dorsoventrally tall (Charig and Milner, 1997; MS, pers. obs. on cast, MNN GDF 214; Barker et al., 2021), but due to the dorsal damage it cannot be said if this was also the case in *Irritator*. The supraoccipital crest is flanked by two funnel-like depressions leading to the posterior openings for the vena cerebralis media (Figures 14, 21A, B). The foramina for the vein are large and placed dorsal to the level of the dorsal rim of the paroccipital processes, being

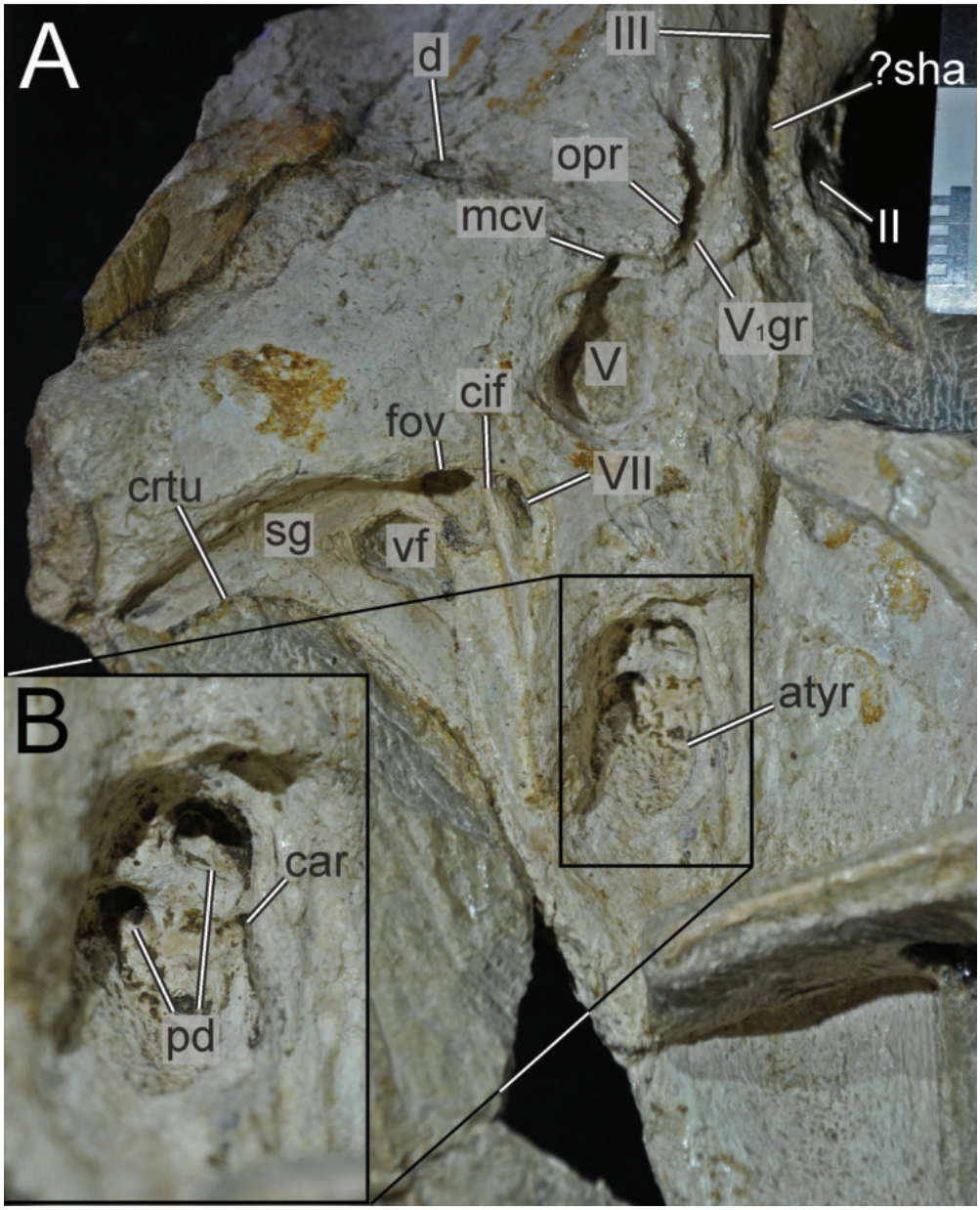

FIGURE 25. Close-up photographs of right lateral braincase of *Irritator challengeri* (SMNS 58022). A, right lateral view; B, magnified anterior tympanic recess. Note that bones are labelled in bold, and other anatomical structures in regular font. Abbreviations: atyr, anterior tympanic recess; car, external foramen for the internal carotid artery (=vidian) canal; cif, crista interfenestralis; crtu, crista tuberalis; d, damage; fov, fenestra ovalis; mcv, mid cerebral vein foramen; opr, ophthalmic ridge defining groove for ophthalmic branch (CN V_1); pd, (blind) pneumatic depression; sg, stapedial groove; vf, (lateral) vagal foramen; ?sha, potential sphenoidal artery opening; II, medially open foramen for optic nerve (CN II); III, oculomotor nerve (CN III) foramen; V, trigeminal nerve (CN V) foramen; V_1gr, ophthalmic groove for V_1 branch; VII, facial nerve (CN VII) foramen.

completely enclosed by the supraoccipital. In contrast to *Allosaurus* (Chure and Loewen, 2020) and *Asfaltovenator* (Rauhut and Pol, 2019), there is no curved groove on the posterior surface of the supraoccipital that connects the exit of the mid-cerebral vein with the posttemporal foramen. The latter opening is difficult to identify even with the aid of CT data, but it seems to be represented by a small foramen between the parietal and supraoccipital slightly ventrolateral to the posterior exits of the mid-cerebral vein, marked by a small notch on the dorsolateral suture with the parietal. The fora-

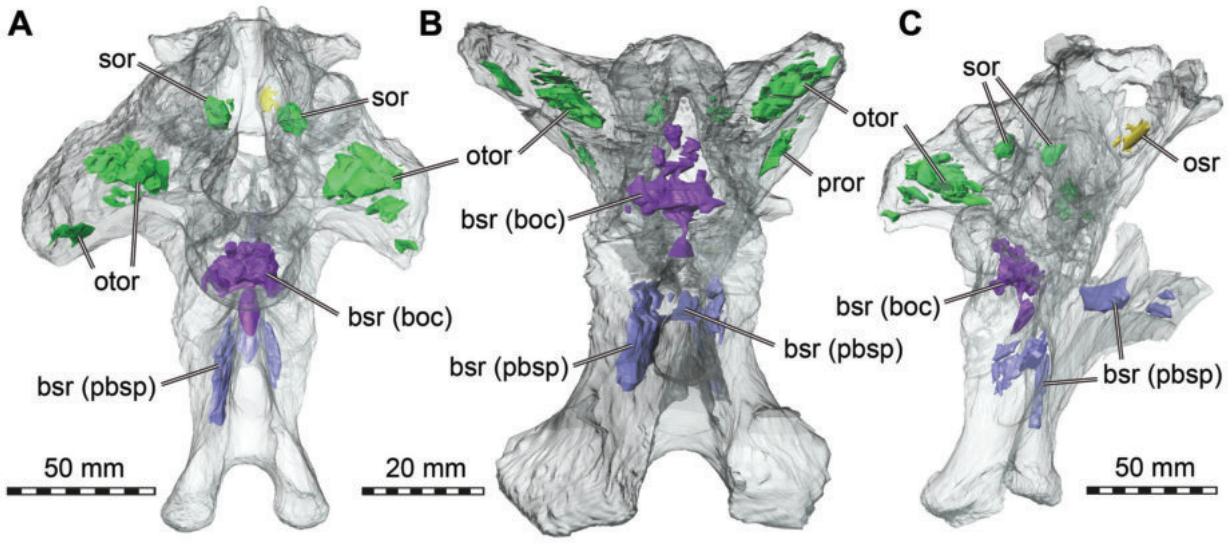

FIGURE 26. 3D renderings of the intracranial cavities within the articulated braincase of *Irritator challengeri* (SMNS 58022). A, posterior view; B, ventral view; C, right anterolateral view. Colours reflect cavity identity, where green cavities are within the otic bones, purple cavities are within the basioccipital (boc), blue cavities are within the parabasisphenoid (pbsp), and yellow recesses are within the orbitosphenoid. Abbreviations: bsr, basisphenoid recess; osr, orbitosphenoid recess; otor, otoccipitical recess; pror, prootic recess; sor, supraoccipital recess.

men is thus within the lateral rim of the funnel-like depression leading towards the opening of the vena cerebralis media, possibly indicating an occipital sinus in this area. On the medial surface of the supraoccipital, a large but shallow depression is present anteroventral to the posterior opening for the mid-cerebral vein, representing the dorsal longitudinal sinus. However, a groove marking the course of the mid-cerebral vein from the sinus towards its anterolateral exit, as is present in other dinosaurs (e.g., Janensch, 1936; Rauhut, 2004), seems to be absent both on the medial side of the supraoccipital and the laterosphenoid/prootic. The dorsal break of the nuchal crest reveals an anterior notch in dorsal view that leads into the brain cavity and separates the left and the right side of the supraoccipital. The notch continues ventrally as a narrow trough at the posterior end of the endocranial cavity towards the dorsal margin of the foramen magnum. Anteriorly, the lateral wall of the supraoccipital articulates with the laterosphenoid. Laterodorsally and presumably dorsally, the bone articulates with the parietals, but due to the dorsal break it cannot be said if a posterior process of the parietal that capped the dorsal surface of the supraoccipital was present, as occurs in many other non-avian theropods. The ventral margin of the supraoccipital forms the entire dorsal roof of the foramen magnum. The ventrolateral suture with the otoccipital is complex (Figure 20C, D). Along the rim of the foramen magnum, each otoccipital sends a stout process dorsomedially, restricting the width of the ventral end of the supraoccipital, though not to the extent seen in some other basal tetanurans (e.g., *Allosaurus*, Chure and Loewen, 2020). Dorsolateral to this otoccipital process, the supraoccipital has a long and slender ventrolateral process, which reaches the level of the dorsal margin of the foramen magnum and slots into a notch in the otoccipital.

On each side, the bone has a ventrolateral bulbous projection that houses parts of the semicircular canals, with an anteroventral facet for the prootic and a posteroventral facet for the otoccipital. The supraoccipital has a distinct ventrolateral groove on the surface that articulates with the prootic, which invades the bone from the medial, endocranial side. Together with a corresponding dorsolateral groove on the articular facet of the prootic, this groove forms a prominent recess from the medial braincase surface for the flocculus, which is narrow, but very long, continuing posterolaterally into the otoccipital. While the opening for the anterior semicircular canal is situated dorsolateral to the channel, the opening for the posterior semicircular canal lies rather posteroventrally. The supraoccipital bears a large cavity posterior to the endosseous canal of the common crus, which is followed posteromedially by another, smaller one (Figure 26). Both cavities do not bear an obvious connection to a pneumatic foramen.

Otoccipital (Exoccipital-Opisthotic)

In most dinosaurs, including *Irritator*, the exoccipital is tightly fused with the opisthotic to form the otoccipital (Sues et al., 2002). Interestingly, this is not the case in the holotype of *Baryonyx* (Charig and Milner, 1997). Both otoccipitals are preserved in *Irritator* and form the lateral borders of the foramen magnum, as well as most of the paroccipital processes (Figures 14, 20C, D). The otoccipital contacts the basisphenoid anteroventrally, the prootic anterodorsally, the supraoccipital mediodorsally, the parietal laterodorsally, the squamosal and possibly the quadrate laterally, and the basioccipital ventrally (Figures 2-4).

While the left paroccipital process is almost complete, the right one misses its distalmost part. Both paroccipital processes are relatively short and project posteriorly and ventrolaterally. In contrast, the paroccipital processes of *Baryonyx*, *Ceratosuchops*, and *Riparovenator* seem considerably longer (Charig and Milner, 1997; Barker et al., 2021); the paroccipital process of *Irritator* is c. 1.1 times longer than tall, whereas that of *Riparovenator* is 2.5 times longer (Barker et al., 2021). In *Irritator*, the dorsal and ventral margins of the paroccipital processes are almost straight and parallel to each other, but the processes are very slightly flexed ventrolaterally. The distal end that articulates with the squamosal is blunt and rounded. The ventral margin of the base of the paroccipital process is placed approximately at the level of the half-height of the occipital condyle, as in most non-avian averostrans, whereas it is placed relatively higher in non-averostran theropods (Rauhut, 2003). On the posterodorsal surface of the proximal part of the paroccipital process is a longitudinal groove that leads to the funnel-like dorsal depressions of the supraoccipital, which articulates with the anterodorsal surface of the otoccipital. The paroccipital process braces the prootic anteriorly, and the parietal and squamosal dorsally. In addition, the distal end of the paroccipital process closes the quadrate facet of the squamosal posteromedially.

Ventral to the paroccipital process, the otoccipital articulates with the basioccipital along a lengthy contact consisting of two processes. One process is posteriorly directed and forms the dorsolateral part of the occipital condyle on either side. These condylar processes of the left and right otoccipital remain separated from one another by a thin median crest of the basioccipital. The contact with the basioccipital continues anteriorly from the floor of the endocranial cavity to the level of the anterior rim of the crista interfenestralis. Within the foramen magnum, the left and right elements diverge anteriorly, making more room for the contribution of the basioccipital to the floor of the endocranial cavity. In ventral view, the broad articular facet for the basioccipital is elongate and semi-oval in outline, being rounded posteriorly. The second process of the otoccipital that contacts the basioccipital forms the crista tuberalis (=crista metotica, metotic strut of other authors [e.g., Gower and Weber, 1998; Rauhut, 2004]). The crista tuberalis is developed as a robust, posterolaterally oriented ridge that is dorsally continuous with the ventral margin of the paroccipital process (Figures 23, 25A). It separates the region of the inner ear, anteriorly, from the occipital region posteriorly. The crista tuberalis extends to the basioccipital/basisphenoid contact and contacts the basisphenoid in the lateral braincase wall. The crista tuberalis and occipital process of the otoccipital define a posterior fossa, the paracondylar recess, ventrolateral to the occipital condyle. Within the paracondylar recess, there are three foramina: two smaller foramina penetrate the bone mediolaterally and can be identified as two foramina for the CN XII (only one was found with the medical CT data in Schade et al., 2020a). The third foramen ('posterior vagal foramen'; see below) penetrates the otoccipital anteroposteriorly and forms a short but broad canal that probably corresponds to the joint passage of CN IX–XI from the recessus scalae tympani to the occipital surface of the braincase.

On the anterior side of the crista tuberalis and below the proximal part of the paroccipital process, the columellar recess (sensu lato) is located. Two large, anteroposteriorly arranged openings are visible within the columellar recess, separated by a robust crista interfenestralis. The posterior aperture within the columellar recess was identified as the metotic foramen by Sues et al. (2002). However, a metotic foramen would only be present if the embryonic fissura metotica does not become subdivied into a vagal foramen (=jugular foramen) and the fenestra pseudorotunda (=fenestra cochlea) during ossification of the chondrocranium (Gower and Weber, 1998; see also discussion in Bronzati and Rauhut, 2018). Whereas the posterior opening seems to be undivided in lateral view (thus justifying its identification as metotic foramen by Sues et al., 2002), the CT data reveal that a separate fenestra pseudorotunda is indeed present (Figure 23A-C), which functioned as a pressure-relief outlet for endolymphatic fluid flow within the inner ear (see Rieppel, 1985; Gower and Weber,

1998).The fenestra pseudorotunda is located medially to the crista interfenestralis and leads anteroposteriorly into the recessus scalae tympani. Although the medial wall of the fenestra pseudorotunda is ventrally broken on both sides of the braincase, it seems that this fenestra was largely or completely separated from the larger, more posteriorly situated opening, which would thus correspond to the vagal foramen. The latter represents the opening through which CN IX-XI and the jugular vein exited the endocranial cavity. The cranial nerves IX-XI probably occupied the dorsal part of the opening and diverged posteriorly, where a shallow groove on the otoccipital leads into the canal of the posterior foramen that opens into the paracondylar recess on the occiput, as described above. The jugular vein (posterior cephalic vein of Bronzati and Rauhut, 2018) thus left the braincase through the ventral part of this opening and might have diverged posteroventrally around the crista tuberalis of the otoccipital. As the posterior division of the vagal nerve group (CN X, and probably its accessories CN IX and XI) is thus a two-step procedure, in which the nerve first leaves the braincase into the recessus scalae tympani and then exits this cavity through a posteriorly directed foramen in the occiput, we suggest the terms 'medial vagal foramen' for the exit of the nerve from the braincase, and 'posterior vagal foramen' for its exit onto the occiput.

The anterior aperture within the columellar recess is the fenestra ovalis (=fenestra vestibuli), which was spanned by a membrane to receive the basal plate of the stapes, on the lateral aspect of the cochlea, and is posteriorly bordered by the crista interfenestralis.

Posterolaterodorsal to the fenestra ovalis, the posterolaterally extending stapedial groove lies ventral to the sutural contact of the otoccipital and prootic on the anteroventral side of the paroccipital process, being bordered posteriorly by the otoccipital and anteriorly by the prootic.

In anterior view, there are three openings posterodorsally to the crista interfenestralis on the articular facet for the prootic of the otoccipital. Medially, a large opening for the posterior ampulla of the vestibular apparatus is situated. Dorsally to the posterior ampulla opening, a fossa for the distal portion of the flocculus invades the otoccipital anteromedially, and the opening for the horizontal semicircular canal can be found further laterally, slightly ventral to the floccular recess. In dorsal view, directly posterior to the floccular recess, there is a small and slit-like opening for the posterior semicircular canal in the broad contact area with the supraoccipital.

In medial view, the otoccipital forms the ventral part of the lateral wall of the endocranial cavity anterior to the foramen magnum. In its ventral part, this wall is pierced by two anteroposteriorly separated foramina for branches of CN XII to exit, the posterior of which is slightly larger than the anterior one. At the anterior end of the medial surface, the large and slightly more dorsally positioned vagal foramen pierces the lateral endocranial wall. Within the posterior portion of the otoccipital, an accumulation of partly webbed and interconnected cavities is visible in our µCT data, but without an obvious connection to a pneumatic foramen. Additionally, each otoccipital bears a smaller, anteroposteriorly elongated cavity on the distalmost portion of the paroccipital process (Figure 26).

Prootic

Both prootics are completely preserved (Figures 1, 20-24), although each bears a dorsoventrally oriented crack posteriorly to the large CN V opening. The prootic contributes to the lateral wall of the braincase and consists of a main body that is relatively short anteroposteriorly and high dorsoventrally, and a posterolateral, wing-like process that overlies the proximal part of the anterior surface of the paroccipital process of the otoccipital. The prootic contacts the laterosphenoid anterodorsally, the supraoccipital posterodorsally, the otoccipital posteriorly, the basioccipital posteroventrally, the basisphenoid anteroventrally, and the other prootic anteroventromedially. Due to the exposure of the supraoccipital on the lateral side of the braincase, there seems to be no prootic-parietal contact, which is usually found in this area in carnosaurs (e.g., Coria and Currie, 2016; Chure and Loewen, 2020). As mentioned above, it cannot be excluded that there might have been a thin lamina of the parietal extending ventrally over the supraoccipital here and thus contacting the prootic over a short distance.

In *Irritator*, the most distinctive feature of the prootic in lateral view is the large opening for CN V, which is developed as a roughly drop-shaped, anterodorsally open notch on the anterior part of the bone, extending over approximately half of the length of the prootic body, excluding the posterolateral process. Unlike in some other non-avian theropods (Bakker et al., 1988), the ophthalmic branch of the trigeminal nerve does not pass through a separate canal in the prootic and laterosphenoid; instead, there is a ventrally open groove under an

overhanging ridge anterior to the trigeminal foramen on the laterosphenoid that provides evidence for the course of this nerve. Because of the absence of an ophthalmic canal, a maxillomandibular foramen sensu Sampson and Witmer (2007) is not present, and the trigeminal ganglion was probably situated in a more extracranial position. Indeed, the opening for the trigeminal nerve in the rather thick prootic is slightly funnel-shaped, with a more marked depression ventral to the opening, as in *Eustreptospondylus oxoniensis* (Sadleir et al., 2008), probably indicating the position of the ganglion just outside the braincase and the ventral course of the mandibular branch of the nerve. Posterior to the trigeminal foramen, the orbitosphenoidal crest starts on the ventral side of the posterolateral wing that flanks the paroccipital process, where it forms the anterolateral border of the stapedial groove (Figures 20A, B, 23A-C). Anterior to this wing, it curves sharply downward, but remains restricted to the posterior edge of the prootic. Thus, a well-developed preotic pendant (ala basisphenoidalis of some authors; see Sampson and Witmer, 2007) is absent, in contrast to most other non-avian theropods (Chure and Madsen, 1998; Rauhut, 2004). Posteroventral to CN V, the slit-like opening for CN VII leaves the braincase. In lateral view, only an incision in the orbitosphenoidal crest indicates the position of this foramen, as it extends anteromedially towards posterolaterally and opens posteriorly below the orbitosphenoidal crest (Figures 23A-C, 25). In contrast to some dinosaurs (e.g., *Efraasia minor*; Bronzati and Rauhut, 2018), there is only a single opening for the facial nerve, indicating that this nerve split into the hyomandibular and palatine rami outside the braincase, as seems to be usual in non-avian theropods. Posterior to the foramen of the facialis nerve, a broad embayment in the posterior margin of the prootic below the paroccipital process forms the anterior margin of the fenestra ovalis.

Posterior and posteroventral to the CN V opening, the medial surface of the prootic bears several depressions and openings for the endosseous labyrinth, flocculus, and cranial nerves (Figure 24). Ventral and slightly posterior to the trigeminal foramen, the anteromedially open entrance for the facial nerve lies within a marked depression. The posterolateroventrally oriented recess for the flocculus is developed as a narrow, but deep, incision on the suture with the supraoccipital and otoccipital, posterior to the trigeminal foramen and approximately at the mid-height level of the latter. Two openings for the anterior and horizontal semicircular canal are found on the medial side of the mediolaterally wide articular facet for the supraoccipital and in the ventral part of the articular facet for the otoccipital, respectively. Below the floccular recess, a large, anteriorly directed recess in the suture with the otoccipital, which posteroventrally leads towards the fenestra pseudorotunda, marks the anterior ampulla and the cochlear duct of the inner ear. The fenestra ovalis makes up a medioventral notch of the prootic. Both branches of CN VIII are situated within the prootic here, their foramina piercing the bone at the dorsal end of the cochlear duct within the osseous labyrinth. In most reptiles, including the megalosauroid *Dubreuillosaurus*, a small opening posterodorsal to CN VII on the medial side of the prootic was identified as the foramen for CN VIII (Allain, 2002). This also seems to be the case in *Irritator*, though this area is damaged on the left side and a small overhanging crest in this position seems to hide the foramina for the acoustic nerve.

Anteriorly, both prootics flex medially and meet on their midline to form the central part of the robust dorsum sellae posterodorsal to the pituitary fossa, between the parabasisphenoid ventrally and the laterosphenoid dorsally. Here, they articulate via a mediolaterally wide surface with the laterosphenoid on the dorsal aspect and with the basisphenoid on the anterior and ventral aspect. The dorsum sellae of each prootic is anteroposteriorly pierced by a canal for the CN VI, which traverses the prootic and exits through a foramen at the basisphenoid-prootic suture from the braincase into the pituitary fossa. In posterior view, the canals are lateral to the anterior interprootic contact (Figure 21A, B). In contrast, in *Dubreuillosaurus*, an opening on the lateral aspect of the braincase, directly ventrally to CN V, has been identified as the exit of CN VI (Allain, 2002).

The posteromedial surface of the prootic meets the otoccipital and, more dorsally, the supraoccipital. The prootic of *Irritator*, and seemingly *Baryonyx* (Charig and Milner, 1997) and *Ceratosuchops* (Barker et al., 2021), makes up a substantial part of the anterolateral surface of the paroccipital process (Figure 20A, B, 21-22). In *Piatnitzkysaurus*, the contact of the prootic and the otoccipital ends shortly posterodorsal to the fenestra ovalis (Rauhut, 2004).

Our CT data reveal that ventral to CN V and anterior to CN VII, a very small and isolated cavity is present on both sides (not shown in Figure 26, but see Schade et al., 2020b; Schade et al., 2022). Further posteriorly, an isolated and complex net-

work of different-shaped and different-sized cavities exists within the prootic portion of the paroccipital process (Figure 26B, C). The right complex is more voluminous.

Basioccipital

The basioccipital is well preserved in *Irritator* (Figure 14). As in all theropods, it is a median unpaired bone that makes up the posterior floor of the endocranial cavity and the ventral part of the occiput (Figure 24). It forms a small median part of the ventral margin of the foramen magnum and the main portion of the occipital condyle. The basioccipital contacts the basisphenoid anteriorly and ventrally, the otoccipital laterally and the prootic anterodorsally (Figures 20-24).

The occipital condyle is ball-shaped and has a slightly constricted neck. In relation to the skull roof, the hemispherical occipital articulation surface for the atlas projects posteroventrally in *Irritator*, *Baryonyx* (Charig and Milner, 1997), and *Suchomimus* (MS, pers. obs. on cast, MNN GDF 214), providing further evidence that the snout of spinosaurids was strongly ventrally inclined in a natural head posture (Schade et al., 2020a).

In posterior view, a triangular, ventrally broadening basioccipital depression is present ventral to the occipital condyle, flanked by ventrolaterally directed ridges leading to the basal tubera. Lateral to these ridges, there is a shallow depression on the suture between the basioccipital and the ventral process of the otoccipital that extends ventrally from the paracondylar recess and becomes shallower ventrally. Thus, well-developed subcondylar recesses, as are present in *Dilophosaurus wetherilli* and some other basal tetanurans (Witmer, 1997; Rauhut, 2004), are absent in *Irritator*.

Dorsolaterally, the basioccipital articulates with the otoccipital via a large, laterally placed articulation surface. The two otoccipital facets are separated from one another by a shallow median ridge of the basioccipital in the floor of the foramen magnum, which widens anteriorly towards the floor of the endocranial cavity. The facet for the otoccipital extends over nearly the entire anteroposterior length of the basioccipital. Anterodorsally, the basioccipital bears a small dorsally directed facet for its anterodorsal contact with the prootic on either side. Lateral to the prootic contacts, the basioccipital forms a short surface that floors parts of the cavum labyrinthicum, has a contact with the crista interfenestralis of the otoccipital, and frames the fenestra pseudorotunda ventrally. Within the floor of the cavum labyrinthicum, the basioccipital and basisphenoid forms a narrow ventral cavity for the distalmost tip of the cochlea.

The short anterodorsal facet of the basioccipital for the prootic is posteriorly separated from the facet for the otoccipital by a dorsally open, U-shaped notch in the dorsolateral margin of the basioccipital. This notch forms the ventral margin of the medial vagal foramen, possibly for CN IX–XI and the jugular vein. The dorsal surface of the basioccipital is concave between the contacts to the bones forming the lateral wall of the braincase. This results in a cup-shaped, oval depression on the anterior part of the basioccipital, which continues anteriorly onto the dorsal surface of the basisphenoid and holds the hindbrain.

Anteriorly, the basioccipital forms a dorsoventrally tall and slightly posteroventrally inclined surface that contacts the basisphenoid. Posteroventrally, two ventrolateral processes of the basioccipital brace the occipital condyle against the basisphenoid. These ventral processes represent the inconspicuous basal tubera, which are only formed by the basioccipital and just slightly wider than the width of the occipital condyle. Although projecting tubera are thus absent, and the left side is damaged, the posterior surface of these processes is rugose (Figure 14), indicating the attachment of craniocervical musculature, as noted by Sues et al. (2002). In contrast to other non-avian theropods, in which the crista tuberalis of the otoccipital forms the lateral margin of the basal tubera (e.g., Sampson and Witmer, 2007), this structure ends above the base of these ventral processes of the basioccipital in *Irritator* (Figure 23). While *Baryonyx* (Charig and Milner, 1997) and possibly *Ceratosuchops* and *Riparovenator* (Barker et al., 2021) bear a posteriorly elevated sutural contact between the basioccipital and the basisphenoid, this is not the case in *Irritator* and *Suchomimus* (MS, pers. obs. on cast, MNN GDF 214). In *Baryonyx, Ceratosuchops*, and *Riparovenator*, the posteriorly elevated sutural contact is roughly W-shaped and produces two dorsoventrally high depressions, flanking the ventral basisphenoid recess depression (Charig and Milner, 1997; Barker et al., 2021). Right and left tubera are separated by a deep, V-shaped incision that is spanned by a transverse lamina with a ventrally concave margin in *Irritator* (Figures 14, 23E, F), *Ceratosuchops*, and *Riparovenator* (Barker et al., 2021). This lamina forms the posterior wall of a dorsally deep cavity (‘median opening’ in Sues et al., 2002) that invades the basioccipital and basisphenoid at their contact in *Irritator* (Figures 24, 26). The internal surface of the

cavity is largely formed by bone of the basioccipital, whereas its ventral border is formed by the basisphenoid.

This opening leads to a partly webbed and irregularly shaped internal cavity network that extends dorsally below the floor of the braincase and to the base of the occipital condyle posteriorly. Sues et al. (2002) assigned the respective opening to the basisphenoid sinus and hence to the median pharyngeal system, a view that we concur with, as the bony relations of this opening—being bordered by the basisphenoid anteroventrally and the basioccipital posteriorly—correspond to the usual placement of this recess. As another part of the basisphenoid recess is placed below this recess in the basisphenoid (see below), this recess is thus subdivided (like the morphology observed in the juvenile *Tyrannosaurus* specimen CMNH 7541; Witmer and Ridgely, 2010; Carr, 2020).

Parabasisphenoid

As in all theropods, the basisphenoid is tightly fused with the parasphenoid, and we thus use the term 'parabasisphenoid' to refer to this compound bone within this section. This unpaired element is well preserved and reversed L-shaped in lateral view (Figures 14, 20-25). The parabasisphenoid includes a relatively robust cultriform process anteriorly. The cultriform process is largely embedded within the sediment but its morphology was uncovered with the medical CT data. The parabasisphenoid forms the anteroventral part of the braincase and contacts the pterygoid through the basipterygoid processes ventrally, the prootic dorsally, and the basioccipital posterodorsally (Figures 1-4).

As in *Baryonyx* (Charig and Milner, 1997), *Ceratosuchops, Riparovenator* (Barker et al., 2021), a braincase referred to *Suchomimus* (MNN GDF 214), and the caenagnathid *Epichirostenotes curriei* (Sues, 1997), but in contrast to all other non-avian theropods, the basisphenoid is oriented vertically, so that the normally ventral surface is confluent with the occipital surface of the basioccipital, and the basipterygoid processes are placed posteroventral to the basal tubera. This results in a dorsoventrally tall but anteroposteriorly short basisphenoid body in lateral view and a posteriorly open basisphenoid recess. In *Irritator*, the basisphenoid body is notably longer than wide, with a maximal length of c. 4.5 cm from the basioccipital-basisphenoid suture to the basisphenoid web and a minimal transverse width of c. 3.5 cm (approximately at mid-length). The inconspicuous basal tubera are connected to the basipterygoid processes by stout, largely parallel, and slightly lateroposteriorly directed lateral laminae, corresponding to the cristae ventrolateralis of other non-avian theropods (Sampson and Witmer 2007).

The posterior surface of the basisphenoid bears two prominent recesses: a smaller, dorsally situated one and a larger, ventral one. Both recesses are in a marked longitudinal depression between the cristae ventrolateralis, which is bordered dorsally by the lamina of the basioccipital that spans between the basioccipital tubera. The normally anterior, here ventral, border of this depression, formed by the basisphenoidal web (Bakker et al., 1988), is rather inconspicuous in *Irritator* so that the depression opens ventrally. This is because the very stout basisphenoid web between the basipterygoid processes is ventrally rather than posteriorly directed. The dorsal recess within the depression is situated directly at the sutural contact between the basioccipital and parabasisphenoid. Our µCT data reveal the complexity of this recess, dorsally leading over to the medial internal cavity below the condyle (already mentioned in the basioccipital section). Additionally, the recess leads to two cavities anteroventral to the subcondylar cavity. These two cavities are dorsoventrally high, anteroposteriorly short, and separated from each other by a mediolaterally oriented bony wall. The two cavities are flanked by two dorsoventrally tall and mediolaterally narrow cavity networks, invading the basipterygoid processes. The left network extends further ventrally than the right one. In the dorsal vicinity of the two separated medial cavities, some minor channels and cavities are present, possibly connecting the medial cavities with the cavity networks of the basipterygoid processes. The ventralmost prominent recess in the posterior surface of the parabasisphenoid ('basisphenoid recess' in Sues et al., 2002) is a rather simple, dorsoventrally high, and anteroposteriorly relatively shallow, cone-shaped depression. In its dorsal orientation, it is largely parallel to the more dorsal recess, from which it is separated by a bony lamina. As noted above in the description of the basioccipital, all these posterior recesses, the one at the basioccipital-basisphenoid suture and the one only enclosed by the parabasisphenoid, are assigned to the basisphenoid recess. While *Irritator* bears depressions assigned to a transversally subdivided basisphenoid recess on the posterior surface of the parabasisphenoid, *Baryonyx, Suchomimus, Ceratosuchops,* and *Riparovenator* do not seem to exhibit a subdivison of this recess

(Charig and Milner, 1997; MS, pers. obs. on cast, MNN GDF 214; Barker et al., 2021).

In *Irritator*, the basipterygoid processes are very robust and short, the anteroposterior length of their articular surface being more than the distance that they protrude ventrally from the basisphenoid web. They project mainly ventrally and diverge only very little laterally, being separated by a broad, U-shaped gap in posterior view. The articular surface is almost parallelogram-shaped in ventral view, with a rounded posterior border and a pointed anteromedial corner. It has a rather complex morphology, being convex anteroposteriorly and mediolaterally in its posterior third, but rather flat to very slightly anteroposteriorly concave anteromedially, and rises slightly anterodorsally. Stout laminae extend anterodorsally from the basipterygoid processes towards the cultriform process and enclose a deep, cone-shaped subsellar recess, which is separated from the posterior depression on the parabasisphenoid by an anteroposteriorly broad, flat ventral surface of the basisphenoid web.

In lateral view, the basisphenoid bears a large, obliquely oval depression, the 'lateral pneumatic recess' of Sues et al. (2002), ventral to the articulation facets for the prootic. This depression corresponds to the anterior (=lateral) tympanic recess (Witmer, 1997b), which represents a theropodan or neotheropodan synapomorphy (Rauhut, 2003; see also Bronzati et al., 2018). The recess deepens dorsally and is markedly asymmetrical on the left and right side. Although it is subdivided into a larger anterior and smaller posterior depression within the recess on either side, the anterior depression is notably larger on the left than on the right side, while the posterior depression is larger on the right side. Furthermore, the large anterior depression of the left side is divided by a thin bony lamina from another, smaller, triangular depression anterior to the anterior tympanic recess; this depression is absent on the right side. The large anterior depression within the anterior tympanic recess was identified as the entrance of the carotid canal for the cerebral carotid artery by Sues et al. (2002), but our CT data suggest that it is a blind-ended pocket extending anterodorsally. The actual openings of the vidian canal are small and inconspicuous, being placed in a narrow groove below this anterior pneumatic depression; and while the entrance of the right vidian canal is placed within the anterior tympanic recess, the left one is placed just below this structure (Figure 22-25). There are minor internal channels in the vicinity of the anterior tympanic recess, partly leading over to the prootic and the basioccipital. Although the lateral sides of the parabasisphenoid body (between the cultriform process, anterior tympanic recess, and the laminae leading towards the parabasisphenoid body from the basipterygoid processes) are slightly concave, there are no additional pneumatic recesses, such as the parasphenoid or basipterygoid recesses, which are present in some other non-avian theropods (Rauhut, 2004).

The cultriform process projects into the interorbital region. As also reported for *Majungasaurus* (Sampson and Witmer, 2007) and present in many other theropods, the 'cultriform process' of *Irritator* is strictly speaking not a singular medial structure but composed of two parasagittal sheets of bone. These sheets arise from the anterior edges of the basipterygoid processes ventrally and converge dorsally, closer to the skull midline, thus confining a dorsally narrowing subsellar recess on the anteroventral surface of the parabasisphenoid, as described above. Left and right sheets are connected in the skull midline by a transverse bar of bone, which leaves deep dorsal and ventral longitudinal grooves between the sheeted parts of the cultriform process (Figure 21). As a result, the cultriform process has an H-shaped cross-section (Figure 20A, B), which, in addition to the abelisaurid *Majungasaurus* (Sampson and Witmer, 2007), has been reported for the megalosauroid *Dubreuillosaurus* (Allain, 2002). In *Irritator*, the cultriform process is flexed anteroventrally and anteriorly pointed, giving the cultriform process a hook-shaped appearance in lateral view (Figure 2B). The dorsal groove on the cultriform process leads posteriorly to a dorsoventrally deep depression, directly in front of a dorsal, plate-like projection (Figures 21A, B, 22). The distal end of this projection is round and points posterodorsally. Such a projection is also present in, e.g., *Allosaurus* (Chure and Loewen, 2020), the juvenile *Tyrannosaurus* specimen CMNH 7541 (Witmer and Ridgely, 2010; Carr, 2020), *Suchomimus* (MS, pers. obs. on cast, MNN GDF 214), and *Ceratosuchops* (Barker et al., 2021). However, it is less prominent in these taxa, and seems to be absent in the megalosauroid *Dubreuillosaurus* (Allain, 2002). This projection may have contacted the orbitosphenoid in *Irritator*, but incomplete preservation of the latter renders this detail unclear. The posterior margin of the dorsal projection is concave, forming a nearly round, window-like transverse opening between the plate itself and the posteriorly adjacent laterosphenoid and prootic. Sampson and Witmer (2007) describe an opening in a similar position in *Majun-*

gasaurus as a fonticulus interorbitalis, and a dorsal plate connecting the cultriform process with the skull roof as a mineralized interorbital septum, and furthermore report on the presence of similar mineralizations in several other ceratosaurs and at least one allosauroid, *Giganotosaurus*. Sampson and Witmer (2007) observe that the surfaces of these structures are usually striated and irregular, which supports their interpretations of the structure as calcified cartilage over the alternative that the structure is a proper ossification. However, in *Irritator*, the surface of the dorsal projection of the cultriform process is smooth, supporting the interpretation that the dorsal plate indeed is an 'interorbital process' of the cultriform process itself rather than a partially mineralized interorbital septum.

Directly anteroventral to the 'interorbital process', the cultriform process bears two small internal cavities, and posteroventral to the 'interorbital process' is a third, larger, anterodorsally inclined and seemingly isolated cavity (Figure 26C). The three cavities cannot be assigned to a pneumatic sinus, because they seem to be unknown in other theropods. Behind the projection, a dorsal groove leads to the sella turcica (pituitary fossa) that housed the pituitary gland. The sella turcica is narrow, cone-shaped, and dorsoventrally deep. Within the floor of this fossa, there is a singular opening for the cerebral carotid artery, representing the joint opening of the left and right vidian canals, which converge within the parabasisphenoid, as in other non-avian theropods. Posterior to the pituitary region, the parabasisphenoid transversely broadens towards its dorsal surface, which bears two large, lateromedially oriented articulation facets for the prootics to form the dorsum sellae. As the prootics meet each other anteriorly and diverge posterolaterally, the prootics form parts of the dorsum sellae, and the parabasisphenoid only has a small dorsal exposure in the cup-shaped depression for the hindbrain, between the prootics anteriorly and the basioccipital posteriorly (Figure 21A, B).

Laterosphenoid

Both laterosphenoids are present in *Irritator*. While the right laterosphenoid is largely intact, the left one bears a large hole in the center of the body (Figures 1, 22). This element contacts the orbitosphenoid anteriorly, the frontal anterodorsally, the postorbital anterolaterally, the parietal dorsally, the supraoccipital posteriorly, and the prootic ventrally (Figures 2-4).

The body of the laterosphenoid has a roughly trapezoidal shape, with the posterior and anterior margins paralleling each other. The posterior margin has a slight anterior inclination. It is perpendicular to the posteroventral margin in lateral view. In posterior view, the posteroventral portion of the laterosphenoid flares laterally. The posterior margin forms the contact with the supraoccipital. Here, the right element has a small, rounded depression (Figure 25), which was identified as the opening for the vena cerebralis media by Sues et al. (2002). However, this opening would be in a much more posterior and dorsal position than in other non-avian theropods, and the µCT data shows that it does not pierce the bone and may rather represent damage; as noted below, the mid-cerebral vein probably exited the braincase through a foramen immediately dorsal to the trigeminal foramen (Figures 23A–C, 25).

The dorsal margin is slightly anterodorsally inclined and articulates with the parietal over its full length. Anteriorly, there is a distinct process for the articulation with the orbitosphenoid, the posterior end of the frontal and a small anterior portion of the parietal. The process is anterodorsally and slightly medially directed and has a blunt anterior end that is anteroventrally directed, forming a small ventral hook (Figure 20A, B). Laterally, the process bears a longitudinal depression. The processes of the left and right side leave a median gap for the olfactory tract, which is ventrally bound by the orbitosphenoid. The ventrally recurved part of the process forms the dorsal and anterodorsal margin for a circular foramen for the passage of the CN IV, which is anteroventrally and ventrally bound by the orbitosphenoid. This foramen is notably large, although not as large as the trigeminal foramen. The anteromedial margin of the laterosphenoid ventral to the CN IV foramen is formed as a blunt ridge, against which the orbitosphenoid articulates. In this area (Figures 20, 22-25), two more foramina are found between the laterosphenoid and the orbitosphenoid, which are easier to see in the fossil than in the CT scans due to the delicate nature of the orbitosphenoid. In agreement with Sues et al. (2002), we identify the dorsal foramen as for the CN III. The more ventrally located foramen could be for the sphenoidal artery (see Sampson and Witmer, 2007), whereas the CN II is completely enclosed by the orbitosphenoid.

Posterior to the anterodorsal process, a second process is present at the dorsal part of the laterosphenoid, the capitate process, which is slightly shorter and projects mainly laterally and slightly

anteriorly. The process contacts the frontal anterodorsally, the parietal dorsally and the postorbital laterally via a blunt head. Ventrally, the capitate process ascends directly from the lateral surface, and there is no expanded antotic crest that buttresses the process, as reported for *Majungasaurus* (Sampson and Witmer, 2007).

At its ventral base, the laterosphenoid bears a medial process that contacts its counterpart (Figure 21A, B). Together, they form a bridge-like contact in anterior view, forming the dorsal margin of the dorsum sellae. The base ends in an acute ventral tip that flanks the parabasisphenoid laterally and forms a small ventral process anterior to the trigeminal foramen. It is formed by the anterior and anteroventral margin of the laterosphenoid. The anterior margin is slightly inclined anterodorsally in lateral view and straight in anterior view. The ventral margin is slightly posterodorsally inclined. It contacts the prootic and forms the dorsal margin of the CN V opening, which is marked as a small, rounded rim in the anterior part of this margin.

The lateral surface of the laterosphenoid is almost flat, with the anterior portion curving slightly medially. Dorsal to the CN V opening, there is a mediolaterally concave overhang of the bone, which houses the exit for the mid-cerebral vein (also partly penetrating the prootic in *Irritator*), as in other non-avian theropods (see, e.g., Rauhut, 2004). Anterior to this overhang, an anterodorsally inclined depression for the ascending CN V1 ramus is present, which has about the same dorsoventral height as the respective opening and is bordered posteriorly by a steeply ascending, slightly anteroventrally overhanging step on the lateral surface of the laterosphenoid.

The medial surface of the laterosphenoid is concave (Figure 24), encapsulating the cerebral region of the braincase (the µCT data allowed for a better separation of the orbitosphenoid, laterosphenoid, and the sediment within the braincase, indicating more voluminous cerebral hemispheres on the new endocast). In dorsal view, the dorsal margin is also medially concave, with the anteromedial process that forms the dorsum sellae being set at an angle of 90° towards the lateral part of the laterosphenoid.

Orbitosphenoid

Only the right orbitosphenoid is present, and it is unclear if the entire element is preserved (Figures 1, 20-25). The bone is extremely thin, and many aspects of its morphology are more readily observed in the fossil than in the µCT data. The orbitosphenoid contacts the laterosphenoid posteriorly and possibly the frontal dorsally (Figure 2). The orbitosphenoid probably articulates dorsally with the ventral hook of the anterodorsal process of the laterosphenoid, hereby enclosing the foramen for the CN IV. However, it is not entirely clear if the orbitosphenoid contacts the frontal (as depicted by Sues et al., 2002), which may be suggested by the right element, or if the laterosphenoid borders the CN IV opening dorsally and anterodorsally and thus separates the orbitosphenoid and the frontal, as our interpretation of the µCT data shows. The orbitosphenoid forms the anteroventral border for CN IV and the anteromedial border for CN III laterally, as well as the lateroventral margin for the olfactory tract and the lateral border for CN II medially. The orbitosphenoid is dorsoventrally tall and generally slender. Its dorsal portion is slightly expanded anteriorly to form a plate-like section that articulates with the anterior margin of the laterosphenoid posteriorly.

The CN III foramen is small and positioned in the sutural contact of the laterosphenoid and orbitosphenoid. Ventrally to the CN III opening, an even smaller opening of unclear identity is present; it may belong to the sphenoidal artery, as noted above. Anteriorly, a large, semicircular medial concavity represents the CN II opening in the particularly thin central part of the orbitosphenoid. The left orbitosphenoid of *Suchomimus* possibly provides evidence for these assignments, as the foramina have a similar distribution (MS, pers. obs. on cast, MNN GDF 214).

Our µCT data show that the interior of the orbitoshenoid of *Irritator* bears one large and one small cavity without an external connection in its dorsal portion, anterior to the opening for CN III (Figure 26). In non-avian theropods, no hollow orbitosphenoid has been reported to date, however, the sauropodomorph *Massospondylus carinatus* bears one cavity per orbitosphenoid (Chapelle and Choiniere, 2018).

Stapes

Only the right stapes is present (Figures 1B, 27). It is preserved on the right basisphenoid and jugal.

The stapedial shaft is a straight and delicate rod. In articulation, the stapes lies within the stapedial groove, between the prootic and otoccipital, and extends between the fenestra ovalis anteriorly and the eardrum that would have been placed posteroventral to the quadrate head-paroccipital process articulation posteriorly (Figures 2A, 4B). Thus,

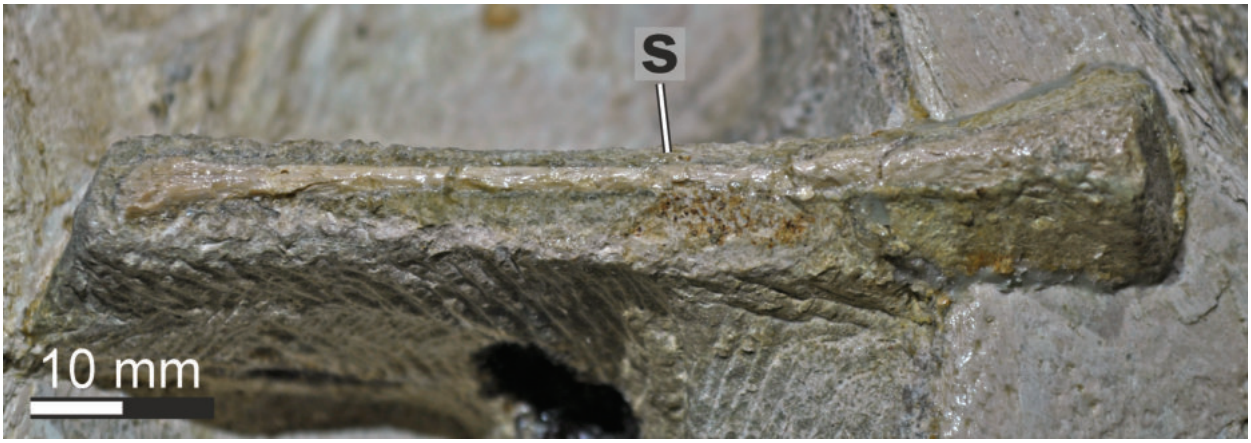

FIGURE 27. Close-up photograph of the stapes of *Irritator challengeri* (SMNS 58022). Abbreviation: s, stapes.

the full length of the stapedial shaft seems to be preserved.

Vomer

In the specimen, only small parts of the posterior portion of the vomer are visible through the right antorbital fenestra (Figure 1B). The vomer is a fused, slender, elongate element preserved in several pieces, as shown by the CT data (Figure 28). The vomer contacts the maxilla laterodorsally and the pterygoid and palatine posteriorly, and, possibly, the premaxilla anterodorsally (Figures 2, 4B). As the premaxillae and anterior ends of the maxillae are missing in *Irritator*, the anterior end of the vomer is also not preserved, and thus its anterior extent cannot be established (Figure 2B). It is unclear if the vomer articulated with the premaxillae in spinosaurids, as it does in other non-avian theropods. The bone visible in ventral view between the premaxillae and identified as the vomer in *Baryonyx* by Charig and Milner (1997) represents the anteromedial processes of the maxillae, and Rayfield et al. (2007) argued that the vomer possibly did not project as far anteriorly as previously thought. Despite the very long anterior ramus of the maxilla, the vomer reaches the level of the anterior part of the antorbital fenestra posteriorly, as in other non-avian theropods with relatively shorter snouts (e.g., Gilmore, 1920; Madsen, 1976; Rauhut et al., 2010).

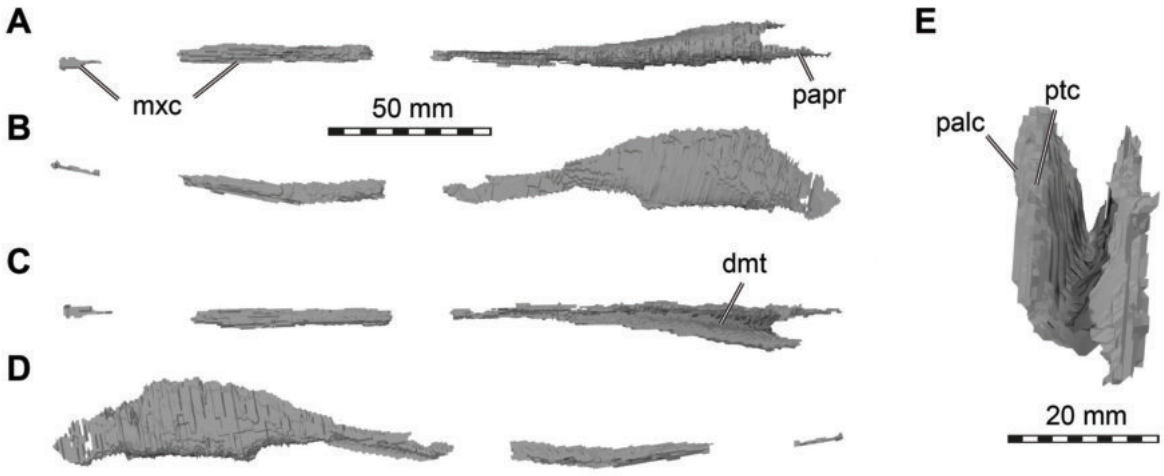

FIGURE 28. 3D renderings of the vomer of *Irritator challengeri* (SMNS 58022). A, ventral view (anterior to left); B, left lateral view; C, dorsal view (anterior to left); D, right lateral view; E, posterior view. Note different scale in E. Abbreviations: dmt, dorsomedian trough of vomer; mxc, maxillary contact, palc, palatine contact; papr, posterior articular process of vomer; ptc, pterygoid contact.

Anteriorly, the preserved part of the vomer forms a thin rod-like process that is wedged ventrally between the median ridges of the maxillae. At the level where the maxillae diverge from the skull midline and lose their contact with one another, the vomer becomes a vertically sheeted plate, which almost immediately bifurcates dorsally into two laminae that bound a deep, median, dorsally open trough (Figure 28C, E). This posterior portion of the vomer becomes dorsoventrally taller, and the lateral sheets of the vomer are almost parallel to one another, only slightly diverging dorsally, resulting in a deep, narrow, U-shaped cross-section to the bone. In dorsal view, the two lateral sheets diverge very slightly posteriorly. At the posteriormost end of the vomer, the two lateral vomerine sheets are ventrally not floored by bone but form short posterior processes for the articulation with the palatine and the pterygoid. These vomerine processes are sandwiched between the pterygoids medially and the palatine laterally, which bear short, plated processes for the vomer articulation.

Palatine

Both palatines are preserved (Figures 1, 29), which have the typical tetraradiate shape found in most non-avian theropods (Rauhut, 2003). The right element lacks the anterior maxillary process (Figure 28A, C, D), but it is present in the left element (Figure 28E, F). On the other hand, the right palatine bears a better preserved posteroventral aspect than its left counterpart (Figure 28B). The palatine contacts the vomer anterodorsally, the maxilla anteroventrally, the jugal and possibly the lacrimal posterolaterally, and the pterygoid posteromedially (Figures 2, 4). Solely, the dorsal portions of the palatines are exposed in the antorbital fenestrae (Figure 1), but their whole morphology is revealed by our CT data. We were able to segment the maxillary process of the left palatine separately from the maxilla, but this is not the case on the right.

The maxillary process is wide at its base but narrows anteriorly to an elongate rod. This rod tapers anteriorly and represents by far the longest process of the palatine. There is a shallow, anteroposteriorly oriented depression on the anteriormost third of the process, which faces ventrolaterally towards the maxilla. With this facet, the palatine articulates with the dorsal surface of the median ridge of the maxilla.

Dorsally, the vomeropterygoid process borders the internal choana anteriorly and the pterygopalatine fenestra posteriorly (Figure 4B). The process has a transversely broad ventral base, the posterior surface of which is excavated by a deep fossa between the posterior processes of the palatine. The vomeropterygoid process ascends dorsomedially and twists from a posterolaterally-anteromedially oriented base into an anteroposteriorly expanded, vertical, wing-shaped bony plate. This plate is more anteriorly expanded and tapers to a point anteriorly. However, a dorsoventrally high but anteroposteriorly short, rounded, posterior expansion is also present, as in most basal tetanurans (e.g., Madsen, 1976; Currie and Zhao, 1994; Eddy and Clarke, 2011), but in contrast to most non-avian coelurosaurs (e.g., Barsbold and Osmolska, 1999; Rauhut et al., 2010). The medial surface of the plate is parallel with the sagittal skull axis, and principally contacts the lateral surface of the vomeropalatine process of the pterygoid. However, anteriorly, the short articular process of the vomer becomes wedged between palatine and pterygoid (Figures 2, 4).

Posteroventral to the vomeropterygoid process, there is a medial process for the pterygoid and a lateral one for the jugal contact, which diverge posteriorly at an acute angle, framing the anteriorly narrow pterygopalatine/suborbital fenestra. The jugal process forms a vertically oriented plate that lies against the medial surface of the jugal. Its dorsal margin is continuous with the posteroventral margin of the vomeropterygoid process, forming a semicircular margin. The ventral margin of the jugal process is offset from the ventral margin of the maxillary process by a small concavity, but otherwise the process is posteriorly continuous with the maxillary process. As in most non-avian averostrans (see Carrano and Sampson, 2008), the jugal process is dorsolaterally more expanded than the maxillary process. At its posterior end, the jugal process bears a notch, possibly separating the process into a dorsal lacrimal process and a ventral jugal process, although it cannot be excluded that this notch might be an artifact of preservation, as this part of the palatine is only preserved on the right side and no contact with the lacrimal is obvious. The pterygoid process of the palatine is anteroposteriorly longer than the jugal process (as preserved). It is dorsoventrally high and lateromedially thin, with its distal end tapering. Its dorsal surface is markedly concave between the more vertical medial side and the lateroventrally flexed ventral margin. The medial margin of the pterygoid process of the palatine extends onto the medial surface of the vomeropterygoid process

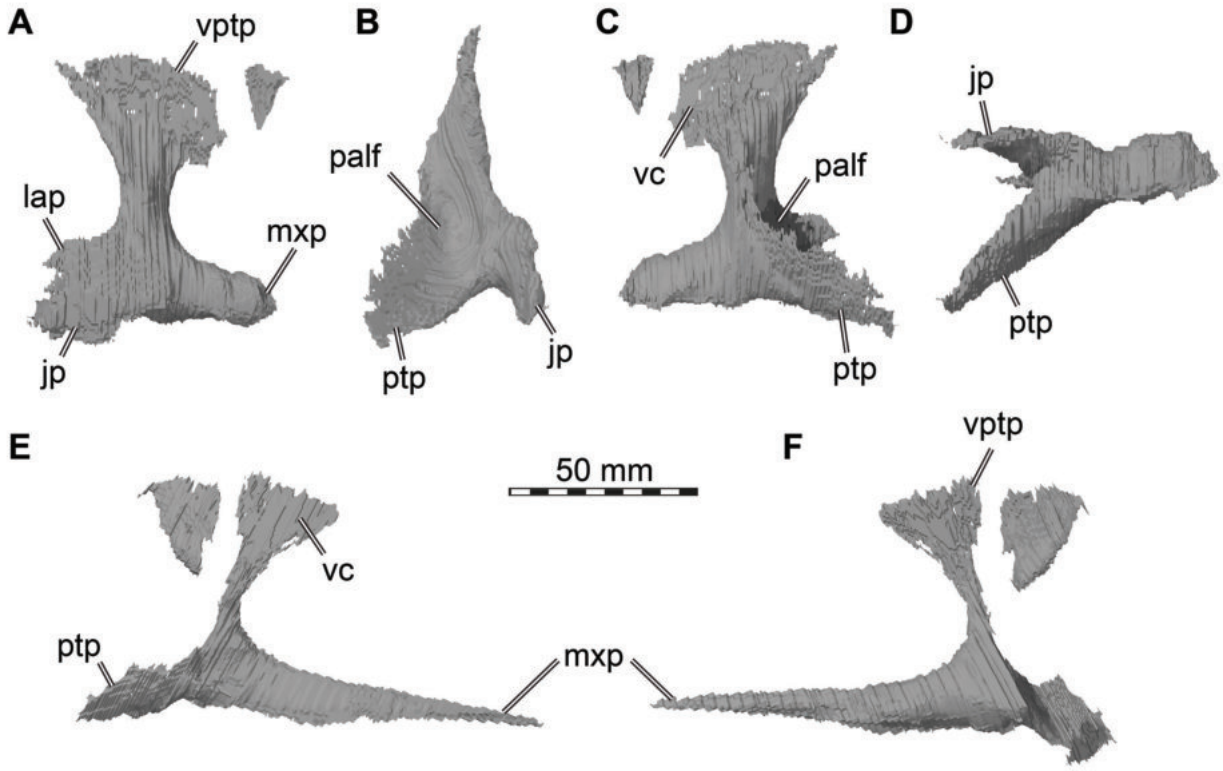

FIGURE 29. 3D renderings of the palatines of *Irritator challengeri* (SMNS 58022). A–D, right palatine in A, lateral view; B, posterior view; C, medial view; D, ventral view (anterior direction to the right). E–F, left palatine in E, medial view; F, lateral view. Abbreviations: jp, jugal process; lap, lacrimal process; mxp, maxillary process; palf, posterior palatine fossa; ptp, pterygoid process; vc, surface for contact with vomer; vptp, vomeropterygoid process.

and forms the medial margin of the posterior fossa on the base of the vomeropterygoid process.

Pterygoid

Both pterygoids are nearly completely preserved, but disarticulated from their life positions (Figures 1, 30). The left pterygoid is rotated clockwise out of its former position, and large parts of it are exposed in the fossil above the left surangular. The posterior portion of the right pterygoid lies ventrolateral to the basisphenoid. Our CT data reveal that both elongated pterygoids are largely intact, except for minor parts of their vomeropalatine processes and the posteriormost portion of the left quadrate wing (Figure 31). The pterygoid forms a connection of the anterior palate with the basicranial region. In contrast to other non-avian theropods, it is composed of only two main structures: an anteriorly directed palatine process, which contacts the ectopterygoid centrally and laterally, and the vomer and palatine at its anterior end, and the posterior quadrate wing, which forms articulation surfaces for the epipterygoid and quadrate (Figures 2-4). In between the two main parts lies the articular facet for the basipterygoid processes of the basisphenoid.

The vomeropalatine process is elongated and mediolaterally thin. It is slightly bowed anterodorsally where it ascends towards the vomeropterygoid process of the palatine. As in most non-avian theropods (e.g., Madsen, 1976; Ostrom, 1969; Currie and Zhao, 1994), the vomeropalatine process is approximately L-shaped in cross-section, with a more vertical medial and a more horizontal lateral part. Both rami are of subequal width and gently curve into each other. From the basipterygoid processes posteriorly, the right and left anterior processes approach one another medially, thus constricting the interpterygoid vacuity. The surface of the anterior process is dorsolaterally concave and ventromedially convex. Around the mid-length of the process, the ectopterygoid articulates laterally on an unremarkable surface of the margin of the vomeropalatine process. This ectopterygoid-pterygoid contact is unusual, both in terms of its position and morphology: usually, the ectopterygoid contacts the pterygoid at the posterior end of the latter along a lateroventral ectopterygoid

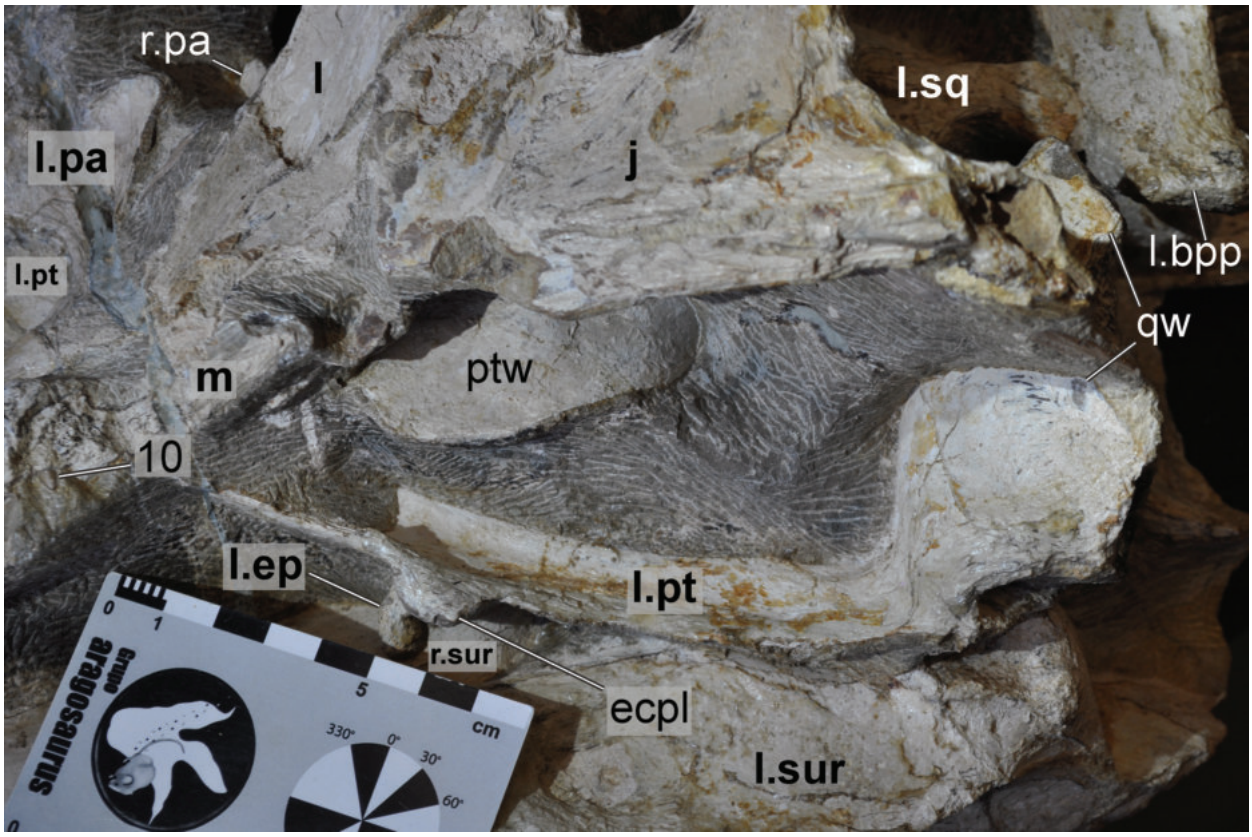

FIGURE 30. Close-up photograph of the left cheek region of *Irritator challengeri* (SMNS 58022). Note that bones are labelled in bold, and other anatomical structures in regular font. Abbreviations: j, jugal; l, lacrimal; l.ep, left ectopterygoid; ecpl, ectopterygoid lamina of the left pterygoid; l.bpp, left basipterygoid process of the parabasisphenoid; l.pa, left palatine; l.pt, left pterygoid; l.sur, left surangular; l.sq, left squamosal; m, maxilla; ptw, pterygoid wing of left quadrate; qw, quadrate wing of left pterygoid; r.pa, right palatine; r.sur, right surangular; 10, tenth preserved tooth position of the left maxilla.

ramus, which projects off the contact point between the vomeropalatine process and quadrate wing of the pterygoid (Madsen, 1976, Eddy and Clarke, 2011; Brusatte et al., 2012; Chure and Loewen, 2020). However, an ectopterygoid ramus of the pterygoid is entirely absent in both pterygoids of *Irritator*. In order to close the pterygopalatine fenestra/suborbital fenestra transversely, the ectopterygoid position is inferred relatively far anteriorly in comparison to other non-avian theropods; this also coincides with the position that both ectopterygoids are preserved in relation to their respective pterygoids in the specimen (see Ectopterygoid section for additional details). Furthermore, both pterygoids show a slight lateral thickening at the approximate site of the ectopterygoid contact, with a small, semicircular ventral expansion of a very thin bony lamina on the left element, which is visible on the fossil (Figures 1A, 30; see also Figure 31A, D). Anterior to the ectopterygoid contact, the anterior third of the vomeroplatine process underlies the ventromedial surface of the palatine in our articulated skull reconstruction. At its anterior tip, the vomeropalatine process bears a short, plate-like process, which is slightly turned downwards regarding the main axis of the vomeropalatine process. This plate-like process articulates with the vomer anteriorly and with the palatine medially (Figures 2, 4B).

Posteriorly, the pterygoid forms a large, more laterally positioned quadrate wing and short posteromedial process; the right wing is posterodorsally more complete and exhibits a small area medial to the right jugal-quadratojugal contact (Figure 1B). The quadrate wing is a posteriorly and slightly laterally directed, transversely thin sheet of bone that is considerably higher dorsoventrally than long anteroposteriorly. The anterior margin of the wing is ventrally slightly thickened and ascends almost perpendicularly from the dorsal margin of the vomeropalatine process. The posterior margin is concave, and the pointed ventral part extends as

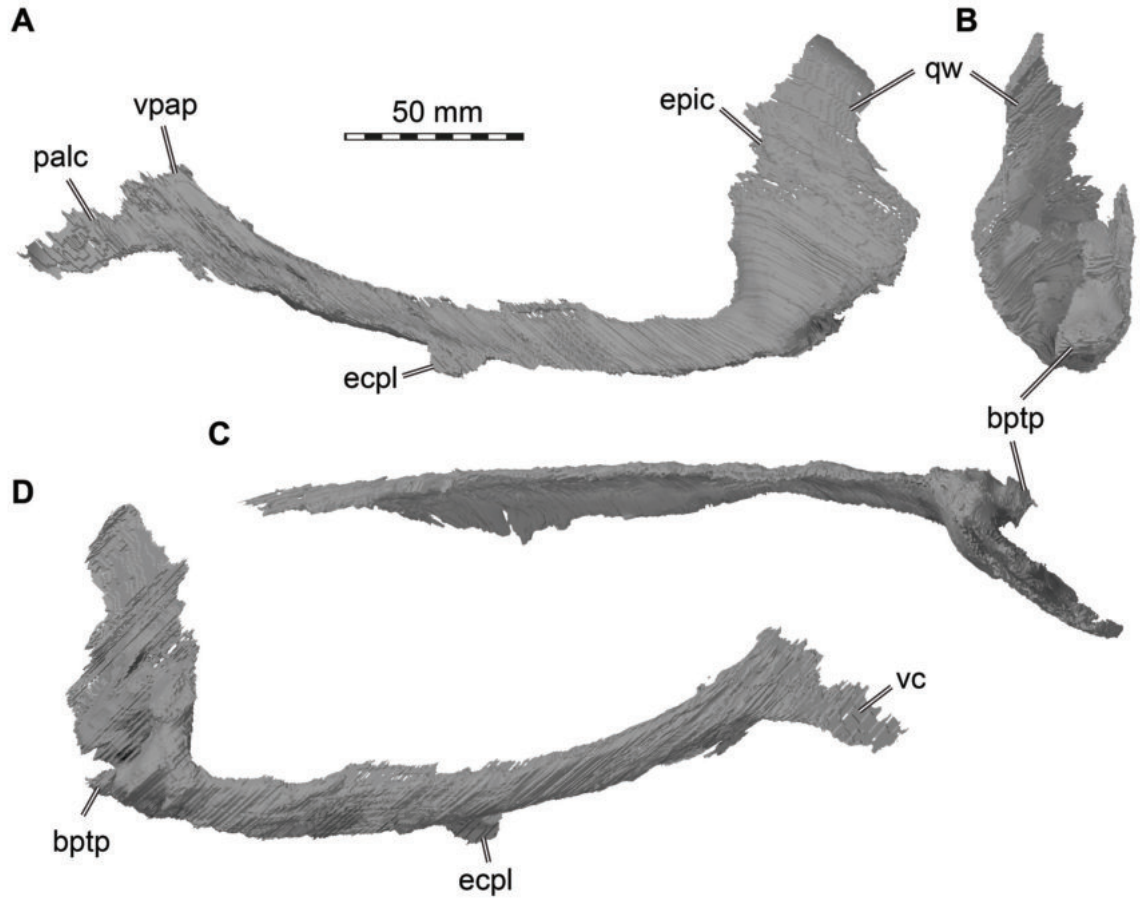

FIGURE 31. 3D renderings of the left pterygoid of *Irritator challengeri* (SMNS 58022). A, lateral view; B, posterior view; C, dorsal view; D, medial view. Abbreviations: bptp, basipterygoid process; ecpl, ectopterygoid lamina; epic, epipterygoid contact; palc, palatine contact; qw, quadrate wing; vc, vomer contact; vpap, vomeropalatine process.

widely posteriorly as the dorsal part. The anterior and posteroventral margins are flexed inwards, so that the medial surface of the quadrate wing is concave, whereas the lateral surface is convex. The lateral surface articulates with the pterygoid flange of the quadrate (Figures 2-4). Ventrally, at the base of the quadrate wing, the pterygoid has a short posteromedial process, which is separated from the quadrate wing by a broad, shallow groove. The process is posteriorly directed and receives the basipterygoid process of the parabasisphenoid dorsomedially. Above the basipterygoid articulation, the parabasisphenoid and pterygoid leave a dorsoventrally tall anteroposterior passage, the cranioquadrate space. A distinct notch is present between the basipterygoid process and the ventral portion of the quadrate wing (Figure 31C).

Ectopterygoid

The CT data reveal that both ectopterygoids are well preserved (Figure 32) but are no longer in articulation with their neighboring bones. Only a small portion of the posteromedial process of the left ectopterygoid is visible on the fossil, below the left pterygoid (Figures 1A, 30). Both elements bear a transverse crack in a very similar manner on the jugal process. The ectopterygoid of *Irritator* is conspicuously small and slender and lacks the typical medial expansion seen in nearly all non-avian theropods (Rauhut, 2003). The ectopterygoid likely contacted the jugal laterally and the pterygoid medially and formed the anterior margin of a large, elongate oval subtemporal fenestra of the articulated skull in ventral view (Figures 2-4).

As is typical for non-avian theropods, the lateral jugal process is hook-shaped, being flexed posterolaterally so that the jugal facet is almost parallel to the pterygoid contact. The medial ectopterygoid body is anteroposteriorly long and dorsoventrally slim. The jugal contact is flexed posteriorly at a perpendicular angle. The lateral-facing contact area is elongated and pointed posteriorly; it

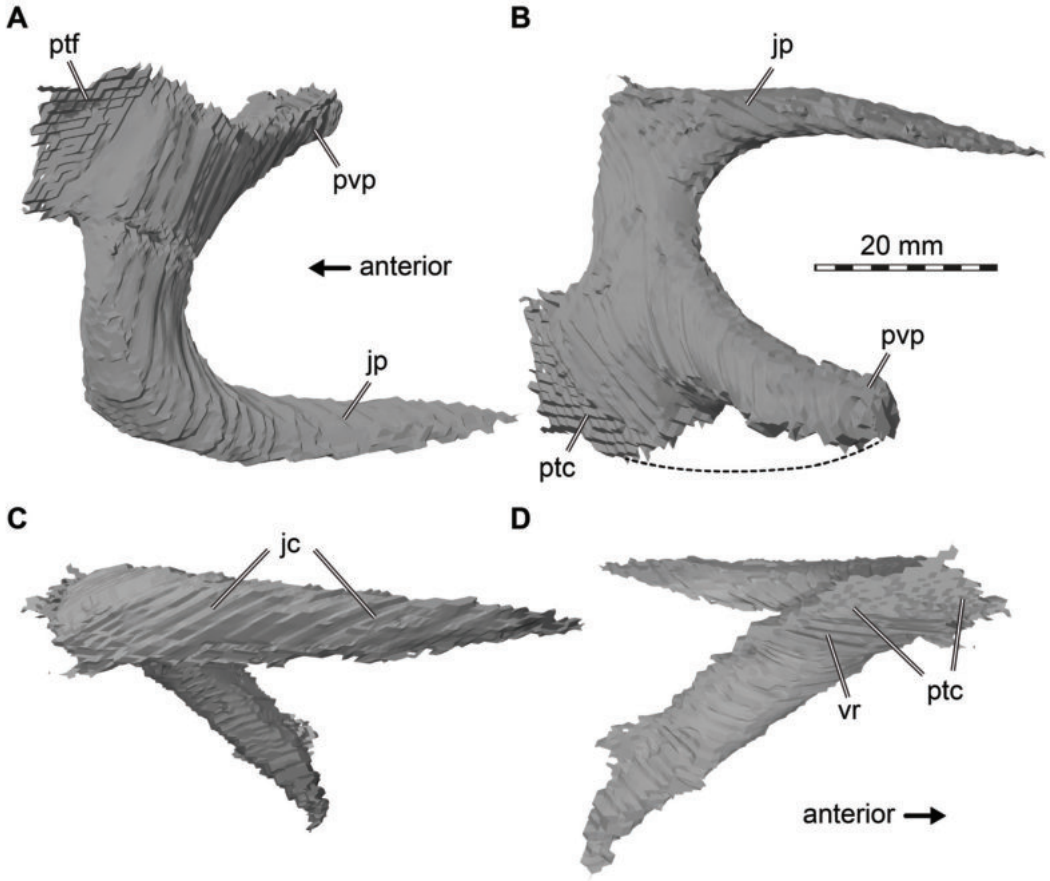

FIGURE 32. 3D renderings of the left ectopterygoid of *Irritator challengeri* (SMNS 58022). A, dorsal view; B, ventral view; C, lateral view; D, medial view. Arrow in A valid for A-C. Note that dashed line indicates approximate former extent of bone. Abbreviations: jc, jugal contact; jp, jugal process; ptc, pterygoid contact; ptf, pterygoid flange; pvp, posteroventral process; vr, ventral recess.

lacks the anteroventral process present in, e.g., *Dubreuillosaurus* (Allain, 2002) and *Asfaltovenator* (Rauhut and Pol, 2019). The ectopterygoid articulates with the jugal at about the mid-length of the latter, which is like other non-avian theropods (Sampson and Witmer, 2007; Brusatte et al., 2012).

The medial ectopterygoid body is angled posteroventrally at an angle of approximately 45° towards the jugal articulation. The pterygoid contact is formed by a short, broad, wing-shaped bony lamina anteriorly and a long, mediolaterally slender, but dorsoventrally thicker posterior process. The articulation surface for the pterygoid is only slightly longer than the articulation surface for the jugal. A marked, posteriorly deepening longitudinal step separates the anterior sheet from the posterior process, thus defining a posteriorly deepening ventral depression on the medial side of the ectopterygoid body (Figure 32D). This depression corresponds to the ventral ectopterygoid fossa that is present in most non-avian neotheropods, except for ceratosaurs (Rauhut, 2003). However, this fossa does not invade the lateral part of the ectopterygoid body, unlike in most other basal tetanurans (e.g., Madsen, 1976; Currie and Zhao, 1994; Eddy and Clarke, 2011).

The combined pterygoid-ectopterygoid morphology of *Irritator* suggests that these elements had a mode of articulation that is unusual for non-avian theropods. Usually, the strongly expanded medial surface of the ectopterygoid contacts both the lateral margin of the base of the vomeropalatine process of the pterygoid and a posteroventrally directed ectopterygoid ramus of the pterygoid, thus accounting for the notable twist between the jugal articulation and the pterygoid contact (Madsen, 1976; Sampson and Witmer, 2007; Eddy and Clarke, 2011; Brusatte et al., 2012; Chure and Loewen, 2020). In *Irritator*, the ectopterygoid ramus of

the pterygoid is entirely absent, but the general morphology of the contact between the pterygoid and ectopterygoid is the same as in other non-avian theropods (Sampson and Witmer, 2007), with the thin anterior lamina of the ectopterygoid body overlapping the pterygoid dorsally, whereas the latter overlaps the thickened ectopterygoid body posteriorly (Figures 2B, 4B). Furthermore, the twist between the articular surfaces is still present, as noted above. As noted in the description of the pterygoid, the narrow mediolateral width of the ectopterygoid in *Irritator* suggests that this bone had a relatively far-forward position in the skull: the ectopterygoid is mediolaterally not wide enough to reach the pterygoid and the jugal simultaneously on the posterior portion of the pterygoid. In this area, the slightly anterodorsally flexed vomeropalatine process of the pterygoid is steeply anterodorsally inclined in the articulated skull, probably explaining why the twist between the articular ends of the ectopterygoid is present despite of the absence of an ectopterygoid wing of the pterygoid. In our articulated skull reconstruction, the ectopterygoid thus contacts the jugal immediately posterior to the posterior end of the 'paperclip-like' maxilla-jugal contact, in a position between the orbit and antorbital fenestra (Figure 4B). Usually, the ectopterygoid articulates with the jugal around its mid-length and below the orbit in non-avian theropods (Sampson and Witmer, 2007; Brusatte et al., 2012; Evers et al., 2020).

Close to the articulation surface for the pterygoid, there are small, discrete cavities within the ectopterygoid body, without a clear connection to a pneumatic foramen.

Epipterygoid

The epipterygoid contacts the pterygoid ventromedially. In our CT data, we found two exceptionally thin elements (Figure 33) that are only partly visible in the fossil, wedged between the posterior portion of the right surangular and articular and the quadratojugal and jugal, and thus not preserved in their original position (Figure 1B). However, comparison with described epipterygoids of other non-avian theropods (Eddy and Clarke, 2011; Brusatte et al., 2012) allows unambiguous identification of the thin elements as this bone. The left epipterygoid is slightly better preserved than the right element, but both agree in general morphology.

The epipterygoid of *Irritator* is a dorsoventrally tall plate with an anteroposteriorly wide base and tapering dorsal end. The anterior margin of the epipterygoid is somewhat thickened compared to the thin blade making up the remainder of the bone. The medial surface, which would lie against the quadrate wing of the pterygoid, is gently concave. Anteroventrally, there is a small, posteriorly recurved flange on the medial surface, which appears to have received the anterior margin of the quadrate wing of the pterygoid, similar to the condition described in *Alioramus* (Brusatte et al., 2012). *Acrocanthosaurus* and *Alioramus* bear a distinct articulation surface for the epipterygoid on their dorsolateral quadrate process of the pterygoid (Eddy and Clarke, 2011; Brusatte et al., 2012). This is not the case in *Irritator*, which makes it difficult to determine its exact position. However, based on the flange for the anterior quadrate wing margin, we placed the epipterygoid along the anterior margin, at a mid-height level of the quadrate wing of the pterygoid (Figure 2A).

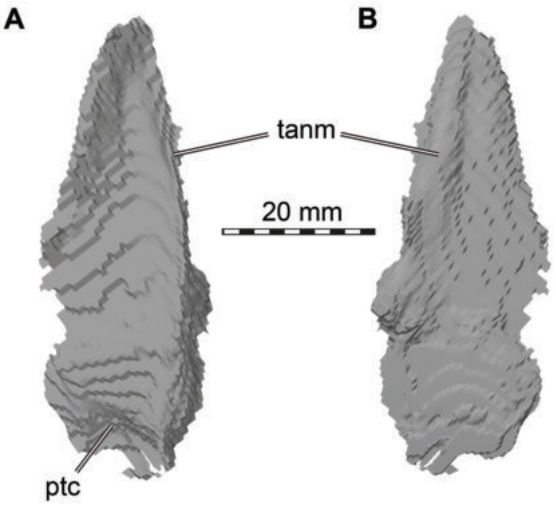

FIGURE 33. 3D renderings of the left epipterygoid of *Irritator challengeri* (SMNS 58022). A, medial view; B, lateral view. Abbreviations: ptc, pterygoid contact; tanm, thickenend anterior margin.

Mandible

As noted by Sues et al. (2002), the mandible is incompletely preserved on both sides, with only the surangular and articular being preserved for both mandibular rami, plus the almost complete prearticular and parts of the angular on the left side (Figure 1). In contrast to most non-avian theropods, the jaw articulation is anteroventrally inclined, so that the posterior end of the mandible is approximately level with the posterior end of the skull (Figure 2). A relatively large mandibular fenestra is present and largely preserved (Figures

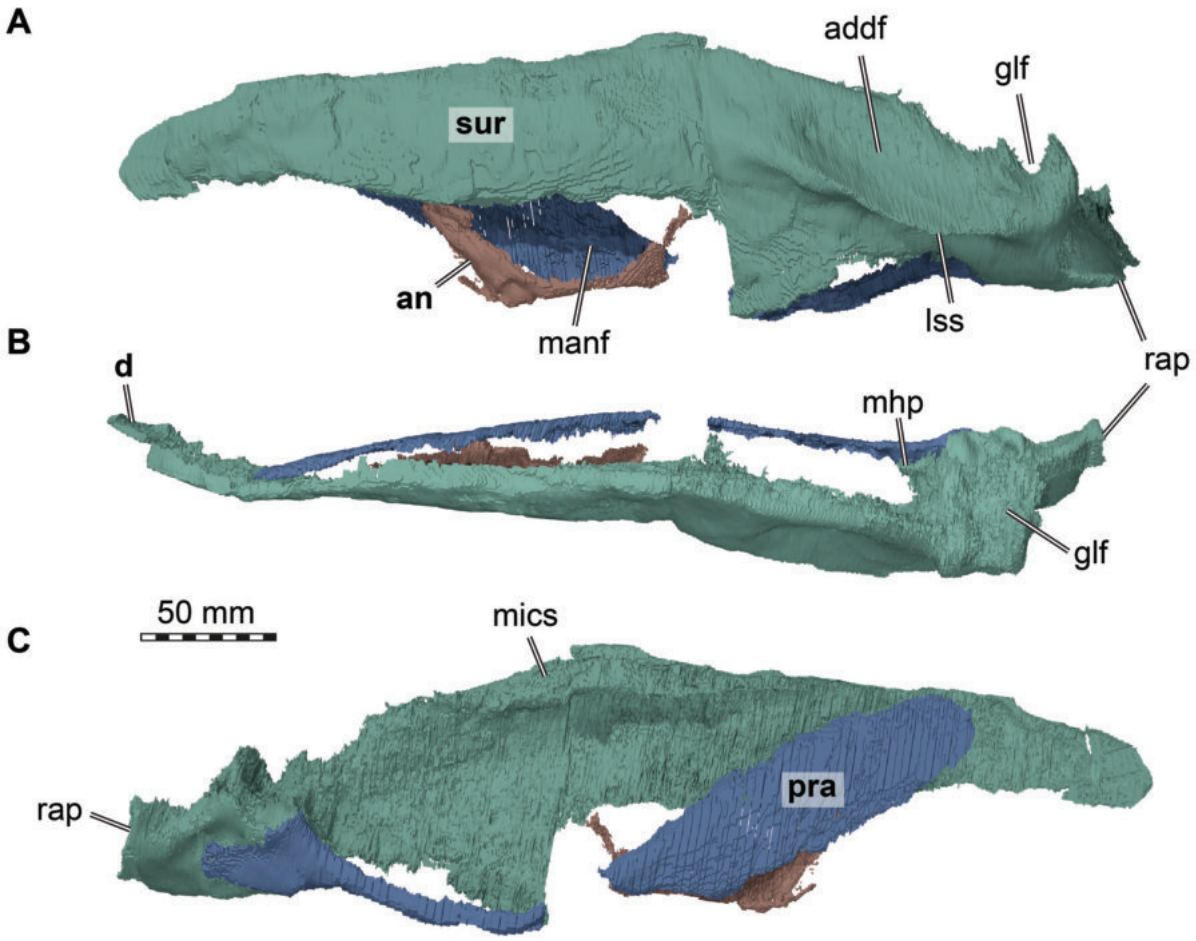

FIGURE 34. 3D renderings of left mandibular elements of *Irritator challengeri* (SMNS 58022). A, lateral view; B, dorsal view; C, medial view. Abbreviations: addf, adductor fossa; an, angular; d, dentary; glf, glenoid fossa; lss, lateral surangular shelf; manf, mandibular fenestra; mhp, medial hook process; mics, medially inclined coronoid shelf; pra, prearticular; rap, retroarticular process; sur, surangular. Note that different bones are rendered in different colours, and that bone labels are in bold. Also note that the articular is fused with the surangular and thus segmented in a joint model with that bone.

1A, 2A, 34A), being bordered dorsally and posterodorsally by the surangular and anteroventrally, ventrally and posteroventrally by the angular; the fenestra is unusual in shape in that the ventral margin is strongly concave, whereas the dorsal rim is rather straight. The fenestra is ventrally placed in the mandible so that the surangular accounts for approximately half the height of the mandible in this area.

Surangular + Articular

Both surangulars are largely complete (Figures 34, 35), but the right element is missing its anterior end. Additionally, both retroarticular processes are damaged and the ventral margins of the surangulars near the contact with the respective angular are unclear, as the morphology differs slightly between the right and left element. In the fossil, the left surangular is largely exposed in lateral view close to its original position in the articulated skull, whereas the right surangular is rotated approximately 180° along its anteroposterior axis regarding its original position, which results in its medial surface being exposed on the right side of the specimen (Figure 1). As preserved, the surangular of *Irritator* contacts the dentary anteriorly, the prearticular medially, the angular ventrally and the articular posterodorsally (Figure 2).

The surangular and articular seem to be fused in both mandibular rami. There is no unequivocal external sutural contact between both bones, and our CT data fail to completely follow sutures internally. Thus, the surangular and articular were seg-

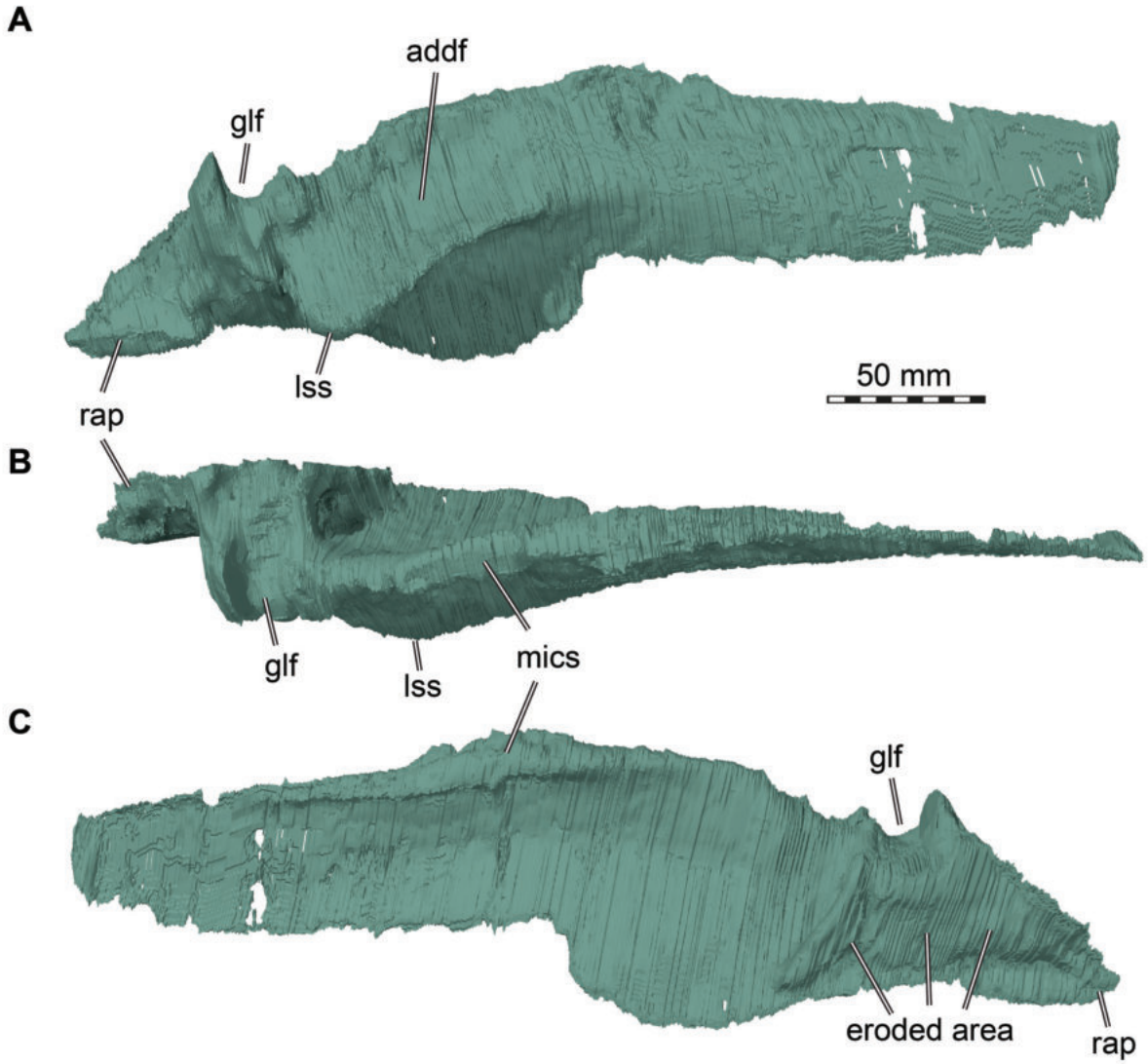

FIGURE 35. 3D renderings of right surangular of *Irritator challengeri* (SMNS 58022). A, lateral view; B, dorsal view; C, medial view. Abbreviations: addf, adductor fossa; glf, glenoid fossa; lss, lateral surangular shelf; mics, medially inclined coronoid shelf; rap, retroarticular process. Note that the articular is fused with the surangular and thus segmented in a joint model with that bone.

mented as single models, and their morphology is described together here.

The surangular is anteroposteriorly elongated. The anterior portion of the bone is mediolaterally thin. The dorsal margin of this anterior part of the bone is straight. The ventral margin parallels the dorsal margin in the area where it forms the dorsal margin of the mandibular fenestra but expands ventrally at the level of the posterior end of this opening. On the better-preserved right side, there is a small, anteriorly open notch at the dorsal end of this expansion, marking the narrowly rounded, dorsally placed posterior end of the mandibular fenestra. However, the exact position, size, and shape of the fenestra can only be estimated based on the angular, as the ventral margin of the anterior surangular ramus itself shows no notch or curvature that would allow identification of the anteroposterior length of the fenestra just based on surangular morphology. Anterior to the mandibular fenestra, the ventral margin of the surangular very slightly converges with the dorsal margin, and the blunt anterior end of the surangular was overlapped laterally by the dentary, of which a small fragment is preserved in this position on the left side, as shown by Sues et al. (2002). In cross-sec-

tion, this anterior part of the surangular is slightly convex laterally and concave medially. On approximately one-fifth of the length of the surangular posterior to its anterior end, the dorsal margin of the anterior surangular ramus becomes gradually thicker until it forms a robust, medially infolding shelf for the articulation with the coronoid. The shelf becomes wider and more robust posteriorly until it turns into a dorsomedially opening groove above the posterior end of the mandibular fenestra, where the dorsal margin of the surangular is strongly thickened and approximately triangular in cross-section. The groove ends at approximately the level of the posterior end of the mandibular fenestra, posterior to which the dorsal margin of the surangular becomes gradually thinner again towards the jaw articulation. The facet for the obviously anteroposteriorly elongate coronoid thus forms a dorsally facing medial shelf anteriorly and a dorsomedially facing groove posteriorly, in contrast to the simple, medially facing facet in other non-avian theropods (e.g., Madsen, 1976; Currie and Zhao, 1994). There is no sign of an anterior surangular foramen and an anteriorly extending groove from that foramen on the lateral side, as is present in many other non-avian theropods (e.g., Madsen, 1976; Currie and Zhao, 1994; Currie, 2003; Sampson and Witmer, 2007; Rauhut et al., 2010).

The laterally rugose coronoid eminence at the level of the posterior end of the mandibular fenestra marks the transition to the posterior portion of the surangular, forming a distinct kink in lateral view so that the straight dorsal margin of the posterior portion slopes ventrally at an angle of approximately 35° with respect to the anterior portion. The dorsal margin is maximally mediolaterally thickened in this area, so that the medial surface of the surangular keeps the concavity seen in the anterior portion.

The lateral surface of the posterior portion bears a prominent surangular shelf, which projects lateroventrally. The shelf starts anteriorly with a marked lateral thickening dorsal and slightly posterior to the posterior margin of the external mandibular fenestra and stretches posteroventrally to below approximately the half-length of the glenoid fossa of the articular. In the left element, the shelf is not completely preserved. Based on CT data of the right surangular, the shelf is posteriorly rounded and expands far lateroventrally. Dorsal to the shelf, a marked, anteroposteriorly long, oval adductor fossa is present, placed somewhat anterolateral to the jaw articulation and directed dorsolaterally and very slightly posteriorly. The shelf seems to be similar in *Baryonyx* (Charig and Milner, 1997), but different in other non-avian theropods, where it is less prominent and projects laterally without a ventral deflection (e.g., Madsen, 1976; Sampson and Witmer, 2007: Eddy and Clarke, 2011; Brusatte et al., 2012). Posteriorly and very slightly dorsally to the shelf, a marked, rounded lateral tubercle is present at the posterior end of the glenoid fossa. Anterodorsal to this tubercle and thus dorsal to the posterior end of the lateral surangular shelf, the anterolateral margin of the glenoid is marked by a raised, slightly laterally overhanging ridge.

Below the lateral surangular shelf, the left side shows two foramina, leading to the medial side of the surangular. The anterior foramen is placed slightly more ventrally, approximately 1 cm anterior to the anterior rim of the glenoid and seeming to pierce the surangular more or less straight mediolaterally, whereas the second foramen is placed slightly more dorsolaterally in the lateral shelf, just below the anterior rim of the glenoid, and opens posterolaterally. Two posterior surangular foramina are also present in some other non-avian theropods, such as *Sinraptor* (Currie and Zhao, 1994), *Proceratosaurus bradleyi* (Rauhut et al., 2010), and *Allosaurus* (Benson, 2010).

Both articulars are present but neither is complete. The articular surface for the quadrate is formed between the articular and surangular, and exact contributions cannot be discerned due to the fusion of the latter two elements. The entire articular region is mediolaterally wide and medially expanded with regard to the vertical plate formed by the anterior parts of the surangular. The articular surface shows two distinct facets that subdivide the glenoid; a mediolaterally smaller, but anteroposteriorly slightly longer, medial one for the entocondyle and a lateral one for the ectocondyle. The posterior margin of the lateral facet of the glenoid is strongly dorsally elevated to form a high, transversely oriented projection that is tongue-shaped in posterior view. This projection is separated from the also slightly elevated posteromedial edge of the medial condyle by a wide incision that forms an obtuse angle in posterior view. The anterior margin of the glenoid is bound by a low ridge on its lateral half. At the anteromedial end of the glenoid fossa, a slightly anteriorly recurved ridge descends along the margin of the articular (‘medial hook process’ of *Alioramus*; Brusatte et al., 2012).

The left surangular bears a medial, anteroventrally facing spur for articulation with the prearticular that seems to be absent in other non-avian

theropods (e.g., Madsen, 1976; Brusatte et al., 2012). The left articular is still in its original contact with the prearticular, and this area appears to be intact in medioventral view, with the entocondyle of the quadrate fitting precisely into the respective glenoid (in the articulated skull reconstruction).

The retroarticular process is unusual in *Irritator*. In lateral view, it is strongly offset ventrally from the glenoid portion of the surangular/articular, being placed entirely below the level of the lateral surangular shelf and forming an almost right angle with the subvertical posterior wall of the glenoid. Some aspects of the retroarticular process are better preserved on the right side (Figure 35) and some are better preserved on the left side (Figure 34). The left retroarticular process is lobe-shaped in medioventral view and rather thin dorsoventrally, being somewhat inclined mediodorsally. In contrast to most other non-avian averostrans (e.g., Madsen, 1976; Sampson and Witmer, 2007), the articular surface for the *m. depressor mandibulae* is not developed as a concavity, but the dorsal surface of the process is gently convex mediolaterally. The posteriormost portion of the left process is missing. In contrast, the right retroarticular process is anteroposteriorly longer than its left counterpart, indicating that the process was originally about twice the anteroposterior length of the glenoid fossa. The medial side of the right glenoid region and retroarticular process is largely eroded, but the left side shows that a ridge extended from the dorsomedial side of the process to the posteromedial edge of the glenoid. A marked, ventrally overhanging angular medial process, as it is present in some non-avian theropods in this region (e.g., Yates, 2005), is absent. The chorda tympani foramen could not be identified in the CT images.

There is a diffuse network of cavities present ventral to the glenoid fossa, close to the surangular and articular articulation surface, made up of many different-sized cavities that are not always interconnected. The cavities of the right network are usually larger. The anteriormost of those are situated anteroventral to the articular surface for the quadrate and seem to bear foramina on the anteromedial articular surface for the prearticular. Posteriorly, cavities of this network extend to the retroarticular process base. Posteroventrally to the glenoid fossa for the ectocondyle, the right surangular bears a comparatively large cavity. Such a cavity is more ventrally situated and smaller in the left surangular.

Angular

Only the left angular is preserved, being in its presumed original position regarding the left surangular, but only a portion of its anterior part is present (Figures 1, 34). Thus, little can be said with certainty about the angular morphology in *Irritator*. As preserved, the dorsal margin of the angular is deeply convex and borders the external mandibular fenestra ventrally. This margin seems to be original and thus indicates the shape of the mandibular fenestra. The dorsal concavity of the bone is more marked than in most other non-avian theropods, with the dorsal margin of the anterior prong being set at an angle of c. 70° in respect to the dorsal margin at the posteroventral part of the mandibular fenestra, similar to the condition in *Acrocanthosaurus* (Eddy and Clarke, 2011). However, this angle is about 30° in *Majungasaurus* (Sampson and Witmer, 2007), 40° in *Allosaurus* (Madsen, 1976), and *Sinraptor* (Currie and Zhao, 1994), and 50° in *Alioramus* (Brusatte et al., 2012). Consequently, the anterior prong of the angular is strongly anterodorsally directed and reaches the level of the ventral margin of the surangular dorsally, as in *Herrerasaurus* (Sereno and Novas, 1993). The anterior end of the anterior prong is pointed. Anterodorsally, a small, laterally facing shelf is developed, which might indicate a contact with the surangular. Here, the medial side is markedly flattened, probably for the contact with the prearticular. At the ventral end of the anterior prong, a small, anteriorly projecting process is present. Whereas the anterior prong of the angular is thickened, as is usual in non-avian theropods, the posterior half of the preserved portion is only represented by a thin, dorsally bent bridge. Posterior to the preserved part, the angular most probably broadly overlapped the ventral lamina of the surangular laterally, but there does not seem to be a marked facet for the angular at the level of the retroarticular process, indicating that the angular did not reach the posterior end of the mandible. Between the posterior bridge of the preserved part of the angular and the surangular, a foreign body has been added to the fossil, which can clearly be discerned in the CT data (Figures 1, 34).

Prearticular

Only the left prearticular of *Irritator* is preserved, but the element is nearly complete except for a central piece that is entirely missing, and possibly a part of the ventral margin in the posterior half of the element (Figures 1, 34). The left prearticular is preserved in articulation with the left

surangular/articular, which it contacts posterolaterally. The other bone contacts are not preserved but based on lower jaw morphology of other non-avian theropods, it probably contacted the splenial anteriorly, the coronoid posterodorsally, the angular anteroventromedially, and possibly the dentary anterodorsally (Figures 2, 3; see, e.g., Zhao and Currie, 1994 for comparison). As preserved, the prearticular is a mediolaterally thin and anteroposteriorly long element. It is ventrally bowed along its mid-length, forming a distinctly concave dorsal and convex ventral margin. The ventral margin in the anterior portion parallels the dorsal margin, although it cannot be completely excluded that minor portions of the very thin ventral bony lamina are broken away here. The anterior part of the prearticular is dorsoventrally expanded with regard to the central portion of the bone. The latter seems to have been very slender, although it is possibly missing minor parts of the ventral lamina, and only the dorsal margin is still intact. There is no incision in the anteroventral margin of the anterior part, which is present in *Allosaurus* (Madsen, 1976) and *Acrocanthosaurus* (Eddy and Clarke, 2011). Posteriorly, the bone ends with a dorsoventrally expanded, triangular surface that lies medially against the surangular and the articular at the level of the glenoid fossa (Figures 1B, 34). Although this expansion seems to taper posteriorly in its ventral part, the prearticular of *Irritator* does not seem to form a thin process that underlies the retroarticular process, a condition seen in many other non-avian theropods, including *Majungasaurus* (Sampson and Witmer, 2007) and *Acrocanthosaurus* (Eddy and Clarke, 2011). Anterior to this posterior expansion, the ventral margin of the prearticular becomes slightly thickened mediolaterally.

Dentition

The only tooth-bearing bone preserved in *Irritator* is the maxilla (Figure 1). One unusual character of *Irritator*, even in comparison to other spinosaurids for which maxillae are known (Charig and Milner, 1997; Sereno et al., 1998; Taquet and Russell, 1998; Dal Sasso et al., 2005), is the extremely wide spacing of the anterior maxillary teeth (Figures 1-2, 4-6). The teeth are more widely spaced in the maxilla anteriorly than posteriorly in *Irritator*. From the first to the seventh preserved alveoli of the left maxilla, the distance between the alveoli is larger than the mesiodistal length of the alveoli. In the last six preserved tooth positions in the detached fragment of the right maxilla (Figure 6), this spacing rather abruptly becomes less than the mesiodistal length of the teeth; this seems also to be the case on the left side. This is the opposite of the condition found in a snout referred to *Spinosaurus*, in which the spacing of the teeth increases in more distal teeth (Dal Sasso et al., 2005). This was apparently also the situation in the maxillary fragment that was part of the holotype of *Spinosaurus* (Stromer, 1915).

The number of teeth in the maxilla of *Irritator*, as well as the identification of the preserved teeth (and thus the total number of teeth originally present in the maxilla) have been contentious. Martill et al. (1996) stated in the diagnosis of the taxon that more than 11 teeth were present in the maxilla, and later mentioned that the snout "bears at least 16 large teeth" (Martill et al., 1996: 6), though they did not clarify if this was the total number of preserved teeth or the estimated number of teeth in one maxilla. Sues et al. (2002) identified nine teeth in the left and 10 tooth positions in the right maxilla and suggested that the total number of maxillary teeth was at least 11. In comparison with other known spinosaurid maxillae, Sales and Schultz (2017) suggested that the first preserved maxillary alveolus of *Irritator* is the third one and identified eight additional tooth positions in the left maxilla, resulting in a total number of nine preserved maxillary teeth; their counting suggested tooth positions three to 11 to be present. However, our results show that 10 tooth positions are preserved in the left maxilla (Figures 4B, 5). Sues et al. (2002) and Sales and Schultz (2017) were only able to identify nine tooth positions in this element, because the crown of the 8th preserved tooth position is lost, and the respective alveolus is covered by sediment. Furthermore, this is exactly the position in which the tooth spacing switches from widely to closely spaced, resulting in the impression that the seventh and ninth preserved tooth positions might be as widely spaced as more anterior teeth. However, an additional alveolus between these positions is clearly visible in the CT data.

In the right maxilla, two tooth positions are preserved in the main body and still articulated with the rest of the skull (contra Sales and Schultz, 2017, who identified the first preserved tooth in the detached fragment as the second preserved tooth position in total), whereas the detached toothed fragment includes preserved teeth or fragments of 10 tooth positions, resulting in a total number of 12 preserved tooth positions on this side (Figure 6). Mirroring the detached fragment of the right maxilla onto the left maxilla, the last two tooth positions would be placed in a short section of the left maxil-

lary body that is broken away posterior to the tenth preserved tooth, so that 12 tooth positions might also have originally been present in the left element. Thus, the number of preserved tooth positions in the holotype of *Irritator* can now be established as 12.

Concerning the question of which tooth positions are preserved and thus how many teeth were originally present in the maxilla of *Irritator*, this is more complicated to answer. As noted above, Sales and Schultz (2017) identified the first preserved tooth position as the third maxillary tooth, arguing that the fourth maxillary tooth is the largest in all known spinosaurid maxillae, which would coincide with the second tooth preserved in the left maxilla of *Irritator*. However, although the second preserved tooth on the left side is indeed larger than the first, the CT data show that the first and second preserved alveoli in *Irritator* are of subequal size. Furthermore, the condition in other spinosaurids is less clear than argued by Sales and Schultz (2017). Although the fourth alveolus is clearly the largest in the snout referred to *Spinosaurus* by Dal Sasso et al. (2005) and apparently also in the spinosaurid snout MNHN SAM 124 (Taquet and Russell, 1998), it is the third alveolus in *Baryonyx* (NHMUK R 9951; Charig and Milner, 1986, 1997), whereas alveoli three to six are largest and are of subequal size in *Suchomimus* (MNN GAD 501). Thus, given the subequal size of the first two alveoli, the first alveolus preserved in *Irritator* might well be tooth position three, four, or five, resulting in a total tooth count of 14 to 16 teeth, which would be more than in the snout referred to *Spinosaurus* (12 maxillary teeth; Dal Sasso et al., 2005), but considerably less than in *Suchomimus* (22 maxillary teeth; Sereno et al., 1998). On the other hand, in all known spinosaur snouts (Charig and Milner, 1997; Sereno et al., 1998; Taquet and Russell, 1998; Dal Sasso et al., 2005), the snout starts to curve upwards approximately at the level of the fourth tooth position, and the alveolar border is already markedly flexed anterodorsally at the level of the third alveolus. This does not seem to be the case in the first preserved alveolus in *Irritator*, indicating that this might represent a tooth position posterior to the third. Given the uncertainty in the tooth count, tooth positions given in the following always refer to preserved positions. Although our tooth position interpretation would invalidate the main argument used by Sales and Schultz (2017) to exclude *Angaturama* from being the same specimen as the holotype of *Irritator*, these authors provide further tentative reasons, such as relative proportional differences and slight differences in the preservational mode (Sales and Schultz, 2017). Based on our observations, we cannot provide any further information that could resolve this question.

The third preserved alveolus of the right maxilla houses a replacement tooth, while the remnants of the respective functional tooth are preserved in the detached maxillary fragment (Figure 6). It is unclear if the fourth preserved position holds the original functional crown, which is anteriorly and posteriorly surrounded by splinters of this same crown, or if three discrete teeth are situated here, which could be interpreted from the CT data. Potentially, this situation is pathologic; the carinae of the anterior 'splinter' are somewhat obliquely oriented in comparison to the definite functional tooth in this position. However, because of this uncertain situation and the fact that the crown of the fourth tooth position is labiolingually thin, more labially situated in comparison to other crowns, and seems—in respect to the third and fifth tooth position—distally shifted, we consider it as artificially glued there. The fifth tooth position is devoid of a functional crown but bears one relatively large and one small replacement tooth. Furthermore, in some tooth positions, breakages may obscure exact conditions, e.g., the left sixth tooth is completely split. Some teeth (the fifth and seventh tooth of the left maxilla and the ninth tooth of the right maxilla) were difficult to segment due to low contrast and show what could be separate fragments of the same tooth at their roots. Most of the tooth positions are represented by at least partially erupted teeth and/or the respective roots on the left side: 1–7 and 9–10 (the eighth alveolus seems to be empty). The right side preserves functional teeth and/or the respective roots in the following alveoli: 1–2 and, within the tooth-bearing fragment, 3–4, 6–11 (the eleventh was just about to erupt). Relatively large replacement teeth can be found in the left maxilla in positions 1–2 and 4–9 (Figure 5D). The right side preserves comparable replacement teeth in the positions 1–3 and 5–9 and 12 (Figure 6D). Relatively younger replacement teeth seem to be preserved within the second left alveolus and within the first, second, and fifth right alveolus. These interpretations are based on relative size and position of individual teeth. The CT data reveal that the replacement teeth in the maxillae of *Irritator* tend to be positioned lingually and slightly distally to the roots of their respective predecessors. Additionally, very small replacement teeth seem to start their growth relatively high up the root base of

functional teeth. Normally, the maxillary replacement teeth of non-avian theropods grew in a ventral direction and migrated labially during growth (Hanai and Tsuihiji, 2019). However, the conditions in *Oxalaia* (Kellner et al., 2010) and *Irritator* seem to suggest that spinosaurid (pre)maxillary replacement teeth additionally moved mesially during growth; possibly a result of the narrowness of spinosaurid snouts (see also Lacerda et al., 2021; Isasmendi et al., 2022). Furthermore, the fragmentary distal dentary of *Iberospinus natarioi* also shows two generations of replacement teeth with a similar pattern of eruption (Mateus and Estraviz-López, 2022), seemingly indicating that it was widespread among spinosaurids (Lacerda et al., 2021; Isasmendi et al., 2022; this study).

The teeth of *Irritator* have been described in some detail by Sues et al. (2002), with additional details being mentioned by Sales and Schultz (2017) and Hendrickx et al. (2019). The teeth have long roots, which are usually longer than the respective crowns. All roots have their bases at the same level within the maxilla, differing from, e.g., *Tarbosaurus bataar* (Hanai and Tsuihiji, 2019). As noted by Sues et al. (2002), the teeth of *Irritator* are conical and weakly recurved. However, whereas Sues et al. (2002: 539) state that the teeth are round in cross-section, the CT data shows that they are quite notably compressed labiolingually, with the ratio between mesiodistal length and labiolingual width at their bases varying between 1.3 and 1.7, whereas most other spinosaurids have considerably more rounded teeth, with ratios between 1.1 and 1.5 (Stromer, 1915; Richter et al., 2013; Hendrickx et al., 2015). The crowns of *Irritator* bear carinae along their full length on the mesial and distal aspect but are devoid of serrations. Both Sues et al. (2002) and Hendrickx et al. (2019) noted that the carinae in *Irritator* have a 'beaded' appearance, mainly referring to the sixth and seventh tooth positions preserved in the detached maxillary fragment (eight and ninth preserved tooth position in total). However, the carinae of these teeth are damaged by numerous cracks traversing them, and the anteriormost teeth in the left maxilla show completely smooth mesial and distal carinae. As noted and illustrated by Sues et al. (2002), Sales and Schultz (2017) and Hendrickx et al. (2019), small, weakly developed undulations are present along the distal carina in several teeth. In agreement with Hendrickx et al. (2019), we cannot confirm the presence of a granulated enamel surface, which is present in *Baryonyx* (Charig and Milner, 1997; Hendrickx et al., 2019) and was stated as present in *Irritator* by Sues et al. (2002). In contrast, the enamel is completely smooth; only under highest magnification and in oblique light can a very fine pitting be noticed, which might, however, be diagenetic.

RESULTS

Parsimony Analyses

The primary aim of our phylogenetic analyses is to investigate the interrelationships of megalosauroids and evaluate the morphological distinctiveness of spinosaurids, including an examination of rates of character evolution based on the Bayesian tip-dating analysis (below). However, as postcranial characters and their codings have not been reviewed in detail and only limited additional postcranial information was added, the results of our analysis should be taken with caution.

The parsimony analysis of the complete data set resulted in 8184 equally parsimonious trees (most parsimonious tree, MPT) with a length of 1515 steps (Supplementary Data 5). The strict consensus tree is rather well resolved, except for a major polytomy within spinosaurids and another within Allosauroidea (Figure 36A). Our parsimony results support the monophyly of Carnosauria, as previously found by, e.g., Rauhut and Pol (2019). However, within this clade, we found a more traditional arrangement of a monophyletic Megalosauroidea (including Spinosauridae) and Allosauroidea (Figure 36), unlike Rauhut and Pol (2019), who recovered Spinosauridae outside a clade containing Megalosauridae and Allosauroidea. Our results do accord with those of Rauhut and Pol (2019) in recovering Piatnitzkysauridae as an early-branching clade within Allosauroidea.

In contrast to most analyses, which generally find Megalosauroidea to be comprised of a sister-taxon arrangement between a monophyletic Megalosauridae and a monophyletic Spinosauridae (e.g., Allain, 2002; Benson, 2010; Carrano et al., 2012; Rauhut et al., 2016), the taxa classically grouped as megalosaurids are here found forming a grade outside of spinosaurids (Figure 36). According to our analysis, the immediate sister taxon to spinosaurids is the late Middle Jurassic *Monolophosaurus* (Figure 36A), which has been found in different phylogenetic positions outside of Megalosauroidea in previous analyses (e.g., Allain, 2002; Benson, 2010; Carrano et al., 2012; Rauhut et al., 2016). The sister taxon to the *Monolophosaurus*-Spinosauridae clade is Megalosaurinae, a clade composed of the taxa *Torvosaurus*, *Megalo-*

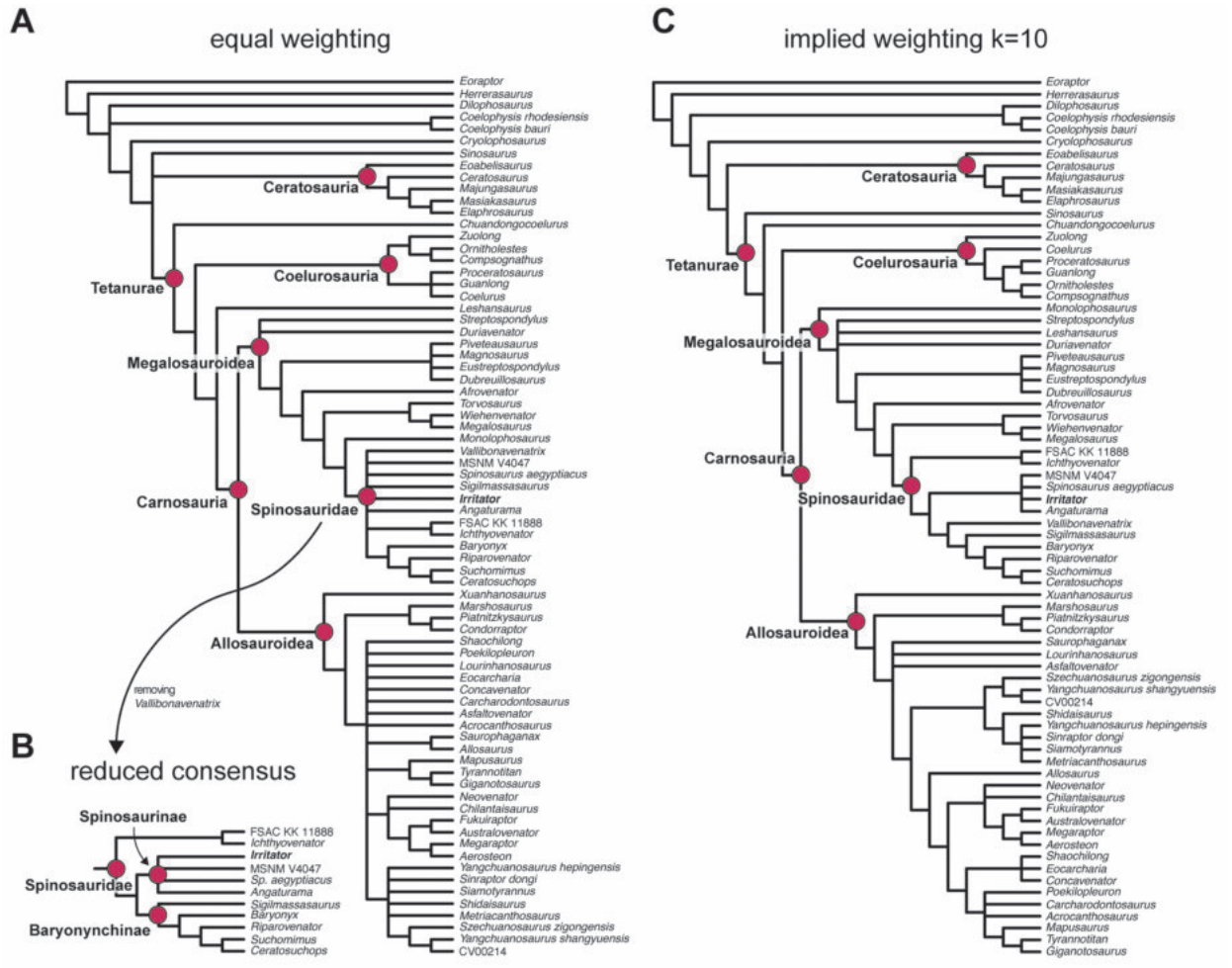

FIGURE 36. Phylogenetic results from parsimony analysis using the full dataset. A, strict consensus tree of 8184 MPTs retained from an equal weighting analysis (see methods for details); B, partial reduced consensus tree, showing the clade Spinosauridae after removal of the taxon *Vallibonavenatrix*; C, strict consensus tree of 406 MPTs retained from an implied weighting analysis using a concavity constant of k=10 (see Methods for details). Important clades are labelled. *Irritator* as the main focus of our study is highlighted in bold face within the clade Spinosauridae.

saurus bucklandii, and *Wiehenvenator* (Figure 36A). The genus *Afrovenator* is one step further outside this clade, followed by a clade including the taxa *Eustreptospondylus, Dubreuillosaurus, Magnosaurus,* and *Piveteausaurus divesensis* (Figure 36A). Finally, *Streptospondylus altdorfensis* and *Duriavenator* are found in a polytomy as the earliest branching members of Megalosauroidea (Figure 36A).

Support for the inclusion of spinosaurids within Megalosauroidea (in contrast to Rauhut and Pol, 2019) is higher than for many other clades: Forcing spinosaurids outside of a megalosaurid-allosauroid clade requires at least 11 additional steps in our current analysis. Uniting the megalosaurids of other analyses in a monophyletic clade is also considerably less parsimonious, requiring at least five additional steps. Creating a monophyletic Avetheropoda (Allosauroidea + Coelurosauria) to the exclusion of Megalosauroidea requires at least an additional 12 steps.

The position of *Monolophosaurus* as sister taxon to spinosaurids is supported by relatively few (four) unambiguous synapomorphies, including the relatively low placement of the dorsal quadrate condyle (CH101:0; below two-thirds of the height of the orbit; also present in *Asfaltovenator, Allosaurus,* coelurosaurs, and some other theropods), the presence of a quadrate foramen (CH108:0; reversal to the plesiomorphic carnosaur condition), dentary teeth that are considerably smaller and more numerous than the maxillary teeth (CH195:1), and

an unexpanded ischial symphysis (CH342:0; reversed in *Ichthyovenator laosensis* and a probable reversal to the plesiomorphic carnosaurian condition). Due to the unusual position of *Monolophosaurus* in our parsimony analysis using equal weights, we herein also report ambiguous synapomorphies that possibly link this taxon with spinosaurids (here, we only comment on those characters that were considered potential apomorphies after evaluation with the 'trace character' option in Mesquite; see Supplementary Data 11 for complete lists of character changes found under ACCTRAN and DELTRAN in PAUP). Thus, the following characters are morphological traits that were considered potential synapomorphies under ACCTRAN, but are currently unknown in *Monolophosaurus* or ambiguous due to other reasons: a long and plate-shaped palatal process of the maxilla (CH17:1; unknown in *Monolophosaurus*); a planar postorbital articulation with the jugal (CH67:0; a reversal to the non-megalosauroid condition; present in a postorbital referred to *Ceratosuchops* [Barker et al., 2021; see discussion in the description of the postorbital] and, probably, *Monolophosaurus*, whereas *Irritator* shows the typical megalosauroid morphology); presence of a suborbital flange of the postorbital (CH68:1; present in *Monolophosaurus* and the postorbital referred to *Ceratosuchops*, but not in *Irritator*); a prefrontal that is exposed on the anterodorsal margin of the orbit (CH79:0; reversal to the non-averostran condition; present in *Monolophosaurus* and *Irritator*, but not in *Baryonyx*); a ventral margin of the pterygoid wing of the quadrate that is confluent with the expansion for the mandibular condyles (CH106:1; spinosaurid synapomorphy, unknown in *Monolophosaurus*); a subrectangular quadrate head shape in dorsal view (CH111:1; spinosaurid synapomorphy, unknown in *Monolophosaurus*); a retroarticular process in which the mediolateral width is higher than the posterior width of the dentary (CH174:1; absent in *Megalosaurus*, present in *Irritator*, otherwise unknown in megalosauroids, including *Monolophosaurus*); extent of the anterior carina of the maxillary and dentary teeth up to the base of the crown (CH186:0; present in spinosaurids, unknown in *Monolophosaurus*); expanded and triangular epipophyses of the atlantal neural arch in lateral view (CH201:1; present in *Monolophosaurus*, unknown in spinosaurids); small size of pneumatic foramen in anterior dorsal vertebrae (CH227:0; reversal to the plesiomorphic carnosaurian condition; present in *Monolophosaurus* and most spinosaurids); absence of pneumaticity in sacral vertebrae (CH237:0; reversal to the plesiomorphic condition of tetanurans; unknown in *Monolophosaurus*); absence of an anterior process on chevrons (CH258:0; unknown in *Monolophosaurus*); a length ratio of the deltopectoral crest with regard to the total length of the humerus ranging between 0.43–0.49 (CH274:1; unknown in *Monolophosaurus*, as are all appendicular characters apart from features of the pelvic girdle); presence of hypertrophied distal ends of the radius and ulna (CH280:1); presence of a transversely compressed, blade-like olecranon process of the ulna (CH284:1); presence of hypertrophied medial and lateral processes on the proximal end of the ulna (CH286:1); a small and lobular morphology of the lateral (fibular) condyle of the tibia (CH365:1); presence of a bluntly rounded vertical ridge on the medial side of the astragalus (CH367:4); a ventral orientation of the distal condyles of the astragalus (CH375:0); and an ascending process of the astragalus that is >1.6 times the depth of the astragalar body (CH377:2). The following DELTRAN synapomorphies are character states that are present in *Monolophosaurus* and spinosaurids, but are unknown or of unclear optimization in further outgroup taxa (so they evolved at the latest at the *Monolophosaurus*+spinosaurid node, but may have a wider distribution among megalosauroids closely related to spinosaurids): the nasal process of the premaxilla extends posterior to the posterior tip of the subnarial process (CH4:2); a partly or fully fused internasal contact (CH38:1); presence of a midline crest on the nasals (CH45:1); absence of a dorsal rim of the antorbital fossa on the anterior lacrimal process (CH49:2; present in *Monolophosaurus*, spinosaurids, *Wiehenvenator*, and *Eustreptospondylus*, but absent in *Torvosaurus, Dubreuillosaurus,* and *Afrovenator*); a frontal that is wider than long (CH83:1); a slightly expanded anterior end of the dentary (CH153:1; present in *Monolophosaurus* and the early branching megalosauroids *Eustreptospondylus* and *Dubreuillosaurus*, but not in megalosaurines); and an intermediate size of the mylohyoid foramen in the splenial (CH163:1). Moving *Monolophosaurus* to the basis of Megalosauroidea or outside the megalosauroid-allosauroid clade requires only two additional steps. Moreover, a position of *Monolophosaurus* as the earliest branching member of Megalosauroidea was found in the analysis using implied weights (Figure 36C; Supplementary Data 7); in this case, the megalosaurines (*Megalosaurus*, *Torvosaurus*, and *Wiehenvenator*) are found as sister taxon to spinosaurids (Figure 36C).

Spinosauridae is supported by 65 (potential) synapomorphies. As one of the primary purposes of our re-description of *Irritator* and phylogenetic analysis is to understand spinosaurid skull evolution and the origin of their unusual skull morphology, we here provide a full list of these synapomorphies. Only seven synapomorphies are unambiguous, and these are largely postcranial, reflecting our still very poor knowledge of spinosaurid skulls: a ratio between mesiodistal length and transverse width at the base of lateral teeth of 1.5 or less (CH184:1); gently sloping demarcation of dorsal surface of neural arch from diapophyseal surface in anterior cervical vertebrae (CH213:0; the baryonychines *Baryonyx* and *Suchomimus* have character state 1, so this character might be optimized as a spinosaurine synapomorphy with different ingroup relationships); a ventral keel in posterior-most cervicals and anterior-most dorsals that forms a straight to slightly convex ventral margin, with the anterior end of the keel protruding ventrally from the anterior articular surface (CH223:1); the presence of pneumaticity/webbing at base of neural spines in middle to posterior dorsals (CH224:1; originally considered to be a baryonychine synapomorphy [Sereno et al., 1998], but also present in *Ichthyovenator* and, probably, *Spinosaurus* [Stromer, 1915]); the height of neural spines of dorsal vertebrae being at least twice as high as the centrum height (CH235:2); flat ventral surface of anterior caudal vertebrae (CH243:0; the plesiomorphic averostran condition [state 1] is present in FSAC KK 11888 [Ibrahim et al., 2020]); and centrodiapophyseal laminae on neural arch of anterior caudal vertebrae are as prominent as in dorsal vertebrae (CH246:1). In addition, this group is supported by eight DELTRAN synapomorphies, which represent morphological characters that are currently unknown or have a problematic distribution in close relatives of spinosaurids. These include the ventral margin of pterygoid wing of the quadrate being confluent with the expansion for the mandibular condyles (CH106:1; unknown in *Monolophosaurus*, absent in other megalosauroids), presence of a mediolateral expansion of the quadrate head in relation to quadrate shaft (CH111:1; unknown in *Monolophosaurus*, absent in other megalosauroids), ventral surface of posterior dorsal vertebral centra is flattened, sometimes with a shallow medial sulcus (CH232:1; absent in *Monolophosaurus*, but present in megalosaurines and spinosaurids), absence of anterior processes in chevrons (CH258:0; unknown in *Monolophosaurus*, absent in other megalosauroids), the obturator foramen being formed as a ventrally open notch (CH323:1; present in *Eustreptospondylus* and spinosaurids, but absent in *Torvosaurus* and *Monolophosaurus*), bluntly rounded vertical ridge on medial side of the anteromedial buttress for the astragalus on the tibia (CH367:4; unknown in *Monolophosaurus*, absent in other megalosauroids), fibular crest does not extend to proximal end of the tibia (CH369:2; present in spinosaurids and *Torvosaurus*, but absent in *Megalosaurus*), and the ascending process of the astragalus has a height relative to the depth of the astragalar body that exceeds 1.6 (CH377:2; unknown in *Monolophosaurus*, absent in other megalosauroids). Furthermore, spinosaurids are found to have a long list of ACCTRAN synapomorphies, which are characters that are either synapomorphies for the group, have a problematic distribution in megalosauroids generally, or could alternatively be apomorphic for more deeply nested spinosaurid subclades. In whichever case, these synapomorphies characterize spinosaurids or spinosaurid subclades (including individual taxa), unless otherwise noted. As expected, these include many of the skull apomorphies that are unknown for most spinosaurid taxa, and thus only optimized as ambiguous synapomorphies. ACCTRAN synapomorphies for Spinosauridae are: a markedly concave ventral margin of the premaxilla in lateral view (CH2:1); position of the posterior end of the external nares that is posterior to the ventral margin of the premaxillary body (CH6:2); presence of a mediolateral constriction of the posterior portion of the premaxialla (CH8:1); interlocking articulation between premaxilla and maxilla (CH11:1); anterior ramus of the maxilla more than twice as long as high (CH12:4); anteriorly angled orientation of anteriormost alveolus in the maxilla (CH14:1); straight or gently curved anterodorsal margin of the ascending process of the maxilla (CH15:0); jugal ramus of the maxilla is subequal in length or shorter than the ascending process (CH16:1); medial wall of the anterior end of the maxillary antorbital fossa lacks depressions or maxillary fenestra (CH27:0); sinusoidal shape of the alveolar border of the maxilla (CH33:2); forked posterior end of the jugal ramus of the maxilla (CH35:1); posterior narial margin on nasal without or with weak fossa (CH39:0; reversal to the morphology in carnosaurian outgroups under the assumption that such a fossa represents a carnosaur synapomorphy, only known in *Monolophosaurus* among non-spinosaurid megalosauroids); pneumatic foramina in nasal absent (CH43:0; condition only known in *Irritator* [state 0] and *Monolo-*

phosaurus [state 1] among megalosauroids); lateral lamina of ventral process of lacrimal forming a continuous sheet of bone between the ventral and anterior processes (CH50:0); anteroposterior expansion of ventral process of the lacrimal begins at the dorsal end of the ventral process (CH51:1); dorsal and ventral portions of antorbital fossa on the lacrimal is continuous, lateral lamina does not project far anteriorly (CH52:1; also present in *Torvosaurus*, but absent in *Monolophosaurus* and *Wiehenvenator*); angle between anterior and ventral rami of lacrimal is < 75° (CH57:1); position of anterior end of jugal is excluded from the internal antorbital fenestra (CH59:0), jugal pneumatization absent (CH60:0; also in *Torvosaurus*, but not in *Monolophosaurus*); there is no antorbital fossa that is clearly offset from the lateral surface by a raised rim on the jugal (CH61:0); presence of a horizontal ridge along the jugal body (CH64:1); presence of a lateral ridge along the postorbital contact on the postorbital process of the jugal (CH65:1); the dorsoventral height of the posterior process of the jugal is less than half the height of the suborbital part (CH66:0); anterior end of the anterior process of the postorbital is downturned (CH76:1); a midline ridge on the frontal is present (CH82:1); frontals in adult individuals are partially or completely fused (CH84:1); the median skull table between supratemporal fossae on the parietals is narrow with a sharp sagittal crest (CH88:2); anterior process of squamosal is as long as or shorter than posterior process (CH95:1; present in *Irritator* and *Dubreuillosaurus*, but absent in *Afrovenator* and *Monolophosaurus*); the orientation of the quadrate in lateral view is anteroventrally inclined, with the mandibular joint being positioned anterior to the quadrate head (CH110:0); absence of a marked depression on the exoccipital lateral to the foramen magnum, above the paracondylar recess (CH117:1); location of basipterygoid processes of the basisphenoid almost directly ventral to basal tubera, with the basisphenoid recess being anteroposteriorly narrower than wide and opening more posteriorly than ventrally (CH128:2); posteroventral orientation of the occipital condyle in respect to the skull table (CH137:1); anterior end of dentary is strongly dorsally expanded, with the dorsal margin extending considerably above the posterior alveolar margin (CH153:2); splenial has a curved, rather than notched, contour of the posterior edge (CH162:1); strong development of horizontal ridge on the lateral surface of the surangular below the mandibular joint (CH166:1); presence of a depressed lateral shelf on the surangular for the attachment of the *m. adductor mandibulae externus superficialis*, bound medially by a dorsally facing ridge (CH167:1; also present in allosauroids, but absent in *Megalosaurus* and *Monolophosaurus*); the retroarticular process of the mandible is elongate, as long as or longer than anteroposterior length of mandibular glenoid (CH173:0); flat or slightly convex attachment area for the *m. depressor mandibulae* (CH176:1); the lateral margin of retroarticular process is strongly offset ventrally from the glenoid (CH177:1); the interdental plates are obscured by an expanded paradental lamina, triangular apices only may be visible (CH179:1); the lateral maxillary and dentary teeth are straight or almost straight, with the tip of the teeth being placed mesial to the distal carina, and the distal carina being straight or convex (CH181:1); crown striations are present on all tooth crowns (CH182:2); presence of more than five premaxillary teeth (CH189:3); the maxillary teeth have an increasingly wide spacing in the mid-section (at least one-third of an alveolar width apart), but spacing decreases again posteriorly (CH193:1); presence of a rapid increase in tooth size at the anterior end of the maxilla (CH194:1); the length/posterior height ratio of mid-cervical centra is 1.75–2.75 (CH220:1); a vertical ridge on lateral surface of the ilium blade dorsal to acetabulum is absent (CH304:0); ridge on the medial ilium surface adjacent to preacetabular notch is strongly developed, forming a shelf (CH314:1); the obturator foramen in the pubis is a ventrally open notch (CH323:1; as noted above, this character has a problematic distribution in megalosauroids, being absent in *Torvosaurus* and *Monolophosaurus*, but present in spinosaurids and *Eustreptospondylus*); and the obturator foramen in the pubis is large and oval (CH332:1; this character can only be properly coded in *Ichthyovenator*, which has a ventrally open, but well-defined margin of the obturator foramen, whereas this opening is absent and only indicated as a shallow ventral notch in the pubis of other spinosaurids).

Within spinosaurids, the strict consensus tree of the analysis using the full dataset and equal weights shows rather poor resolution (Figure 36A), with a basal polytomy and otherwise two monophyletic groups. One of these clades includes the Asian spinosaurid *Ichthyovenator* and the specimen FSAC KK 11888 (the proposed neotype of *Spinosaurus aegyptiacus*; Ibrahim et al., 2014), whereas the other represents the Baryonychinae, containing the taxa *Sigilmassasaurus brevicollis, Baryonyx, Ceratosuchops, Riparovenator,* and

Suchomimus. Reduced consensus methods remove the Spanish spinosaurid *Vallibonavenatrix*, as this taxon can appear in multiple positions within this clade. After removal of *Vallibonavenatrix*, three clades are found within spinosaurids (Figure 36B, Supplementary Data 8). The earliest branching of these is the *Ichthyovenator*+FSAC KK 11888 clade (Figure 36B). This clade forms the sister group to a Spinosaurinae-Baryonychinae dichotomy, with the Spinosaurinae showing a polytomy including the OTUs *Angaturama*, *Irritator*, MSNM V 4047, and *Spinosaurus* (Figure 36B). Some runs of the pcrprune algorithm also removed *Angaturama* from the reduced consensus tree; in this case, the snout MSNM V 4047 was found as sister taxon to *Spinosaurus aegyptiacus* (see below). Within the Baryonychinae, *Sigilmassasaurus* was found as the earliest branching taxon (Figure 36B), followed by a pectinate arrangement of *Baryonyx, Riparovenator, Suchomimus,* and *Ceratosuchops*, as in the strict consensus tree (Figure 36A–B).

The placement of FSAC KK 11888 is based on several shared postcranial characters with *Ichthyovenator* and several quadrate characters that are different from the condition seen in *Irritator*, *Baryonyx*, and *Suchomimus*. Unambiguous synapomorphic characters shared between *Ichthyovenator* and FSAC KK 11888 are the absence of L-shaped neural spines in the mid-caudals (CH244:0; a reversal to the non-carnosaurian condition, within 'higher' spinosaurids only known in *Riparovenator*; Barker et al., 2021), the presence of a spinodiapophyseal ridge or lamina on the caudal neural spines (CH247:1), a straight dorsal margin of the ilium (CH318:1), and a heart-shaped cross-section of the articulated ischia (CH343:1). The quadrate characters excluding FSAC KK 11888 from the Spinosaurinae-Baryonychinae clade include the medially flexed ventral margin of the pterygoid wing (CH107: 0; the normal theropod condition, whereas *Baryonyx* and *Irritator* apomorphically show a sharp-edged ventral margin), the lack of a mediolateral expansion of the quadrate head (CH 112: 0; apomorphically present in *Irritator*, *Baryonyx*, and *Suchomimus*), and the presence of a foramen on the medial side of the ventral quadrate body (CH113: 1; a character shared with *Afrovenator* and *Torvosaurus* and interpreted as a synapomorphy of the *Afrovenator*-Megalosaurinae-Spinosauridae clade that is reversed in 'higher' spinosaurids). Moving FSAC KK 11888 into Spinosaurinae or as sister taxon to *Spinosaurus* requires six additional steps. It might be worth noting, however, that several characters that might unite this specimen with spinosaurines (mainly dental and postcranial characters) could either not be evaluated or have not been included in this analysis, so our results should not be seen as a test of the proposed spinosaurine affinities of this specimen, or its proposed referral to *Spinosaurus*.

The parsimony analysis of skull characters (i.e., removing all postcranial characters, see methods) resulted in 153 equally parsimonious trees with a length of 778 steps (Supplementary Data 6). The strict consensus largely conforms to the results of the analysis of the entire data set (Figure 37A), especially in respect to showing a monophyletic Carnosauria within Tetanurae, although with relatively poor resolution within this clade. Clades found in the strict consensus tree include Spinosauridae (with the same basic topology as in the entire dataset, see below), a *Sinraptor-Yangchuanosaurus* spp. clade, and Carcharodontosauria (Figure 37A). In the reduced consensus tree, monophyletic Megalosauroidea and Allosauroidea are found, with very similar taxonomic compositions as those in the analysis of the entire dataset (Figure 37B). One notable exception is *Megalosaurus*, which is, although placed in its traditional position within Megalosauroidea in some MPTs, recovered as a basal member of Allosauroidea in a different subset of MPTs in the skull dataset analysis. Strictly speaking (i.e., adhering to phylogenetic nomenclature), this would mean that the 'Megalosauridae' (as usually understood, minus *Megalosaurus*)-Spinosauridae clade should not be called Megalosauroidea under the current hypothesis (it would become Spinosauroidea); however, we retain this name here for ease of discussion. Within Megalosauroidea, *Afrovenator* is found as an early branching taxon, followed by a clade composed of *Torvosaurus, Wiehenvenator,* and *Leshansaurus qianweiensis*, and finally a monophyletic Spinosauridae (Figure 37B). Within spinosaurids, FSAC KK 11888 forms the sister taxon to a Baryonichinae-Spinosaurinae clade (Figure 37), which shows the same taxonomic composition and interrelationships as in the analysis of the complete data set (except for the taxa *Sigilmassasaurus* and *Ichthyovenator*, for which no skull material is known).

Reduced consensus methods also show that *Monolophosaurus, Dubreuillosaurus*, and *Eustreptospondylus* can take variable positions within Megalosauroidea (Figure 37B). *Monolophosaurus* is either found as the earliest branching taxon within this clade (as also in the implied weights analysis of the entire dataset: Figure 36B), or as sister taxon to spinosaurids (Figure 37B), as in the

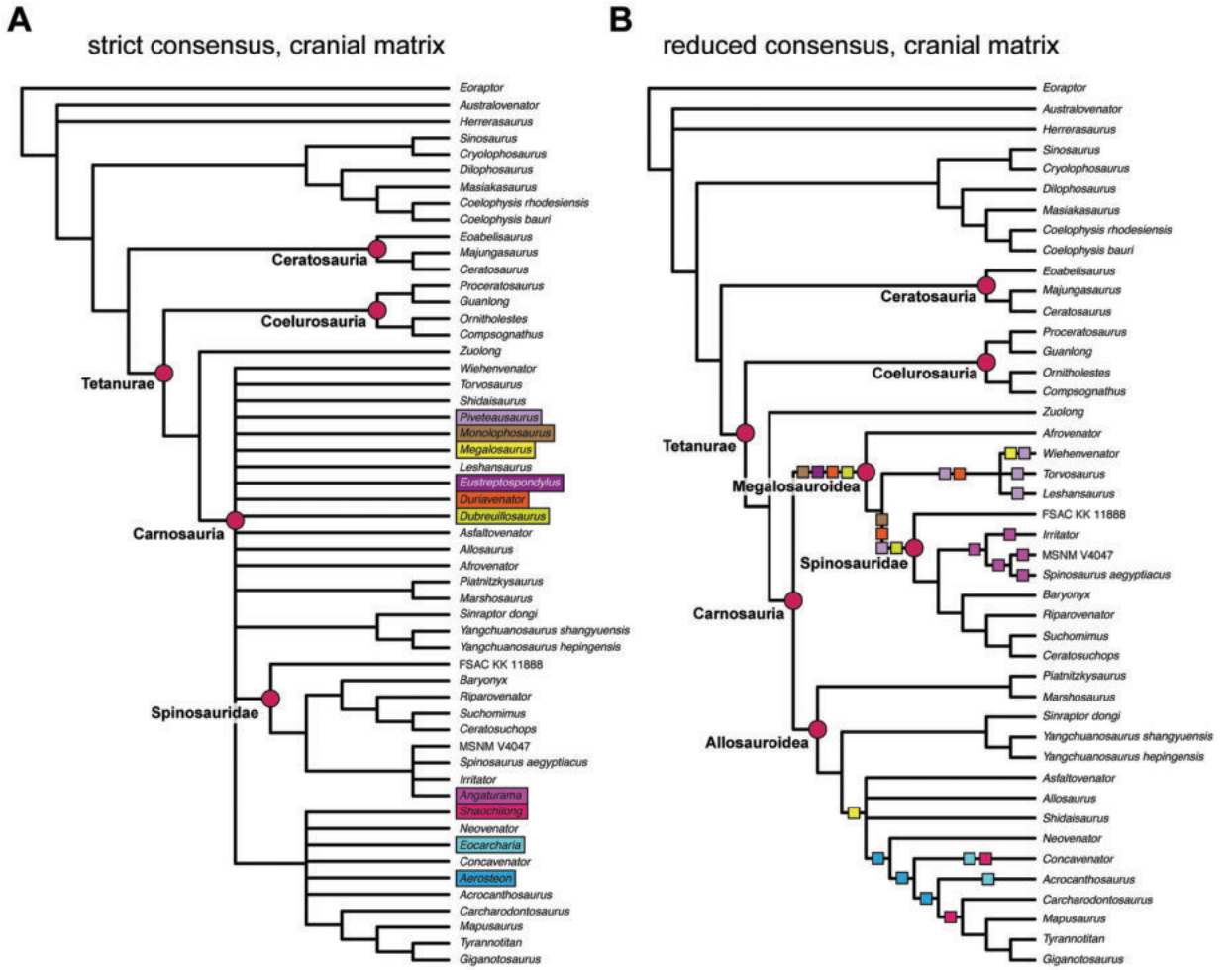

FIGURE 37. Phylogenetic results from parsimony analysis using the cranial dataset. A, strict consensus tree of 153 MPTs retained from an equal weighting analysis (see Methods for details); B, reduced consensus tree, pruning wild card taxa from the strict consensus. Wild card taxa are highlighted with coloured boxes in A, and their possible topological positions are shown with same coloured squares in B. Important clades are labelled.

equal weights analysis of the entire dataset (Figure 36A). Likewise, and depending on the position of *Monolophosaurus, Eustreptospondylus,* and *Dubreuillosaurus* are either found as early branching megalosauroids (if *Monolophosauruus* forms the sister taxon to spinosaurids) or as closely related to spinosaurids (if *Monolophosaurus* is placed at the base of megalosauroids) (Figure 37B). Skull characters shared between *Dubreuillosaurus* and/or *Eustreptospondylus* and spinosaurids include the anteroventrally angled anteriormost maxillary teeth (Ch14:1; in *Eustreptospondylus*; Sadleir et al., 2008), the absence of a pneumatic recess on the medial side of the maxilla posterior to the maxillary fenestra (CH27:0; in *Eustreptospondylus*, but not in *Dubreuillosaurus*; within carnosaurs, this recess is also absent in the megalosaurines *Torvosaurus* and *Wiehenvenator* and in the allosauroid *Asfaltovenator*), the presence of a lateral ridge along the postorbital facet on the jugal (CH65:1; only known in *Dubreuillosaurus* and convergently also present in allosauroids), the straight or slightly concave dorsal margin of the postorbital (CH71:1; in both *Dubreuillosaurus* and *Eustreptospondylus*; reversal to the non-carnosaurian condition, convergently also in carcharodontosaurs and again reversed in *Ceratosuchops*), the reduced and anteriorly placed laterosphenoid facet on the medial side of the postorbital (CH72:1; in both *Dubreuillosaurus* and *Eustreptospondylus*, again reversed in *Ceratosuchops*), absence of a supraorbital brow in the postorbital (CH75:0; in both *Dubreuillosaurus* and *Eustreptospondylus*, reversal to the non-carnosaurian condition, and again reversed in *Ceratosuchops*), possibly the absence of a constriction of the infratemporal fenestra

through the ventral process of the squamosal (CH91:0; under DELTRAN, unknown in most megalosauroids), possibly a relatively elongate posterior process of the squamosal (CH95:1; under DELTRAN, in *Dubreuillosaurus* and spinosaurids, unknown in megalosaurines and *Eustreptospondylus*), a broad exposure of the supraoccipital on the margin of the foramen magnum (CH121:0), a dorsoventrally expanded anterior end of the dentary (CH153:1; convergently present in *Monolophosaurus*, *Marshosaurus*, *Asfaltovenator*, and some other allosauroids within carnosaurs), and the presence of a pronounced lateral groove on the dentary housing the neurovascular foramina (CH158:1; convergently present in many allosauroids).

Another interesting result of the reduced consensus tree of the skull character matrix is that, within spinosaurines, the exclusion of *Angaturama* results in the snout MSNM V4047 from Morocco being clustered with *Spinosaurus aegyptiacus* (Figure 37B), lending support to the interpretation of Dal Sasso et al. (2005) that this specimen is referable to *Spinosaurus*. This relationship is based on a single character, an increase of tooth spacing in the posterior part of the maxilla (CH193:2; see Stromer, 1915; Dal Sasso et al., 2005), whereas other spinosaurids, such as *Suchomimus* and *Irritator*, show more widely spaced teeth in the midsection of the maxilla, but a decrease of spacing posteriorly (CH193:1).

Bayesian Topology, Time-calibration and Rates of Character Evolution

The topology of the posterior tree sample from the Bayesian analysis was summarized as an "allcompat" tree with the sumt command of MrBayes, which produces a 50% majority rule tree to which all compatible groups are added. High resolution of the "allcompat" tree indicates that many clades are consistently recovered across the posterior tree sample, although the posterior probabilities (PP) for many clades are low (Figure 38). The Bayesian topology agrees with parsimony analyses in recovering many large clades of theropods with relatively high branch support, including Spinosauridae (PP = 86%), Allosauroidea (PP = 62%), Ceratosauria (PP = 93%), and Coelurosauria (PP = 98%) (Figure 38). The Bayesian topology furthermore agrees with parsimony results in finding a monophyletic Megalosauroidea that includes spinosaurids (PP = 45%), and a monophyletic Carnosauria (PP = 20%; Figure 38). However, both nodes are associated with posterior probabilities below 50%. Although differences in the exact relationships of taxa could be reported between the Bayesian and parsimony topologies, we focus on differences within megalosauroids and spinosaurids as they are the primary taxa of interest.

An important difference from the parsimony analysis is the placement of *Monolophosaurus*, which is recovered outside of Megalosauroidea according to our Bayesian analysis, and which is instead found as the sister taxon to *Chuangdongcoelurus primitivus* (PP = 86%) forming the earliest branching clade within Carnosauria (see Figure 38; treating Carnosauria as a stem-based taxon including Allosauroidea+Megalosauroidea; see, e.g., Rauhut and Pol, 2019). As in the parsimony analysis, non-spinosaurid megalosauroids are recovered as a grade with respect to spinosaurids rather than united in a sister-clade to spinosaurids, but the arrangement of taxa and subclades of non-spinosaurid megalosauroids differs from the parsimony analyses (Figures 36-38). All relationships within Megalosauroidea outside of Spinosauridae have low posterior probabilities, below 50% (Figure 38). According to the Bayesian results, *Eustreptospondylus*, *Streptospondylus*, *Magnosaurus*, and *Dubreuillosaurus* form a clade (PP = 29%) that is the sister to spinosaurids (PP = 19%; Figure 38). This node marks the split of spinosaurids from other meglaosauroids and is dated to the Toarcian–Aalenian boundary (c. 174 Ma) according to the time calibration. As the origination date of Spinosauridae is estimated to be at 135.9 Ma, this implies a ghost lineage of roughly 38 million years. When the internal megalosauroid nodes associated with posterior probabilities below 50% are collapsed, this ghost lineage increases to a maximum of 53.2 million years (Figure 39). The remaining taxa of Megalosauroidea are arranged in a large clade (Megalosaurinae, PP = 25%; Figure 38).

The Bayesian analysis finds relatively good support for the split between Baryonychinae and Spinosaurinae within Spinosauridae, with these clades having posterior probabilities of 45% and 86%, respectively (Figure 38). One spinosaurid taxon, *Vallibonavenatrix*, is recovered outside of this divergence but within spinosaurids, and thus as the earliest branching spinosaurid (Figure 38). Barynonychinae includes *Baryonyx, Suchomimus, Riparovenator,* and *Ceratosuchops*, whereas Spinosaurinae includes all other taxa (except for *Vallibonavenatrix*; Figure 38). Thus, with respect to the parsimony topology, *Sigilmassasaurus* is removed from Baryonychinae and instead proposed to be a spinosaurine.

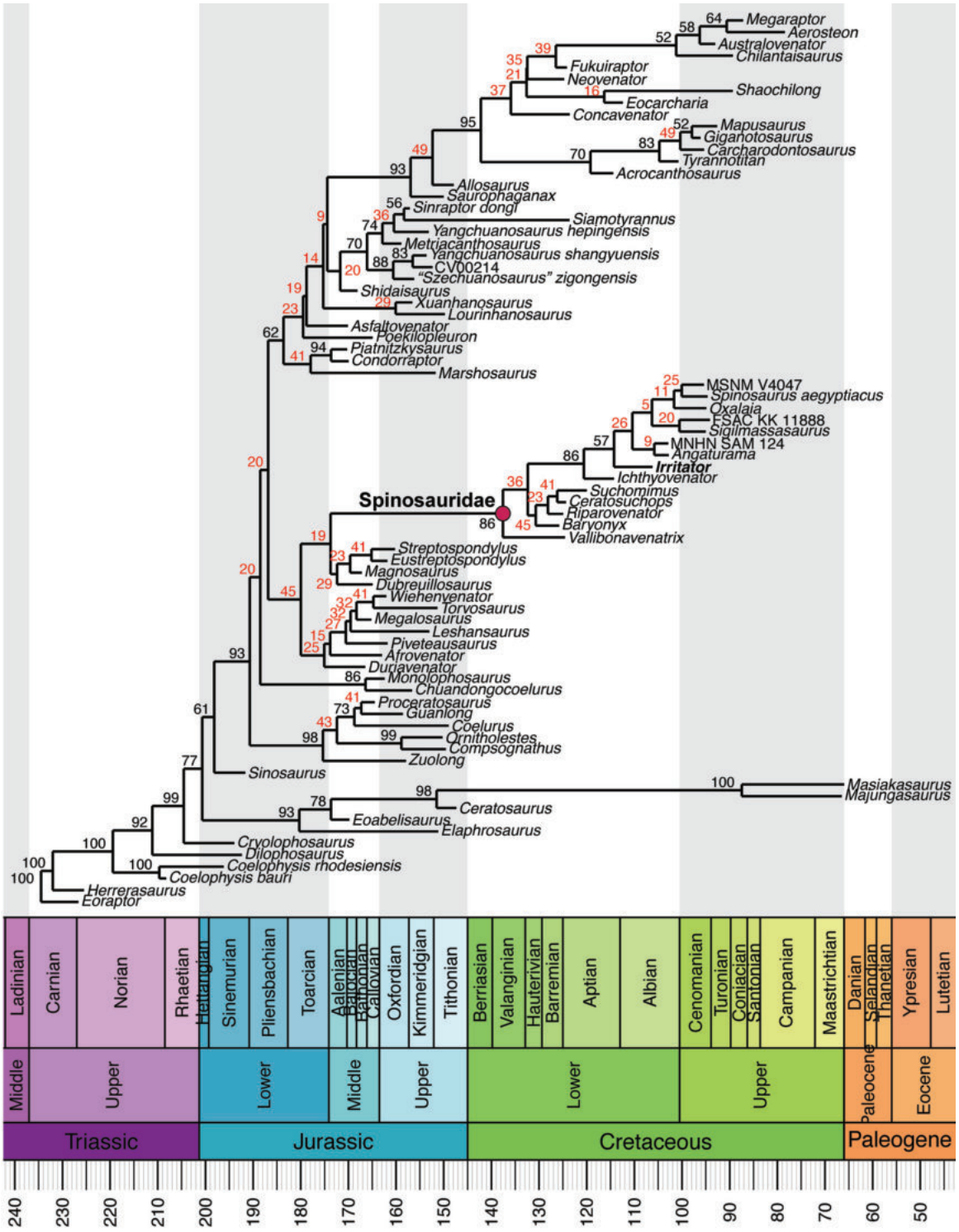

FIGURE 38. Tip-dated allcompat tree from posterior sample of Bayesian analysis (with full dataset), showing posterior probability values for internal nodes. Red values represent nodes below 50% posterior probability.

The character transition rates estimated in the Bayesian analysis show evolutionary rate variations across all branches spanning two orders of magnitude, ranging from a minimum rate of 0.047 character transitions per million years to a maximum of 3.65 character transitions per million years (Figure 39). The lowest rates (lowest 20% quantile, rates < 0.32) are generally associated with branches that lead to tips (Figure 39). High rates (highest 20% quantile, rate > 1.43) are largely found among deep internal branches of the phylogeny that signifiy the evolution of large clades, such as Ceratosauria+Tetanurae (rate = 2.59), Tetanurae (rate = 2.54), Tetanurae minus *Sinosaurus* (rate = 3.65), Allosauroidea (rate = 1.85), and Coelurosauria (rate = 1.78; see Figure 39). The branch leading to spinosaurids also has a high rate of character evolution, with a value of 1.75 (Figure 39). This is noteworthy, as this branch is extremely long (53.2 Ma), particularly so in comparison to the branches leading to most other large clades. Thus, although spinosaurids had a long evolutionary duration to accumulate their defining morphological characters, this happened at a relatively fast evolutionary rate over a sustained evolutionary period. The only other branch with a comparable duration (64 million years) is that which connects *Masiakasaurus knopfleri*+*Majungasaurus* with earlier ceratosaurs and is associated with much lower rates of 0.45 character transitions per million years (Figure 39). High evolutionary rates are also found within spinosaurids, for example in the terminal branches leading to *Vallibonavenatrix* (rate = 1.71), FSAC KK 11888 (rate = 2.07), as well as in Spinosaurinae (rate = 1.74; see Figure 39), indicating that spinosaurids continued to sustain high rates of character change after their evolutionary origin.

DISCUSSION

Phylogeny and the Evolutionary History of Spinosaurids

Due to the limited taxon sampling (especially for non-carnosaurian theropods) and the uneven treatment of skull and postcranial characters, the primary aim of our phylogenetic analyses was not to present a novel hypothesis of theropod or carnosaur interrelationships. Instead, we evaluated the morphological disparity of spinosaurid skulls and the influence of spinosaurid skull characters on the phylogeny of carnosaurs and especially megalosauroids, based on the new anatomical information presented herein. Whereas we revised the character definitions and codings of Rauhut and Pol (2019) for cranial, mandibular, and dental characters rather thoroughly and added several new characters, we did not do the same for the postcranial characters, for which the *Irritator* holotype provides no novel information. For postcranial characters, we mainly used the character definitions and codings presented by Rauhut and Pol (2019), which, in turn, were largely based on definitions and codings of Carrano et al., 2012). Nevertheless, we will offer a short discussion on some aspects of our phylogenetic analyses.

As for several recent analyses (e.g., Cau, 2018; Rauhut and Pol, 2019), our current parsimony-based phylogeny robustly supports the inclusion of most large-bodied basal tetanurans in a clade, Carnosauria. Although this is also recovered in the “allcompat” tree of the Bayesian analysis, support for this clade is low (PP = 20%). In contrast to the results of Rauhut and Pol (2019), who found three major carnosaurian subclades (Spinosauridae, Megalosauridae, and Allosauroidea), in a pectinate arrangement within Carnosauria, we found a more conventional arrangement of a monophyletic Megalosauroidea (including Spinosauridae) across all analytical settings and methods. However, in contrast to most previous analyses that recovered Spinosauridae within Megalosauroidea (e.g., Benson et al., 2010; Carrano et al., 2012; Rauhut et al., 2016), the remaining (i.e., non-spinosaurid) megalosauroids were not found to form a monophyletic Megalosauridae as sister taxon to Spinosauridae, but rather to represent different grades on the evolutionary lineage towards Spinosauridae (again in both parsimony and Bayesian analyses). An unusual finding is the placement of *Monolophosaurus* as a member of Meglosauroidea, which we recovered in all parsimony analyses. In earlier works, this taxon was sometimes found to be a basal allosauroid (e.g., Sereno, 1997). More recent phylogenetic studies, which were conducted after the publication of detailed anatomical accounts of the cranium and postcranium (Brusatte et al., 2010; Zhao et al., 2010), generally recovered *Monolophosaurus* outside of Megalosauroidea in relatively basal positions in either Tetanurae (e.g., Carrano et al., 2012) or Carnosauria (Rauhut and Pol, 2019). Especially surprising is the position of *Monolophosaurus* as the immediate sister to spinosaurids (and thus as deeply nested within Megalosauroidea) according to our equally weighted parsimony analysis of the full dataset, given the amount of plesiomorphic character states in this taxon (e.g., Brusatte et al., 2010; Zhao et al., 2010). However, as it takes only

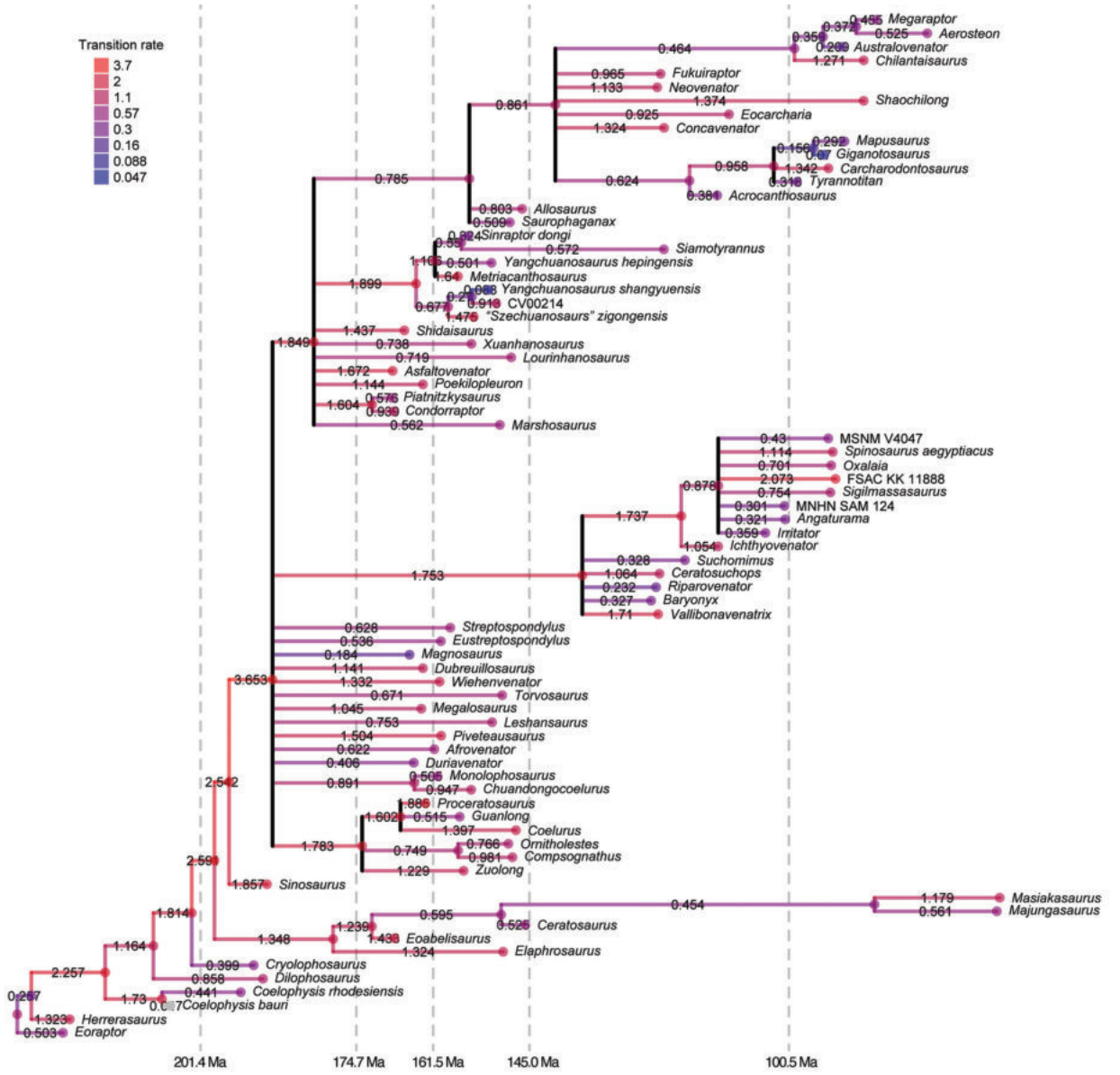

FIGURE 39. Tip-dated allcompat tree from posterior sample of Bayesian analysis (with full dataset). Branch colours show evolutionary character state transition rates (in character transitions per million year). Nodes below 50% posterior probability are collapsed into polytomies for which evolutionary rates cannot be calculated.

two additional steps to remove *Monolophosaurus* from Megalosauroidea, our dataset is potentially compatible with earlier hypotheses on the phylogenetic position of the taxon (e.g., Carrano et al., 2012). The implied weighting analysis of the same (full) dataset finds *Monolophosaurus* less deeply nested at the base of Megalosauroidea, suggesting that its position in the equally weighted analysis is, at least in part, driven by characters that are prone to homoplasy in basal tetanurans (see Rauhut and Pol, 2019). Indeed, the unambiguous and DELTRAN synapomorphies of *Monolophosaurus*+Spinosauridae (i.e., all apomorphic characters that are demonstrably shared between these taxa) have an average consistency index of 0.3, which is slightly lower than the average of all characters (CI = 0.33). We suspect that the spinosaurid sister-relationship of *Monolophosaurus* in the equally weighted analysis is largely driven by our skull character modifications, as postcranial characters have only marginally changed regarding Carrano et al. (2012), and as our skull-only dataset recovers the same result as the full dataset at least in a subset of the MPTs. However, the Bayesian tip-dating

analysis recovers *Monolophosaurus* in a more traditional position, outside of Megalosauroidea and basally within Carnosauria.

In comparison with previous hypotheses, the paraphyletic assemblage of non-spinosaurid megalosauroids that is common to parsimony and Bayesian results (regardless of the placement of *Monolophosaurus*) slightly reduces the ghost lineage for spinosaurids compared to previous topologies that united all non-spinosaurid megalosauroids into a megalosaurid sister clade to Spinosauridae (e.g., Barker et al., 2021: 36 Ma). However, from the appearance of the possible sister taxon *Monolophosaurus* in the (probable) late Callovian (c. 164 Ma) to the first occurrence of spinosaurids in the early Barremian (c. 129 Ma), a vast ghost lineage of some 35 million years remains, assuming that our equally weighted parsimony topology is correct. The Bayesian results imply a longer ghost lineage of approximately 38 million years when the "allcompat" topology is used, but this duration may increase (or decrease slightly) with alternative in-group topologies within meglaosauroids that remain possible, given the low posterior probabilities found for these nodes in our analysis.

Spinosaurids show highly derived skull anatomy among theropods, based on the numbers of characters that are derived with respect to close relatives. A total of 45 character transitions of craniodental characters were recovered under ACCTRAN at the node of Spinosauridae in our analysis (based on character optimization on the parsimony analysis; Supplementary Data 11), and 35 craniodental transformations were found by DELTRAN at the next less inclusive node within Spinosauridae that includes taxa with craniodental information (i.e., Baryonychinae+Spinosaurinae, excluding the clade uniting *Ichthyovenator* and FSAC KK 11888, which have no or only very limited skull material preserved). These were by far the highest numbers of transformations recorded at any internal node within Megalosauroidea. The spinosaurid ghost lineage could potentially explain the high number of craniodental modifications in spinosaurids when compared to other megalosaurids, as changes could simply accumulate over time. It is not clear if the disparate cranial and mandibular morphology of spinosaurids, compared to other basal tetanurans, reflects a gradual accumulation of modifications over the long ghost lineage or a sudden acquisition of a unique skull morphology. However, even a gradual process implies high rates of morphological evolution at the base of Spinosauridae, indicating that spinosaurid skull anatomy is not just a consequence of slow accumulation of changes over long time spans: our Bayesian analysis recovers a rate of 1.75 character transitions per million year, which is in the upper 20% quantile of rates detected among branches of the tree. This high rate of morphological evolution over a sustained duration of time reflected in the ghost lineage can explain the morphological distinctiveness of spinosaurids regarding closely related theropods, especially in the skull. Moreover, spinosaurids seem to retain high rates of morphological evolution after their origination, as high rates are detected at the internal branch leading to Spinosaurinae as well as those leading to several individual spinosaurid taxa.

Why spinosaurids are associated with such a long ghost lineage can currently only be speculated on. One possibility might be that spinosaurids originated in the southern hemisphere and are thus missing from the known fossil record, considering the generally abysmal Gondwanan theropod record from the Middle Jurassic to the late Early Cretaceous (see Rauhut and López-Arbarello, 2008; Rauhut and Pol, 2021). Evidence in favour of this explanation might include the presence of possible spinosaurid teeth in the (probably) Middle Jurassic Tiourarén Formation of Niger (Serrano-Martínez et al., 2015, 2016) and the Late Jurassic Tendaguru Formation of Tanzania (Buffetaut, 2011). However, the spinosaurid identity of both occurrences has been questioned (Rauhut, 2011; Hendrickx et al., 2019). An isolated spinosaurid tooth from the Berriasian of Brazil described by Sales et al. (2017) nevertheless documents the presence of this clade in the earliest part of the Cretaceous. Based on our phylogenetic results, the closest known relative of spinosaurids either occurred in eastern Asia (*Monolophosaurus*, under unweighted parsimony of the entire data matrix) or Europe (Megalosaurinae under weighted parsimony of the entire data matrix, or *Eustreptospondylus* and *Dubreuillosaurus* if only skull characters are considered, or a clade composed of *Eustreptospondylus*, *Dubreuillosaurus*, *Streptospondylus*, and *Magnosaurus* when the Bayesian results are consulted); all options indicate a non-Gondwanan origin of the group. A European origin (see also Barker et al., 2021) might also be in line with the hypothesis that Europe (which probably resembled an archipelago during the Jurassic; Smith et al., 1994) was a center of megalosauroid evolution in the Middle Jurassic (Rauhut et al., 2020). However, due to the extremely poor Jurassic theropod record

of Africa and other Gondwanan continents, it also cannot be ruled out that this impression represents an artefact of the fossil record. Another aspect worth mentioning is our generally poor knowledge of megalosauroid skulls. In the matrix including skull characters only, megalosauroids in general could be scored for only 44.5% (on average) of skull characters (whereas, as mentioned in the materials and methods section, the average of coded characters for all included OTUs was 49%), and this proportion is not evenly distributed among all relevant taxa (i.e., those with skull remains preserved). Only two megalosauroid taxa (*Monolophosaurus* [in the equal weighted parsimony result] and *Irritator*) have more than 75% of the skull characters coded, while eight out of the 18 included megalosauroids have less than 25% coded. Indeed, the second highest number of transformations under DELTRAN (26) was found for *Irritator*, one of the few taxa for which an almost complete skull is known. Assuming that the cranial and mandibular anatomy of this taxon is not unusually strongly modified, this probably reflects our very poor knowledge of the skull anatomy of spinosaurids, especially spinosaurines. This is reflected by the amount of missing data, which is 58% for non-spinosaurid megalosauroids, but 68.5% for spinosaurids.

Our phylogenetic in-group results for spinosaurids support the traditionally recovered distinction of baryonychines and spinosaurines (e.g., Sereno et al., 1998; Carrano et al., 2012; Barker et al., 2021). Baryonychines include *Baryonyx*, *Suchomimus*, *Riparovenator*, and *Ceratosuchops* across all our analyses, but the content of Spinosaurinae is more variable, with *Ichthyovenator* (Bayesian and all parsimony analyses) and/or FSAC KK 11888 (all parsimony analyses) sometimes excluded from the clade, although a Spinosaurinae including these OTUs is supported by high posterior probabilities in the Bayesian analysis (PP = 86%). In order to fully scrutinize the in-group relationships of spinosaurids further, the known but as-of-yet poorly described materials from several OTUs (e.g., *Suchomimus* and FSAC KK 11888) should receive thorough anatomical descriptions. In addition, character observations from the snout region (e.g., Sales and Schulz, 2017; Lacerda et al., 2021) could be integrated with our work, which we did not do here due to the lack of an anterior snout region in *Irritator*.

Head Posture

Based on the orientation of the lateral semicircular canal (LSC) in the endosseous labyrinth and the orientation of the occipital condyle, we have recently proposed a strongly ventrally inclined habitual head posture (c. 45°) for *Irritator* (Schade et al., 2020a). Although the new anatomical observations on the *Irritator* skull confirm this strong inclination for the rostrum, the skull anatomy shows that this is caused by a distinct ventral angulation of the rostrum regarding the postrostral skull region, while the orientation of the occipital condyle indicates a horizontally orientated braincase, as is typical for non-avian theropods. Thus, it is not the entire head that is downturned, but the snout is angled with regard to the braincase. This ventral angulation of the rostrum is caused by a posteroventral rotation of the orbital and postorbital regions of the skull against the snout, evidenced by the different lengths of the jugal and ascending rami of the maxilla, the markedly acute angle between the ventral and anterior processes of the lacrimal, the ventrally concave margin of the jugal, the slightly vaulted frontal and anteroventrally directed anterior process of the postorbital, and the placement of the infratemporal fenestra posteroventral to the orbit. Interestingly, the same angulation is also evident in the mandible, with the distinct ventral kink of the anterior portion of the surangular and the more anterior elements with respect to the region of the jaw articulation and insertion area of the main jaw muscles. In other words, if the foramen magnum faces in a straight posterior direction, the snout shows a strong ventral inclination of around 45°, confirming previous assessments based on the LSC plane (Schade et al., 2020a), which is indirectly rotated with regard to the rostrum as it is firmly embedded within the braincase. With the mentioned inclination of the snout and the arrangement and morphology of the preorbital bones, a field of binocular vision in front of the skull is indicated in *Irritator*. The mediolaterally narrowest portion of the skull roof above the orbit is situated where the frontals articulate with the prefrontals (Figures 4A, 8). This produces an anterodorsally open area that minimizes potential obstruction of the lacrimal and anterior portions of the snout (Figures 2A-4A). The morphological similarities of the lacrimal, orbital, and occipital region of other spinosaurids, including material assigned to *Suchomimus* (MS, pers. obs. on cast, MNN GDF 214), *Baryonyx* (Charig and Milner, 1997), *Ceratosuchops*, and *Riparovenator* (Barker et al., 2021), may indicate that these theropods probably had a

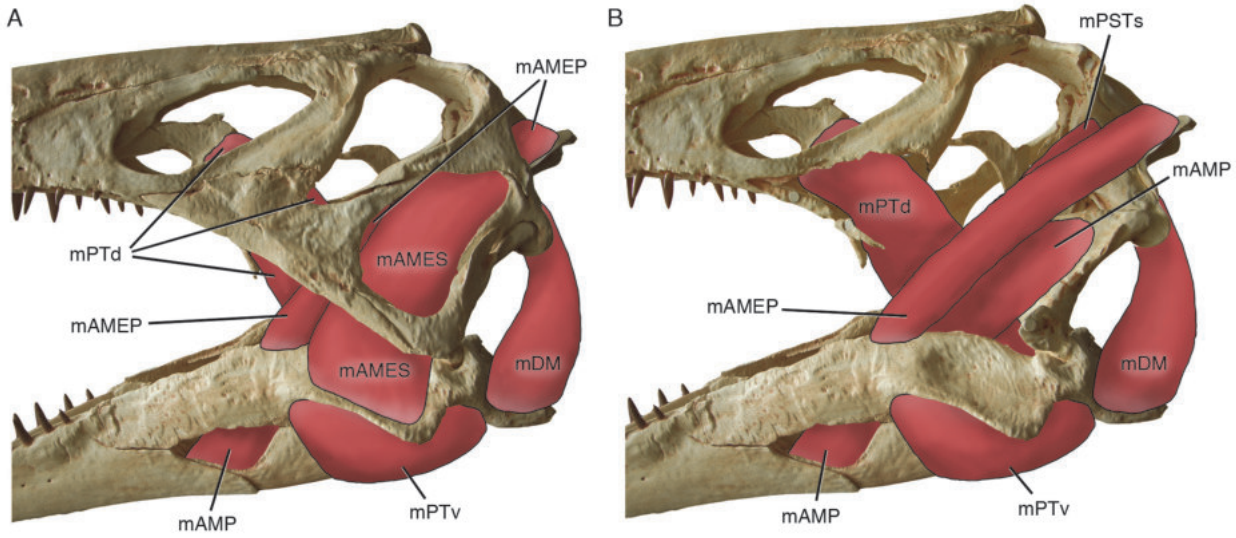

FIGURE 40. Medical CT data-based 3D print of *Irritator challengeri* (SMNS 58022) with reconstructed jaw muscle anatomy in left lateral view. A, with superficial muscles; B, with removed cheek bones, revealing deeper muscles. mAMEP, *m. adductor mandibulae externus profundus*; mAMES, *m. adductor mandibulae externus superficialis*; mAMP, *m. adductor mandibulae posterior*; mDM, *m. depressor mandibulae*; mPSTs, *m. pseudotemporalis superficialis*; mPTd, *m. pterygoideus dorsalis*; mPTv, *m. pterygoideus ventralis*.

similar head posture to *Irritator*, with binocular vision.

Functional Anatomy of the Jaws

Further evidence concerning the ecology of *Irritator* (and, by inference, other spinosaurids) comes from the biomechanics of its skull. Vertebrate mandibles can biomechanically be understood as third-order levers, as the adductor muscles insert on the lower jaw between the potential load anteriorly and the jaw joint, serving as the fulcrum, posteriorly (Figure 40; see also, e.g., Barel, 1983; Westneat, 1994, 2003). In a third-order lever, the mechanical advantage is defined as the input moment arm (distance between fulcrum and adductor muscles, i.e., jaw joint–coronoid eminence, as the most anterior insertion point of the adductor muscles; Holliday and Witmer, 2007; Holliday, 2009) divided by the output moment arm (distance between fulcrum and load, e.g., anteriormost tooth position for anterior mechanical advantage). Lower mechanical advantage values indicate speedy but low forced bites and vice versa. Thus, the ratio between pre- and postcoronoid lengths determine the relative speed and force of bites in vertebrate mandibles. One crucial feature for the functional anatomy is thus the configuration of the articulation of the skull with the lower jaw. There are three main types of the squamosal-quadrate-articular setup in non-avian theropods. First, the squamosal-quadrate articulation can be in a straight vertical line with the quadrate-articular articulation. This seems to be the most widespread condition in non-avian theropods (Rauhut, 2003). In the second setup, the dorsal contact of the quadrate is slightly to considerably more anteriorly situated in comparison with its ventral articulation with the lower jaw, as can be seen in many ceratosaurs (e.g., Gilmore, 1920; Sampson and Witmer, 2007; Zaher et al., 2020). In contrast, *Irritator* shows the third setup, in which the dorsal contact of the quadrate is positioned more posteriorly than the ventral one (in relation to the long axis of the mandible, the downward orientation of the snout mentioned above notwithstanding), as can be seen in some maniraptoriformes, e.g., *Archaeopteryx* (Rauhut, 2014) and Ornithomimosauria (Makovicky et al., 2004). Assuming a comparable relative position of the coronoid eminence and thus the insertions of the jaw muscles, this third arrangement of bones results in different jaw mechanisms, which likely produced a weak bite (lower mechanical advantage) in comparison to other large-bodied theropods (see Henderson, 2002; Therrien et al., 2005). This is partially because, in comparison to theropods with posteroventrally inclined or straight quadrates, the leverage for the jaw closing muscles (the input moment arm) is shortened in taxa with an anteroventrally inclined quadrate, such as spinosaurids, as the jaw

joint moves closer to the insertion areas of the main jaw closing muscles. This is exemplified by the insertion areas of the *m. adductor mandibulae externus* group (see Holliday and Witmer, 2007; Holliday, 2009). This and our other inferences of muscle attachments are modelled after those of other theropod dinosaurs, which, in turn, were inferred based on phylogenetic bracketing of birds and crocodilians (Witmer, 1995; Holliday and Witmer, 2007; Holliday, 2009; Cost et al., 2022). The insertion of the *m. adductor mandibulae externus profundus* of *Irritator*, the most anterior of the *m. adductor mandibulae externus* group (on the lower jaw), is marked as a slightly elevated, laterally placed and rugose patch at the point where the dorsal margin of the surangular flexes ventrally. This patch is posterior to the mid-length between the jaw articulation and the surangular-dentary suture in *Irritator*, whereas it is at approximately two-thirds of that length in taxa with a posteroventrally inclined quadrate, such as *Majungasaurus* (Holliday, 2009: fig. 8C) and in a similar position in animals with a more vertical quadrate, such as *Tyrannosaurus* (Gignac and Erickson 2017). Likewise, in *Majungasaurus*, the large insertion area for *m. adductor mandibulae externus superficialis* is anteriorly offset from the jaw articulation and extends anteriorly to the middle of the anterior half of the surangular (Holliday, 2009). In most large-bodied theropods, an anteroposteriorly elongate, flattened, or slightly depressed facet for the attachment of this muscle is present on the dorsal surface of the surangular, anterior to the jaw joint. In *Irritator*, we interpret the well-marked depression on the surangular shelf as the insertion facet for this muscle, which is restricted to the posterior half of this bone and partially overlaps the mandibular articulation laterally at its posterior end. Thus, the jaw anatomy (i.e., the osteological correlates of the adductor muscles) in *Irritator* indicates a shortening of the input moment arm not only by anterior rotation of the jaw joint, but also a relatively more posterior placement of the main jaw closing muscles on the mandible. Apart from reducing the input moment arm, this reduction in distance between the jaw joint and the closing muscle insertions also increases the angular momentum of the lower jaw: the jaws close more rapidly, as less muscle contraction (in terms of distance) is needed to adduct the mandible. In extant archosaurs with fast jaw closure (i.e., crocodilians), this is facilitated by the pterygoideus musculature (Busbey, 1989; Iordansky, 2000; Sellers et al., 2017). In *Irritator*, this muscle group is markedly different, as its main anterior attachment on the posterior end of the palatine is comparatively close to the ventral attachment on the surangular, and a ventrolateral flange of the pterygoid, which is usually hypertrophied in crocodilians, is poorly developd in *Irritator*. Thus, the *m. pterygoideus* of *Irritator* is markedly shorter and more dorosoventrally oriented than in crocodiles.

A second, and likely even stronger, effect on mechanical advantage comes from elongation of the out-lever, i.e., the part of the jaw anterior to the anteriormost insertion point of the adductor muscles, which clearly is elongated in *Irritator* and other spinosaurids with known mandibles. Low mechanical advantages and bite forces in *Irritator* and other spinosaurids are in line with the rather slender snouts and lower jaws of these animals, which are less resistant to bending stresses resulting from biting than those of high-snouted oreinirostral theropods (see Rayfield, 2011).

The lower jaw of *Irritator* bears an enlarged retroarticular process in comparison to most other non-avian averostran theropods. This structure forms the attachment site for the *m. depressor mandibulae*, which must have been rather strongly developed in *Irritator* (see Holliday and Witmer, 2007; Snively and Russell, 2007; Holliday, 2009). The *m. depressor mandibulae* stretched between the posterolateral surface of the paroccipital process and the posterodorsal surface of the retroarticular process (Holliday, 2009), permitting a powered and fast opening movement (Holliday and Witmer, 2007) in *Irritator*.

In addition, the quadrate-jaw articulation in *Irritator* supports potential lateral mandibular spreading, as proposed by Hendrickx et al. (2016). These authors suggested that the lower jaws of spinosaurids had kinetic mandibular rami which displaced laterally when being depressed, based on the lateromedial orientation of the intercondylar sulcus of the quadrate. The sulcus orientation and lateromedially wide ectocondyle, which morphologically differs strongly from most other non-avian theropods, forced the articular and surangular laterally during jaw opening. Indeed, our digitally reconstructed and articulated models of *Irritator* suggest that the entocondyle of the quadrate intersects with the mandibular articular facet and the posterior edge of the articular fossa cuts into the quadrate when the lower jaw gets depressed, unless compensatory lateral movement of the mandibular rami is introduced (Figure 41). We illustrate this in two supplementary videos using digital models in Blender and physically printed 3D models (Supplementary Data 13, Supplementary Data

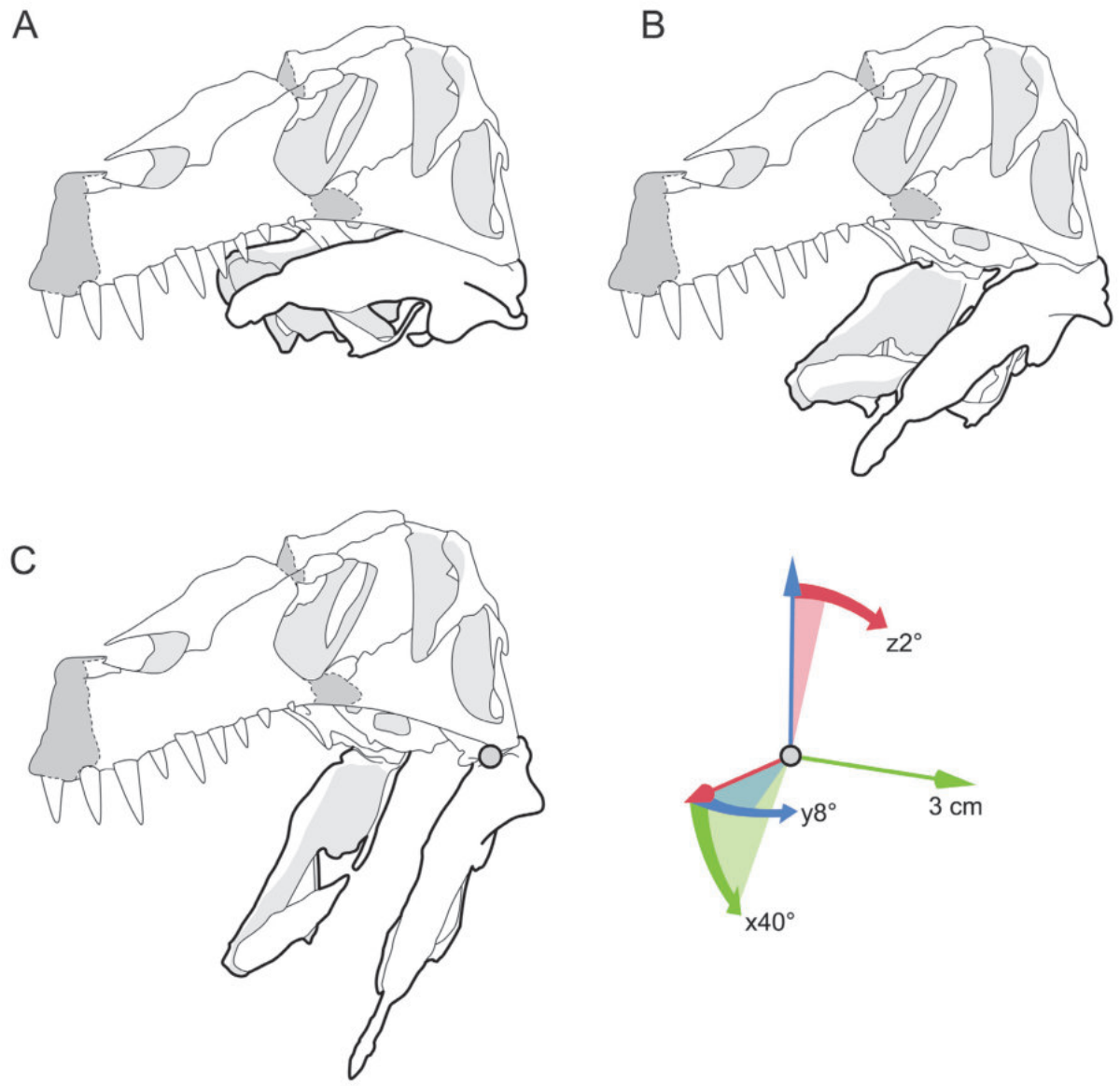

FIGURE 41. Line drawings of the re-arranged and articulated skull of *Irritator challengeri* (SMNS 58022). A, completely closed lower jaw; B, laterally spreading and rotating lower jaw rami during depression; C, the maximum opening angle of around 40° (in wider angles, the raised posterolateral margin of the glenoid fossa hits the quadrate). The lower jaw rami spread approx. 8° sideways, producing a pharynx mediolaterally widened around 3 cm per side. Additionally, each lower jaw ramus is rotating around the long axis by approx. 2° (dorsally lateral and ventrally medial). These values are measured from the point of origin for the maximum opening angle in relation to the closed position.

14). To keep a tight but non-intersecting articulation between quadrate and articular, a maximal range of jaw opening of approximately 40° is expected for *Irritator* (with the jaw joint covered by cartilage, there might be slightly higher ranges of motion possible). As the mandibular symphyses of spinosaurids are unfused and show the typical, rather unspecialized morphology of most theropods (Stromer, 1915; Charig and Milner, 1997), indicating that the jaws were held together anteriorly by soft tissues (Holliday and Nesbitt, 2013), a certain lateral expansion of the jaws with lateral stretching of the connective tissue situated in the symphyses might have been possible (see Charig and Milner, 1997; Sereno et al., 1998; Holliday and Nesbitt, 2013; Hendrickx et al., 2016). However, this setting

would need considerable muscle effort of the abductors, including the *m. depressor mandibulae* (see above). This is because the lateral expansion of the lower jaw would create additional tension on the bone and the adductor muscles, including the *m. pterygoideus ventralis* (inserting on the ventral surface of the prominent lateral surangular shelf) of the internal adductor musculature. Reaching the point of maximal tension, the relaxation of the abductor muscles would reinforce the contraction speed of the adductor muscles, further supporting the hypothesis of a very rapid jaw closure. In summary, the skull morphology of *Irritator* indicates fast, rather than strong biting, supporting previous studies on skull strength and bite force in non-avian theropods (Henderson 2002; Therrien et al., 2005; Rayfield 2011).

Further evidence for the feeding ecology of spinosaurids comes from the anterior jaw morphology and dentition. The articulated premaxillae and maxillae of these animals are narrow, but rather robust and closely appressed, mainly due to the medially swollen and ventrally expanded paradental lamina that covers the (apparently fused) paradental plates medially (see description above; Charig and Milner, 1997; Sereno et al., 1998; Dal Sasso et al., 2005). Together with the deep (in relation to the tooth-bearing bones) roots of the teeth, this results in a rather rigid implantation of teeth in the jaws of spinosaurids. The more rounded cross section of the teeth and presence of longitudinal fluting further increase their robustness. The long, slender snouts of spinosaurids were certainly less suited to withstand the high impact forces created by other large theropod skulls upon impact on prey animals that were large with regard to the body size of the predator (Rayfield et al., 2001; Henderson, 2002; Rayfield, 2004, 2011; Cuff and Rayfield, 2013). However, the elongate snouts and mandibles, the high angular momentum created by the jaw muscles and the resulting rapid closing of the jaws, together with the enlarged teeth in the anterior part of the maxilla and dentary, are ideally suited to capture and secure elusive prey of relatively small size (compared to the body size of spinosaurids), including fish and other relatively small vertebrates, such as pterosaurs (Buffetaut et al., 2004) or juvenile dinosaurs (Charig and Milner, 1997). During snapping, the large, conical teeth would puncture the prey item at high speed, leading to severe injuries. The prey could then be lifted off the ground or out of the water, with the deep implantation and rigid medial anchoring of the teeth by the expanded paradental lamina, the more rounded cross section and longitudinal flutings all helping to prevent tooth loss or breakage caused by the struggling prey. The unusually high tooth replacement rates in spinosaurids (Heckeberg and Rauhut, 2020) might be a further indication that tooth loss by struggling prey and the need for rapid replacement was an issue during feeding in spinosaurids.

Ecology

Hypotheses on the stance and ecology of spinosaurids, and in particular *Spinosaurus*, have changed over the last decades. Stromer (1936) interpreted anatomical pecularities of *Spinosaurus*, particularly in the jaw and dorsal vertebrae, as indicative of some unusual specialisation among theropods that was not further detailed. He explicitly mentioned that no good extant analog seems to exist for this animal. The earliest reconstruction (in the same paper) depicted *Spinosaurus* as a tyrannosaur-like creature with an erect posture, albeit with a sail on its back (Stromer, 1936: Abb. 8). Following the initial suggestion of a piscivorous diet for spinosaurids by Taquet (1984), based on fragmentary remains from the late Early Cretaceous of Niger, the discovery of *Baryonyx* in the Barremian Wessex Formation of England, half a century after the first reconstruction by Stromer, led to a reinterpretation of spinosaurids as long-snouted, piscivorous predators with a terrestrial lifestyle and facultative quadrupedality (Charig and Milner, 1986). Later, Charig and Milner (1997) reconstructed *Baryonyx* as a piscivorous predator with a typical theropod-like bipedal posture. The same general body plan was later found in the closely related *Suchomimus* from the Aptian Elrhaz Formation of Niger (Sereno et al., 1998).

It is by now generally accepted that spinosaurids were probably largely (but not exclusively) piscivorous predators (as mainly indicated by tooth and jaw morphology, although gut contents and other fossils indicate a mixed diet; e.g., Charig and Milner, 1997; Buffetaut et al., 2004), and likely possessed a greater affinity to water bodies than other large-bodied theropods (Amiot et al., 2010a, b; Ibrahim et al., 2014, 2020; Sales et al., 2016; Hassler et al., 2018; Fabbri et al., 2022). Rauhut et al. (2016) furthermore found statistical evidence that megalosauroids in general preferred nearshore over inland environments. Certain anatomical traits of the skull, neck, and manus of spinosaurids have occasionally been interpreted as potential adaptations to piscivory (e.g., Charig and Milner, 1986; Sereno et al., 1998; Evers et al., 2015; Arden et al.,

2019; Schade et al., 2020a). However, most of these interpretations remain speculative and have not been tested by biomechanical studies or comparative statistical analyses using extant analogs (but see Henderson, 2018; Ibrahim et al., 2020a; Fabbri et al., 2022a, b; Sereno et al., 2022).

Newly discovered cranial and postcranial materials referred to *Spinosaurus* have recently led to reinterpretations of the anatomy and ecology of this taxon. In an initial study, Ibrahim et al. (2014) proposed reduced hind leg–pelvis proportions based on a partial skeleton that led these authors to suggest that *Spinosaurus* was quadrupedal when moving terrestrially. Some of the hypotheses proposed in this study (e.g., foot webbing) were highly speculative and not further tested (see Hone and Holtz, 2021). In another study, Ibrahim et al. (2020) reported a nearly complete tail (likely of the same specimen presented in their earlier paper) with elongated neural spines and other peculiarities of the caudals. These were interpreted as adaptations for tail-based propelling, which the authors tested with analog biomechanical models (Ibrahim et al., 2020a; however, see also Hone and Holtz, 2021; Sereno et al., 2022). However, based on biomechanical modelling of the whole body, Henderson (2018) and Sereno et al. (2022) argued that *Spinosaurus* was a slow, unstable swimmer that was unable to dive. Likewise, using a robotic model of the tail, Fish et al. (2021) found that, although keeled tails are generally better at producing thrust under water than tapering tails, the tail of *Spinosaurus*, as reconstructed by Ibrahim et al. (2020a), produced considerably less thrust in water than that of modern *Crocodylus*. On the other hand, Fabbri et al. (2022a, b) found evidence for high bone compactness in *Spinosaurus* and *Baryonyx*, which are statistically indistinct from equally high compactness values exclusively found among aquatic tetrapods when accounting for allometry and demonstrated that these high compactness values are best interpreted as indicating frequent aquatic submersion based on a large comparative phylogenetic sample of amniotes. However, spinosaurids seem to have had a certain degree of ecological disparity as indicated by bone compactness, as values for *Suchomimus* indicate non-diving foraging behaviour (Fabbri et al., 2022a, b). Many of the anatomical traits and their interpretations have been questioned on various anatomical and ecological grounds (Hone and Holtz, 2021; Myhrvold et al., 2022; Sereno et al., 2022). The papers by Ibrahim et al. (2014, 2020) and Fabbri et al. (2022a, b) provide separate inferences for various traits that have varying levels of support from the evidence. For example, phylogenetic comparative statistical evidence for habitual submersion of *Spinosaurus* on the basis of bone compactness is high (Fabbri et al., 2022a, b), but this does not mean that claims that are less substantiated, such as the hypothesis of quadrupedality based on the proposed relative pelvis size and reconstructed center of gravity or the hypothesis of webbed feet (Ibrahim et al., 2014), must be accepted at the same time (see Sereno et al., 2022). Hone and Holtz (2021) argue that *Spinosaurus* and other spinosaurids were possibly generalist, mainly bipedal predators preying along shorelines (see also Henderson, 2018; Sereno et al., 2022). Wading behaviour that is explicitly part of this model, however, is not supported by comparative statistical evidence of bone compactness, as modern waders (including herons) have bone compactness values like those of non-aquatic amniotes (Fabbri et al., 2022a). However, it might be questionable whether flying birds with a body weight approximately three orders of magnitude less than spinosaurids are good biomechanical analogs, and Sereno et al. (2022) instead argue that the observed bone compactness in *Spinosaurus* might be due to the bone mechanics of such a large, short-limbed animal. Despite the lack of consenus on an exact interpretation of the above-mentioned features, it does seem clear that spinosaurids (or at least *Spinosaurus*) were better adapted to foraging in and/or around water bodies than other large theropods.

Although *Irritator* does not preserve postcranial material that could advance this debate, it represents the spinosaurid with the most complete cranial and mandibular remains. Thus, anatomical and functional considerations based on the skull may help to specify the feeding style of this taxon, which is related to its foraging, and thus, ecology. We interpret the rather weak bite force proposed herein (in relation to other large-bodied theropods), in combination with a rapid jaw closure and robust dentition, as indicating that the animal hunted prey considerably smaller than its own body size, which could still include large fishes and smaller dinosaurs. We scrutinize viewpoints previously published by some of us that the floccular lobe and size of the anterior semicircular canal (ASC) indicate a particularly agile lifestly in *Irritator* (Schade et al., 2020a). ASC lengthening in dinosaurs generally has since been shown to be related to the evolution of an erect stance or bipedality (Bronzati et al., 2021), and the ASC shape of *Irritator* is thus unlikely to indicate any specializations for agility

relative to other, closely related bipedal dinosaurs. Also, semicircular canal shape in general has recently been shown to have low predictive power over ecological adaptations, based on empirical studies on reptiles (e.g., Bronzati et al., 2021; Evers et al., 2022; whereas it has proven insightful in synapsids, e.g., Pfaff et al., 2015; 2017; Schwab et al., 2019; Araújo et al., 2022) and theoretical considerations on biomechanics (David et al., 2022; however, see also Hanson et al., 2021; 2022 and references therein). A link between floccular lobe size and agility should also be evaluated formally considering comparative data before it is used as an indicator of specific ecological traits (see also Walsh et al., 2013; Ferreira-Cardoso et al., 2017). Despite these reservations concerning neuroanatomical evidence in support of agile hunting behaviour, *Irritator* still preserves other osteological features that are at least consistent with the interpretation of it applying ambush hunting behaviour. This includes the posteriorly placed external nares (which may enable the snout to have been partially submerged whilst hunting aquatic prey), the position and orientation of the eyes (which may have facilitated binocular vision; see also Stevens, 2006; Arden et al., 2019), and the jaw anatomy that indicates spreading lower jaws capable of rapid closure to capture, injure, and swallow prey. This ecological interpretation of spinosaurids as predators applying ambush hunting behaviour may be separate from the question of the frequency of their submersion in water. Ambush predator behaviour of spinosaurids can easily be reconciled with the compactness data of Fabbri et al. (2022a), which suggests habitual aquatic submersion in water of some spinosaurids without detailing the mode of locomotion. Lastly, we do not think that the ecological debate surrounding spinosaurids should simply be reduced to comparisons with individual extant taxa (e.g., “heron model” or “crocodile model” or “pursuit predator model”; e.g., Arden et al., 2019; Hone and Holtz, 2021). We may have to accept that the exact ecology of spinosaurids cannot currently be determined with great certainty, and that there is no extant analog that fully mirrors its ecology or behaviour—much as Stromer (1936) initially argued.

Data Availability

The CT slice data and 3D files of SMNS 58022, are published online, in the repository MorphoSource, projects ‘Schade et al., 2020. *Irritator challengeri* SMNS 58022 neuroanatomy’ (https://www.morphosource.org/projects/00000C951) and ‘Schade et al., 2022. *Irritator challengeri* SMNS 58022 osteology’ (https://www.morphosource.org/projects/000372273).

The phylogenetic data matrices can be found on Morphobank (morphobank.com) under project 3955 (https://morphobank.org/index.php/MyProjects/List/select/project_id/3955).

The MrBayes output files can be found at: https://doi.org/10.5281/zenodo.7785634.

ACKNOWLEDGMENTS

We are deeply grateful to Rainer Schoch for access to SMNS 58022 and permission to loan the specimen in order to conduct CT examinations. We thank Nicole Kreuzer and Stephan Tomaschko (Zeiss in Essingen) as well as Jacqueline Jendick and Cornelia Pankalla (Deutsches Herzzentrum in Munich) for the CT examinations of the skull of *Irritator.* We are very thankful for the support of Martin Nose (Freunde der Bayerischen Staatssammlung für Paläontologie und Geologie München e.V. for financial support), Tanja Schulz-Mirbach (Lehre@LMU for financial support), Nils Knötschke, Benjamin Englich, Brian Bernecker, Jens Kosch (Dinosaurier-Park Münchehagen for general support and casts), and Heinrich Mallison (Palaeo3D for 3D prints). Susannah Maidment took photographs and provided access to material of *Baryonyx.* Additionally, we thank Ingelore Hinz-Schallreuter, Stefan Meng, Marie Hörnig, Jakob Krieger, Georg Brenneis, Steffen Harzsch, Gertrud Rößner, Christoph Kettler, Roger Benson, Max Kellermann, Julia Desojo, Chris Barker, Mario Bronzati, Guilherme Hermanson, Gabriel Ferreira, and Alexander Kellner for help and discussions. We also thank three anonymous reviewers and Elisabete Malafaia for their thoughtful reviews of an initial version of this manuscript, as well as Christian Kammerer and Heinrich Mallison for their editorial work. MS is supported by the Bogislaw PhD scholarship of the University of Greifswald. CF is supported by the Swiss National Science Foundation (PZ00P2_174040).

Ethics Statement

As the specimen described here originates from Brazil, and there currently is a debate about the legality and ethics of working with Brazilian specimens deposited outside of this country (Cisneros et al., 2021, 2022), we acknowledge the possibly problematic status of SMNS 58022. Thus, we want to present some background and considerations on this matter.

The type specimen of *Irritator challengeri* was purchased by the Staatliches Museum für Naturkunde Stuttgart from a German fossil dealer in 1991. The specimen was imported to Germany prior to 1990, when the decree on the export of fossils and the handling of type specimens from Brazil was passed (Cisneros et al., 2022); the previous legislation in Brazil (Decreto-Lei 4.146 from March 1942) governs the need of permits for the collection of specimens, but not their export (see Cisneros et al., 2022). Most fossils from the Araripe Basin are collected and sold by local collectors (Vila Nova et al., 2011; Vilas Boas et al., 2013; Cisneros et al., 2022). D. Martill (in Sues et al., 2002) mentioned that local collectors recalled seeing the specimen (later becoming the holotype of *Irritator challengeri*), so that it is likely that it was purchased from such collectors prior to its export. Currently, as part of the collection of the Staatliches Museum für Naturkunde Stuttgart, the specimen is property of the German Bundesland (province) of Baden-Württemberg, and a clarification of its legal status lies neither within our nor the local curator's power.

Since the acquisition of the specimen by the Staatliches Museum für Naturkunde Stuttgart, it has been studied repeatedly. The new taxon *Irritator challengeri* was established and initially described by Martill et al. (1996), with additional information having been provided by Sues et al. (2002), Hendrickx et al. (2016, 2019), Sales and Schultz (2017), and Schade et al. (2020). As the specimen is part of a public collection and thus available for additional study for anybody with a scientific interest in it, we provide new information here.

In order to make our data available to the broader scientific community, we already deposited the available neuroanatomical models and CT data (a medical CT of the entire skull and a µCT of the braincase) in the online repository MorphoSource (Schade et al., 2020b) in the framework of our previous publication on the endocranial anatomy of *Irritator* (Schade et al., 2020a). These CT data, which also formed the basis for the current work, are freely available for download from that platform. All new 3D models created from that data, in addition to photogrammetric models of the fossil, are also deposited on MorphoSource (Schade et al., 2022).

Author Contributions

MS and OWMR designed the project. MS organized CT scans. MS segmented the medical and µCT data. OM segmented the medical CT data and produced the skull rearrangement and videos. MS, OM, CF, SWE, and OWMR coded and scored phylogenetic characters, and OWMR performed the cladistic analyses. SWE performed the character optimization of parsimony results. SWE performed the Bayesian analysis. MS and OWMR prepared photographic figures, MS and OM prepared line drawings, and OWMR and OM prepared muscle reconstructions, and SWE prepared the digital anatomical and phylogeny figures. MS, OM, CF, SWE, and OWMR interpreted the data, discussed the phylogeny, and wrote the manuscript.

REFERENCES

Agnarsson, I. and Miller, J. 2008. Is ACCTRAN better than DELTRAN? Cladistics, 24:1032-1038. https://doi.org/10.1111/j.1096-0031.2008.00229.x

Allain, R. 2002. Discovery of a megalosaur (Dinosauria, Theropoda) in the Middle Bathonian of Normandy (France) and its implications for the phylogeny of basal Tetanurae. Journal of Vertebrate Paleontology, 22:548-563. https://doi.org/10.1671/0272-4634(2002)022[0548:domdti]2.0.co;2

Allain, R. and Chure, D.J. 2002. *Poekilopleuron bucklandii,* the theropod dinosaur from the Middle Jurassic (Bathonian) of Normandy. Palaeontology, 45:1107-1121. https://doi.org/10.1111/1475-4983.00277

Allain, R., Xaisanavong, T., Richir, P., and Khentavong, B. 2012. The first definitive Asian spinosaurid (Dinosauria: Theropoda) from the Early Cretaceous of Laos. Naturwissenschaften, 99:369-377. https://doi.org/10.1007/s00114-012-0911-7

Amiot, R., Buffetaut, E., Lécuyer, C., Wang, X., Boudad, L., Ding, Z., Fourel, F., Hutt, S., Martineau, F., Medeiros, M.A., Mo, J., Simon, L., Suteethorn, V., Sweetman, S., Tong, H., Zhang, F., and Zhou, Z. 2010a. Oxygen isotope evidence for semi-aquatic habits among spinosaurid theropods. Geology, 38:139-142. https://doi.org/10.1130/G30402.1

Amiot, R., Wang, X., Lécuyer, C., Buffetaut, E., Boudad, L., Cavin, L., Ding, Z., Fluteau, F., Kellner, A.W.A., Tong, H., and Zhang, F. 2010b. Oxygen and carbon isotope compositions of Middle Cretaceous vertebrates from North Africa and Brazil: ecological and environmental significance. Palaeogeography, Palaeoclimatology, Palaeoecology, 297:439-451. https://doi.org/10.1016/j.palaeo.2010.08.027

Andres, B., Clark, J.M., and Xu, X. 2010. A new rhamphorhynchid pterosaur from the Upper Jurassic of Xinjiang, China, and the phylogenetic relationships of basal pterosaurs. Journal of Vertebrate Paleontology, 30:163-187. https://doi.org/10.1080/02724630903409220

Arai, M. and Assine, M.L. 2020. Chronostratigraphic constraints and paleoenvironmental interpretation of the Romualdo Formation (Santana Group, Araripe Basin, Northeastern Brazil) based on palynology. Cretaceous Research, 116:104610. https://doi.org/10.1016/j.cretres.2020.104610

Araujo, R., David, R., Benoit, J.K., Lungmus, J., Stoessel, A., Barrett, P.M., Maisano, J.A., Ekdale, E., Orliac, M., Luo, Z.-X., Martinelli, A.G., Hoffman, E.A., Sidor, C.A., Martins, R.M.S., Spoor, F., and Angielczyk, K.D. 2022. Inner ear biomechanics reveals Late Triassic origin of mammalian endothermy. Nature, 607:726-731. https://doi.org/10.1038/s41586-022-04963-z

Arden, T.M., Klein, C.G., Zouhri, S., and Longrich, N.R. 2019. Aquatic adaptation in the skull of carnivorous dinosaurs (Theropoda: Spinosauridae) and the evolution of aquatic habits in spinosaurids. Cretaceous Research, 93:275-284. https://doi.org/10.1016/j.cretres.2018.06.013

Bakker, R.T., Williams, M., and Currie, P.J. 1988. *Nanotyrannus,* a new genus of pygmy tyrannosaur, from the latest Cretaceous of Montana. Hunteria, 1:1-30.

Bapst, D.W. 2012. Paleotree: An R package for paleontological and phylogenetic analyses of evolution. Methods in Ecology and Evolution, 3:803-807. https://doi.org/10.1111/j.2041-210X.2012.00223.x

Barel, C.D.N. 1983. Toward a constructional morphology of cichlid fishes (Teleostei, Perciformes). Netherlands Journal of Zoology, 33:357-424.

Barker, C.T., Hone, D.W.E., Naish, D., Cau, A., Lockwood, J.A.F., Foster, B., Clarkin, C.E., Schneider, P., and Gostling, N.J. 2021. New spinosaurids from the Wessex formation (Early Cretaceous, UK) and the European origins of Spinosauridae. Scientific Reports, 11:19340. https://doi.org/10.1038/s41598-021-97870-8

Barker, C.T., Naish, D., Newham, E., Katsamenis, O.L., and Dyke, G. 2017. Complex neuroanatomy in the rostrum of the Isle of Wight theropod *Neovenator salerii*. Scientific Reports, 7(1):3749. https://doi.org/10.1038/s41598-017-03671-3

Barsbold, R. and Osmólska, H. 1999. The skull of *Velociraptor* (Theropoda) from the Late Cretaceous of Mongolia. Acta Palaeontologica Polonica, 44:189-219.

Bell, M.A. and Lloyd, G.T. 2015. Strap: An R package for plotting phylogenies against stratigraphy and assessing their stratigraphic congruence. Palaeontology, 58:379-389. https://doi.org/10.1111/pala.12142

Beer, D. and Beer, A. 2019. phylotate: Phylogenies with Annotations. R package version 1.3. https://CRAN.R-project.org/package=phylotate

Benoit, J., Legendre, L., Farke, A., Neenan, J., Mennecart, B., Costeur, L., Mérigeaud, S., and Manger, P. 2020. A test of the lateral semicircular canal correlation to head posture, diet and other biological traits in “ungulate” mammals. Scientific Reports, 10:19602. https://doi.org/10.1038/s41598-020-76757-0

Benson, R.B.J. 2008. A redescription of *‘Megalosaurus’ hesperis* (Dinosauria, Theropoda) from the Inferior Oolite (Bajocian, Middle Jurassic) of Dorset, United Kingdom. Zootaxa, 1931:57-67.

Benson, R.B.J. 2010. A description of *Megalosaurus bucklandii* (Dinosauria: Theropoda) from the Bathonian of the UK and the relationships of Middle Jurassic theropods. Zoological Journal of the Linnean Society, 158:882-935. https://doi.org/10.1111/j.1096-3642.2009.00569.x

Britt, B.B. 1991. Theropods of Dry Mesa Quarry (Morrison Formation, Late Jurassic), Colorado, with emphasis on the osteology of *Torvosaurus tanneri*. BYU Geology Studies, 37:1-72.

Brochu, C.A. 2001. Crocodylian snouts in space and time: phylogenetic approaches toward adaptive radiation. American Zoologist, 41(3):564-585.

Bronzati, M., and Rauhut, O.W.M. 2018. Braincase redescription of *Efraasia minor* Huene, 1908 (Dinosauria: Sauropodomorpha) from the Late Triassic of Germany, with comments on the evolution of the sauropodomorph braincase. Zoological Journal of the Linnean Society, 182:173-224. https://doi.org/10.1093/zoolinnean/zlx029

Bronzati, M., Langer, M.C., and Rauhut, O.W.M. 2018. Braincase anatomy of the early Sauropodomorph *Saturnalia tupiniquim* (Late Triassic, Brazil). Journal of Vertebrate Paleontology, 38:e1551973. https://doi.org/10.1080/02724634.2018.1559173

Bronzati, M., Benson, R.B., Evers, S.W., Ezcurra, M.D., Cabreira, S.F., Choiniere, J., Dollman, K.N., Paulina-Carabajal, A., Radermacher, V.J., Roberto-da-Silva, L., and Sobral, G. 2021. Deep evolutionary diversification of semicircular canals in archosaurs. Current Biology, 31(12):2520-2529.

Brusatte, S., Benson, R.B.J., Zhao, X.-J., and Currie, P. J. 2010. The skull of *Monolophosaurus jiangi* (Dinosauria: Theropoda) and its implications for early theropod phylogeny and evolution. Zoological Journal of the Linnean Society, 158:573-607.

Brusatte, S.L., Benton, M.J., Ruta, M., and Lloyd, G.T. 2008. Superiority, Competition, and Opportunism in the Evolutionary Radiation of Dinosaurs. Science, 321:1485-1488. https://doi.org/10.1126/science.1161833

Brusatte, S.L., Carr, T.D., and Norell, M.A. 2012. The osteology of *Alioramus*, a gracile and long-snouted tyrannosaurid (Dinosauria: Theropoda) from the Late Cretaceous of Mongolia. Bulletin of the American Museum of Natural History, 366:1-197. https://doi.org/10.1206/770.1

Buffetaut, E. 1989. New remains of the enigmatic dinosaur *Spinosaurus* from the Cretaceous of Morocco and the affinities between *Spinosaurus* and *Baryonyx*. Neues Jahrbuch für Geologie und Paläontologie, Monatshefte, 2:79-87.

Buffetaut, E. 1992. Remarks on the Cretaceous theropod dinosaurs *Spinosaurus* and *Baryonyx*. Neues Jahrbuch für Geologie und Paläontologie Monatshefte, 2:88-96.

Buffetaut, E., Martill, D., and Escuillie, F. 2004. Pterosaurs as part of a spinosaur diet. Nature, 430:33. https://doi.org/10.1038/430033a

Busbey, A.B. III. 1989. Form and function of the feeding apparatus of *Alligator mississippiensis*. Journal of Morphology, 202:99-127.

Canale, J., Apesteguía, S., Gallina, P., Mitchell, J., Smith, N., Cullen, T.M., Shinya, A., Haluza, A., Gianechini, F., and Makovicky, P. 2022. New giant carnivorous dinosaur reveals convergent evolutionary trends in theropod arm reduction. Current Biology, 32(14): P3195-3202.E5. https://doi.org/10.1016/j.cub.2022.05.057

Carr, T.D. 2020. A high-resolution growth series of *Tyrannosaurus rex* obtained from multiple lines of evidence. PeerJ, 8:e9192. https://doi.org/10.7717/peerj.9192

Carrano, M.T. and Sampson, S.D. 2008. The phylogeny of Ceratosauria (Dinosauria: Theropoda). Journal of Systematic Palaeontology, 6:182-236.

Carrano, M.T., Benson, R.B.J., and Sampson, S.D. 2012. The phylogeny of Tetanurae (Dinosauria: Theropoda). Journal of Systematic Palaeontology, 10:211-300. https://doi.org/10.1080/14772019.2011.630927

Chapelle, K.E.J. and Choiniere, J.N. 2018. A revised cranial description of *Massospondylus carinatus* Owen (Dinosauria: Sauropodomorpha) based on computed tomographic scans and a review of cranial characters for basal Sauropodomorpha. PeerJ, 6:e4224. https://doi.org/10.7717/peerj.4224

Charig, A.J. and Milner, A.C. 1986. *Baryonyx*, a remarkable new theropod dinosaur. Nature, 324:359-361.

Charig, A.J. and Milner, A.C. 1997. *Baryonyx walkeri*, a fish-eating dinosaur from the Wealden of Surrey. Journal of Systematic Palaeontology, 53:11-70.

Chure, D.J. and Loewen, M.A. 2020. Cranial anatomy of *Allosaurus jimmadseni*, a new species from the lower part of the Morrison Formation (Upper Jurassic) of Western North America. PeerJ, 8:e7803. https://doi.org/10.7717/peerj.7803

Chure, D.J. and Madsen, J.H. 1998. An unusual braincase (?*Stokesosaurus clevelandi*) from the Cleveland-Lloyd dinosaur quarry, Utah (Morrison formation; Late Jurassic). Journal of Vertebrate Paleontology, 18:115-125. https://doi.org/10.1080/02724634.1998.10011038

Cisneros, J.C., Raja, N.B., Ghilardi, A.M., Dunne, E.M., Pinheiro, F.L., Fernández, O.R.R., Sales, M.A.F., Rodríguez-de la Rosa, R.A., Miranda-Martínez, A.Y., González-Mora, S., Bantim, R.A.M, de Lima, F.J., and Pardo, J.D. 2022. Digging deeper into colonial palaeontological practices in modern day Mexico and Brazil. Royal Society Open Science, 9:210898. https://doi.org/10.1098/rsos.210898

Cisneros, J.C., Raja, N.B, Stewens, P., and Ghilardi, A.M. 2021. The moral and legal imperative to return illegally exported fossils. Nature Ecology and Evolution, 6;2-3. https://doi.org/10.1038/s41559-021-01588-9

Conrad, J.L. 2008. Phylogeny and systematics of Squamata (Reptilia) based on morphology. Bulletin of the American Museum of Natural History, 310:1-182.

Conrad, J.L., Rieppel, O., Gauthier, J.A., and Norell, M.A. 2012. Osteology of *Gobiderma pulchrum* (Monstersauria, Lepidosauria, Reptilia). Bulletin of the American Museum of Natural History, 362:1-88.

Coria, R.A. and Currie, P.J. 2002. The braincase of *Giganotosaurus carolinii* (Dinosauria, Theropoda) from the Upper Cretaceous of Argentina. Journal of Vertebrate Paleontology, 22:802-811.

Coria, R.A. and Currie, P.J. 2016. A new megaraptoran dinosaur (Dinosauria, Theropoda, Megaraptoridae) from the Late Cretaceous of Patagonia. PLoS ONE, 11:e0157973. https://doi.org/10.1371/journal.pone.0157973

Cost, I., Sellers, K., Rozin, R., Spates, A., Middleton, K., and Holliday, C. 2022. 2D and 3D visualizations of archosaur jaw muscle mechanics, ontogeny and phylogeny using ternary diagrams and 3D modeling. The Journal of Experimental Biology, 225(Suppl_1):jeb243216. https://doi.org/10.1242/jeb.243216

Cuff, A.R. and Rayfield, E.J. 2013. Feeding mechanics in spinosaurid theropods and extant crocodilians. PLoS ONE, 8:e65295. https://doi.org/10.1371/journal.pone.0065295

Currie P.J. and Zhao, X.-J. 1994. A new carnosaur (Dinosauria, Theropoda) from the Jurassic of Xinjiang, People's Republic of China. Canadian Journal of Earth Sciences, 30:2037-2081. https://doi.org/10.1139/e93-179

Currie, P.J. 2003. Cranial anatomy of tyrannosaurid dinosaurs from the Late Cretaceous of Alberta, Canada. Acta Palaeontologica Polonica, 48(2):191-226.

Dal Sasso, C., Maganuco, S., Buffetaut, E., and Mendez, M.A. 2005. New information on the skull of the enigmatic theropod *Spinosaurus*, with remarks on its size and affinities. Journal of Vertebrate Paleontology, 25:888-896. https://doi.org/10.1671/0272-4634(2005)025[0888:NIOTSO]2.0.CO;2

David, R., Bronzati, M., and Benson, R.B.J. 2022. Comment on "The early origin of a birdlike inner ear and the evolution of dinosaurian movement and vocalization". Science, 376(6600). https://doi.org/10.1126/science.abl6710

De França, T.C., Brilhante, N.S., De Oliveira Monteiro Nobre, Y., Medeiros, M.A., Lindoso, R.M., and Costa, F.R. 2022.The first record of a spinosaurid pedal ungual from Brazil (Boca do Forno Ravine, Itapecuru Formation, Parnaíba Basin). Historical Biology, 34(9):1817-1826. https://doi.org/10.1080/08912963.2021.1981890

Eddy, D.R. and Clarke, J.A. 2011. New information on the cranial anatomy of *Acrocanthosaurus atokensis* and its implications for the phylogeny of Allosauroidea (Dinosauria: Theropoda). PLoS ONE, 6(3):e17932. https://doi.org/10.1371/journal.pone.0017932

Evers, S.W., Foth, C., and Rauhut, O.W.M. 2020. Notes on the cheek region of the Late Jurassic theropod dinosaur *Allosaurus*. PeerJ, 8:e8493. https://doi.org/10.7717/peerj.8493

Evers, S.W., Joyce, W.G., Choiniere, J.N., Ferreira, G.S., Foth, C., Hermanson, G., Yi, H., Johnson, C.M., Werneburg, I., and Benson, R.B.J. 2022. Independent origin of large labyrinth size in turtles. Nature Communications, 13:5807. https://doi.org/10.1038/s41467-022-33091-5

Ezcurra, M.D., Nesbitt, S.J., Bronzati, M., Dalla Vecchia, F.M., Agnolin, F.L., Benson, R.B.J., Egli, F.B., Cabreira, S.F., Evers, S.W., Gentil, A.R., Irmis, R.B., Martinelli, A.G., Novas, F.E., da Silva, L.R., Smith, N.D., Stocker, M.R., Turner, A.H., and Langer, M.C. 2020. Enigmatic dinosaur precursors bridge the gap to the origin of Pterosauria. Nature, 588(7838):445-449. https://doi.org/10.1038/s41586-020-3011-4

Fabbri, M., Navalón, G., Benson, R.B.J., Pol, D., O'Connor, J.K., Bhullar, B.-A.S., Erickson, G.M., Norell, M.A., Orkney, A., Lamanna, M.C., Zouhri, S., Becker, J., Emke, A., Dal Sasso, C., Bindellini, G., Maganuco, S., Auditore, M. and Ibrahim, N. 2022a. Subaqueous foraging among carnivorous dinosaurs. Nature 603:852-857. https://doi.org/10.1038/s41586-022-04528-0

Fabbri, M., Navalón, G., Benson, R., Pol, D., O'Connor, J., Bhullar, B.-A., Erickson, G., Norell, M., Orkney, A., Lamanna, M., Zouhri, S., Becker, J., Dal Sasso, C., Bindellini, G., Maganuco, S., Auditore, M., and Ibrahim, N. 2022b. Sinking a giant: quantitative macroevolutionary comparative methods debunk qualitative assumptions. bioRxiv. https://doi.org/10.1101/2022.05.05.490811

Ferreira-Cardoso, S., Araújo, R., Martins, N.E., Martins, G.G., Walsh, S., Martins, R.M.S., Kardjilov, N., Manke, I., Hilger, A., and Castanhinha, R. 2017. Floccular fossa size is not a reliable proxy of ecology and behaviour in vertebrates. Scientific Reports, 7:2005. https://doi.org/10.1038/s41598-017-01981-0

Fischer, V., Benson, R.B., Druckenmiller, P.S., Ketchum, H.F., and Bardet, N. 2018. The evolutionary history of polycotylid plesiosaurians. Royal Society Open Science, 5(3):172177. https://doi.org/10.1098/rsos.172177

Fish, F.E., Rybczynski, N., Lauder, G.V., and Duff, C.M. 2021. The role of the tail or lack thereof in the evolution of tetrapod aquatic propulsion. Integrative and Comparative Biology, 61:398-413. https://doi.org/10.1093/icb/icab021

Gauthier, J.A. 1986. Saurischian monophyly and the origin of birds. In Padian, K. (ed.), The Origin of Birds and the Evolution of Flight. Memoirs of the California Academy of Sciences, 8:1-55.

Gelman, A. and Rubin, D.B. 1992. Inference from iterative simulation using multiple sequences. Statistical Science, 4:457-511.

Gilmore, C.W. 1920. Osteology of the carnivorous Dinosauria in the United States National Museum, with special reference to the genera *Antrodemus (Allosaurus)* and *Ceratosaurus*. Bulletin of the United States National Museum, 110:1-154.

Gignac, P. and Erickson, G. 2017. The biomechanics behind extreme osteophagy in *Tyrannosaurus rex*. Scientific Reports, 7:12. https://doi.org/10.1038/s41598-017-02161-w

Goloboff, P.A. and Catalano, S.A. 2016. TNT version 1.5, including a full implementation of phylogenetic morphometrics. Cladistics, 32:221-238. https://doi.org/10.1111/cla.12160

Gower, D.J. and Weber, E. 1998. The braincase of *Euparkeria*, and the evolutionary relationships of birds and crocodilians. Biological Reviews, 73:367-411. https://doi.org/10.1111/j.1469-185X.1998.tb00177.x

Hanai, T. and Tsuihiji, T. 2019. Description of tooth ontogeny and replacement patterns in a juvenile *Tarbosaurus bataar* (Dinosauria: Theropoda) using CT-scan data. The Anatomical Record, 302:1210-1225. https://doi.org/10.1002/ar.24014

Hanson, M., Hoffman, E.A., Norell, M.A., and Bhullar, B.S. 2021. The early origin of a birdlike inner ear and the evolution of dinosaurian movement and vocalization. Science, 372(6542):601-609. https://doi.org/10.1126/science.abb4305

Hanson, M., Hoffman, E.A., Norell, M.A., and Bhullar, B.S. 2022. Response to Comment on “The early origin of a birdlike inner ear and the evolution of dinosaurian movement and vocalization”. Science, 376(6600):eabl8181. https://doi.org/10.1126/science.abl8181

Hassler, A., Martin, J.E., Amiot, R., Tacail, T., Arnaud Godet, F., Allain, R., and Balter, V. 2018. Calcium isotopes offer clues on resource partitioning among Cretaceous predatory dinosaurs. Proceedings of the Royal Society B, 285:20180197. https://doi.org/10.1098/rspb.2018.0197

Heath, T.A., Huelsenbeck, J.P., and Stadler, T. 2014. The fossilized birth-death process for coherent calibration of divergence-time estimates. Proceedings of the National Academy of Sciences, 111(2):E2957–E2966. https://doi.org/10.1073/pnas.1319091111

Heckeberg, N. and Rauhut, O.W.M. 2020. Histology of spinosaurid dinosaur teeth from the Albian-Cenomanian of Morocco: implications for tooth replacement and ecology. Palaeontologia Electronica, 23:a48. https://doi.org/10.26879/1041

Henderson, D.M. 2003. The eyes have it: the sizes, shapes, and orientations of theropod orbits as indicators of skull strength and bite force. Journal of Vertebrate Paleontology, 22:766-778. https://doi.org/10.1671/0272-4634(2002)022[0766:TEHITS]2.0.CO;2

Hendrickx, C. and Mateus, O. 2014. *Torvosaurus gurneyi* n. sp., the largest terrestrial predator from Europe, and a proposed terminology of the maxilla anatomy in nonavian theropods. PLoS ONE, 9:e88905. https://doi.org/10.1371/journal.pone.0088905

Hendrickx, C., Mateus, O., Araújo, R., and Choiniere, J. 2019. The distribution of dental features in non-avian theropod dinosaurs: Taxonomic potential, degree of homoplasy, and major evolutionary trends. Palaeontologia Electronica, 22(3.74):1-110. https://doi.org/10.26879/820

Hendrickx, C., Mateus, O., and Buffetaut, E. 2016. Morphofunctional analysis of the quadrate of Spinosauridae (Dinosauria: Theropoda) and the presence of *Spinosaurus* and a second spinosaurine taxon in the Cenomanian of North Africa. PLoS ONE, 11:e0144695. https://doi.org/10.1371/journal.pone.0144695

Henderson, D.M. 2018. A buoyancy, balance and stability challenge to the hypothesis of a semi-aquatic *Spinosaurus* Stromer, 1915 (Dinosauria: Theropoda). PeerJ, 6:e5409. https://doi.org/10.7717/peerj.5409

Holliday, C.M. 2009. New insights into dinosaur jaw muscle anatomy. The Anatomical Record, 292:1246-1265. https://doi.org/10.1002/ar.20982

Holliday, C. and Nesbitt, S. 2013. Morphology and diversity of the mandibular symphysis of archosauriforms. Geological Society of London Special Publications, 379:555-571. https://doi.org/10.1144/SP379.2

Holliday, C.M. and Witmer, L.M. 2007. Archosaur adductor chamber evolution: integration of musculoskeletal and topological criteria in jaw muscle homology. Journal of Morphology, 268:457-484. https://doi.org/10.1002/jmor.10524

Hone, D.W.E. and Holtz, T.R., Jr. 2017. A century of spinosaurs – a review and revision of the Spinosauridae with comments on their ecology. Acta Geologica Sinica, English Edition, 93:1120-1132. https://doi.org/10.1111/1755-6724.13328

Hone, D.W.E., and Holtz, T.R., Jr. 2021. Evaluating the ecology of *Spinosaurus*: Shoreline generalist or aquatic pursuit specialist? Palaeontologia Electronica, 24:a03. https://doi.org/10.26879/1110

Ibrahim, N., Maganuco, S., Dal Sasso, C., Fabbri, M., Auditore, M., Bindellini, G., Martill, D.M., Zouhri, S., Mattarelli, D.A., Unwin, D.M., and Wiemann, J. 2020a. Tail-propelled aquatic locomotion in a theropod dinosaur. Nature, 581:67-70. https://doi.org/10.1038/s41586-020-2190-3

Ibrahim, N., Sereno, P.C., Dal Sasso, C., Maganuco, S., Fabbri, M., Martill, D.M., Zouhri, S., Myhrvold, N., and Iurino, D.A. 2014. Semiaquatic adaptations in a giant predatory dinosaur. Science, 345:1613-1616. https://doi.org/10.1126/science.1258750

Iordansky, N. 2000. Jaw Muscles of the Crocodiles: Structure, Synonymy, and Some Implications on Homology and Functions. Russian Journal of Herpetology, 7(1):41-50.

Isasmendi, E., Navarro-Lorbés, P., Sáez-Benito, P., Viera, L.I., Torices, A., and Pereda-Suberbiola, X. 2022. New contributions to the skull anatomy of spinosaurid theropods: Baryonychinae maxilla from the Early Cretaceous of Igea (La Rioja, Spain). Historical Biology. https://doi.org/10.1080/08912963.2022.2069019

Janensch, W. 1936. Über Bahnen von Hirnvenen bei Saurischiern und Ornithischiern, sowie einigen anderen fossilen und rezenten Reptilien. Paläontologische Zeitschrift, 18:181-198.

Kellermann, M. 2021. New data on dinosaur diversity in the “middle” Cretaceous (Albian, Cenomanian) of North Africa. Unpublished Master’s thesis. Ludwig-Maximilians-Universität Munich, Germany.

Kellner, A.W.A. and Campos, D. 1996. First Early Cretaceous theropod dinosaur from Brazil with comments on Spinosauridae. Neues Jahrbuch Geologie und Paläontologie Abhandlungen, 199:151-166.

Kellner, A.W.A., Azevedo, S.A.K., Machado, E.B., Carvalho, L.B. de, and Henriques, D.D.R. 2011. A new dinosaur (Theropoda, Spinosauridae) from the Cretaceous (Cenomanian) Alcântara Formation, Cajual Island, Brazil. Anais de Academia Brasileira de Ciências, 83:99-108.

Lacerda, M.B.S., Grillo, O.N., and Romano, P.S.R. 2022. Rostral morphology of Spinosauridae (Theropoda, Megalosauroidea): premaxilla shape variation and a new phylogenetic inference. Historical Biology, 34(11):2089-2109. https://doi.org/10.1080/08912963.2021.2000974

Lakin, R. and Longrich, N. 2018. Juvenile spinosaurs (Theropoda: Spinosauridae) from the middle Cretaceous of Morocco and implications for spinosaur ecology. Cretaceous Research, 93:129-142. https://doi.org/10.1016/j.cretres.2018.09.012

Lepage, T., Bryant, D., Philippe, H., and Lartillot, N. 2007. A general comparison of relaxed molecular clock models. Molecular Biology and Evolution, 24(12):2669-2680. https://doi.org/10.1093/molbev/msm193

Lewis, P.O. 2001. A likelihood approach to estimating phylogeny from discrete morphological character data. Systematic Biology, 50(6):913-925.

Maddison, W.P. and Maddison, D.R. 2021. Mesquite: a modular system for evolutionary analysis. Version 3.70. http://www.mesquiteproject.org

Madsen, J.H., Jr. 1976. *Allosaurus fragilis*: a revised osteology. Utah Geological and Mineral Survey Bulletin, 109:1-163.

Madsen, J.H., Jr. and Welles, S.P. 2000. *Ceratosaurus* (Dinosauria, Theropoda): a revised osteology. Utah Geological Survey, Miscellaneous Publications, 2:1-80.

Malafaia, E., Gasulla, J.M., Escaso, F., Narváez, I., Sanz, J.L., and Ortega, F. 2020. A new spinosaurid theropod (Dinosauria: Megalosauroidea) from the Upper Barremian of Vallibona, Spain: implications for spinosaurid diversity in the Early Cretaceous of the Iberian Peninsula. Cretaceous Research, 106:104221. https://doi.org/10.1016/j.cretres.2019.104221

Makovicky, P.J., Kobayashi, Y., and Currie, P. J. 2004. Ornithomimosauria, p. 137-150. In Weishampel, D.B., Dodson, P., and Osmólska, H. (eds.), The Dinosauria (2nd ed.). University of California Press, Berkley, California, USA.

Martill, D.M., Cruickshank, A.R.I., and Frey, E. 1996. A new crested maniraptoran dinosaur from the Santana Formation (Lower Cretaceous) of Brazil. Journal of the Geological Society, 153:5-8.

Marugan-Lobon, J., Chiappe, L.M., and Farke, A.A. 2013. The variability of inner ear orientation in saurischian dinosaurs: Testing the use of semicircular canals as a reference system for comparative anatomy. PeerJ, 1:e124. https://doi.org/10.7717/peerj.124

Mateus, O. and Estraviz-López, D. 2022. A new theropod dinosaur from the early cretaceous (Barremian) of Cabo Espichel, Portugal: Implications for spinosaurid evolution, PLoS ONE, 17:e0262614. https://doi.org/10.1371/journal.pone.0262614

Milner, A. 2001. Fish-eating theropods: A short review of the systematics, biology and palaeobiogeography of spinosaurs. II Jornadas de Paleontología de Dinosaurios y su Entorno, 2:129-138.

Molnar, R.E., and Farlow, J.O. 1990. Carnosaur paleobiology, p. 210-224. In Weishampel, D.B, Dodson, P., and Osmolska, H. (eds.), The Dinosauria. University of California Press, , Berkley, California, USA.

Motta, M., Aranciaga Rolando, A., Rozadilla, S., Agnolin, F., Chimento, N., Brissón, E.F., and Novas, F. 2016. New theropod fauna from the Upper Cretaceous (Huincul Formation) of northwestern Patagonia, Argentina. New Mexico Museum of Natural History and Science Bulletin, 71: 231-253.

Munt, M., Blackwell, G., Clark, J., Foster, B., Gostling, N., Lockwood, J., Murray, K., Peaker, A., Rankin, K., and Sweetman, S. 2017. New spinosaurid dinosaur finds from the Wessex Formation (Wealden Group, Early Cretaceous) of the Isle of Wight. Poster.

Myhrvold, N., Sereno, P.C., Baumgart, S.L., Formoso, K.K., Vidal, D., Fish, F.E., and Henderson, D.M. 2022. Spinosaurids as 'subaqueous foragers' undermined by selective sampling and problematic statistical inference. bioRxiv. https://doi.org/10.1101/2022.04.13.487781

Ostrom, J.H. 1969. Osteology of *Deinonychus antirrhopus*, an unusual theropod dinosaur from the Lower Cretaceous of Montana. Peabody Museum of Natural History Bulletin, 30:1-165.

Paradis, E. and Schliep, K. 2019. Ape 5.0: an environment for modern phylogenetics and evolutionary analyses. R. Bioinformatics, 35:526-528. https://doi.org/10.1093/bioinformatics/bty633

Paulina-Carabajal, A. 2015. Guía para el studio de la neuroanatomía de dinosaurios saurischia, con énfasis en formas sudamericanas. Publicación Electrónica de la Asociación Paleontológica Argentina, 15:108-142. https://doi.org/10.5710/PEAPA.15.06.2015.102

Paulina-Carabajal, A. and Canale, J.I. 2010. Cranial endocast of the carcharodontosaurid theropod *Giganotosaurus carolinii* Coria and Salgado, 1995. Neues Jahrbuch für Geologie und Paläontologie Abhandlungen, 258:249-256. https://doi.org/10.1127/0077-7749/2010/0104

Paulina-Carabajal, A. and Currie, P.J. 2017. The braincase of the theropod dinosaur *Murusraptor*: osteology, neuroanatomy and comments on the paleobiological implications of certain endocranial features. Ameghiniana, 54:617. https://doi.org/10.5710/AMGH.25.03.2017.3062

Pêgas, R.V., Holgado, B., and Leal, M.E.C. 2021. On *Targaryendraco wiedenrothi* gen. nov. (Pterodactyloidea, Pteranodontoidea, Lanceodontia) and recognition of a new cosmopolitan lineage of Cretaceous toothed pterodactyloids. Historical Biology, 33:1266-1280. https://doi.org/10.1080/08912963.2019.1690482

Pfaff, C., Czernym, S., Nagel, D., and Kriwet, J. 2017. Functional morphological adaptations of the bony labyrinth in marsupials (Mammalia, Theria). Journal of Morphology, 278:742-749. https://doi.org/10.1002/jmor.20669

Pfaff, C., Martin, T., and Ruf, I. 2015. Bony labyrinth morphometry indicates locomotor adaptations in the squirrel-related clade (Rodentia, Mammalia). Proceedings of the Royal Society B, 282:20150744. https://doi.org/10.1098/rspb.2015.0744

Pol, D. and Escapa, I. 2009. Unstable taxa in cladistic analysis: Identification and the assessment of relevant characters. Cladistics, 25:515-527. https://doi.org/10.1111/j.1096-0031.2009.00258.x

Pol, D. and Rauhut, O.W.M. 2012. A Middle Jurassic abelisaurid from Patagonia and the early diversification of theropod dinosaurs. Proceedings of the Royal Society B, 279:3170-3175. http://doi.org/10.1098/rspb.2012.0660

Porfiri, J., Novas, F., Calvo, J., Agnolin, F., Ezcurra, M., and Cerda, I. 2014. Juvenile specimen of *Megaraptor* (Dinosauria, Theropoda) sheds light about tyrannosauroid radiation. Cretaceous Research, 51:35-55. https://doi.org/10.1016/j.cretres.2014.04.007

Raath, M.A. 1977. The anatomy of the Triassic theropod *Syntarsus rhodesiensis* (Saurischia: Podokesauridae) and a consideration of its biology. Unpublished PhD thesis. Rhodes University, Makhanda, Eastern Cape, South Africa.

Rambaut, A., Drummond, A.J., Xie, D., Baele, G., and Suchard, M.A. 2018. Posterior summarization in Bayesian phylogenetics using Tracer 1.7. Systematic Biology, 67(5):901-904. https://doi.org/10.1093/sysbio/syy032

Rauhut, O.W.M. 2001. Morphology and mechanics of the jaws of spinosaurid theropods (Dinosauria): implications for predation. Ameghiniana, Suplemento-Resumenes, 38:4.

Rauhut, O.W.M. 2003. The interrelationships and evolution of basal theropod dinosaurs. Special Papers in Palaeontology, 69:1-213.

Rauhut, O.W.M. 2004. Braincase structure of the Middle Jurassic theropod dinosaur *Piatnitzkysaurus*. Canadian Journal of Earth Sciences, 41:1109-1122.

Rauhut, O.W.M. and Carrano, M.T. 2016. The theropod dinosaur *Elaphrosaurus bambergi* Janensch, 1920, from the Late Jurassic of Tendaguru, Tanzania. Zoological Journal of the Linnean Society, 178:546-610. https://doi.org/10.1111/zoj.12425

Rauhut, O.W.M. and Pol, D. 2019. Probable basal allosauroid from the early Middle Jurassic Cañadón Asfalto Formation of Argentina highlights phylogenetic uncertainty in tetanuran theropod dinosaurs. Scientific Reports, 9:18826. https://doi.org/10.1038/s41598-019-53672-7

Rauhut, O.W.M. and Pol, D. 2021. New theropod remains from the Late Jurassic Cañadon Calcáreo Formation of Chubut, Argentina. Journal of South American Earth Sciences, 111:103434. https://doi.org/10.1016/j.jsames.2021.103434

Rauhut, O.W.M., Foth, C., and Tischlinger, H. 2018. The oldest *Archaeopteryx* (Theropoda: Avialiae): a new specimen from the Kimmeridgian/Tithonian boundary of Schamhaupten, Bavaria. PeerJ, 6:e4191. https://doi.org/10.7717/peerj.4191

Rauhut, O.W.M., Hübner, T.R., and Lanser, K.-P. 2016. A new megalosaurid theropod dinosaur from the late Middle Jurassic (Callovian) of north-western Germany: Implications for theropod evolution and faunal turnover in the Jurassic. Palaeontologia Electronica, 19:26A. https://doi.org/10.26879/654

Rauhut, O.W.M., Milner, A.C., and Moore-Fay, S. 2010. Cranial osteology and phylogenetic position of the theropod dinosaur *Proceratosaurus bradleyi* (Woodward, 1910) from the Middle Jurassic of England. Zoological Journal of the Linnean Society, 158:155-195. https://doi.org/10.1111/j.1096-3642.2009.00591.x

Rauhut, O.W.M., Schwermann, A.H., Hübner, T.R., and Lanser, K.-P. 2020. The oldest record of the genus *Torvosaurus* (Theropoda: Megalosauridae) from the Callovian Ornatenton Formation of north-western Germany. Geologie und Paläontologie in Westfalen, 93:31-43.

Rayfield, E.J. 2004. Cranial mechanics and feeding in *Tyrannosaurus rex*. Proceedings of the Royal Society of London B, 271:1451-1459.

Rayfield, E.J. 2011. Structural performance of tetanuran theropod skulls, with emphasis on the Megalosauridae, Spinosauridae and Carcharodontosauridae. Special Papers in Palaeontology, 86:241-253.

Rayfield, E.J., Norman, D., Horner, C., Horner, J., Smith, P., Thomason, J., and Upchurch, P. 2001. Cranial design and function in a large theropod dinosaur. Nature, 409:1033-1037. https://doi.org/10.1038/35059070

Rayfield, E.J., Milner, A.C., Xuan, V.B., and Young, P.G. 2007. Functional morphology of spinosaur 'crocodile-mimic' dinosaurs. Journal of Vertebrate Paleontology, 27:892-901. https://doi.org/10.1671/0272-4634(2007)27[892:FMOSCD]2.0.CO;2

Richter, U., Mudroch, A., and Buckley, L.G. 2013. Isolated theropod teeth from the Kem Kem Beds (Early Cenomanian) near Taouz, Morocco. Paläontologische Zeitschrift, 87:291-309. https://doi.org/10.1007/s12542-012-0153-1

Rieppel, O. 1985. The recessus scalae tympani and its bearing on the classification of reptiles. Journal of Herpetology, 19:373-384.

Ronquist, F., van der Mark, F.P., and Huelsenbeck, J.P. 2009. Bayesian phylogenetic analysis using Mr Bayes, p. 210-266. In Lemey, P., Salemi, M., and van Damme, A.M. (eds.), The Phylogenetic Handbook, second edition. Cambridge University Press, Cambridge, UK.

Sadleir, R., Barrett, P.M., and Powell, H.P. 2008. The anatomy and systematics of *Eustreptospondylus oxoniensis,* a theropod dinosaur from the Middle Jurassic of Oxfordshire, England. Monograph of the Palaeontographical Society, London, 160:1-82.

Sales, M.A.F. and Schultz, C.L. 2017. Spinosaur taxonomy and evolution of craniodental features: evidence from Brazil. PLoS ONE, 12:e0187070. https://doi.org/10.1371/journal.pone.0187070

Sales, M.A.F., Lacerda, M.B., Horn, B.L.D., de Oliveira, I.A.P., and Schultz, C.L. 2016. The "χ" of the matter: testing the relationship between paleoenvironments and three theropod clades. PLoS ONE, 11:e0147031. https://doi.org/10.1371/journal.pone.0147031

Sales, M.A.F., Liparini, A., de Andrade, M.B., Aragão, P.R.L., and Schultz, C.L. 2017. The oldest South American occurrence of Spinosauridae (Dinosauria, Theropoda). Journal of South American Earth Sciences, 74:83-88. https://doi.org/10.1016/j.jsames.2016.10.005

Sampson, S.D. and Witmer, L.M. 2007. Craniofacial anatomy of *Majungasaurus crenatissimus* (Theropoda: Abelisauridae) from the Late Cretaceous of Madagascar. Society of Vertebrate Paleontology Memoir, 8:32-102.

Schade, M., Rauhut, O.W.M., and Evers, S.W. 2020a. Neuroanatomy of the spinosaurid *Irritator challengeri* (Dinosauria: Theropoda) indicates potential adaptations for piscivory. Scientific Reports, 10:211. https://doi.org/10.1038/s41598-020-66261-w

Schade, M., Rauhut, O. W. M., and Evers, S. W. 2020b. Project: Schade et al., Irritator challengeri SMNS 58022 neuroanatomy. MorphoSource, available at https://www.morphosource.org/projects/00000C951.

Schade, M., Rauhut, O. W. M., Foth, C., Moleman, O., and Evers, S. W. 2022. Project: Schade et al., Irritator challengeri SMNS 58022 osteology. MorphoSource, available at https://www.morphosource.org/projects/000372273.

Schwab, J.A., Kriwet, J., Weber, G.W., and Pfaff, C. 2019. Carnivoran hunting style and phylogeny reflected in bony labyrinth morphometry. Scientific Reports, 9:70. https://doi.org/10.1038/s41598-018-37106-4

Sellers, K.C., Middleton, K.M., Davis, J.L., and Holliday, C.M. 2017. Ontogeny of bite force in a validated biomechanical model of the American alligator. Journal of Experimental Biology, 220:2036-2046. https://doi.org/10.1242/jeb.15628

Sereno, P. and Brusatte, S. 2008. Basal abelisaurid and carcharodontosaurid theropods from the Elrhaz Formation (Aptian-Albian) of Niger. Journal of Vertebrate Paleontology, 26:46A.

Sereno, P.C. and Novas, F. 1993. The skull and neck of the basal theropod *Herrerasaurus ischigualastensis*. Journal of Vertebrate Paleontology, 13:451-476.

Sereno, P.C., Beck, A.L., Dutheil, D.B., Gado, B., Larsson, H.C.E., Rauhut, O.W.M., Sadleir, R.W., Sidor, C.A., Varricchio, D.J., Wilson, G.P., and Wilson, J.A. 1998. A long-snouted predatory dinosaur from Africa and the evolution of spinosaurids. Science, 282:1298-1302. https://doi.org/10.1126/science.282.5392.1298

Sereno, P.C., Forster, C.A., Larsson, H.C.E., Dutheil, D.B., and Sues, H.-D. 1994. Early Cretaceous dinosaurs from the Sahara. Science, 266:267-271. https://doi.org/10.1126/science.266.5183.267

Sereno, P., Myhrvold, N., Henderson, D., Fish, F., Vidal, D., Baumgart, S., Keillor, T., Formoso, K., and Conroy, L. 2022. *Spinosaurus* is not an aquatic dinosaur. eLife, 11:80092. https://doi.org/10.7554/eLife.80092

Smith, A.G., Smith, D.G., and Funnell, B.M. 1994. Atlas of Mesozoic and Cenozoic coastlines. Cambridge University Press, Cambridge, UK.

Smith, J.B., Lamanna, M.C., Mayr, H., and Lacovara, K.J. 2006. New information regarding the holotype of *Spinosaurus aegyptiacus* Stromer, 1915. Journal of Paleontology, 80:400-406. https://doi.org/10.1666/0022-3360(2006)080[0400:NIRTHO]2.0.CO;2

Smith, J. 2007. Dental morphology and variation in *Majungasaurus crenatissimus* (Theropoda: Abelisauridae) from the Late Cretaceous of Madagascar. Journal of Vertebrate Paleontology, 27:103-126.

Smyth, R.S.H., Ibrahim, N., and Martill, D.M. 2020. *Sigilmassasaurus* is *Spinosaurus*: a reappraisal of African spinosaurines. Cretaceous Research, 114:104520. https://doi.org/10.1016/j.cretres.2020.104520

Snively, E. and Russell, A.P. 2007. Functional morphology of neck musculature in the Tyrannosauridae (Dinosauria, Theropoda) as determined via a hierarchical inferential approach. Zoological Journal of the Linnean Society, 151:759-808. https://doi.org/10.1111/j.1096-3642.2007.00334.x

Stadler, T. 2010. Sampling-through-time in birth-death trees. Journal of Theoretical Biology, 267:396-404.

Stevens, K.A. 2006. Binocular vision in theropod dinosaurs. Journal of Vertebrate Paleontology, 26:321-330. https://doi.org/10.1671/0272-4634(2006)26[321:BVITD]2.0.CO;2

Stromer, E. 1915. Ergebnisse der Forschungsreisen Prof. E. Stromers in den Wüsten Ägyptens. II. Wirbeltier-Reste der Baharîje -Stufe (unterstes Cenoman). 3. Das Original des Theropoden *Spinosaurus aegyptiacus* nov. gen., nov. spec. Abhandlungen der Königlichen Bayerischen Akademie der Wissenschaften. Mathematisch-Physikalische Klasse, 28:1-28.

Stromer, E. 1936. Ergebnisse der Forschungsreisen Prof. E. Stromers in den Wüsten Ägyptens. VII. Baharije-Kessel und -Stufe mit deren Fauna und Flora. Eine ergänzende Zusammenfassung. Abhandlungen der Bayerischen Akademie der Wissenschaften, Mathematisch-Naturwissenschaftliche Abteilung, 33:1-102.

Sues, H.D. 1997. On *Chirostenotes*, a Late Cretaceous oviraptorosaur (Dinosauria: Theropoda) from Western North America. Journal of Vertebrate Paleontology, 17:698-716. https://doi.org/10.1080/02724634.1997.10011018

Sues, H.-D., Frey, E., Martill, D.M., and Scott, D.M. 2002. *Irritator challengeri*, a spinosaurid (Dinosauria: Theropoda) from the Lower Cretaceous of Brazil. Journal of Vertebrate Paleontology, 22:535-547. https://doi.org/10.1671/0272-4634

Taquet, P. 1984. Une curieuse spécialisation du crâne de certains Dinosaures carnivores du Crétacé: Le museau long et étroit des Spinosauridés. Comptes Rendus de l'Académie des Sciences, Paris, série II, 299:217-222.

Taquet, P. and Russell, D.A. 1998. New data on spinosaurid dinosaurs from the Early Cretaceous of the Sahara. Comptes Rendus de l'Académie des Sciences, Paris, série II, 327:347-353.

Therrien, F. and Henderson, D.M. 2007. My theropod is bigger than yours … or not: estimating body size from skull length in theropods. Journal of Vertebrate Paleontology, 27:108-115. https://doi.org/10.1671/0272-4634(2007)27[108:MTIBTY]2.0.CO;2

Therrien, F., Henderson, D.M., and Ruff, C.B. 2005. Bite me: biomechanical models of theropod mandibles and implications for feeding behavior, p. 179-237. In Carpenter, K. (ed.), The Carnivorous Dinosaurs. Indiana University Press, Bloomington and Indianapolis, USA.

Vila Nova, B.C., Saraiva A.A., Moreira J.K., and Sayão, J.M. 2011. Controlled excavations in the Romualdo formation lagerstatte (Araripe Basin, Brazil) and pterosaur diversity: remarks based on new findings. Palaios, 26:173-179. https://doi.org/20110310091832

Vilas Boas, M., Brilha, J.B.R., and De Lima, F.F. 2013. Conservação do patrimônio paleontológico do Geopark Araripe (Brasil): enquadramento, estratégias e condicionantes. Boletim Paranaense de Geociências, 70:156-165. https://doi.org/10.5380/geo.v70i0.31418

Walsh, S.A., Iwaniuk, A.N., Knoll, M.A., Bourdon, E., Barrett, P.M., Milner, A.C., Nudds, R.L., Abel, R.L., and Sterpaio, P.D. 2013. Avian Cerebellar Floccular Fossa Size Is Not a Proxy for Flying Ability in Birds. PLOS ONE, 8(6):e67176. https://doi.org/10.1371/journal.pone.0067176

Wellnhofer, P. 1975. Die Rhamphorhynchoidea (Pterosauria) der Oberjura-Plattenkalke Süddeutschlands. II: Systematische Beschreibung. Palaeontographica A, 148:132-186.

Westneat, M.W. 1994. Transmission of force and velocity in the feeding–mechanisms of labrid fishes (Teleostei, Perciformes). Zoomorphology, 114:103-118.

Westneat, M.W. 2003. A biomechanical model for analysis of muscle force, power output and lower jaw motion in fishes. Journal of Theoretical Biology, 223:269-281.

Wilkinson, M. 1995. Coping with abundant missing entries in phylogenetic inference using parsimony. Systematic Biology, 44:501-514. https://doi.org/10.2307/2413657

Witmer, L.M. 1997a. The evolution of the antorbital cavity of archosaurs: a study in soft-tissue reconstruction in the fossil record with an analysis of the function of pneumaticity. Society of Vertebrate Paleontology, Memoir, 3:1-76. https://doi.org/10.1080/02724634.1997.10011027

Witmer, L.M. 1997b. Craniofacial air sinus systems, p. 151-159. In Currie, P.J. and Padian, K. (eds.), Encyclopaedia of Dinosaurs. Academic Press, New York, USA.

Witmer, L.M. and Ridgely, R.C. 2010. The Cleveland tyrannosaur skull (*Nanotyrannus* or *Tyrannosaurus*): New findings based on CT scanning, with special reference to the braincase. Kirtlandia, 57:61-81.

Yates, A. 2005. A new theropod dinosaur from the Early Jurassic of South Africa and its implication for the early evolution of theropods. Palaeontologia Africana, 41:105-122.

Zaher, H., Pol, D., Navarro, B.A., Delcourt, R., and Carvalho, A.B. 2020. An Early Cretaceous theropod dinosaur from Brazil sheds light on the cranial evolution of the Abelisauridae. Comptes Rendus Palevol, 19:101-115. https://doi.org/10.5852/cr-palevol2020v19a6

Zhao, X.-J. and Currie, P.J. 1994. A large crested theropod from the Jurassic of Xinjiang, People's Republic of China. Canadian Journal of Earth Sciences, 30:2027-2036.

SUPPLEMENTAL DATA 1

Here is a list of things which were changed by OM on the digital *Irritator* skull reconstruction to make it mostly symmetrical and articulate properly.

Where bones seemed to be mostly intact, OM opted to not deform those bones and instead focused on making other, less well preserved or obviously deformed bones, fit. OM did not include repositioning of bones in this list.

- Restoring the fossils original shape before breaking

The original fossil was broken in two at one point and has been incorrectly glued back together. The whole anterior part of the skull was rotated slightly to the left side. OM put this back in place, rotating it to the right, using all the bones that were present in both the anterior and posterior half of the fossil. Aligning this, fixed bending in the nasals, maxillae, palatines, pterygoids and surangulars.

- Bending of the nasals and adjacent bones

Lateral bending of the nasals in two main places. As mentioned above, the fossil had a bend at the break of the fossil, so OM corrected for the lateral shift and rotated the anterior snout piece slightly to the right. The second location is just behind the posterordorsal processes of the maxillae. This is probably where the nasals and lacrimals are deformed the most. OM bent the nasals and anterodorsal processes of the lacrimals to the left. These two changes made the nasals roughly straight.

- Bending and shifting of the maxillae

Much of the skull was pushed in medially on the right side. This effectively collapsed much of the skull laterally. As a result, the posterior half of both maxillae was laterally pushed to the left. OM corrected this, making them more symmetrical. Around the mid-point of the maxillae, there is a break in the bones where minerals go through the break. OM used this as a rough rotation point to shift the posterior halves of the maxillae back into place. Besides aiming for symmetry, it was hard to know how wide the jaw should be around the posteroventral processes of the maxillae. OM used the connection to the other bones (jugals, lacrimals, palatines, pterygoids, vomer) to figure out how wide it should be. Especially the palatines were very informative to know roughly how wide the skull should be at this point, since these needed to attach to the pterygoids medially and jugals, lacrimals and maxillae laterally.

- Bending the quadratojugals

There were always some bones that did not fit when OM put the skull together. In the end, OM rotated the dorsal process of the quadratojugals forward to the anterior position to make it fit with the squamosals and quadrates. The right quadratojugal was still in tight articulation with the jugal, so OM left that in place. The problem was that the angle of the dorsal process did not line up correctly with the quadrate and the squamosal. OM rotated this dorsal process around 10 degrees forward. The quadratojugal itself is a very thin element and did also seem to have sustained damage. OM felt fairly safe bending this bone instead of others that were less likely to have substantial changes to their shape during fossilization or after.

- Shifting of the right lacrimal and prefrontal

When viewed perfectly from the side, it becomes clear that the lacrimals did not line up. The right lacrimal is in good condition and showed little deformation. The left lacrimal was in much worse shape. OM opted to change the left lacrimal instead of the right one. The posterior margin of the left lacrimal is badly damaged. But the anterior margin is still in good shape and OM used that to align the two lacrimals. There was a gap, filled with matrix behind the prefrontal between it and the frontal bone. Since we know the nasals were bent to the right, it seems that it had taken the left lacrimal and tightly articulated prefrontal with it, pulling them forward. Thus, together with the nasals that needed to be bent to the left, OM needed to shift the left lacri-

mal and prefrontal back to a more posterior position that matched the right lacrimal and better articulated with the frontal.

Fixing small broken pieces of bone and putting them back into place to match the rest of the skull anatomy. Small pieces of bone were sometimes bent, or disarticulated entirely that needed to be changed.

Bones that OM bent

- The small remnant of the dentary was bent badly, OM straightened this.

- The ventral halves of the lacrimals were slightly bent due to larger stresses in the whole skull. OM laterally shifted these slightly so they articulated with the jugals and other bones better.

- The left jugal was in bad shape and OM laterally bent both the anterior half, and the posterodorsal process to better articulate with other bones.

- OM bent the right parasphenoid process to the right so it is oriented better. But OM left the smaller details as they were, as they don't articulate with anything else.

- OM did some very slight bending of the pterygoids to make them fit all the other bones they interact with (basisphenoid, ectopterygoid, palatine and vomer). OM felt okay with bending these slightly due to these bones being very thin and broken. It seems probable there was some deformation.

- OM very slightly bent the nasal and frontal dorsally around the point of the articulation with the nasal and prefrontals. Two reasons: There are several very small longitudinal cracks in the nasal that can be seen in the CT scans. This resulted in the whole complex of the braincase to move ventrally very slightly. As previously mentioned, the quadratojugal did not fit. Bending the nasal and frontal resulted in very slightly raising the whole braincase complex + postorbitals, squamosals and quadrates. This in turn made the quadratojugals articulate better and the posterodorsal process of the jugal articulates better with the ventral process of the postorbital.

Broken bones OM put back together

- OM used the breaks in the pterygoids to fit them around the rest of the bones. This resulted in a slightly smaller gap between the preserved parts.

- Small parts of the left postorbital and left squamosal were disarticulated. OM put these back as good as possible.

- Large parts of the vomer are missing. OM shifted the posterior piece back a little more so that it articulates better with the pterygoids. This results in a longer vomer.

- A small part of the ventromedial lip of the left maxilla was broken off. Initially, OM interpreted this as part of the vomer, but it seems to fit the maxilla better.

- Both ectopterygoids were broken and had a slight gap in the middle. OM narrowed those gaps to better reflect their original width.

SUPPLEMENTAL DATA 2

Characters for the phylogenetic analysis, modified from Rauhut and Pol 2019.

1. Premaxilla, height/length ratio ventral to external naris (length measured along ventral border of bone): < 0.5 (0), 0.5-0.99 (1), 1-1.49 (2), 1.5 or higher (3). ORDERED.

2. Ventral margin of the premaxilla in lateral view: straight to slightly convex (0), markedly concave (1) (new).

3. Participation of the maxilla in the ventral border of naris: absent, subnarial process of the premaxilla contacts the nasal (0), subnarial process of premaxilla reduced or absent, maxilla expressed on the ventral margin of the nares (1) (modified from Rauhut and Pol 2019).

4. Premaxilla, posterior extent of nasal process relative to posterior tip of subnarial process: considerably more anterior (0), even (1), posterior (2). ORDERED.

5. Premaxilla, form of premaxilla-nasal suture: V-shaped (0), W-shaped (1).

6. Position of anterior end of external nares: over anterior half of ventral margin of premaxillary body (0), over the posterior half of the ventral margin of the premaxillary body (1), posterior to the ventral margin of the premaxillary body (2). ORDERED.

7. Premaxilla, diastema adjacent to maxilla along dentigerous margin: absent (0), present, with alveolar margin being continuous between premaxilla and maxilla (1), present, with alveolar margin being discontinuous between premaxilla and maxilla ("subnarial gap") (2) (modified from Rauhut and Pol 2019).

8. Premaxilla, mediolateral constriction of posterior portion: absent (0), present (1).

9. Premaxilla, development of subnarial (maxillary) process: well-developed, rod or plate-like (0), reduced to a short, stout triangle, as long as or shorter than its basal width (1).

10. Subnarial foramen on the premaxilla–maxilla suture: absent (0), present (1).

11. Premaxilla, articulation with maxilla: planar (0), interlocking (1).

12. Anterior ramus of the maxilla: absent, anterior margin of maxillary body confluent with anterior margin of the ascending process (0), present but very short (length/height ratio less than 1) (1), present moderately long (1-1.35) (2), present, long (1.35-1.7) (3), present, very long (more than 2) (4). ORDERED.

13. Subnarial fossa on the maxilla: absent (0), present (1) (new).

14. Maxilla, orientation of anteriormost alveolus: vertical (0), angled anteriorly (1).

15. Anterodorsal margin of the ascending process of the maxilla: straight or gently curved (0), with pronounced kink at about mid-length, with a more anteriorly facing margin ventral and a more dorsally facing margin dorsal to the kink (1).

16. Relative posterior length of the ascending process and jugal ramus of the maxilla: jugal ramus extends considerably further posteriorly than ascending process (0), subequal in length or ascending process longer (1) (new).

17. Maxilla, morphology of palatal process: long, ridged or fluted prong (0), long and plate-shaped (1).

18. Maxilla, position of palatal process: ventral, immediately dorsal to paradental plates (0), dorsal, immediately ventral to dorsal surface of maxillary anterior ramus (1).

19. Maxilla, horizontal ridge (prominent 'lingual bar') between palatal process and antorbital fenestra: absent (0), present (1).

20. Maxilla, depth of paradental plates relative to anteroposterior width: low, < 1.8 (0), tall > 1.8 (1).

21. Maxilla, ventral extent of paradental plates relative to lateral wall: as far ventral (0), fall short (1).

22. Maxilla, arrangement of nutrient foramina on lateral surface: single row or no distinct pattern (0), a second, more dorsally placed row is present anteriorly and converges with the ventral row posteriorly (1), a second, dorsally placed row is present and extends posteriorly more or less parallel to the ventral row (2).

23. Maxilla, anteroventral border of antorbital fossa: graded or stepped (0), demarcated by raised ridge (1).

24. Maxilla, anterior margin of antorbital fossa: rounded (0), squared (1).

25. Maxilla, ventral extent of antorbital fossa (as measured from the rim of the antorbital fenestra to the highest point of the ridge marking its border) at the level of about the half length of the antorbital fenestra: small or absent, less than 1/3 the height of the maxillary body at this level (0), moderate, between 1/3 and half the height (1), dorsoventrally deep, more than half the height (2). ORDERED.

26. Maxilla, position of anterior end of antorbital fossa: posterior to or level with posterior rim of external nares (0), ventral to external nares (1).

27. Medial wall of the anterior end of the maxillary antorbital fossa: lacking depressions or foramina (0), with a large depression without sharply defined margins (1), with a sharply rimmed maxillary fenestra (2).

28. Development of maxillary fenestra: opens medially into a small maxillary antrum with a robust medial wall (0), opens medially into a large maxillary antrum that is medially open or only covered by a very thin bony wall (1), opens anteriorly into a large antrum within the ascending process of the maxilla (2) This character is inapplicable in taxa that lack a maxillary fenestra.

29. Promaxillary foramen: absent (0), present and opens anteriorly into pneumatic recesses in the ascending process of the maxilla (1).

30. Size of the promaxillary foramen in relation to the maxillary fenestra: smaller (0), larger (1). This character is inapplicable in taxa that lack a maxillary fenestra.

31. Maxilla, development of pneumatic fossa (excavatio pneumatica) in ascending process: absent (0), present (1).

32. Maxilla, pneumatic region on medial side of maxilla posteroventral to maxillary fenestra: absent (0), present (1).

33. Shape of the alveolar border of the maxilla: straight (0), convex (1), sinusoidal (2) (new).

34. Maxilla, posterior end of tooth row relative to orbit: beneath (0), anterior (1).

35. Posterior end of the jugal ramus of the maxilla: single (0), forked (1) (new).

36. Posteriormost end of the jugal ramus of the maxilla: straight, in line with alveolar border (0), markedly downturned (1) (new).

37. Maxilla and nasal, external surface texture: smooth (0), sculptured (1).

38. Nasal, inter-nasal contact in adults: separate (0), partly or fully fused (1).

39. Nasal, posterior narial margin: absent or weak fossa (0), large fossa (1), laterally splayed hood (2).

40. Posteriorly pointed, sharply rimmed depression on the lateral side of the nasal posterodorsal to the external nares: absent (0), present (1).

41. Nasal, participation in antorbital fossa: absent or at edge (0), present (1).

42. Nasal, antorbital fossa in lateral view: visible (0), occluded by ventrolaterally overhanging lamina (1).

43. Nasal, pneumatic foramina: absent (0), present (1).

44. Nasal, development of dorsolateral surfaces: none, nasals low and dorsally convex (0), pronounced dorsolateral rims, sometimes with lateral crests (1), tall, parasagittal crests (2) (modified from Rauhut and Pol 2019).

45. Midline crest on the nasals: absent (0), present (1) (modified from Rauhut and Pol 2019).

46. Posterior end of nasal crest on the nasal: not expanded, crest stays of subequal width throughout length (0), transversely broadened into a notable tubercle (1) (new).

47. Nasal, sculpturing: smooth or low rugosity (0), deeply rugose, bears large excresences (1) (modified from Rauhut and Pol 2019).

48. Posterior end of the nasals: thin, plate-like (0), strongly thickened, robust (1) (new).

49. Antorbital fossa and dorsal rim on the anterior process of the lacrimal: present, but fossa is largely hidden in lateral view by an overhanging lateral lamina and only exposed anteriorly (0), present, widely exposed laterally and confluent with the antorbital fossa of the dorsal part of the ventral process (1), dorsal rim absent, no differentiation between fossa and rim on the lateral surface of anterior process (2).

50. Lacrimal, morphology of lateral lamina of ventral process of lacrimal: forming a continuous sheet of bone between the ventral and anterior processes (0), invaginated dorsally and convex anteriorly, anteriormost point situated dorsal to midheight of ventral process (1), anteriormost point situated around midheight of ventral process (2).

51. Anteroposterior expansion of ventral process of the lacrimal: begins at two thirds of the height of the ventral process or lower (0), begins at the dorsal end of the ventral process (1) (new).

52. Lacrimal, dorsal and ventral portions of antorbital fossa: separated by anterior projection of lateral lamina (0), continuous, lateral lamina does not project far anteriorly (1).

53. Lacrimal fenestra: absent (0), present (1).

54. Lacrimal, openings in lacrimal recess: single (0), multiple (1).

55. Lacrimal horn: absent (0), small dorsal rugosity (1), low, broad, rugose bar (2), large triangular horn (3). ORDERED.

56. Lacrimal, suborbital process: absent (0), present (1).

57. Lacrimal, angle between anterior and ventral rami: ~90° (0), < 75° (1).

58. Lacrimal, length of anterior process relative to ventral process: more (0), or less than 80% (1).

59. Jugal, position of anterior end: excluded from internal antorbital fenestra (0), posterior to internal antorbital fenestra, but reaching its posterior rim (1), expressed at rim of internal antorbital fenestra, with distinct anterior process extending beneath it (2) (modified from Rauhut and Pol 2019). ORDERED.

60. Jugal, pneumatisation: absent (0), internally hollowed and transversely inflated by foramen in posterior rim of antorbital fossa (1).

61. Jugal, antorbital fossa that is clearly offset from the lateral jugal surface by a raised rim: absent (0), present (1) (modified from Rauhut and Pol 2019).

62. Anterior end of jugal: slender and not or only slightly expanded (0), strongly expanded, and expansion forms at least a small part of the anterior margin of the orbit (1).

63. Jugal, orientation of orbital margin on postorbital process: angled posterodorsally (0), vertical (1) (modified from Rauhut and Pol 2019).

64. Horizontal ridge along the jugal body: absent (0), present (1) (new).

65. Lateral ridge along the postorbital contact on the postorbital process of the jugal: absent (0), present (1) (new).

66. Dorsoventral height of the posterior process of jugal: less than half the height of the suborbital part (0), more than half the height, but less than height of suborbital part (1), or subequal or more than dorsoventral height of suborbital part (2) (modified from Rauhut and Pol 2019).

67. Postorbital, articulation with jugal: planar or with a shallow, V-shaped groove dorsally (0), with a deep, broad groove posteriorly, ventral process with U-shaped cross-section (1).

68. Postorbital, suborbital flange: absent (0), present (1).

69. Development of suborbital flange of postorbital: small, triangular eminence (0), dorsoventrally elongate, large rounded flange (1), jugal process curved anteroventrally and suborbital process developed as large, sharply angled, triangular flange (2). This character is not applicable to taxa that do not have a suborbital flange.

70. Postorbital, ventral extent relative to ventral margin of orbit: substantially above (0), approximately same level (1).

71. Dorsal margin of postorbital above jugal process in lateral view: convex (0), straight to slightly concave (1), with pointed, triangular cornual process that is anteriorly offset from a possible step at the beginning of the squamosal articulation (2) (new).

72. Laterosphenoid facet on medial side of the postorbital: large and placed at the junction of the three postorbital processes (0), reduced in size and placed entirely on the anterior process (1) (new).

73. Medial side of posterior process of the postorbital: straight or concave, dorsal margin forms a sharp rim (0), convex, medial margin curves into dorsal margin (supratemporal fossa extends onto process) (1).

74. Supratemporal fossa on the anterior process of the postorbital and posterior end of frontal: forms a large shelf on the dorsal surface of the process (0), reduced, restricted to the posteriormost part and faces more posterodorsally than dorsally (1).

75. Supraorbital brow: absent, anterior end of postorbital tapers (0), present as a dorsoventrally expanded, anteriorly rounded, rugose swelling over the posterior part of the orbit (1), large, strongly rugose supraorbital brow (possible formed by a separate palprebal ossification fused to the postorbital) that connects the postorbital with the lacrimal present (2). ORDERED.

76. Anterior process of the postorbital: straight (0), downturned anteriorly (1) (new).

77. Posterior process of the postorbital: Pointed and transversely narrow (0), broadened transversely posteriorly and wider than high (1).

78. Parietal-postorbital contact at the anterior end of the supratemporal fenestra: absent, parietal and postorbital separated by posterior process of frontal that reaches the laterosphenoid (0), present, frontal excluded from laterosphenoid in dorsal view (1).

79. Prefrontal in adult individuals: Exposed on the anterodorsal margin of the orbit (0), reduced, not exposed at the anterior margin of the orbit, might only be visible at the dorsal margin of the orbit (1), absent as separate ossification (2).

80. Frontal-prefrontal contact: prefrontal contacts anterolateral margin of the frontal, placed mainly lateral to the frontal (0), prefrontal contacts anterior margin of the frontal, placed mainly anterior to frontal (1) (new).

81. Frontal, exposure along orbital rim: broad, one third or more of the dorsal orbital margin (0), reduced, less than one third of the dorsal orbital margin (1).

82. Midline ridge on the frontal: absent (0), present (1) (new).

83. Proportions of frontal (as exposed on the skull roof): longer than wide (0), wider than long (1).

84. Frontals in adult individuals: unfused (0), partially or completely fused (1) (Carrano and Sampson 2008).

85. Clearly offset lateral postorbital process of the frontal: absent (0), present (1) (new).

86. Nasal-frontal suture: anterior end of articulated frontals medially tapering or rounded (0), anterior end of articulated frontals separated by a broad medial posterior process of the nasal (1).

87. Overlap of the parietal over the median supraoccipital ridge/thickening: absent (0), present (1) (modified from Rauhut and Pol 2019).

88. Parietal, development of median skull table between supratemporal fossae: flat, but relatively narrow (less than 50% of width of supratemporal fenestrae) (0), separated by a triangular plate of bone anteriorly, but narrowing to a sagittal crest posteriorly (1), narrow with sharp sagittal crest (2), very broad, widely separating upper temporal fenestrae, skull table at least 50% of width of supratemporal fenestra and fossa (3).

89. Parietal, size and elevation of nuchal wedge and alae: small to moderate, height of alae less than height of base of paroccipital process (0), expanded, height more than height of base of paroccipital process (1).

90. Supratemporal fossa, anteromedial corner: open dorsally (0), partially roofed over by a small shelf of the frontalparietal (1).

91. Squamosal, constriction of lower temporal fenestra: absent (0), present (1).

92. Squamosal, anterodorsal lamina: emarginated by upper temporal fenestra (0), continuous (1).

93. Strongly developed and sharply defined horizontal ridge extending from the ventral margin of the postorbital facet towards the quadrate articulation on the lateral side of the squamosal body: absent (0), present (1) (new).

94. Posterior extent of postorbital facet on squamosal: ends anterior to or at the anterior border of the ventral process (0), extends posteriorly to at least the half-width of the ventral process (1) (new).

95. Relative length of anterior and posterior processes of squamosal: anterior process considerably longer than posterior process (0), anterior process as long as or shorter than posterior process (1) (new).

96. Squamosal, flange covering quadrate head laterally: absent (0), present, covers the posterior part of the head and separated from quadratojugal process of squamosal by a wide, U-shaped incision (1), present, covers most of quadrate head and separated from quadratojugal process only by a narrow, slit-like incision (2). ORDERED.

97. Squamosal-quadratojugal contact: present (0), absent (1) (modified from Rauhut and Pol 2019).

98. Squamosal, articulation with quadratojugal: at tip (0), broad (1) (modified from Rauhut and Pol 2019).

99. Quadratojugal, anteriormost point of ventral process relative to lower temporal fenestra: ventral, no further than two thirds of the length of the fenestra from the posterior border (0), further anterior, subequal to the anterior border of the fenestra (1).

100. Large pneumatic foramen in quadrate: absent (0), present (1). (modified from Rauhut and Pol 2019).

101. Position of the quadrate head in relation to the orbit: low, below two-thirds of the height of the orbit (0), at two-thirds of the height of the orbit or higher (1).

102. Angle between quadrate ridge and distal quadrate condyles in posterior view: more than 70° (0), less than 70° (1) (modified from Rauhut and Pol 2019).

103. Medial side of quadrate ridge at mid-height in posterior view: straight or concave (0), convex (1) (new).

104. Proportion of the length of the quadrate that is occupied by the pterygoid wing: less than 70% (0) or 70% or more (1).

105. Proximal part of the dorsal margin of the pterygoid wing of the quadrate: forms a sharp crest (0), notably thickened mediolaterally (1) (new).

106. Ventral margin of pterygoid wing of the quadrate: Offset from mandibular condyles (0), confluent with expansion for mandibular condyles (1) (new).

107. Ventral margin of the pterygoid wing of the quadrate: flexed medially to form a medial shelf or ridge (0), forms a sharp ventral edge , only the most proximal part flexes medially (1) (new).

108. Quadrate foramen: present (0), absent(1) (modified from Rauhut and Pol 2019).

109. Development of quadrate foramen in the quadratojugal flange of the quadrate: semioval notch, widely open laterally (0), with a ventrally flexed lateral spur at at least the dorsal margin (1), completely enclosed in the quadrate (2) (modified from Rauhut and Pol 2019).

110. Orientation of the quadrate in lateral view: anteroventrally inclined, mandibular joint notably anterior to quadrate head (0), more or less vertical, mandibular joint approximately straight below quadrate head (1), posteroventrally inclined, mandibular joint notably posterior to quadrate head (2) (modified from Rauhut and Pol 2019).

111. Quadrate, head shape in dorsal view: oval (0), subrectangular (1).

112. Mediolateral expansion of quadrate head in relation to quadrate shaft: absent (0), present (1) (new).

113. Quadrate, medial foramina adjacent to condyles: absent (0), present (1).

114. Medial condyle of the quadrate: anteroposteriorly narrow and long axis of condyle mainly mediolaterally oriented (0), anteroposteriorly expanded and more anteroposteriorly oriented (1) (new).

115. Ventral rim of the basis of the paroccipital processes: above or level with the dorsal border of the occipital condyle (0), situated at mid-height of occipital condyle or lower (1).

116. Paroccipital processes: directed laterally or slightly ventrolaterally (0), directed strongly ventrolaterally, with distal end entirely below the level of the foramen magnum (1).

117. Marked depression on the exoccipital lateral to the foramen magnum, above the paracondylar recess: present (0), absent (1) (new).

118. Supraoccipital, anteroposterior depth of median ridge relative to occipital condyle length: less (0), greater (1).

119. Maximal width of dorsal expansion of supraoccipital ridge: less than or subequal to width of foramen magnum (0), notably greater than width of foramen magnum (1).

120. Posterior exit of mid-cerebral vein: on the posterior surface of the supraoccipital, without any associated marked depressions (0), placed within a notable, funnel-shaped depression (1), associated with a curved groove leading towards the posttemporal fenestra (2) (new).

121. Supraoccipital, participation in foramen magnum: present, ventral margin of supraoccipital forms a more or less straight line above the foramen, forming most of its dorsal rim (0), narrow, formed by a small median ventral process of the supraoccipital separating the exoccipitals on the dorsal edge of foramen (1), absent, exoccipitals meet in the midline above the foramen magnum (2) (modified from Rauhut and Pol 2019). ORDERED.

122. Attachment for proatlas on dorsolateral rim of foramen magnum: inconspicuous (0), marked as paired raised lips (1) (new).

123. Basioccipital, ventrolateral pair of pneumatic cavities invading neck of occipital condyle and joining medially: absent (0), present (1).

124. Morphology of posterior basioccipital surface below the condyle: with undivided longitudinal median groove (0), median groove divided dorsally by small median lamina (1), with large longitudinal ridge separating two large lateral depressions (2).

125. Basioccipital, fossa ventral to occipital condyle in basioccipital apron: narrow and groove-like, one half or less of the width of the occipital condyle (0), broad depression, approximately two thirds or more the width of the occipital condyle (1) (Carrano et al., 2012).

126. Notch on the basioccipital-basisphenoid suture separating a medial basioccipital portion of the basal tubera from a lateral basisphenoid portion: absent (0), present (1) (modified from Rauhut and Pol 2019).

127. Width of basioccipital ventral to the occipital condyle: greater than width of occipital condyle (0), subequal to or less than the width of the occipital condyle (1).

128. Basisphenoid, location of basipterygoid processes relative to basal tubera: anterior or slightly anteroventral, basisphenoid recess opens ventrally (0), anteroventrally, basisphenoid recess opens posteroventrally (1), almost directly ventral, basisphenoid recess anteroposteriorly narrower than wide and opens more posteriorly than ventrally (2).

129. Basisphenoid, presence and depth of basisphenoid recess: absent (0), shallow, longer than deep (1), deep, deeper than long (2). ORDERED.

130. Basisphenoid, shape of opening for basisphenoid recess: elongate oval (0), teardrop-shaped, narrowing posteriorly (1), subcircular (2), anteroposteriorly compressed, slit-like (3), trapezoidal, widening posteriorly (4).

131. Longitudinal lamina at least partially dividing the basisphenoid recess in its interior into left and right compartments: present (0), absent (1) (new).

132. Subdivision of basisphenoid recess into anterior and posterior recesses: absent (0), present (1) (new).

133. Posterior part of the ventral margin of the basisphenoid between the basal tubera and the basipterygoid processes: gently concave in lateral view (0), straight or slightly convex in lateral view (1).

134. Basipterygoid processes: on elongate stalks, with rather small articular surface (0), broad, enlarged articular surface facing anteroventrolaterally at lateral sides of the anterior end of the basisphenoid (1) (modified from Rauhut and Pol 2019).

135. Exit of cranial nerves X and XI: laterally through the metotic foramen (0), posteriorly through a foramen in the paracondylar recess (1).

136. Subcondylar recess on the occiput: small, restricted to the occiput lateral to the occipital condyle (0), extended ventrally, developed as deep depression on the lateral sides of the ventral part of the occiput (1)

137. Orientation of the occipital condyle in respect to the skull table: posteriorly (0), posteroventrally (1) (modified from Rauhut and Pol 2019).

138. Angle between the posterior end of the dorsal skull roof and the main body of the supraoccipital:

approximately 90° (0), notably obtuse (1).

139. Braincase, morphology of trigeminal foramen: single (0), partly split (1), fully split (2). ORDERED.

140. Exit of the abducens nerve (cranial nerve VI): placed within the pituitary fossa or the depression surrounding it (0), placed lateral to the pituitary fossa and its surrounding depression (1).

141. Dorsal process on the parasphenoid rostrum anterior to the pituitary fossa: absent (0), present (1) (new).

142. Well-developed anterior tympanic recess in the braincase: absent (0), present (1).

143. Braincase, ossification of interorbital region: weak or absent (0), extensive, ossified sphenethmoid and interorbital septum (1).

144. Length of the anterior, maxillary process of the palatine (as measured from the anterior end of the junction with the vomerine process to the anterior tip) in relation to length of jugal process (as measured from the posterior end of the junction with the pterygoid process to the posterio tip): less or subequal (0), longer (1).

145. Palatine, pneumatic recess on the dorsolateral side of the base of the vomerine process: absent (0), present (1) (modified from Rauhut and Pol 2019).

146. Deep, posterodorsally opening recess at the confluence of the jugal, pterygoid and vomerine processes of the palatine: absent (0), present (1) (new).

147. Pterygoid, pocket on ectopterygoid flange: absent (0), present (1).

148. Anteroventral expansion of jugal process of ectopterygoid: absent (0), present (1)

149. Ectopterygoid, ventral fossa: absent (0), present (1).

150. Ventral fossa of the ectopterygoid: simple depression (0), invaginates the lateral ectopterygoid body (1).

151. Size of external mandibular fenestra: Large, surangular above the fenestra accounts for less than half of the height of the mandible (0), reduced, surangular accounts for more than half the height of the mandible (1).

152. Mandible, position of anterior end of external mandibular fenestra relative to last dentary tooth: posterior (0), ventral (1).

153. Anterior end of dentary: not expanded (0), slightly expanded (1), strongly dorsally expanded, dorsal margin considerably above posterior alveolar margin (2) (modified from Rauhut and Pol 2019). ORDERED.

154. Shape of the anterior end of the dentary: rounded (dorsoventrally convex) (0), squared (dorsoventrally straight) (1).

155. Anteroventral flange or process at the anterior end of the dentary: absent (0), present (1).

156. Enlarged tooth or teeth in the anterior end of the dentary: absent (0), present, usually in the third and/or fourth dentary alevolus (1).

157. Dentary, shape in dorsal view: straight (0), curves anteromedially (1).

158. Dentary, longitudinal groove housing dorsally situated row of neurovascular foramina on lateral surface: absent or weak (0), present and well-defined (1).

159. Dentary, number of Meckelian foramina: one (0), two (1).

160. Posterior end of the dentary: with dorsal and ventral processes subequal in length or dorsal process slightly longer (0), sloping posteroventrally, ventral end extends considerably further posteriorly than dorsal end (1).

161. Morphology of posterior margin of dentary: forked (0), posteroventrally sloping margin with incision for mandibular fenestra (1).

162. Splenial, contour of posterior edge: straight (0), curved (1), notched (2).

163. Splenial, size of splenial ('mylohyoid') foramen: small (height less than 15 % of height of splenial at the level of the foramen) (0), intermediate (height between 15 % and 25 % (1), large (height 25% or more) (2). ORDERED.

164. Splenial, foramen in ventral part: completely enclosed by bone (0), open anteroventrally (1).

165. Deep incision in the anteroventral part of the prearticular: absent (0), present (1) (new).

166. Surangular, horizontal ridge on lateral surface below mandibular joint: weak or absent (0), strong (1).

167. Surangular, depressed lateral shelf for the attachment of the M. adductor mandibulae externus superficialis, bound medially by a dorsally facing ridge: absent, dorsal surface of the surangular mediolaterally convex anterior to the glenoid (0), present (1) (new).

168. Shelf on surangular for the attachment of the M. adductor mandibulae externus superficialis: faces mainly dorsally (0), faces notably laterodorsally (1)

169. Surangular, number of posterior surangular foramina: one (0), two (1).

170. Articular: rectangular ventral projection below the foramen for the chorda tympani on the medial side at the posteriomedial margin of the mandibular glenoid: absent, ventromedial margin of glenoid rounded (0), present (1) (modified from Rauhut and Pol 2019).

171. Anterior rim of the mandibular glenoid in lateral view: confluent with the dorsal margin of the surangular (0), raised above the dorsal margin of the surangular (1).

172. Ossified antarticular in the mandible: absent (0), present (1).

173. Retroarticular process of the mandible: elongate, as long as or longer than anteroposterior length of mandibular glenoid (0), short, shorter than length of mandibular glenoid (1).

174. Retroarticular process, mediolateral width relative to posterior width of dentary: ≤ (0), > (1).

175. Retroarticular process, orientation of attachment surface: posterodorsal (0), posterior (1).

176. Attachment area for the M. depressor mandibulae: mediolaterally notably concave (0), flat to slightly convex (1).

177. Lateral margin of retroarticular process: more or less aligned with glenoid (0), strongly offset ventrally from glenoid (1).

178. Paradental plates, continuity and replacement groove: separated, groove present (0), forming a continuous medial lamina ('fused'), groove absent (1).

179. Interdental plates, visibility in medial view: widely exposed, subpentagonal and moderate–tall (0), obscured by an expanded paradental lamina, triangular apices only may be visible (1).

180. Paradental plates, surface texture: smooth (0), vertically striated or ridged (1).

181. Lateral maxillary and dentary teeth: recurved, so that tip of the tooth is placed distal to distal carina, distal carina concave (0), straight or almost straight, tip of tooth placed mesial to distal carina, distal carina straight or convex (1).

182. Teeth, crown striations: absent (0), present on premaxillary and/or anterior dentary teeth only (1), present on all tooth crowns (2).

183. Teeth, enamel wrinkles: absent (0), pronounced marginal enamel wrinkles (1).

184. Lateral teeth, ratio between mesiodistal length and transverse width at the base: more than 1.5 (0), 1.5 or less (1) (modified from Rauhut and Pol 2019).

185. Teeth, maxillary and dentary, serrations: present (0), absent (1).

186. Teeth, maxillary and dentary, extent of anterior carina: to base of crown (0), at mid-height of crown or more apically (1).

187. Premaxillary teeth, arrangement of carinae: nearly symmetrical, on opposite sides (0), more asymmetrical, both on lingual side (1).

188. Premaxillary teeth, serrations: present (0), absent (1).

189. Premaxillary teeth, number: three (0), four (1), five (2), more than five (3). ORDERED.

190. Premaxillary teeth, spacing: even (0), paired and spaced (1).

191. Size of first premaxillary tooth (or alveoli): subequal to second premaxillary tooth (0), less than two thirds of the size of the second premaxillary tooth (1), less than half the size of the second premaxillary tooth (2). ORDERED.

192. Maxillary teeth, number: > 17 (0), 11–17 (1), < 11 (2). ORDERED.

193. Maxillary teeth, mid-tooth spacing: adjacent, closely spaced (0), more widely spaced in the mid-section (at least one-third of an alveolar width apart), but spacing decreases posteriorly again (1), more widely spaced, spacing increases posteriorly towards the end of the tooth row (2) ORDERED.

194. Rapid increase in tooth size at the anterior end of the maxilla: absent (0), present (1) (new).

195. Dentary teeth, size and number relative to maxillary teeth: approximately equal (0), smaller and

approximately 1.5 times as numerous (1).

196. Cervical vertebrae, anterior articular facet: concave (0), flat (1), convex (2). ORDERED.

197. Pneumatic feature posterior or posterodorsal to parapophysis (anterior pleurocoel) in cervical vertebrae: absent (0), large, blind depressions (1), large foramina (2).

198. Pneumatic feature on the posterior half of the vertebral centrum in cervical vertebrae: absent (0), large depression (1), foramen (2).

199. Presacral vertebrae, extent of anterior pleurocoel: anterior dorsals only (0), to sacrum (1).

200. Vertebrae, internal structure of pneumatic centra: absent (0), camerate (1), camellate (2).

201. Epipophysis of the atlantal neural arch in lateral view: slender, rod-like (0), expanded, triangular (1).

202. Axial neural spine: anteroposteriorly extensive, sheet-like, with convex or only gently ascending dorsal margin (0), anteroposteriorly reduced, rod-like, with steeply ascending dorsal margin (1).

203. Axis, orientation of intercentrum ventral surface: horizontal or slightly anteroventral (0), tilted anterodorsally (1).

204. Length of epipophyses of the axis: short, approximately level with posterior end of postzygapophyses (0), long, overhang postzygapophyses posteriorly for more than half the length of the postzygapophyseal articular facet (1).

205. Spinopostzygapophyseal laminae of the axis: Extensive, connecting the spine with the postzygapophyses in a large arch, resulting in a large, triangular to rhomboid fossa on the posterior side of the neural arch (0), reduced, strongly invaginated between spine and postzygapophyses, so that at least the distal part of the spine has parallel borders and the posterior fossa is reduced (1).

206. Development of parapophysis on axis: well-developed facet on the anteroventral side (0), indistinct, or only developed as a slightly roughened patch (1).

207. Development of diapophysis on axis: indistinct, probably absent (0), developed as distinct ventrolateral projection (1).

208. Axis, pleurocoels: absent (0), present (1).

209. Neural spine of third cervical vertebra: not significantly different from other postaxial cervical neural spines (0), slender and strongly backswept (1)

210. Cervical vertebrae, morphology of anterior pleurocoel: single opening (0), two openings oriented anteroventralposterodorsal or very plastic morphology (1).

211. Cervical vertebrae, middle, shape of anterior pleurocoel: round (0), anteroposteriorly elongate (1).

212. Cervical vertebrae, anterior, ventral keel: present (0), absent or weak ridge (1).

213. Cervical vertebrae, anterior, demarcation of dorsal surface of neural arch from diapophyseal surface: gently sloping (0), pronounced edge or ridge that offsets the dorsal from the lateral surface (1), elevated prezygoepipophyseal lamina, dorsal surface concave between neural spine and the lamina (2).

ORDERED.

214. Cervical vertebrae, articular surface of prezygapophyses: planar (0), flexed (1).

215. Cervical vertebrae, perimeter of anterior articular surface: not rimmed by a flattened peripheral band (0), flat, forming a distinct rim (1).

216. Cervical vertebrae, anterior, transverse distance between prezygapophyses relative to width of neural canal: < (0), >, prezygapophyses situated lateral to neural canal (1).

217. Cervical vertebrae, anterior, morphology of epipophyses: low, wider than high, posteriorly pointed (0), transversely narrow, high (1), high, robust (2).

218. Neural spine of mid-cervical vertebrae: anteroposteriorly longer than dorsoventrally high (0), higher than long (1).

219. Cervical vertebrae, longest post-axial elements: first five (0), last five (1).

220. Length/posterior height ratio of mid-cervical centra: less than 1.75 (0), 1.75-2.75 (1), more than 2.75 (2). ORDERED.

221. Width/height ratio of anterior articular surface of posteriormost cervical and anteriormost dorsal vertebrae: less than 1.3 (0), more than 1.3 (1) (new).

222. Height of anterior dorsal neural spines (as measured from the dorsal margin of the postzygapophysis): less (0) or more (1) than 1.25 times the height of the neural arch (as measured from the dorsal rim of the centrum to the dorsal margin of the postzygapophysis).

223. Ventral keel in posterior-most cervicals and anterior-most dorsals: ventrally concave, a rounded hypapophysis might be present anteriorly (0), forming a straight to slightly convex ventral margin, anterior end of keel protrudes ventrally from the anterior articular surface and is separated from the latter by a distinct step (1).

224. Dorsal vertebrae, pneumaticity/webbing at base of neural spines in middle to posterior dorsals: absent (0), present (1).

225. Middle to posterior dorsal vertebrae, accessory centrodiapophyseal lamina: absent (0), present (1).

226. Dorsal vertebrae, anterior, ventral keel: absent or developed as a weak ridge (0), pronounced, around 1/3 the height of centrum and inset from lateral surfaces (1).

227. Dorsal vertebrae, anterior, size of pneumatic foramen in centrum: small (0), enlarged (1).

228. Dorsal vertebrae, elevation of parapophyses: slightly elevated from centrum (0), project far laterally, more than half the diapophyseal length (1).

229. Dorsal vertebrae, orientation of hyposphene laminae: diverge ventrolaterally (0), parallel and sheet-like (1).

230. Dorsal vertebrae, position of parapophyses in posteriormost elements: on the same level as transverse process (0), distinctly below transverse process (1).

231. Dorsal vertebrae, distinct step-like ridge lateral to hyposphene, running posterodorsally from dorsal border of neural canal to posterior edge of postzygapophyses: absent (0), present (1), ridge present and is developed into a prominent lamina that bisects the infrapostzygapophyseal fossa in posterior dorsal vertebrae (2). ORDERED.

232. Posterior dorsal vertebrae, shape of ventral surface of vertebral centra: transversely rounded (0), flattened, sometimes with a shallow medial sulcus (1) (new).

233. Dorsal vertebrae, morphology of neural spines: transversely compressed sheets (0), transversely broad anteriorly and posteriorly, central regions of lateral surface embayed by deep vertical troughs (1).

234. Dorsal vertebrae, posterior, inclination of neural spines: vertical or posterior (0), anterior (1).

235. Dorsal vertebrae, height of neural spines relative to centrum height: low, ≤ 1.3x (0), moderate, 1.4-1.8x (1), tall, ≥ 2.0x (2). ORDERED.

236. Middle to posterior dorsal vertebrae, centrum length relative to height: centrum higher than long (0), centrum longer than high (1), centrum more than 1.5 times longer than high (2) (modified from Rauhut and Pol 2019). ORDERED.

237. Sacral vertebrae, centrum pneumaticity: absent (0), pleurocoelous fossae (1), pneumatic foramina (2).

238. Sacral vertebrae, number: 2 [primordial sacrals only] (0), 5 [1 dorsosacral, 2 caudosacrals] (1), 6 [2 dorsosacrals, 2 caudosacrals] (2). ORDERED.

239. Sacral vertebrae, transverse dimensions of middle centra relative to other sacrals: equivalent (0), constricted (1).

240. Sacral vertebrae, orientation of ventral margin of middle centra: approximately horizontal (0), strongly arched (1).

241. Sacral vertebrae, dorsal edge of neural spines: as thin as remainder of spine (0), transversely thickened (1).

242. Sacral vertebrae, pneumaticity of neural arches: weak or absent (0), paired fossa ventral to diapophyses (1).

243. Caudal vertebrae, anterior, morphology of ventral surface: flat (0), groove (1), ridge (2).

244. Caudal vertebrae, L-shaped neural spines: absent (0), present (1).

245. Anterior to mid-caudal vertebrae, depressions or pneumatic foramina in centrum: absent (0), large, pronounced pleurocentral depressions on the dorsal part of the lateral side (1), pneumatic foramina (2).

246. Caudal vertebrae, anterior, centrodiapophyseal laminae on neural arch: weak or lacking (0), only anterior centrodiapophyseal lamina well developed, defining a deep prezygodiapophyseal fossa (1), as prominent as in dorsal vertebrae, defining deep infradiapophyseal fossa that penetrates neural arch (pneumatic) (2).

247. Spinodiapophyseal ridge or lamina in at least mid-caudal vertebrae: absent (0), present (1) (new).

248. Caudal vertebrae, anterior, proportions of neural arch base relative to centrum proportions: < (0), ≥

(1).

249. Caudal vertebrae, middle, morphology of neural spines: rod-like and posteriorly inclined (0), sub-rectangular and sheet-like (1), rod-like and vertical (2).

250. Cervical ribs, length of anterior process: short (0), long (1).

251. Gastralia, posteriormost gastral segments: separate (0), united into single, boomerang-shaped elements (1).

252. Sacral ribs, articulations in adults: separate (0), fused together (1).

253. Sacral ribs, position of posterior attachment to ilium: ventral (0), posterodorsal (1).

254. Sacral ribs, depth relative to ilium height: < 85% (0), ≥ 90% (1).

255. Chevrons, morphology in middle caudal vertebrae: rodlike or only slightly expanded ventrally (0), L-shaped (1).

256. Chevrons, proximal articular surface: divided into anterior and posterior facets by distinct transverse ridge (0), no ridge, but low lateral mounds may be present, one on each side (1).

257. Chevrons, curvature: straight or gently curved (0), strongly curved (1).

258. Chevrons, anterior process: absent (0), present (1).

259. Chevrons, morphology of distal end in anterior and middle elements: expanded anteroposteriorly (0), unexpanded, tapers ventrally (1).

260. Scapula, angle between blade and acromion: gradual, oblique (0), abrupt, perpendicular (1).

261. Scapula, size of acromion process: moderate (0), marked (1).

262. Scapula, midshaft expansion of blade: absent (0), present (1).

263. Scapula, distal expansion of blade: marked (0), weak/absent (1).

264. Scapula, length:width ratio of blade: ≤ 7 (0), 7.5–9 (1), > 10 (2). ORDERED.

265. Scapulocoracoid, shape of anterior margin: indented or notched between acromial process and coracoid suture (0), smoothly curved and uninterrupted across scapula–coracoid contact (1).

266. Scapulocoracoid, glenoid lip: moderate (0), marked (1).

267. Coracoid, development of posteroventral process: low, rounded posteroventral eminence (0), pronounced, posteroventrally tapering process (1).

268. Coracoid, development of biceps tubercle (= acrocoracoid process): absent or poorly developed (0), conspicuous and well developed as tuber (1), developed as a posteroventrally oriented ridge (2).

269. Coracoid, prominent fossa on ventral surface posteroventral to glenoid (subglenoid fossa): absent (0), present (1).

270. Humerus, shape of head: elongate (0), globular (1).

271. Humerus, longitudinal torsion of shaft: absent (0), present (1).

272. Humerus, size of trochanters relative to midshaft diameter: < (0), > 150% (1) > 250% (2). ORDERED.

273. Humerus, development of internal tuberosity: low/rounded (0), hypertrophied (1).

274. Humerus, length of deltopectoral crest relative to total bone length: < 0.4 (0), 0.43–0.49 (1) > 0.52 (2). ORDERED.

275. Humerus, development of deltopectoral crest: large rectangular crest (0), reduced to a low, rounded flange (1).

276. Humerus, orientation of deltopectoral crest apex: anteriorly (0), anterolaterally (1).

277. Humerus, relative orientation of proximal and distal condyles in anteroposterior view: parallel, humerus straight (0), distal canted (1).

278. Humerus, anterior surface of bone adjacent to ulnar condyle: smooth or gently depressed (0), bears well-defined fossa (1).

279. Humerus, shape of distal condyles: rounded (0), flattened (1).

280. Radius and ulna, development of radial external tuberosity and ulnar internal tuberosity: low, rounded (0), hypertrophied distal ends of radius and ulna broadened (1).

281. Radius, shaft: straight (0), curves laterally (1).

282. Radius, development of medial biceps tubercle: small or indistinct (0), hypertrophied (1).

283. Ulna, olecranon process: absent (0), present (1).

284. Ulna, morphology of olecranon process: transversely robust (0), transversely compressed and ‘blade-like’ (1).

285. Ulna, crest extending distally along posterior surface from olecranon process: absent (0), present (1).

286. Ulna, hypertrophied medial and lateral processes on proximal end: absent (0), present (1).

287. Ulna, length relative to minimum circumference: stout, < 2.3 (0), gracile > 2.6 (1).

288. Carpus, morphology and articulations of distal carpals: separate dc1 and dc2 over separate metacarpals, flattened proximodistally (0), fused dc1 and dc2, dc1 overlaps metacarpals I and II, flattened proximodistally (1), fused dc1 and dc2, dc1 overlaps metacarpals I and II, strongly arched proximodistally (2).

289. Manus, length of digit II relative to length of humerus: < (0), > (1)

290. Manus, composition: digit IV and V present (0), digit IV present, digit V absent (1), MC IV present, IV phalanges and digit V absent (2), digits IV and V absent (3). ORDERED.

291. Manual digits, lengths: III longest (0), II longest (1).

292. Metacarpals, transverse width of proximal articular ends relative to minimum transverse shaft width: < (0), ≥ 2x (1).

293. Metacarpal I, length to minimum width ratio: 1.4–1.9 (0), ≥ 2.4 (1).

294. Metacarpal I, length relative to length of metacarpal II: > 57% (0), < 57% (1).

295. Metacarpal I, extent of contact with metacarpal II relative to shaft length: < 1/3 (0), 1/2 (1).

296. Metacarpal I, angle between facet for metacarpal II and proximal articular facet: perpendicular (0), obtuse (1).

297. Metacarpal III, position of base relative to those of other metacarpals: at same level (0), on palmar surface (1).

298. Metacarpal III, shape of proximal end: rectangular (0), triangular (1).

299. Metacarpal III, width relative to width of metacarpal II: > 50% (0), < 50% (1).

300. Manual ungual I, length:height ratio: < 2.5x (0), > 2.5x (1).

301. Manual unguals, proximal height:width ratio: transversely broad, < 2.0 (0), transversely narrow, > 2.4 (1).

302. Pelvic elements, articulations in adults: separate (0), fused (1).

303. Ilium, large external pneumatic foramina and internal spaces: absent (0), present (1).

304. Ilium, vertical ridge on lateral surface of blade dorsal to acetabulum: absent (0), low swollen ridge (1), low double ridge (2).

305. Ilium, posterior width of brevis fossa: subequal to anterior width, fossa margins subparallel (0), twice anterior width, fossa widens posteriorly (1).

306. Ilium, height of lateral wall of brevis fossa relative to medial wall: taller along whole length (0), shorter anteriorly, exposing medial wall in lateral view (1).

307. Ilium, morphology between supraacetabular crest and brevis shelf on lateral surface: gap (0), continuous ridge (1).

308. Ilium, ventrolateral development of supraacetabular crest: large/pendant ‘hood’ (0), reduced shelf (1).

309. Ilium, orientation of pubic peduncle: mostly ventral (0), mostly anterior or ‘kinked’ double facet with anterior and ventral components (1).

310. Ilium, shape of acetabular margin of pubic peduncle: transversely convex or flat (0), transversely concave (1).

311. Ilium, relative sizes of pubic and ischial articulations: subequal (0), pubic articulation ≥ 130% of

iliac articulation (1).

312. Ilium, morphology of ischial peduncle: rounded (0), acuminate (1).

313. Ilium, pubic peduncle length to width ratio: ≤ 1 (0), 1.3–1.75 (1), > 2 (2). ORDERED.

314. Ilium, ridge on medial surface adjacent to preacetabular notch: absent (0), present (1), strongly developed, forming a shelf (2). ORDERED.

315. Ilium, preacetabulum length relative to anterior edge of pubic peduncle: reaches anteriorly to same point as ('brachyiliac') (0), or well past ('dolichoiliac') (1).

316. Ilium, depth of preacetabular process: shallow (0), deep (1).

317. Ilium, anteroventral lobe of preacetabular process: absent (0), present (1).

318. Ilium, shape of dorsal margin: convex (0), straight (1).

319. Ilium, postacetabulum length relative to ischial peduncle length: ≤ (0), > (1).

320. Ilium, depth of postacetabular process: shallow (0), deep (1).

321. Shape of posterior margin of postacetabular process of ilium: rounded, dorsal margin curves gradually into posterior margin (0), only slightly convex or straight, dorsal margin offset from posterior margin by marked posterodorsal angle (1), concave (2), tapering (3).

322. Posterior process on the dorsal end of the posterior margin of the postacetabular blade, formed by a posterior expansion of the medial brevis shelf: absent (0), present (1).

323. Obturator foramen in pubis: completely enclosed in bone (0), ventrally open notch (1), absent (2). ORDERED.

324. Pubic fenestra below obturator foramen: absent (0), present (1)

325. Obturator plate of ischium: largely continuous with pubic articulation (0), with large notch below the pubic peduncle, obturator process offset from pubic articulation (1) (modified from Rauhut and Pol 2019).

326. Foramen in obturator plate of ischium: absent (0), present (1) (modified from Rauhut and Pol 2019).

327. Pubis, shaft orientation: anterodorsally curved (0), straight (1), posteroventrally curved (2) (modified from Rauhut and Pol 2019).

328. Pubis, articulation between apices in adults: unfused (0), fused (1).

329. Pubis, contact between distal portions: separate distally (0), contacting (1), contacting with slit-like opening proximal to distal expansion (interpubic fenestra) (2).

330. Pubis, angle between long axes of shaft and boot: 75–90° (0), < 60° (1).

331. Pubis, morphology of symphysis: marginal (0), broad (1).

332. Pubis, morphology of obturator foramen: small and subcircular (0), large and oval (1).

333. Pubis, anterior expansion of distal end: absent (0), present (1).

334. Pubis, boot length relative to shaft length: < (0), > 30% (1), > 60% (2). ORDERED.

335. Pubis, shape of boot in ventral view: broadly triangular (0), narrow, with subparallel margins (1).

336. Pubis, articulation with ilium: planoconcave (0), peg-and-socket (1).

337. Ischium, length relative to pubis length: 75–80% (0), ≤ 70% (1), > 80% (2).

338. Ischium, shaft orientation: straight (0), ventrally curved (1).

339. Ischium, articulation with ilium: planoconcave (0), peg-and-socket (1).

340. Ischium, morphology of antitrochanter: large and notched (0), reduced (1).

341. Ischium, notch ventral to obturator process: absent (0), present (1).

342. Ischium, morphology of symphysis: unexpanded (0), expanded as apron (1).

343. Ischium, cross-sectional shape of paired midshafts: oval (0), heart-shaped, medial portions of shafts extend posteriorly as midline flange (1).

344. Ischium, morphology of distal end: rounded (0), expanded, triangular (1).

345. Ischium, articulation at distal end in adults: separate (0), fused (1).

346. Femur, head orientation: 45° anteromedial (0), 10–30° anteromedial (1), medial (2). ORDERED.

347. Femur, head angle: ventromedial (0), horizontal (medial) (1), dorsomedial (2). ORDERED.

348. Femur, groove on proximal surface of head oriented oblique to long axis of head (‘articular groove’): absent (0), present (1).

349. Femur, oblique ligament groove on posterior surface of head: shallow, groove bounding lip does not extend past posterior surface of head (0), deep, bound medially by well-developed posterior lip (1).

350. Femur, placement of lesser trochanter relative to femoral head: does not reach ventral margin (0), rises past ventral margin (1), rises to proximal surface (2). ORDERED.

351. Femur, morphology of anterolateral muscle attachments at proximal end: continuous trochanteric shelf (0), distinct lesser trochanter and attachment bulge (1).

352. Femur, development of fourth trochanter: prominent semioval flange (0), very weak or absent (1).

353. Femur, distinctly projecting accessory trochanter (derived from lesser trochanter): weak, forms slightly thickened margin of lesser trochanter (0), present as triangular flange (1).

354. Femur, M. femorotibialis externus origin medially on anterodistal surface: faint, small rugose patch

(0), pronounced rugose depression that extends to distal femur (1).

355. Femur, development of medial epicondyle: rounded (0), ridge (1).

356. Femur, distal extensor groove: absent (0), present (1).

357. Femur, morphology and orientation of tibiofibularis crest: broad (0), narrow, longitudinal (1), lobular, oblique (2).

358. Femur, infrapopliteal ridge connecting medial distal condyle and crista tibiofibularis: absent (0), present (1).

359. Femur, orientation of long axis of medial condyle in distal view: anteroposterior (0), posterolateral (1).

360. Femur, projection of lateral and medial distal condyles: approximately equal (0), lateral projects distinctly further than medial, distal surface of medial is gently flattened (1).

361. Femur, morphology of distal end: central depression connected to crista tibiofibularis by a narrow groove (0), anteroposteriorly oriented shallow trough separating medial and lateral convexities (1).

362. Tibia, lateral malleolus: backs astragalus (0), overlaps calcaneum (1).

363. Tibia, shape of edge of lateral malleolus: smoothly curved (0), tabular notch (1).

364. Tibia, morphology of distal cnemial process: rounded (0), expanded proximodistally (1).

365. Tibia, morphology of lateral (fibular) condyle: large (0), small and lobular (1).

366. Tibia, anterolateral process of lateral condyle: absent or horizontal projection (0), prominent, curves ventrally (1).

367. Tibia, anteromedial buttress for astragalus: absent (0), ventral (1), marked oblique step-like ridge (2), reduced oblique ridge (3), bluntly rounded vertical ridge on medial side (4).

368. Tibia, morphology of fibular crest: narrow (0), bulbous (1).

369. Tibia, development of fibular crest: extends to proximal end of tibia as high crest (0), extends to proximal end of tibia as low ridge (1), does not extend to proximal end of tibia (2). ORDERED.

370. Groove or depression on the medial side of the proximal end of the fibula: absent or only shallow concavity present (0), deep groove on the posterior half of the medial side of the proximal end, offset from anterior margin and opening at least partially posteromedially (1), large, deep depression that opens medially and is offset from the anterior margin only by a thin ridge or lip (2)

371. Ridge on the medial side of the proximal end of the fibula that extends anterodistally from the posteroproximal part: absent (0), present (1).

372. Fibula, size of iliofibularis tubercle: faint scar (0), large (1), anterolaterally curving flange (2).

373. Fibula, size of proximal end relative to width of proximal tibia: < 75% (0), ≥ 75% (1).

374. Astragalus, articulation between ascending process and fibula in adults: separate (0), fused (1).

375. Astragalus, orientation of distal condyles: ventral (0), 30-45° anterior (1).

376. Astragalus, ascending process morphology: blocky (0), laminar (1).

377. Astragalus, ascending process height relative to depth of astragalar body: less (0), subequal (1), > 1.6 times (2).

378. Astragalus, prominent proximolateral extension: absent (0), present (1).

379. Astragalus, round fossa at base of ascending process: absent (0), small (1), large (2). ORDERED.

380. Astragalus, development of articular surface for distal end of fibula: large, dorsal (0), reduced, lateral (1).

381. Astragalus, posterolateral crest: absent (0), present (1).

382. Astragalus, posteromedial crest: absent (0), present (1).

383. Astragalus, articulation with calcaneum in adults: separate (0), fused (1).

384. Metatarsal I, length relative to length of metatarsal II: ≥ 50% (0), < 50% (1).

385. Metatarsal III, shape of proximal end: rectangular (0), shallow notch (1), deep notch (2). ORDERED.

386. Metatarsal III, midshaft cross-sectional shape: rectangular (0), wedge-shaped, plantar surface pinched (1).

387. Metatarsal III, relative proportions of shaft: short and thick, length:transverse width ratio < 12.0 (0), long and gracile, ratio > 12.5 (1).

388. Metatarsal IV, proportions of distal end: broader than tall (0), taller than broad (1).

389. Metatarsal V, morphology of distal end: articular (0), non-articular (1).

390. Metatarsal V, length relative to length of metatarsal IV: > 50% (0), < 50% (1).

391. Antarctometatarsus: absent (0), present (1).

392. Pedal unguals, morphology of lateral and medial grooves: single (0), double (1).

393. Pedal unguals, digits III and IV, cross-sectional shape: triangular (0), elliptical (0).

394. Pedal unguals, digit II, mediolateral symmetry: symmetrical (0), asymmetrical (1).

395. Pedal digit phalanges, length of I-1 + I-2 relative to III-1: greater (0), less than or equal

SUPPLEMENTAL DATA FILES 3-14.

The following supplemental files are available for download.

Suppl. Data 3. Irritator_full_matrix

Suppl. Data 4. Irritator_cranial_matrix

Suppl. Data 5. Irritator_full_matrix_equal_weighting_MPTs+strict_consensus

Suppl. Data 6. Irritator_cranial_matrix_equal_weighting_MPTS+strict_consensus

Suppl. Data 7. Irritator_full_matrix_implied_weighting_MPTs+strict

Suppl. Data 8. Irritator_full_matrix_reduced_consensus

Suppl. Data 9. Irritator_optimization_tree

Suppl. Data 10. Irritator_optimization_matrix

Suppl. Data 11. Irritator_optimization

Suppl. Data 12. Irritator_MrBayes_script

Suppl. Data 13. Irritator_jaw_movement_digital

Suppl. Data 14. Irritator_jaw_movement_print